OPTIMISATION OF PROCESS PARAMETERS OF HIGH POWER CO_2 LASER CUTTING FOR ADVANCED MATERIALS

By

HAYAT A. ELTAWAHNI, B.Sc., M.Sc.

A Thesis Submitted in Fulfilment of the Requirements for the Degree of Doctor of Philosophy (PhD)

Supervisor

Dr. Abdul-Ghani Olabi

School of Mechanical and Manufacturing Engineering

Dublin City University

July 2011

DECLARATION

I hereby certify that this material, which I now submit for assessment on the programme of study leading to the award of Doctor of Philosophy is entirely my own work, that I have exercised reasonable care to ensure that the work is original, and does not to the best of my knowledge breach any law of copyright, and has not been taken from the work of others save and to the extent that such work has been cited and acknowledged within the text of my work.

Signed: HAYAT ELTAWAHNI

(Candidate) ID No.: 52149706

Date: 05/07/2011

ACKNOWLEDGEMENTS

First of all I would like to express my sincere thanks and gratitude to Almighty Allah, who helped and blessed me during the course of my studies. Olabi

Also, I would like to thank Dr. Abdul Ghani Olabi for his supervision and guidance during the course of this work. His constructive suggestions, comments and advice throughout the project were invaluable.

I also would express my acknowledgment to Prof. M. S. J. Hashmi for his financial support of this research and his constant assistance and guidance.

Also, I would like to thank the culture affairs office in London for paying the tuition fee for the third year.

I also would like to take this opportunity to extend my thanks to Dr. K. Y. Benyounis, Walid Magdy and Mr. Martin Johnson for their invaluable help during this research.

I am thankful to my, husband and my kids, whose have given me the chance of discovering what I like, and of devoting myself to it.

I would like to thank the technical staff of the School of Mechanical & Manufacturing Engineering, especially Mr. Liam Domican and Mr. Michael May.

Finally, I would like to take this opportunity to extend my thanks to each one of my friends, here in Ireland and back home, for their honest and sincere concerns about my study and myself.

Optimisation of Process Parameters of High Power CO_2 Laser Cutting for Advanced Materials

Hayat A. Eltawahni, B. Sc., M. Sc.

ABSTRACT

Nowadays, advanced materials such as composite materials, thermoplastics, fibre glass etc. are replacing other materials in many different industrial applications. This is due to the improvements achieved in their engineering properties. The demand on these advanced engineering materials necessitates the development of advanced material processing techniques. Laser beam cutting (LBC) is an advanced processing technique applied widely in industry to cut different materials with high production rates. In order to optimise the LBC process, it is essential to first model the process accurately. In fact, an optimised cutting procedure is crucial to insure the high quality of the products. This procedure should contain the values, or ranges of values, for process parameters that produce cuts with the quality levels required by the end user.

Accordingly, the aim of the current research is to apply response surface methodology (RSM) via Design-expert software to develop empirically based mathematical models that relate the process input parameters to the quality features (responses). Once these mathematical models have been developed and checked for their adequacy they can be used to optimise the process, and thus, achieve the desired quality levels. The LBC input parameters considered herein are: laser power, cutting speed, assist gas pressure, focal point position, nozzle diameter and stand-off distance. The quality features investigated are: upper kerf width, lower kerf width, ratio between two kerfs, heat affected zone (HAZ), roughness of the cut section and operating cost. Materials, commonly used in industry, in sheet form with different thicknesses, have been investigated namely: medical grade austenitic stainless steel AISI316L, medium density fibre board (MDF), Ultra-high molecular weight polyethylene (UHMWPE), polymethyl-methacrylate (PMMA) and glass fibre reinforced plastic (GFRP). A CW 1.5 kW CO_2 Rofin laser is used to perform the cutting operations.

Different models were successfully developed to predict the responses for each material and thickness including operating cost. Moreover, the main effects and interaction effects of the process parameters on the responses were determined, discussed and illustrated graphically. In addition, the process has been optimised and the optimal cutting conditions have been recorded for each material and thickness. These records could be used as a standard procedure for LBC because they provide the relevant parameters and allowable ranges that should be used for optimal laser cutting for each material and thickness.

TABLE OF CONTENTS

CHAPTER III

CHAPTER IV

CHAPTER V

CHAPTER VI

CHAPTER VII

LIST OF FIGURES

LIST OF TABLES

CHAPTER I
INTRODUCTION

1. INTRODUCTION

The name LASER is an acronym for "Light Amplification by the Stimulated Emission of Radiation". In 1917, Albert Einstein was the first to conceive the process called "Stimulated Emission", which makes lasers possible. In 1958, Charles Townes and Arthur Schawlow wrote and published papers about producing light with a wavelength in the visible range. In fact, different materials can be used as lasing material. Some, like the ruby laser, produce short pulses of laser light. Others, like helium-neon gas lasers or liquid dye lasers produce a continuous beam of light [1].

The first gas laser appeared in 1961 when a Helium-Neon (He-Ne) laser was developed at the Bell Telephone Laboratories. Since then newer types of lasers that are more powerful and reliable have been developed. However, only a relatively small number of them are in use for materials processing. The two main types that have been used for the longest period of time and the most frequently used in all applications are the carbon dioxide laser (CO_2) and the Nd-YAG laser. In recent times, a number of other laser types have been developed with the intention that they can also be used in material processing [2 and3].

CO_2 lasers offer the highest average power for materials processing. CO_2 lasers with output power of 1 kW or less are considered low-power laser. High-power laser with average power up to 50 kW are also available, but most lasers in industrial application are under 15 kW, with the majority under 3 kW. Compared with other lasers, the higher power capability of the CO_2 type allows their use in processing different materials in mass production in many industrial applications. Consequently, they are often selected for automotive and other steel parts fabrication [3].

Over the past two decades, the laser has become the tool of choice for most manufacturers in many industrial applications, such as prototype fabricating, welding and machining etc. The role of laser continues to increase in industrial applications especially with the invention of advanced materials, which are difficult to process. The high power laser beam cutting process has advantages in comparison with conventional

cutting processes like plasma arc cutting and mechanical cutting. These advantages are the following: [3 and4].

1. The process can be carried out under atmospheric conditions.
2. There is no force between the workpiece and the laser beam. Therefore there is no need for rigid clamping.
3. The processing speed is very high.
4. There is a small heat-affected zone (HAZ) due to the relatively small total heat input. Thus, there is very little damage to the base material, making it suitable for heat sensitive and combustible materials.
5. The laser beam can be transmitted by optical fibres over long distance.
6. Different materials can be processed by the same laser beam system by controlling the beam parameters.
7. There is a high degree of flexibility (which may facilitate the cutting of complex geometries) and there is a low level of noise.
8. The systems are suitable for both very soft (highly deformable) materials such as paper and very hard (difficult to cut) materials such as diamond.
9. The process is user-friendly since no dangerous radiation ray such as X-rays are produced. However, some safety guidelines still have to be observed.

On the other hand, the main disadvantages of laser beam cutting are as follows:

1. Highly reflective and conductive materials such as gold, copper and silver are difficult to cut using lasers.
2. Laser cutting is limited to cutting through the material. Blind slots, pockets, holes or thin materials are difficult to cut accurately using a laser.
3. The initial capital cost of a laser cutting system is relatively high.
4. Laser cutting of some materials, such as polycarbonate, may produce dangerous exhaust gases.

Laser cutting in general is an effective way to reduce production and manufacturing costs. This is due to the advantage of high production rates as well as the fact that lasers can be mechanised, computer controlled and integrated into assembly lines. Many industries have been revolutionized by the application of laser equipment in their production lines. This is because of the high-quality and low distortion characteristics of the cutting action which can be achieved. Most materials can be cut by the process including metals, wood, plastics, rubber and composites etc. On the other hand, some materials cannot be cut by this process due to safety reasons [4].

The fundamental scientific principles involved in laser cutting of most materials are the same as those occurring in CO_2 lasers. The laser beam is focused onto the surface of the material to be cut by means of a focusing lens. This results in the heating of a small amount of the material surface. This locally heated volume melts and vaporizes rapidly due to the high temperature, and then it is blown away by a jet of gas, leaving an edge with a high quality surface finish. As the beam moves along the surface, a groove of materials vaporizes and the diameter of this groove is usually slightly greater than the diameter of the focused beam. The molten material is ejected with the aid of a high-pressure gas jet called assist gas. This gas usually flows in the same direction as the laser beam [4].

If a manufacturer wishes to introduce laser cutting as a technique in a manufacturing process, it is necessary to study the effect of the process in a new material. A number of preferred characteristics such as accuracy of the cut and quality of the surface finish can be specified and also process characteristics such as high speed and low power usage can be also stipulated. It is then necessary to vary the laser input parameters and test whether or not the desired quality features are achieved or not. This procedure is usually performed by skilled workers. However, this procedure of selection of parameters is based on trial-and-error and is usually time-consuming. Moreover, the conventional one by one technique is not systematic and usually does not lead to an optimised combination of laser cutting parameters. This is due to the fact that the laser cutting process is affected by complex interactions of the different input and output parameters. A systematic study, based on Design of Experiment (DOE) techniques

followed by the analysis of the results using Response Surface Methodology (RSM), will allow the detection and visualisation of the interactive effects of the input parameters on the results. Once a study of this kind has been done, the optimum combinations of laser cutting parameters can be selected and then used to produce the desired specifications.

1.1 Thesis Objective

The main objective of the current work is to apply RSM to develop mathematical models, in the form of function showing the relationships between all the laser cutting parameters. These models would add a significant knowledge to help scientists and researchers in conducting experiments. It would also assist technicians and engineers to achieve the required cutting characteristics. This approach minimises the process start-up costs, guarantees the highest reliability in laser cut products as well as improving the quality of the final parts.

In addition to this, the models to be developed would be useful in predicting responses. This would allow the selection of the optimal settings of the process input parameters to minimise or maximise certain responses. The response could be surface roughness or kerf width etc.

The principal aims of the present research can be summarized in the following points:

1. To build up mathematical models using RSM with the aid of Design-Expert version-7 statistical software to predict the following responses:
    a) Upper kerf width.
    b) Lower kerf width.
    c) Ratio between the upper kerf width to lower kerf width.
    d) Width of HAZ.
    e) Roughness of the cut section.
2. To identify the most influential laser cutting parameters and to clarify their interactions on the above-mentioned responses.

3. To present the developed models in 3D plots and contour graphs etc.
4. To demonstrate the individual effect of a certain factor on a given response at set values of the remaining parameters.
5. To estimate the operating cutting cost.
6. To identify the optimal combinations of the process input parameters, using numerical and graphical optimisation, to achieve a specific target criterion.

Different materials are to be investigated in this work, namely: medical grade stainless steel AISI316L, Ultra-high molecular weight polyethylene (UHMWPE), medium density fibre board (MDF), polymethyl-methacrylate (PMMA) and glass fibre reinforced plastics (GFRP). A 1.5 kW CW CO_2 Rofin laser is to be used as the cutting tool. The process input parameters that under control are laser power, cutting speed, assist gas pressure, nozzle diameter and focus point position.

1.2 Structure of Thesis

Chapter 1 is a general introduction including the thesis objective. Chapter 2 contains a comprehensive literature review. This includes an overview of types of laser with some emphasize on high power CO_2 laser, and a general summary of the laser materials processing and in particular laser beam cutting including CO_2 laser cutting parameters effects. The characteristics of laser cut edge are explained along with the quality features of the laser cutting section and a summary of some other issues such as process economy, process hazard and safety as well as a comparison between laser beam cutting the common traditional cutting processes. Work done by other researches in the area of laser cutting of different materials are also reviewed and discussed. Finally, modelling and optimisation techniques in common laser beam processes are also addressed. Chapter 3 illustrates a discussion of the statistical Design of Experiment (DOE) method used in this work and the optimisation method details. Chapter 4 details the equipment and experimental methods used in this work. The materials used in the study are also demonstrated. The laser machine used is explained in detail. The experiment layout for each material and thickness are presented. The procedure and

equipments utilized in measuring the responses are also shown. Moreover, details of operating cost estimation are given. Finally, information on visual basic program and the layout of the windows are demonstrated. Chapter 5 presents the results and discussion achieved for all materials investigated herein. Chapter 6 illustrates the results of the numerical and graphical optimisations along with the optimal cutting setting for each material and thickness for a given criterion. The conclusions drawn from this investigation and some recommendations for future work are outlined in Chapter 7.

CHAPTER II
LITERATURE REVIEW

2. LITERATURE REVIEW

Lasers are coherent, monochromatic and highly directional beams of light which can be focused to very small spot sizes and are therefore, capable of delivering high energy-densities to small areas of a material. This localized high energy can be used to melt or vaporize the material to perform a cut [5]. There are many types of laser systems that are currently in use for materials processing. In the following section the most common types of laser utilized in materials processing will be briefly discussed and compared.

2.1 Types of Lasers

Lasers can be classified easily according to their lasing mediums, which are divided into three main categories: gas, liquid, or solid. In addition, all laser types operate in one of two temporal modes: continuous wave (CW) and pulsed modes. In the CW mode, the laser beam is emitted without interruption. In the pulsed mode, the laser beam is emitted periodically [6]. Lasers, which can be used for materials processing at present, use lasing media which are either in the form of a solid or a gas. Three main types of solid-state laser have been developed: the ruby laser, neodymium glass laser and the neodymium yttrium aluminium garnet (Nd-YAG) laser. The Nd-YAG, which has an output wave length of 1.06 μm, has practically replaced the other two types as it can maintain higher powers for longer periods. On the other hand, the gas lasers which are utilized in materials processing are currently nearly all 10.6 μm wavelength carbon dioxide (CO_2) lasers as they have proven to be the most efficient and produce the highest power [7]. There are some other types of laser system that are used principally in industry for materials processing such as the carbon monoxides (CO) laser, the Excimer laser etc. A comparison between these lasers can be made in several ways as illustrated in Fig. 2.1 and Fig. 2.2. Fig 2.1 presents a selection of material processing lasers, plotted as a chart with axes of wavelength and average power. The operating regions of the different lasers can thus be distinguished, and power levels appropriate for material processing can be selected. Lines in Fig. 2.1 indicate the principal output wavelengths,

and laser that are used mainly in industrial material processing are shaded [8]. Fig. 2.2 presents a comparison between the principle material processing lasers in terms of capital cost per output power and in terms of operating cost versus output energy [9]. It is well know that Nd-YAG lasers and CO_2 lasers are the best among other laser systems for laser cutting of different materials. In the current study, a CO_2 laser was chosen to perform the cutting operation as it is available in the workshop of the School of Mechanical Engineering. Therefore, a detailed review including its nature, recent development and applications is important.

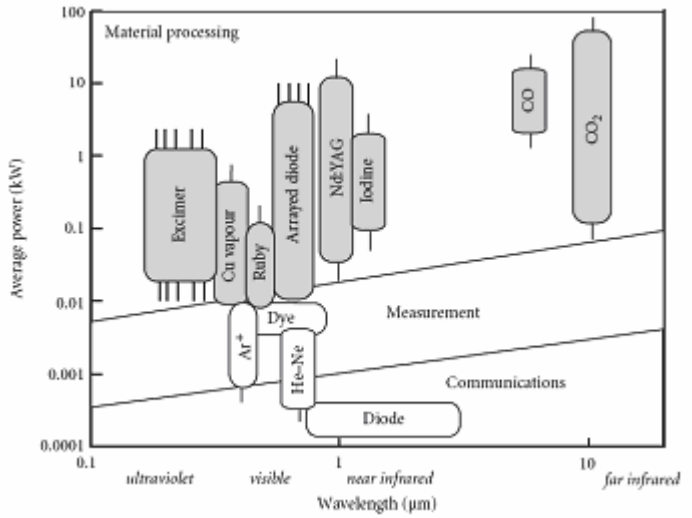

Fig. 2.1: A selection of commercial lasers characterized by wavelength and average power, shown on a background of applications [10].

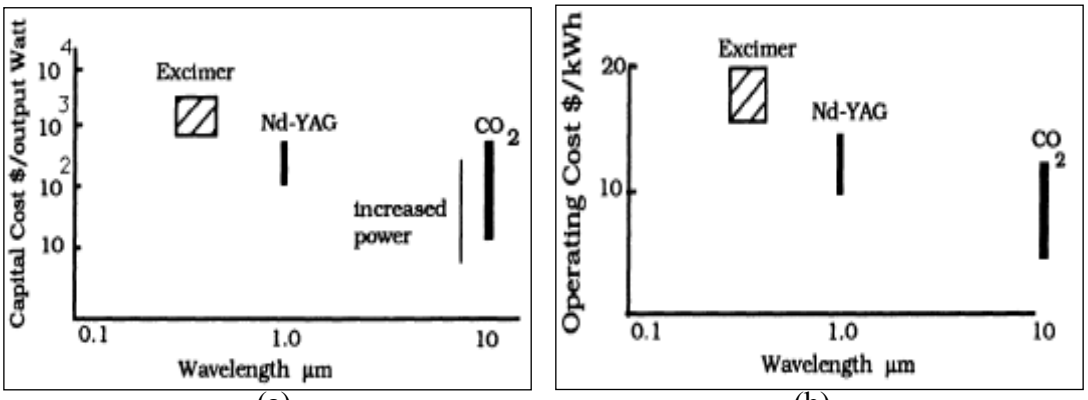

(a) (b)

Fig. 2.2: Various comparisons between the principle materials processing lasers: (a) capital cost/output power and (b) operating cost/output energy [9].

2.2 The High-Power CO_2 Laser

All lasers consist of three main elements: an active medium (lasing material that generates the light), a power supply (a source of energy to excite the active medium) and a resonant cavity (an optical resonator consisting of two parallel mirrors which amplify the light). An example of the configuration of the axial flow CO_2 laser is shown in Fig. 2.3 [10].

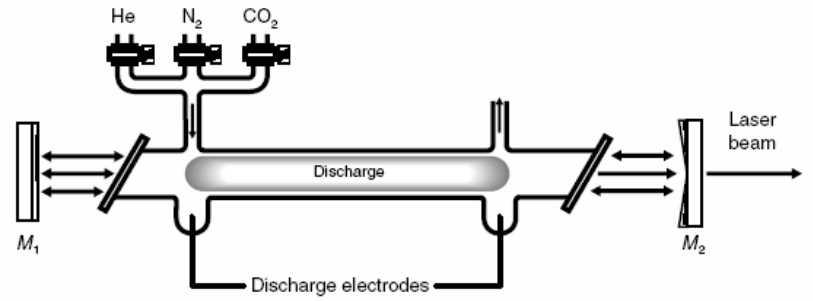

Fig. 2.3: Typical configuration of the axial flow CO_2 laser [10].

In CO_2 lasers, which have a mixture of gases as the active medium, the amount of carbon dioxide gas (CO_2) in the active medium is between 1 and 9%. The remaining volume consists of helium (60–85%), nitrogen (13–35%) and small amounts of other gases. The exact composition depends on the design of the optical cavity, the gas flow rate and the output coupler used. This gas mixture is kept in an excited state with a power supply which produces a high electrical potential [6].

The resonant cavity consists of a discharge tube containing the excited gas mixture between two end mirrors. One of the mirrors is made fully reflective, while the other is partially transparent to allow for beam output. In order to achieve the required beam stability, an acceptable beam divergence and high efficiency, a variety of mirror configurations can be used in the resonant cavity.

The amplification of light in a laser is accomplished by the optical resonator described above. The aligned mirrors in the resonant cavity channel the light back into the lasing medium. As the photons pass back and forth through the lasing medium, they stimulate more and more emissions. Photons that are not aligned with the resonator are

not redirected by the mirrors to stimulate more emission, so that the mirrors will only amplify those photons with the proper orientation, and a coherent beam develops quickly as illustrated in Fig. 2.4 [6].

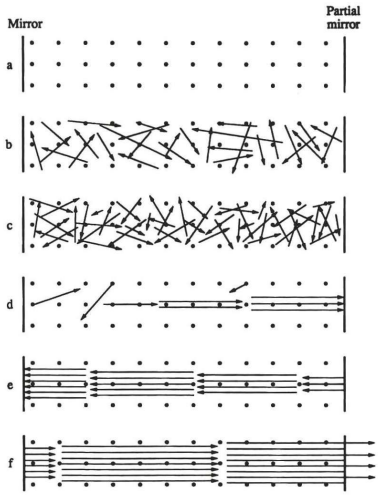

Fig. 2.4: Amplification states (a) laser off, (b) and (c) Initial random states, (d) Initial simulation, (e) Amplification and (f) Coherent beam [6].

Commercial CO_2 lasers are available in five basic configurations, which characterize the geometry of gas flow in the optical cavity: sealed; transversely excited atmospheric pressure (TEA), slow axial flow, fast axial flow and transverse flow. Typical characteristics of these designs are given in Table 2.1.

Table 2.1: Characteristics of commercial CO2 laser designs [8].

	Sealed	TEA	Slow axial flow	Fast axial flow	Transverse flow
Gas, He-N_2-CO_2.N_2-O_2-CO (vol. %)	72-16-8-0-4	72-16-8-0-4	72-19-9-0-0	67-30-3-0-0	60-25-10-5-0
Gas flow rate (m s^{-1})	-	-	5-10	300	20
Gas pressure (mbar)	6-14	1000	6-14	70	50
Gain (W cm^{-3})	20-30	0.5	0.5	5-10	4-6
Gain (W cm^{-1})	50	100	100	1000	6000
Wall plug efficiency (%)	5-15	5-20	5-15	5-15	5-10
Cooling	Conduction	Conduction	Conduction	Convection	Convection
Ergonomics	Portable	Portable	Fixed	Fixed	Fixed

2.2.1 Sealed tube lasers

The gas mixture is contained in an enclosed chamber across which the electric discharge is applied as illustrated in Fig. 2.5. However, the discharge causes CO_2 to dissociate into CO and O_2, which reduces output power. This can be prevented by adding a small amount of water vapour (H_2O) or by using a Ni cathode that is heated to 300 °C as a catalyst. As a result, a laser can be used for over 10^4 h. Typical output powers for sealed tube lasers are of the order of 60W/m. The output beam of the sealed tube CO_2 laser normally operates in the low-order mode. Therefore, it has been used in microsurgery and micromachining where the high accuracy of the low-order mode beam is essential. Machining applications include drilling and cutting of thin metal sheets (about 0.5–1.5 mm in steels), and non–metals [6 and 10].

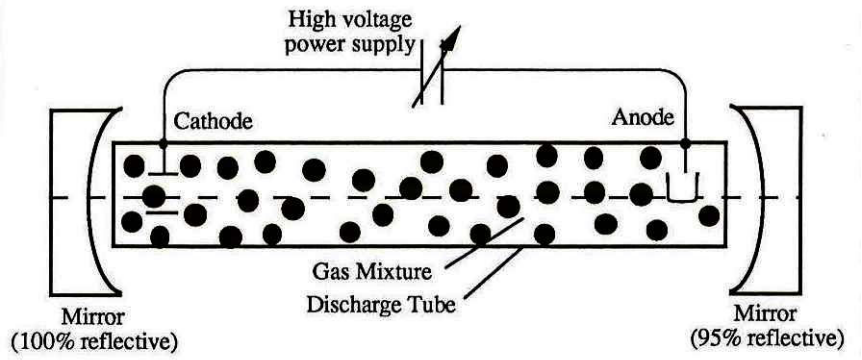

Fig. 2.5: Sealed tube lasers [6].

2.2.2 Transversely excited atmospheric pressure lasers

In this type of laser CO and hydrogen (H_2) may be added to counteract the dissociation of CO_2, and increase the output power. Since the gas pressure is relatively high, large voltages are required for excitation. In TEA lasers only pulsed output is possible, due to discharge instabilities are easily produced in the high pressure gas media, which degrade the output power. TEA lasers can produce short pulses of high peak power (1-50 MW) at a rate of 20-100 Hz. TEA lasers have a small power supply and a lightweight laser head. The applications of this laser are marking the product coding on aluminium cans, and marking plastic packages [8 and 10].

2.2.3 Slow axial flow lasers

In this type of laser, the gas mixture flows at a relatively slow speed (about 20 L/min) and contains a high amount of helium to facilitate cooling. Heat is removed by conduction from the tube centre to the walls. The output power is typically about 50–500W overall, and does not depend on the tube diameter which is about 25 mm. The higher output powers are obtained by increasing the optical path length of the beam in the resonator, using folding mirrors to redirect the beam along different paths as shown in Fig. 2.6. The lower power levels are used in laser surgery, while the higher powers are more appropriate for scribing, resistor trimming, welding of thin sheets, and cutting non-metals [8 and 10].

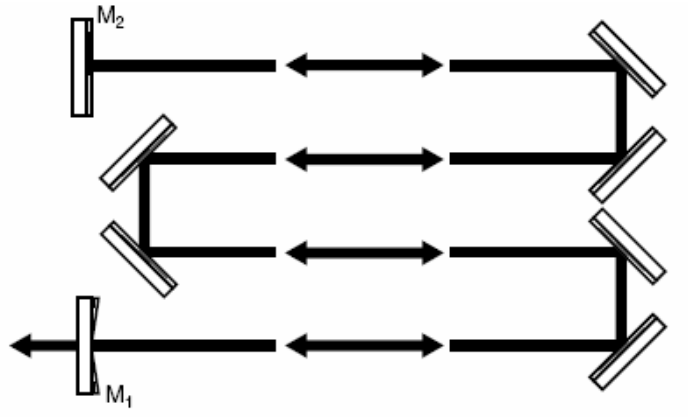

Fig. 2.6: One possible resonator configuration [10].

2.2.4 Fast axial flow lasers

In this type of laser, the removal of the dissipated heat can be made more efficient by moving the gas mixture through the tube at much higher speeds of about 300–500 m/s to get rid of the heat by convection. The gas is then recycled through a heat exchanger. This enables the power to be greatly increased to about 500 W to 6 kW in overall power output and laser systems as large as 20 kW have been built. These types of lasers are extensively used in materials processing, for example, welding and cutting. They tend to have better beam characteristics than transverse flow lasers described in the following section [10].

2.2.5 Transverse flow lasers

The geometry of this type of laser, shown in Fig. 2.7, has a number of advantages over the fast axial flow design. Gas flow rates are typically one tenth those of the fast axial flow design, which reduces the requirements on the blowers, and reduces flow rate losses that lead to increased temperature and reduced beam power. Transverse flow lasers can be made relatively easily in modules, enabling designs to be scaled to high power outputs. The capital cost per kW is lower, and the compact design results in a smaller footprint. The maximum power achieved by this type of laser could reach 9 kW or 15 kW depending on the way the discharge is maintained. These high power lasers are frequently used for material processing operations such as thick section welding and large area surface treatment [8 and 10].

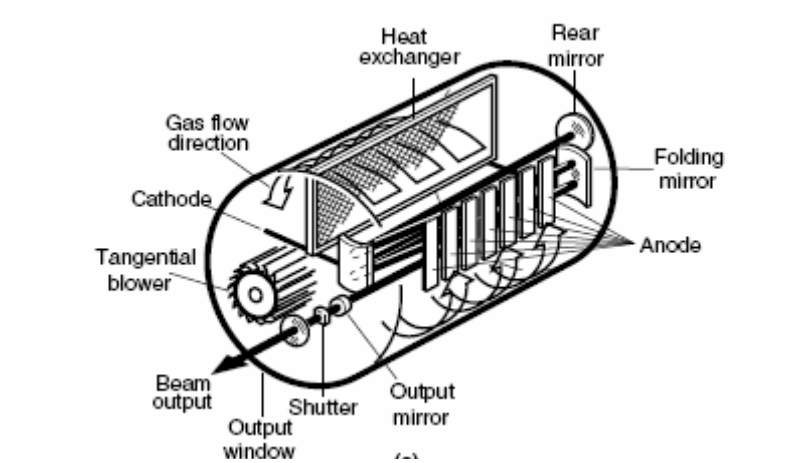

Fig. 2.7: Three-dimensional view of a transverse flow CO_2 laser [10].

2.3 Laser Materials Processing

While the form of energy in a laser is light, when the laser is used for processing materials, the energy density is so high that it can act as a source of heat. Accordingly, it can be a useful source of intense heat when focused on a small area. Lasers are able to produce high power densities because of their monochromatic, coherent, and low divergence properties as compared with normal light. As a result, they can be used to

heat, melt, and vaporize most materials. Lasers are commonly used in materials processing such as: welding, cutting, surface modification and forming. The power densities and exposure times necessary for various processes are shown in Fig. 2.8. In the subsequent sections a detailed review of laser beam cutting (LBC) is outlined [10].

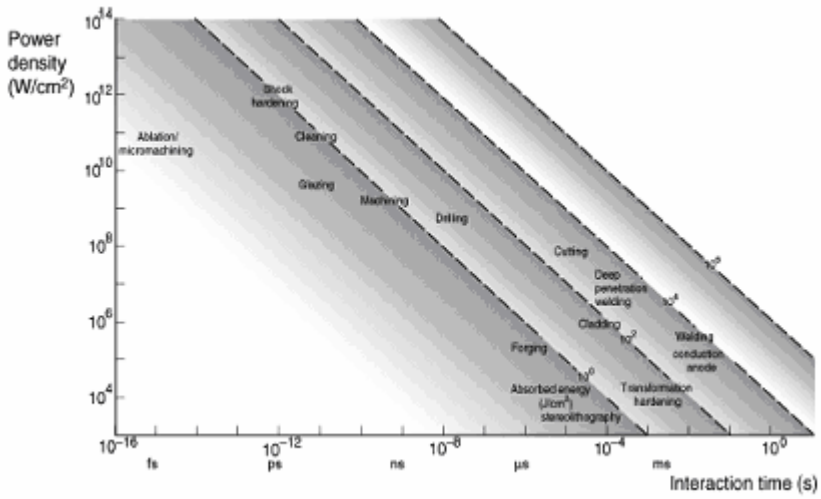

Fig. 2.8: Power densities and interaction times for various laser processes [10].

2.4 Laser Beam Cutting

Soon after the 1960s when lasers were discovered they became popular in many applications in industry especially in materials processing such as the cutting of engineering structures due to their high power density and accuracy. The power density required for cutting metals is normally about 10^6–10^7 W/cm^2. In LBC, the laser beam is focused onto the surface of the material to be cut to rapidly heat it up, resulting in melting and/or vaporization, depending on the beam intensity and material properties as shown in Fig. 2.9. The molten metal and/or vapour are then blown away using an assist gas. Different types of assist gases react either positively, neutrally or negatively in chemical reactions during the cutting operation [4, 10 and11]. In LBC the cutting operation can be classified into different categories depending on the mechanisms involved. These mechanisms are described in this review.

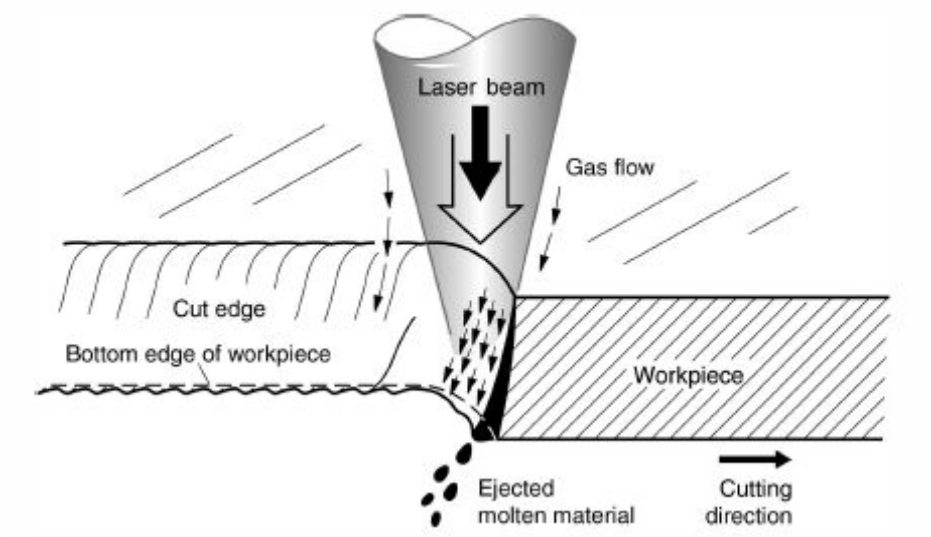

Fig. 2.9: Schematic of the laser cutting process [5].

Lasers can be used effectively to cut metal plates of thicknesses up to about 10 cm. However, the total heat input required for laser cutting is relatively small. This results in a small heat-affected zone size of about 0.1 mm around the cut edge. In addition, the small size of the focused beam results in very narrow kerf sizes, typically about 0.05–1 mm. In fact, the diverging nature of the laser beam results in a slightly tapered cut surface. The workpiece thickness that can be cut with parallel sides is determined by the depth of focus. Plates that are thicker than the depth of focus normally result in tapered surfaces [4 and 10].

By means of LBC both straight and curved cutting of sheet and plate stock in a wide variety of advanced materials can be achieved. Materials include: metals, plastics, rubbers, wood, ceramics and composites. Two types of laser predominate in industrial application for cutting materials at present. These are the CO_2 gas laser and Nd-YAG solid state laser. Most non-metallic materials are cut by CO_2 lasers, due to the fact that they are highly absorptive at the CO_2 wavelength of 10.6 μm. Table 2.2 shows a comparison between CO_2 and Nd-YAG lasers and their capability to cut different materials [4 and 11].

Table 2.2: Summary of processing capability [11].

Material	CO_2 Laser	Nd-YAG laser
Metals		
Mild steel	Excellent	Excellent
Stainless Steel	Excellent	Excellent
Alloy Steel	Excellent	Excellent
Tool Steel	Excellent	Excellent
Aluminium & Aluminium alloys	Fair-good	Good
Copper & Copper alloys	Difficult	Fair
Titanium	Good	Good
Gold & Silver	Poor	Difficult
Non-Metals, Organics		
Plastics (Polymers)	Good- excellent	Poor
Composites	Poor- excellent	Poor-fair
Rubber	Good	Poor
Wood	Excellent	Poor
Paper and Cardboard	Excellent	Poor-good
Leather	Excellent	Poor-good
Synthetic Textiles	Excellent	Poor-good
Non-Metals Inorganic		
Quartz	Good- excellent	Not possible
Glass	Difficult	Not possible
Ceramics	Fair-good	Fair
Stone and Rock	Poor	Poor

2.4.1 Mechanisms of LBC

The cutting process can take place by different mechanisms. The mechanism can be determined for a given combination of material, assist gas and laser. The mechanisms are divided into five different categories: inert gas melt shearing; active gas melt shearing; vaporization; chemical degradation; and scribing. Table 2.3 presents the main cutting mechanisms for the various engineering materials [4 and 8].

2.4.1.1 Inert gas melt-shearing.

Inert gas melt shearing cutting involves melting of the base material, which is then ejected using a high-pressure inert assist gas. In this case the energy for melting is provided entirely by the laser beam. The term fusion or clean cutting is sometimes

used to indicate inert gas assisted cutting. A major problem with this cutting mechanism is the formation of striations (valleys and peaks that run along the thickness) on the cut surface and dross (molten material that sticks to and solidifies on the underside of the cut edge forming a burr on the lower cut edge). However, this type of cutting is more efficient, requiring less energy per unit volume of material removed as compared to the other methods [8 and 10].

Table 2.3: Mechanisms of laser cutting for various engineering materials [8].

Material	Inert gas melt shearing	Active gas melt shearing	Vaporization	Chemical degradation	Scribing
Ferrous alloys	☺	☺	-	-	-
Non-ferrous alloys	☺	☺ (Ti)	-	-	-
Polymers	☺ (Thermoplastics)	☺ (Thermosets)	☺ (PMMA)	☺ (Thermosets)	-
Ceramics	☺	-	-	-	☺
Glasses	☺	-	-	-	☺
Rubber	-	-	-	☺	-
Composites	☺	-	-	☺ (woods)	☺

☺ : Suitable mechanism.

2.4.1.2 Active gas melt-shearing.

Active gas melt shearing cutting process (or sometimes referred to as a gas cutting) involves melting of the base material, which is then ejected using a high-pressure active assist gas. In this case, additional process energy may be generated through an exothermic chemical reaction. As a result, cutting speeds can be increased in comparison with inert gas melt shearing. Ferrous alloys and some thermoset polymers are cut by active gas melt shearing. Temperatures are higher than in the inert gas process, which can lead to edge charring in carbon-based materials, and a poorer edge quality, particularly in thicker metallic sections. The active gas could be O_2 or air. However, air is considered to be active when cutting aluminium but inert when cutting alumina. This cutting mechanism has the same major problems mentioned for the inert gas melt shearing mechanism [8 and 10].

2.4.1.3 Vaporisation

In this case, the material is heated rapidly to its vaporization temperature before extensive melting caused by thermal conduction can occur. Then, the material is removed by vaporization and the ejection of liquid by an inert gas jet normally flows coaxially with the laser beam. PMMA and polyacetal are the common plastics cut using the vaporization mechanism. The cut edge has an extremely high quality and the kerf width is narrow. This form of cutting is limited to thin sections since more energy is required to remove a unit volume of material as compared to melt shear cutting [4and 8].

2.4.1.4 Chemical degradation

In this mechanism, the laser beam modifies the integrity of the material by breaking the chemical bonds. For example, in wood cutting, the large cellulose molecules are reduced to their basic parts of carbon and water vapour. Most thermoset polymers, wood based products, rubber products and epoxy resins are cut by this mechanism. The cut edge produced by this mechanism tends to be flat and smooth; also, its quality is superior to edges produced by mechanical action as it is smooth and splinter free. However, the cut edge produced by this mechanism is covered by a fine layer of residual carbon dust, which may require cleaning [4 and 8].

2.4.1.5 Scribing

In this form of cutting, the structure of the material is weakened by making a groove or line of holes in the material, so that it can be mechanically broken. Sometimes the holes penetrate to the other side of the material, sometimes the holes are not so deep. Low energy, high power density pulses cause vaporization with a small HAZ. This mechanism is used to laser cut alumina, some glasses and composites. Very high processing rates are possible [8 and 9].

2.5 CO_2 Laser Cutting Parameters

The LBC process is a complicated process as it is affected by a large number of parameters. The process parameters can be divided into laser parameters, material parameters and process parameters [8 and 9].

2.5.1 Laser parameters

2.5.1.1 Laser power

Laser power plays an important role in the laser cutting process, as any increase in the laser power will allow the process to be performed at higher cutting speeds and thicker sections can be cut. In practice, lower laser power can lead to partial penetration. The molten material cannot be ejected and the cutting cannot be initiated. On the other hand, if the laser power is too high, this will result in full penetration and a wide kerf of the cut zone, but it causes burning of the cut corners, an increase in dross and poorer cutting quality [8 and 9].

2.5.1.2 Laser beam spatial mode

The beam mode is an indication of how the energy is distributed over the beam cross-section as shown in Fig. 2.10. In LBC the laser beam mode that has the fundamental Gaussian distribution gives the smallest focused spot, the highest power density and the largest depth of focus as compared with other beam modes. This reduces the kerf width, and increases both the cutting speeds and the thicknesses of materials which can be cut. The higher order or multimode beams shown in Fig. 2.10 are more spread out and result in larger focal spot sizes and lower power densities [8 and 9].

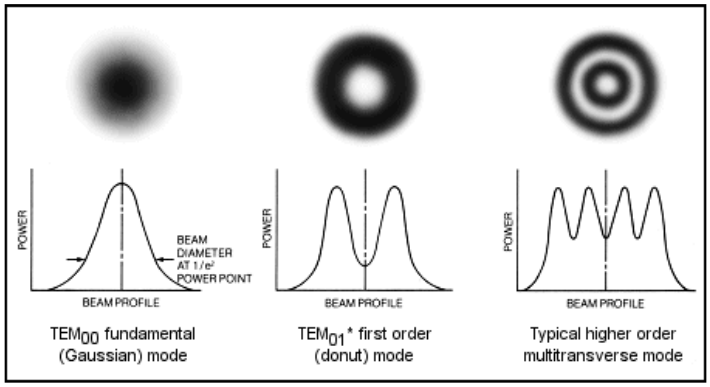

Fig. 2.10: Some types laser beam modes.

2.5.1.3 Laser beam temporal mode

Both continuous wave (CW) and pulsed laser beams are commonly used in laser cutting, however, the CW is normally used. A CW laser beam is often chosen for

smooth cutting in mass-production, especially with thicker sections. A lower energy pulsed laser beam is usually selected for precision cutting of fine components [8].

2.5.1.4 Wavelength

The way in which the materials absorb the laser beam can be highly dependent on the beam wavelength. Therefore, certain lasers will be more suitable for cutting certain classes of materials. Aluminium and copper have low absorption characteristics at the CO_2 wavelength. Therefore, to laser cut these metals, either a high power laser or one with a different wavelength must be used. However, most non-metallic materials and steels are cut by CO_2 laser, due to the fact that they are highly absorptive at the CO_2 wavelength of 10.6 μm [4 and 6].

2.5.1.5 Polarization

In a polarized beam the magnetic and electrical vectors of the photons are aligned parallel to each other. This alignment of vectors indicates that the light beam, as a whole, has highly directional properties [4]. The effect of the orientation of a linearly polarized beam on the cut quality is illustrated schematically in Fig. 2.11. As the figure shows, when the beam is polarized in the cutting direction, the resulting cut may have a narrow kerf with sharp, straight edges. However, as the plane of polarization is oriented away from the cutting direction, the energy absorption decreases. As a result, the cutting speed is reduced, the kerf becomes wider, and the edges rougher and not square to the material's surface.

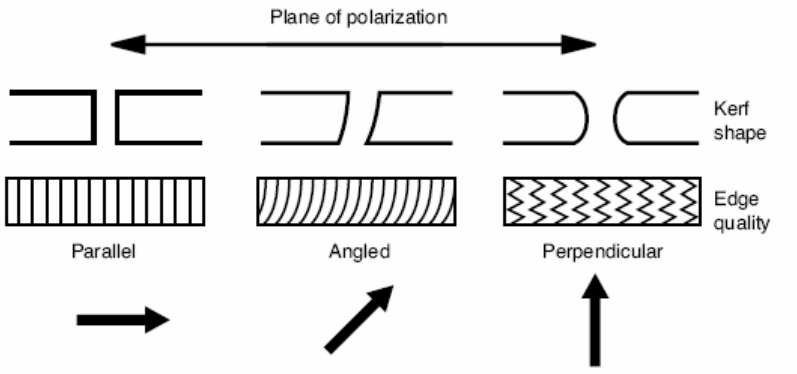

Fig. 2.11: Effect of plane-polarized laser orientation on cut quality [10].

2.5.2 Material parameters

2.5.2.1 Thermal proprieties

Generally speaking, materials can be classified into two groups, metals and non-metals. Metals normally have high thermal conductivity, high melting temperature and optical reflectivity. As a result, metals are more difficult to cut by laser than non-metals, as they required high laser power density and low cutting speeds to raise their temperature to that required for melting. However, as the cutting speed is reduced, instabilities occur that can result in abnormal molten regions and poor edge quality [8].

2.5.2.2 Reflectivity

The reflectivity or absorption of a material is an important parameter in LBC. The reflectivity of any metal is affected by several factors as follows: As the wavelength of the laser becomes shorter the reflectivity decreases and the absorptivity of the surface increases. Also, most metals, which are characterized by a high electric conductivity such as Al and Cu, have extremely high reflectivities (about 98%) for the CO_2 laser. However, the reflectivity will decrease markedly with a rise in the temperature of the metal. In addition, as the reflectivity is a surface phenomenon, so surface films may have a large effect on it. Fig. 2.12 shows the variation in the absorption for CO_2 radiation caused by a surface oxide film. The reflectivity of a workpiece also depends on the polarization and on the angle of incidence as shown in Fig. 2.13. The reflectivity can be significantly reduced (nearly 80% absorption is achieved) if the polarization is parallel to the cut with a CO_2 laser working on steel.

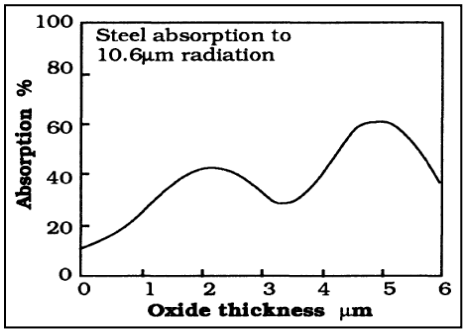

Fig. 2.12: Absorption as a function of thickness of an oxide film on steel for 1.06 μm radiation [9].

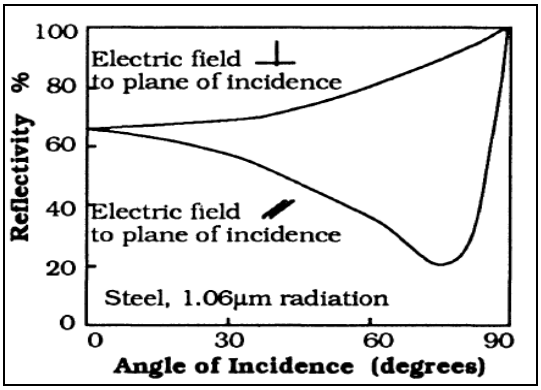

Fig. 2.13: Reflectivity of steel to polarized 1.06 μm radiation [9].

2.5.3 Process Parameters

When the laser type and the material to be cut are known, many of the above parameters are identified and under control. However, there are still parameters that have to be controlled in order to obtain the desirable high quality cut. These parameters are the process parameters.

2.5.3.1 Cutting speed

In industry, LBC is widely used due to the fact that the cutting process can be performed with very high rates. For a given laser power the cutting speed must decrease with increasing thickness of the workpiece as shown in Fig. 2.14. For the laser power indicated in Fig. 2.14, the curve illustrates the maximum cutting speed that can be applied for the successful cutting of a given thickness. If the cutting speed is above this curve the laser does not penetrate through the thickness of the material. Below this curve the extra heat destroys the cut edge [10].

2.5.3.2 Assist gas

The use of an assist gas in LBC has four major functions which affect the cutting efficiency; ejection of molten metal, protection of the lens from back splatter, cooling the cut edge and an additional heat source due to an exothermic reaction in case where an active gas is used. However, when using an active gas such as O_2 to assist the cutting process an oxide layer is deposited on the cut surface, which may need cleaning. On the other hand, the use of inert gases or nitrogen eliminates the formation of the

oxide layer. Yet, this may significantly reduce the cutting speed. In some cases, the pressure of the assist gas has a role in reducing the formation of the dross and restricting the width of the HAZ. The higher the pressure of the assist gas, the smaller the dross formation and the smaller the HAZ. The purity of the assist gas also affects the cutting performance. A small amount of impurity can either reduce the maximum cutting speed or increase the dross formation. Different types of gases are in use in LBC. N_2 is the most common inert gas used, because it is relatively inexpensive. N_2 is usually used when cutting stainless steel and nickel-based alloys. Argon is a common choice when cutting titanium and its alloys, to prevent the formation of titanium oxides or brittle titanium nitrides. O_2 is used for cutting mild steel and stainless steels when a high cutting speed is necessary, with edge quality and discoloration of secondary importance. Helium is also used when a very high quality cut is essential. Finally, compressed air is normally utilized in LBC when cutting aluminium, polymers, wood, composites, alumina and glass because it is easily available [4, 8 and 10].

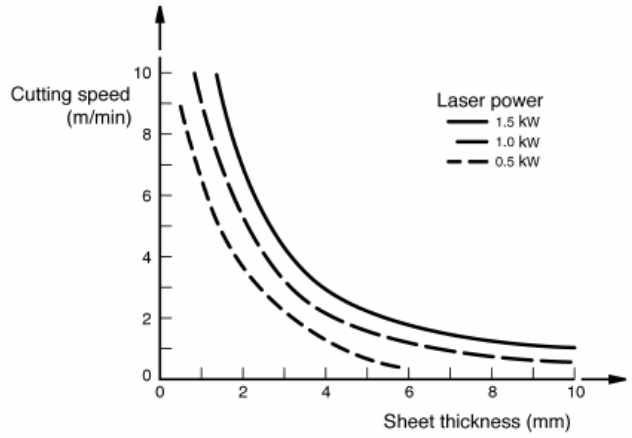

Fig. 2.14: Variation of cutting speed with workpiece thickness in oxygen-assisted laser cutting of steel [10].

2.5.3.3 Nozzle shape

The nozzle has three main roles: to guide the gas coaxially with the laser beam, to reduce the pressure around the lens to minimise lens movement and

misalignment and to minimise turbulence in the met pool by stabilizing the pressure on the workpiece surface. In LBC, the design of the nozzle and its orifice determines the shape of the cutting gas jet which significantly affects the quality of the cut. The diameter of the nozzle orifice ranges between 0.8 and 3 mm, depending on the material and the workpiece thickness. A nozzle with a small diameter creates difficulties in alignment and localizes the gas, resulting in a rough edge. On the other hand, a nozzle with large diameter supplies insufficient gas flow to eject molten material, and results in high gas consumption. The alignment of the nozzle with the laser beam has a significant effect on the quality of the cut. Misalignment causes gas to flow across the top of the cut zone, which can lead to undesirable burning of the cut edge, and a poor quality cut. The different nozzle designs which are commonly used in industry for coaxial application of gas jet during LBC are presented in Fig. 2.15. In fact, no single nozzle design is superior in all applications [8 and 10].

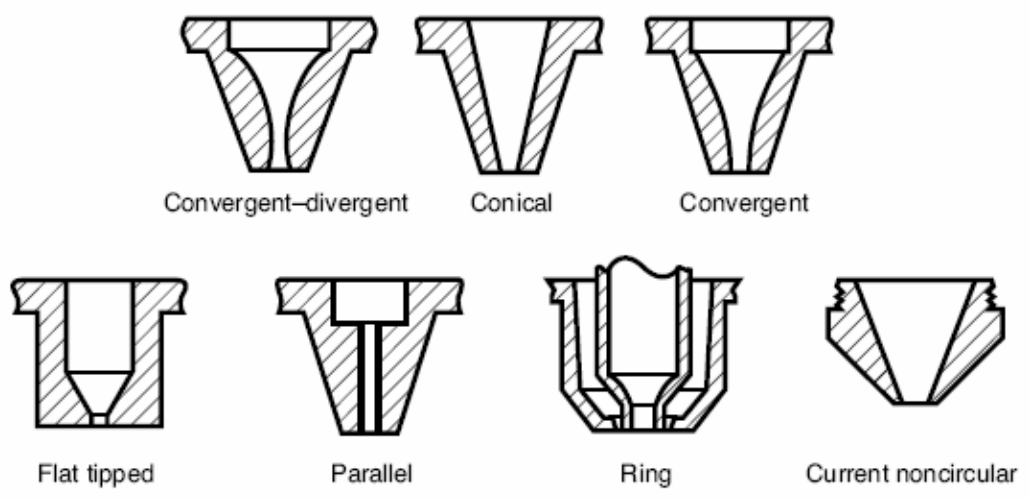

Fig. 2.15: Nozzle designs for laser cutting [10].

2.5.3.4 Stand-off distance

The distance between the nozzle and the workpiece surface is call the stand-off distance. This distance affects the flow patterns of the assist gas. The stand-off distance is normally selected between 0.5 and 1.5mm to minimise turbulence. A short

stand-off distance gives stable cutting conditions, although the risk of damage to the lens from spatter is increased [8].

2.5.3.5 Focal plane position and focal length

The laser beam beyond the focal plane is normally divergent as shown in Fig. 2.16. For that reason, it is vital to monitor the position of the focal plane with respect to the workpiece surface, to obtain a straight kerf (i.e. a non-tapered cut surface). Another reason to have consistency in the location of focal plane (i.e. focal position) is that the maximum power density is achieved at the minimum spot diameter for a given output power.

In fact, the spot diameter at the focal plane and depth of focus (DOF) shown in Fig. 2.16 are defined by: beam diameter before focusing, beam wavelength and the focal length of the focusing lens. For a TEM_{00} CO_2 laser beam of diameter 15 mm and a 127mm focal length lens produces a spot diameter of about 0.15 mm, with a DOF around 1mm. If the DOF is too small, there may be a difficulty in fitting a thicker workpiece within the DOF limits. On the other hand, increasing the DOF, by replacing the lens with one which has larger focal length, will increase the spot diameter and decrease the power density.

Therefore, to cut thicker sections it is preferable to use a focusing lens with a longer focal length, because the DOF should be around half of the section thickness to avoid a tapered cut surface. For thin sections (less than 4 mm) a lens with a shorter focal length is recommended. This should lead to a narrower kerf and smoother cut edge, as a result of the small spot size [8 and 9].

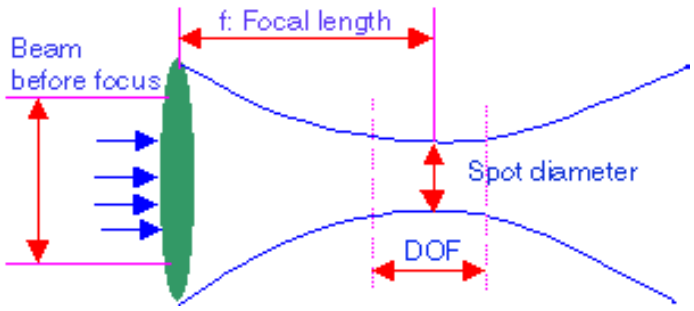

Fig. 2.16: Spot diameter and depth of focus for laser beam [12].

2.5.4 Effect of some process parameters on the cut performance

This is a summary of the preceding sections. The effect of the process parameters on the cut performance for metals may vary when the parameter is set too high or too low. Table 2.4 presents this variation between the low level and high level of some process parameters on the cut performance.

Table 2.4: Cut performance vs. process parameters for metals [11].

Process parameter	Cut performance	
	Too High	**Too Low**
Laser power	Kerf increases, recast & dross increase, wavy striations	Kerf decreases, loss of cut
Cutting speed	Kerf decreases, Loss of cut Increased surface roughness, wavy striations	Kerf increases Recast & dross increase, Increased taper
Focus position	Kerf increases, Recast & dross increase Deep striations, Loss of cut	Kerf increases Recast & dross increase, Loss of cut
Assist gas pressure	Prominent striations Erosion at bottom of cut, Excessive burning	Dross, Inadequate ejection Partly closed kerf
Stand-off distance	Dross	Prominent striations
Nozzle diameter	Dross & high gas consumption	Centring critical* Inadequate ejection & Partly closed kerf

* Focused beam not centred with nozzle orifice yields dross on one side and clean on the other.

2.6 Characteristics of Laser Cut Edge

The quality of the cut is determined by its quality features such as kerf width, cut edge roughness, cut edge squareness, dross and width of HAZ. The quality features of the cut depend on the setting of the process parameters. These quality features (sometimes called quality characteristics) will be discussed in the following section.

2.6.1 Kerf

The kerf is the gap that is formed during through-thickness cutting as presented in Fig. 2.17a. Normally, it is defined as the width of the bottom of the cut and it is slightly larger than the spot diameter in optimised laser cutting. One of the requirements of

having a high quality cut is achieved when the kerf width is as small as possible [8]. In the current research, three quality features for kerf width are considered: upper kerf, lower kerf and the ratio between the upper kerf and the lower kerf.

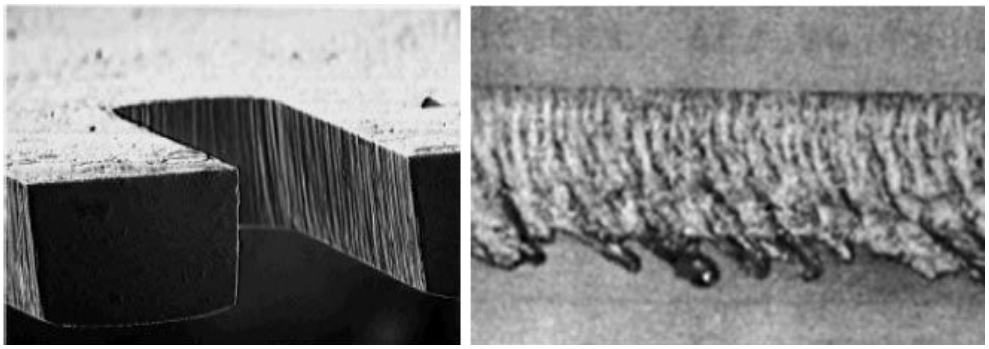

(a) (b)

Fig. 2.17: Cut edge quality features [10].

2.6.2 Striations and surface roughness

Striation is a common characteristic of the surfaces generated by LBC. The surfaces cut using a laser beam normally have a nearly periodic striation pattern, as shown in Fig. 2.17b, which results in a rough surface. The formation of the striations could be caused by: vibrations in the equipment, fluctuations in the laser power, fluctuations in the gas flow and hydrodynamics of the molten metal flow [10]. In order to achieve optimised laser cutting the striation has to be minimised and this produces minimum surface roughness.

2.6.3 Dross

After laser cutting, material which sticks to the lower edge of the workpiece is called dross, and appears as solidified drops as illustrated in Fig. 2.17b. The dross could be either solidified material in the case where the inert gas is used as the assist gas, or a solidified oxide if O_2 is used as the assist gas. The formation of dross depends on the surface tension and viscosity of the molten material. Materials that have a high surface tension or viscosity tend to form more dross. Inert gas-assisted cutting has a greater tendency to form dross when compared to oxygen-assisted cutting of the same material,

since the surface tension of the pure metal is generally greater than that of its oxide. Furthermore, the dross formed during inert gas assisted cutting is usually more difficult to remove than the more brittle oxide dross formed when oxygen is used as an assist gas. Dross can be removed by using a gas jet directed towards the underside of the workpiece, or it is removed mechanically after cutting [4, 8 and 10].

2.6.4 Cut edge squareness

As mentioned earlier the laser beam can be either converging or diverging, and, if so, this can result in a tapered cut edge as demonstrated in Fig. 2.17a. In order to obtain square cut edge it is recommended that the focal plane position and the other process parameters should be adjusted in order to achieve the same widths for the upper kerf and lower kerf. In other words, the ratio between the two kerfs should be approximately 1.

2.6.5 Heat-affect zone

In LBC, the HAZ is produced because of the high localized heat and it is limited to a small area near the cutting zone. The HAZ width increases as the energy input per unit length and cut thickness increases. The HAZ width is important if cuts are to be made near heat-sensitive components. However, it is not normally included in a quality assessment of the laser cut [8].

2.7 Process Economics

In contrast with other processes, laser processing often requires a large investment as shown in Fig. 2.18. However, the productivity, and cut quality available from present industrial laser cutting systems allows the process to offer economical cutting. The total cost of any process including LBC can be divided into two terms which are the fixed and the variable costs. The fixed costs consist of: capital investment (equipment costs), employees' salaries, maintenance (fixed agreement), insurance etc. The variable costs are the running costs related to the process including: lasing gases, lens and mirrors, electrical consumption, chiller additives, assist gas, preventive maintenance and the cost of spares or services consumed during the processing [8]. Therefore, it is important to

estimate the variable cost (or operating cost) for LBC for each cutting condition in order to contrast between the different cutting conditions and to find out the optimal cutting from a cost viewpoint.

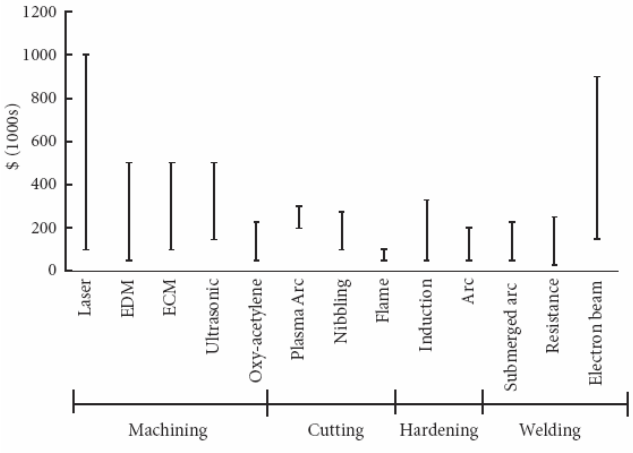

Fig. 2.18: Capital costs of various processes [8].

2.8 Process Hazards and Safety

The basic hazards to humans associated with laser processing concern damage to the eyes, skin and respiratory system. Firstly, the basic hazard of the laser light to the eye is the absorption of the focused laser light which will cause damage to the eye tissue. Secondly, the radiation from high power infrared lasers can cause skin burns, which may result in erythematic, skin cancer etc. Thirdly, there is a hazard of inhaling small particles if these particles go into the respiratory system, and thus cause a health risk when absorbed into the bloodstream. Also, some materials can produce toxic vapours, which can be dangerous for human.

It is essential that operators know the requirements for the safe use of lasers, and that a laser safety officer ensures that those requirements are fulfilled. The fundamental safety procedures are: (i) that only trained authorized technicians may operate lasers, (ii) that protective eye glasses must be always worn, (iii) that laser protective housing must be used and (iv) that no one should work alone on a laser machine. However, the explanations and recommendations given in this section are general guidelines only. For more details one can refer to standards [8].

2.9 Comparison of Laser Cutting with Conventional methods

Both the technical and economical features of each process have to be considered to facilitate a comparison between laser cutting and some other traditional cutting methods. Normally, if the desirable cut quality can be achieved by using several processes, then the process with the lowest cost is selected. In the same way, if the cost of using different processes is similar, then the process which provides the highest quality is the preferred option. However, it is worth remembering that laser cutting may provide a unique solution to a manufacturing requirement that cannot be met by competing methods. The technical characteristics of cuts made using the principal techniques are shown in Fig. 2.19. On the other hand, the capital cost of laser cutting is very high as shown in Fig. 20. The laser cutting process is the ideal alternative in many applications for example: cutting a complex profile, cutting a square edge with high accuracy in both thick and thin materials, cutting the same part in very large quantities (i.e. mass production) or cutting both soft and hard-to-cut materials such as paper or diamond.

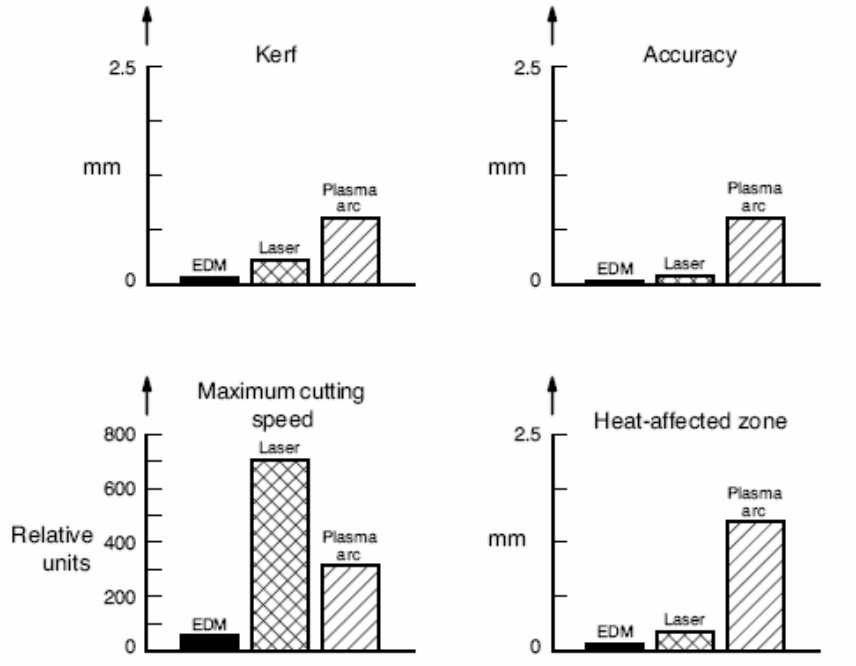

Fig. 2.19: Comparison of electrical discharge machining (EDM), laser cutting, and plasma arc cutting processes [10].

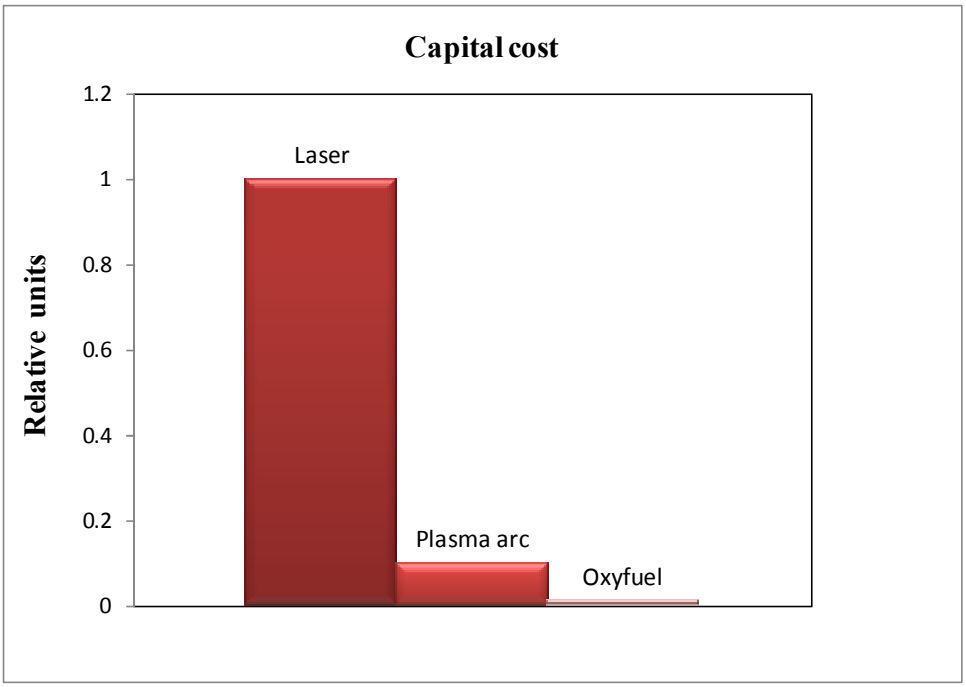

Fig. 2.20: Capital cost of some thermal cutting processes [8].

2.10 Review on Laser Cutting of Different Materials

LBC has wide applications in industry for cutting different materials. In the next sections investigations carried out by other researchers on laser cutting for some engineering materials will be reviewed in terms of the effect of the process parameters on the end product quality, and then modelling of the process, with the aim of predicting the quality features of the end product, or for optimisation purpose.

2.10.1 Laser cutting of metals

Laser cutting of metals including steels and stainless steels has been the main aim of many investigations since steel and its alloys are in massive demand in many industries such as automobile and power plant industries. The nature of the LBC process, and the effect of process parameters on the quality of the cut sections were studied by many researchers.

Uslan [13] has utilized CO_2 lasers to cut high-strength low alloy steel and to investigate the influence of laser power and cutting speed variations on the kerf width size. It was found that increasing the laser power intensity increases the kerf width size and this is more pronounced when the cutting speed is reduced. It was reported that a small variation in laser power results in a large variation in the kerf size. He reported that the influence of the cutting speed was less than that corresponding to the laser power. Also, he mentioned that when using an unfocused laser beam, which in turn reduces the laser power density, the kerf width increases.

Gonsalves et al. [14] have investigated the interdependence of the laser parameters on the cut width when cutting thin sheet of 302 stainless steels. It was demonstrated that the cut width decreases with increasing cutting speed. Also, they verified that only some of the available power is utilized.

The effect of process parameters on the kerf width during CO_2 laser cutting has also been studied by Yilbas [15]. It was found that increasing the laser power and the energy coupling factor increases the kerf width size. It was reported that even slight variations in laser power, cutting speed and energy coupling factor modify the kerf size remarkably. It was mentioned that at low cutting speed and high laser power, increasing the energy coupling factor increases the kerf width as a result of increasing the size of the melt zone in the kerf. On the other hand, any increase in the cutting speed reduces the kerf width. However when the cutting speed decreases, then the rate of energy available at the surface increases and this in turn, increases both the melt size and the striation size. He reported that laser power has a highly significant effect on the kerf size.

A theoretical model has been derived by Chen [16] to investigate the effect of the manufacturing parameters on the three-dimensional cutting front and cut kerf cross-section using a CW CO_2 laser working on mild steel. He analysed the effects of oxide files, polarization, cut front shape, cutting speed and laser power. It was reported that very small levels of impurity in the oxygen would significantly affect the cutting performance. Also, it was mentioned that the kerf width was significantly decreased from 1.86 to 1.66 mm and the maximum kerf depth was considerably reduced from

73.91 to 34.73 mm when laser power decreased from 1500 to 750 W. Moreover, he stated that a higher laser power makes the cut kerf larger and the cut-through performance better. In addition to that he found that the kerf width produced using pure oxygen is larger when compared with the kerf produced using an inert gas. Finally, he reported that the tendency of the experimental results of many previous researchers agrees with the predictions of his theoretical model.

Yilbas [17] has also presented a study to examine the effect of laser cutting parameters on cutting quality when cutting mild steel. The parameters he investigated were workpiece thickness, assist gas pressure, cutting speed and laser power. He extended the study by monitoring the surface plasma, which in turn affects the formation of striations and cutting quality. It was concluded that self-burning occurs at very low cutting speed and increases with increasing oxygen pressure. Also he reported that once the jet velocity reaches sonic velocity, the critical cutting speed drops due to the cooling effect of the jet. Furthermore, it was found that at high oxygen pressure a substantial amount of surface plasma occurs, which in turn may partially block the incident laser beam, resulting in less energy from the laser beam reaching the surface. This plasma then expands due to the pressure differential in the plasma. As a result, more incident energy reaches the surface, which in turn increases the removal rate of molten metal from the kerf, causing more surface plasma. This process occurs periodically and leads to the development of strias around the kerf edge.

Yilbas et al. [18] have conducted a study to assess cut edge quality in terms of waviness and flatness of stainless steel with different thicknesses. They considered cutting speed, oxygen pressure and workpiece thickness as working parameters. They extended the study to detect the light emission from surface plasma. It was found that the cut quality is mainly affected by the oxygen pressure and cutting speed. However, they reported that flatness depends significantly on the thickness. Also, they reported that as the oxygen gas pressure increases the waviness increases.

Evaluating the optimum laser cutting parameters for cutting samples of austenitic stainless steel with a thickness of 1.2 mm, has been investigated by Abdel Ghany and Newishy [19]. It was shown that all the process input parameters have an effect on the

cut quality. They reported that the optimal cutting conditions are: power 210 W, frequency from 200 to 250 Hz, speed 1.5 m/min, focus position from -1 to -0.5, nitrogen pressure from 9 to 11 bar and oxygen pressure from 2 to 4 bar. It was found that increasing the frequency and cutting speed cases a decrease in the kerf width and the roughness of the cut surface, while increasing the power and gas pressure increase the kerf width and roughness. It was mentioned that when nitrogen is used as an assist gas, it produces brighter and smoother cut surfaces with smaller kerf. It was reported that when using the CW mode, the cutting speed could be increased to 8 m/min with the same power and gas pressure setting mentioned above.

The effect of high-pressure assistant-gas on CO_2 laser cutting of 3 mm thick mild steel samples has been investigated by Chen [20]. It was shown that an acceptable quality cutting region does not exist for pure oxygen at a pressure of 10 bar, with power ranging from 0.6 to 1.4 kW and cutting speeds from 40 to 120 mm/s. It was recorded that for inert-gas cutting, dross was formed under the cut kerf with most of the cutting parameters. However it was found that a clean cut was obtained with an argon gas pressure of 10 bar, at a cutting speed of 25 mm/s. Also, he advised that for this metal oxygen cutting is still the best, although argon and nitrogen may be used instead. Finally, it was mentioned that compressed air is inferior to these gases as an assistant gas. However, the cut surface roughness of 28 μm is better than that of pure oxygen of 110 μm and poorer than that of argon of 14 μm.

Assessments of laser cutting quality and thermal efficiency analysis have been carried out by Yilbas [21]. A statistical method based on factorial analysis was introduced to identify the effect of cutting parameters on the resulting cut quality. It was found that increasing laser beam scanning speed (the cutting speed) reduces the kerf width, while the kerf width increases with increasing laser power. It was reported that the main effects of all the parameters employed have a significant influence on the cut quality.

Hamoudi [22] has studied the effect of cutting speed and assist gas type and pressure, on kerf width, striation frequency and heat-affected zone in mild and stainless steels. It was reported that for exothermic cutting, a wide kerf size was associated with

high roughness and large HAZ, while a narrow kerf occurred with a smooth cut and a small HAZ. It was found that the kerf width and the HAZ decrease with increasing cutting speed but increase with increasing gas pressure. It was mentioned that exothermic cutting of stainless steel produced smaller roughness values as compared with the roughness of fusion cutting.

Sheng and Joshi [23] have performed a numerical study on the development of the heat-affected zone during the laser cutting of 304 stainless steel. This numerical model was validated using laser cutting experiments which revealed good agreement. It was concluded that this model is useful as a process planning aid for laser cutting to determine the process parameters that will optimise the material removal rate, the HAZ and the kerf taper.

Dilthey et al. [24] have investigated the laser cutting of steel and stainless steel. The results they achieved have revealed that both mild steel up to a thickness of 12 mm can be cut to an excellent quality and stainless up to a thickness of 6 mm can be cut to a good quality using TEM_{00} up to 1.5 kW. It was mentioned that when cutting stainless steel, it is essential to be able to make exact adjustments of both focus position and gas jet in order to obtain dross free cutting. Also, they reported that corrosion is likely to occur when cutting stainless steel with oxygen or vice versa when cutting stainless steel using inert gas.

Cadorette and Walker [25] have investigated laser cutting using new laser equipment in an operational manufacturing environment to explore the conditions under which the equipment performance could be improved. It was concluded that cut quality highly sensitive to changes in the input variables-particularly O_2 purity.

Wang and Wong [26] have studied the laser cutting of sheet steels coated with zinc and aluminium with thickness ranging from 0.55 to 1 mm. It was shown that by proper control of the cutting parameters good-quality cuts are possible at a high cutting speed of 5000 mm/min. It was revealed that high laser power above 500 W results in a poor-quality cut. They reported that the kerf width generally increases with increasing gas pressure and laser power, and with a decrease in cutting speed. They recommended a method of setting the parameters to control and optimise the process.

Pietro and Yao [27] have conducted an investigation into characterizing and optimizing laser cutting quality. Their aim was to investigate and review the current status of laser cutting and associated quality techniques, including research efforts undertaken in the fields of modelling, regulation, diagnosis and monitoring. They defined the quality of the laser cut in terms of: kerf width, cut edge squareness, inner side slope of the kerf, HAZ extent, dross appearance and surface roughness (striations). It was reported that the arithmetic average roughness parameter R_a was a reliable parameter for characterizing the profile. Also, it was mentioned that a roughness profile can be measured when a complete cut surface is produced. It was reported that the measurements of R_a can only be recorded soon after performing the cut.

The combined effects of laser power and cutting speed on kerf width, surface roughness, striation and size of HAZ of 4130 steel have been studied by Rajaram et al. [28]. It was observed that the laser power had a major effect on the kerf width and size of HAZ, while the cutting speed effects were secondary. It was shown that the cutting speed had a major role in determining the surface roughness and striation frequency. It was reported that a low laser power leads to a smaller kerf width and HAZ, while a low cutting speed gives a small surface roughness and a low striation frequency.

The quality of the final part is an essential issue in industry. It depends on many factors. However, in laser cutting the surface roughness and the striation patterns are of particular importance. It is well know that surface roughness affects the fatigue life and the corrosion of the manufactured part. Therefore, investigating the laser process input parameters and their effect on these surface features is essential. The pattern of periodic lines appearing on the cut surface is known as striation. It affects the surface roughness, appearance and geometry precision of laser cut products. Over the last three decades, many investigations have been carried out to understand the mechanism involved in striation formation and to optimise the laser cutting process by minimizing the striations.

Yilbas [29] has conducted an investigation to understand the striation formation mechanism and its relationship with the process parameters. It was found that the mathematical model which he introduced, represents the physical phenomena well and the prediction of the striation frequency, and striation width agrees with the experimental

findings. It was reported that sideways burning, liquid layer oscillation at the surface and variation in the absorbed power due to surface plasma are the main reasons for the striation.

Li et al. [30] have reported an investigation into achieving striation-free laser cutting of 2 mm thick EN43 mild steel. A 1 kW single mode fibre laser was used in this work. They proposed a theoretical model to predict the cutting speed at which striation-free cutting occurs. It was indicated that above the critical speed of 33 mm/s striation occurs and the surface roughness increases.

Prasad et al. [31] have discussed the laser beam machining of metallic coated steels with the goal of determining the process parameters which have an influence on the outcome of the cutting process. It was found that oxygen is quite effective as an assist gas for cutting coated steels. However, localised overheating and oxidised edges were observed in the case of GALVABOND specimens. This could be eliminated by using nitrogen or helium as an assist gas. It was proven that cutting speed is a function of the input power and that laser processing of these materials is a commercially possible option.

A theoretical work has been undertaken by Simon and Gratzke [32] for the purpose of investigating the instabilities in laser gas cutting. It was suggested that these instabilities could be causes of the formation of striations.

The effects of gas composition on the CO_2 laser cutting of mild steel has been addressed by Chen [33]. It was found that a high purity of oxygen is required for high-performance CO_2 laser cutting of mild steel as only a tiny oxygen impurity of 1.25% will reduce the cutting speed by 50%. He reported that for 3 mm thick mild steel a good-quality cut was obtained using inert gas with a low pressure (up to 6 bar). It was stated that a good-quality cut would be achieved when cutting 3 mm thick mild steel using pure oxygen with pressure ranged between 0.75 and 2.0 bar, a laser power of 1500 W and cutting speed ranged from 20 to 40 mm/s. It was reported that the energy density at the bottom of the workpiece is decreased by a ratio of $½^{.44}$, so that the total input energy may not be sufficient to vaporize the material in the lower part of the cut front within a very short time, although it is sufficient to melt the material. If the pressure of the

assistant gas is not enough to quickly blow away the viscous molten material, the high temperature molten material (adhering to the cut surface) continues its oxidation reaction (or burning). This makes the cut surface more irregular, the undercut angle not very sharp and striation on the cut face more curved. In inert gas cutting, the reduction of energy intensity between the top and the bottom of the sample may also have a large affect on the cutting performance (surface roughness, dross adhesion and maximum cutting speed). Therefore, the striation on the upper part of the cut surface is more flat than on the lower part of the cut surface. Therefore, the surface roughness of the upper part is normally smaller.

Atansov [34] has performed an experimental and theoretical investigation of high-pressure nitrogen assisted CO_2 laser cutting of Aluminium and stainless steel. It was found that the quality of the cut improved significantly with this combination. He recommended this approach for cutting of Al-alloys and stainless steels with thickness less than 5 mm when the cut quality is of particular importance.

Grum and Auljan [35] have investigated the heat effects in the cutting front and its surroundings when cutting both low carbon steel and stainless steel by monitoring the heating phenomena in the specimen material. It was mentioned that the amount of energy input transferred to the cutting front varies due to oscillations in the laser source, changes in the heat released in exothermic reactions and heat losses. The theoretical calculation they made indicates that with a cutting speed of 30 mm/s, power oscillation frequency of the laser source of 300 Hz produces 10 striations per millimetre. They confirmed this theoretical calculation by experimentally measuring the striation widths at the cut surface of low carbon steel. It was assumed that the alloying elements in the stainless steel, especially the chromium, have an influence on the oscillation frequency and therefore on the striation widths at the cut surface.

Duan et al. [36] have analysed the effects of laser cutting process parameters on cut kerf quality. It was confirmed that the theoretical predictions could be verified by practical experiments. It was found that the flow field depends strongly on the geometrical shape of the cutting front, which is affected by other laser parameters such as: laser power, cutting speed, focal position etc. It was mentioned that an increase in the

nozzle to cut kerf displacement is beneficial in reducing the gas consumption. Finally, it was concluded that the mathematical model can be used to build up an optimal group of cutting parameters in order to obtain a high-quality cut edge.

CO_2 laser cutting of Incoloy 800 HT alloy has been studied by Yilbas and Rashid [37]. They monitored the dross ejection from the kerf. The frequency of the dross ejection correlated with the striation frequency and out of flatness. Also, a statistical analysis was conducted to determine the significance levels of cutting speed, laser output intensity, thickness and pulse frequency. It was found that the dross ejection frequency is directly related to the striation frequency. They reported that the overall quality of the cut edge improves within at a pulse frequency of 600 Hz and the rate of dross ejection from the kerf becomes almost steady at this frequency. It was mentioned that the cutting speed and thickness have a significant effect on the out of flatness. They indicate that the cut quality can be improved by varying the combination of pulse frequency and laser output intensity.

Dross formation during CO_2 laser cutting has been studied by Yilbas and Abdul Aleem [38]. It was found that the liquid layer thickness increases with increasing laser power and reduces with increasing assisting gas velocity. It was mentioned that the droplet formed is spherical and the predicted droplet sizes agree well with the experimental results. It was concluded that compounds are formed in the droplets and that the main compound formed in the droplet is FeO. This is due to high temperature oxidation reactions.

The surface roughness of CO_2 laser cutting of mild steel sheets has been investigated by Radovanovic and Dasic [39]. It was observed that the cut surface has two zones, the upper zone in the area where the laser beam enters the sample, the lower one in the area where laser beam leaves the sample. The lower zone has a rougher surface. It was reported that the surface roughness increases with increasing the sheet thickness, but decreases with increasing laser power.

An investigation into the effect of laser cutting operating parameters on surface quality of mild steel has been carried out by Neimeyer et al. [40]. It was indicated that the average surface roughness may be best at high cutting speed and low assist gas

pressure. They confirmed that the workpiece thickness had little effect on the cut surface quality. It was concluded that the profiles of the cut surface of the top and bottom edges yield the same values for average surface roughness, despite the significant visual difference in the striation pattern. The same observation of two striation patterns was reported by Schuocker [41] and Lee et al. [42]. They observed a regular pattern near the upper surface and a less regular pattern nearer the lower surface as show in Fig. 2.19 below.

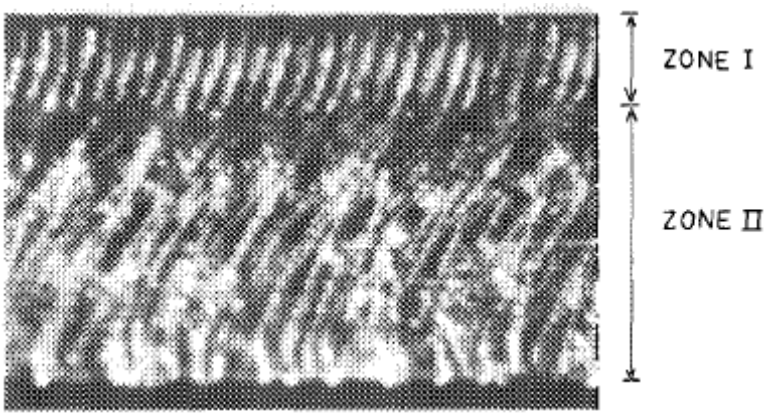

Fig. 2.21: Micrograph showing the two zones of striation patterns.

CO_2 laser cutting of wedge surfaces and normal surfaces of mild steel has been considered by Yilbas et al. [43]. They assessed the end product quality using the international standards for thermal cutting. The cut surfaces were examined by optical microscopy and geometric features of the cut edges such as out of flatness and dross height were measured from the micrographs. It was found that the dross height and out of flatness are influenced significantly by the laser output power, particularly for the wedge-cutting situation. Moreover, the cut quality improves at a certain value of the laser power intensity.

CO_2 laser cutting of advanced high strength steels has been reported by Lamikiz et al. [44]. They considered the influence of the material and, more importantly, the effect of coating on the quality of the cut. It was demonstrated that there were very different behaviours between the thinnest and thickest sheets. However, the variation in the

cutting parameters due to the influence of the material was less significant. They succeeded in determining the optimum cutting conditions. It was mentioned that if a high speed of 8000 mm/min is required, the power should be increased to 300 W. Finally, it was found that the best position for the laser beam is underneath the sheet.

The effect of beam waist position and material thickness on the kerf size and striation formation of steel sheets has been considered by Karatas et al. [45]. They modelled the kerf width using group parameters analysis. It was found that the beam waist position has a significant effect on the kerf size especially when the thickness is small. They reported that the minimum kerf width could be achieved for a thicker workpiece when the beam waist position is moved below the surface of the workpiece. It was confirmed that the predictions of kerf width agree well with the experimental data. It was observed that (no specific striation patterns except) the stria width and depth increase with increasing workpiece thickness.

The laser micro-processing of a metallic stent (i.e. artificial tube) for medical therapy made from SS316L has been investigated by Kathuria [46]. He described the fabrication of a metallic stent of length 20 mm and diameter of 2.0 mm with from a tube thickness of 0.1 mm. He discussed some characteristics such as HAZ and dross. It was found that the desirable taper and quality could be achieved using a laser short pulses with a high pulse repetition rate.

The correct choice of laser cutting parameters is essential in order to minimise the quantity of the heat transferred to a part during the cutting operation. In this way, the part will be cut with the smallest amount of thermal damage. The magnitude of the heat input (contribution of heat) depends on the cutting power and speed. Therefore, the cutting speed should be maximised and the power minimised in order to minimise the thermal damage.

Lamikiz et al. [47] have also investigated the laser cutting of a different series of advanced high-strength steels. They studied the influence of the laser cutting parameters on different metallurgical characteristics. It was found that good-quality cuts for sheet thicknesses of 0.7 and 0.8 mm were achieved using a large range of cutting speeds

between 2000 and 7000 mm/min. It was reported that a level of power of 200 W was sufficient to working at a speed of 4000 mm/min and 300 W for speed of 8000 mm/min. It was mentioned that a gas pressure of 6 bar was sufficient for all speeds mention above. They found that if the sheet thickness was more than 1 mm, good-quality cuts were achieved by using a speed of 3000 mm/min, a power of 300 W and O_2 pressure of 4 bar. They recommended that the O_2 flow should be reduced as the thickness increases to ensure that the exothermic reaction is not too aggressive and does not damage the cut area. Finally, they indicated that the optimal focal position should be near the under-surface of the sheet.

2.10.2 Laser cutting of plastics and its composites

It is well know that laser cutting machines have valuable applications in many industries. One of these industries is the plastic industry where lasers are utilized to cut and make engraving in plastics and acrylics with a high degree of precision and to make complex shapes with a superior cut quality. As mentioned earlier because the laser cutting process is characterized as having many advantages (see chapter one), it has attract many researchers to explore the process fundamentals in order to understand the process more completely. The effect of the CO_2 laser cutting parameters on the resulting cut quality for different plastics was reviewed as follows:

Caiazzo et al. [48] have investigated the laser cutting of three different polymeric plastics namely: polyethylene (PE), polypropylene (PP) and polycarbonate (PC) with thickness ranging from 2 to 10 mm. It was found that high cutting speeds do not always lead to good process efficiency. However, for all three polymers, cutting speeds have the most significant effect on the different aspects of the quality of the cutting edge. It was concluded that in many cases a high power laser is not necessary because 200 Watts may be sufficient to cut these plastics. It was recorded that the quality of the cut edges and faces was much better when working with PP rather than when working with PE. They concluded that the different gases, employed at a constant pressure of 3 bar, indicated no

significant variations in the quality of the cut edges or the value of the critical speed, except when the cutting was carried out at the lowest power setting, i.e. 200W.

Choudhury and Shirley [49] have investigated the CO_2 laser cutting of three polymeric materials (PP), (PC) and Polymethyl-methacrylate (PMMA). They reported that the quality of the cut in the case of PMMA is much better than in the case of PP and PC. It was found that the roughness is inversely proportional to the laser power, the cutting speed and the compressed air pressure. However, they mentioned that the cutting speed and the compressed air pressure have a more significant effect on the roughness than the effect of laser power. It was observed that PMMA has a smaller HAZ, followed by PC and PP and for all the polymers the dimensions of the HAZ is directly proportional to the laser power and inversely proportional to the cutting speed and the compressed air pressure.

Davim et al. [50] have evaluated the cutting quality of PMMA using a CO_2 laser. They reported that the HAZ increases with the laser power and decreases with the cutting speed. Also, they found that the surface roughness increases with a decrease in laser power and an increase in cutting speed. It was presented that the dimensions of the HAZ ranged between 0.12 and 0.37 mm and the surface roughness measurements were less than 1 μm. Finally, they reported that the CO_2 laser cutting of PMMA is widely used in industrial applications.

Kurt et al. [51] have investigated the effect of the CO_2 laser cutting process parameters on the dimensional accuracy and surface roughness of engineering plastics (PTFE and POM). It was concluded that the cutting speed and laser power must be regulated and optimised in order to obtain the desired dimensions and also, to enhance the surface quality and reduce roughness. It was found that the effect of gas pressure on the dimensions can be negligible. It was reported that the relationship between the cutting speed and the surface roughness is not linear. It was reported that the reason for the surface defects could be high gas pressure and high laser power.

The CW CO_2 laser cutting of plastics has been studied experimentally and theoretically by Atanasov and Baeva [52]. They investigated PMMA, a Teflon-PMMA-Teflon sandwich structure and Si-rubber. It was observed that a good agreement was

achieved between the theoretical predictions and the experimental data. They mentioned that it is possible to predict from the model relationships such as the cutting speed as a function of the substrate thickness or laser power and to use these relationships to determine the optimum setting for the process parameters.

Bäha et al. [53] have studied the laser cutting of plastic scintillator and light guide materials. It was found that the optical reflection factor R is a reliable measure for evaluating the quality of a cut surface. It was reported that the light guide materials based on pure PMMA have an average optical factor of 80 – 90% depending on the thickness. It was found that a scintillator with thickness of up to 10 mm can be laser cut with a reflection factor of 80%. It was concluded that all laser cutting parameters should be optimised in order to obtain the required surface optical quality.

Davim et al. [54] have presented a preliminary study to evaluate the effect of processing parameters (laser power and cutting speed) on the laser cut quality of polymeric materials with different thicknesses. It was found that the HAZ increases with the laser power and decreases with the cutting speed. It was reported that when cutting samples of PMMA, parts could be made with acceptable dimensions and without burrs. It was mentioned that the CO_2 laser of polymeric composites is widely used in industrial applications.

Sheng and Cai [55] have developed a procedure that integrates process models for laser cutting with an interactive scheme for selecting the operating conditions. They succeeded in developing an optimisation scheme for laser cutting, which is able to predict the laser power and cutting speed that satisfy the constraints for material removal rate (MRR), entrance taper, exit taper and kerf width. It was shown that the critical criterion (MRR in this case) controls the final cutting conditions. It was concluded that this predictive process planning model will eliminate the trial-and-error procedure that is currently used in laser-based manufacturing.

Berrie and Birkett [56] have investigated experimentally and theoretically the effect of laser parameters on the cutting and drilling rate in samples of Perspex. It was verified that the experimental results agree with the theoretical predictions and provide a sound basis for the assessment of laser machining of other materials which behave in a

similar manner. It was found that increasing the power, increases the depth of the cut, (i.e. thicker samples can be cut successfully) whereas, increasing cutting speed decreases the depth of the cut. Also, they mentioned that moving the focal plane of the lens towards the top surface of the Perspex increases the depth of the cut. It was proved that the gas pressure has no effect on the cut depth.

Romoli et al. [57] have studied CO_2 laser machining in order to create 3D cavities by vaporizing PMMA layer by layer. They used a theoretical model to predict the depth and width of the groove. It was shown that complex shapes can be machined even with sharp corners due to the small radius of the focused spot. It was concluded that further investigations should be performed on forming cavities in different plastic materials which have different responses to CO_2 radiation.

The laser cutting of perspex (PMMA) has also been studied by Black [58]. He reported that samples of PMMA up to 12.5 mm thick could be cut fairly easily with relatively low-power lasers (around 400 W) and cutting speeds of 1500 mm/min. It was found that the pressure of the shielding gas (normally air) must be kept above 0.1 bar, to prevent vapour ignition. This is achieved by creating as air stream of sufficiently high velocity to ensure that the vapour forming from the plastic flows to the bottom of the kerf. He suggested an inert gas for the assistant gas for a better quality of cut and to avoid frosting of the top edge of the cut as the pressure increases. However, the gas cost would be substantially greater than if compressed gas is used.

Di Illio et al. [59] have studied the laser cutting of aramid fibre-reinforced plastics. They discussed the effect of process parameters on the quality of the laser cut. They succeeded in presenting a new method of digital image processing for evaluating the cut quality.

Zhou and Mahdavian [60] have discussed the capability of a low power CO_2 laser in cutting various non-metallic materials including plastics. They developed a theoretical model to estimate the depth of cut that can be achieved if the material properties and cutting speed are known. It was found that the theoretical model agrees with the experimental cutting results. It was mentioned that this development will assist those in manufacturing industries to choose a suitable laser system for cutting or marking non-

metallic materials. Also, it was demonstrated that a 60 W laser power can be used for cutting non-metallic materials and is suitable for plastic board cutting. Finally, it was concluded that the deeper the cutting depth, the more energy is required.

CO_2 laser cutting of reinforced plastic mould parts has been carried out and the cutting results have been compared with other cutting techniques, such as water jet cutting, milling punching, sawing, using a conventional knife, and using an ultrasonic excited knife. This work was carried out by Nuss [61]. It was shown that laser cutting is faster and cleaner and reduces the time spent on post-operation work.

The laser cutting of composites of aramide, graphite and glass cloth-reinforced polyester have been studied by Tagliaferri et al. [62]. They examined the morphology of the cut surfaces by scanning electron microscopy. It was found that the thermal properties of the fibres and matrix are the principal factors which affect cutting performance. It was concluded that the quality of the cut surfaces depends on the type of composite being cut.

Caprino and Tagliaferri [63] have proposed a simple analytical model to predict the kerf depth and optimal working conditions. It was confirmed that in the laser cutting of carbon reinforced plastic composite materials, the poor quality of the cut surface is due to the difference in the thermal properties of the carbon fibre and the resin matrix. In fact, they observed the best results when laser cutting of AFRP due to the polymeric nature of both of the fibre and matrix. It was reported that their experimental results are in excellent agreement with their theoretical predictions for GFRP, AFRP and GFRP-composites. It was proven that the depth of penetration is linearly correlated with the laser power. In addition, they formulated criteria for the classification of cut quality, based on kerf geometry and heat affected zone size to help in selecting the optimum cutting conditions.

Caprino et al. [64] investigated the CO_2 laser cutting of GFRP composites. They introduced an analytical model which allows the depth of kerf to be predicted as a function of the direction of the beam in relation to the direction of travel of the material being worked. They reported a substantial agreement between the experimental results and the theoretical predictions. They stressed the importance of the following when laser

cutting of GFRP. This is to characterize the spatial distribution of power of the laser beam and to relate this to the distribution of the fibre in the matrix.

The CO_2 laser cutting of glass fibre reinforced plastic (GFRP) composites has been investigated separately by Caprino et al. [65]. They again proposed an analytical model which allows the depth of the kerf to be predicted. It was found that the theoretical model is in substantial agreement with the experimental results. They developed an equation to determine the influence of the parameters of the material structure on the kerf depth. It was concluded that the optimal cutting conditions are strongly affected by any non-uniform distribution of the fibres across the thickness of the sample.

Cenna and Mathew [66] have presented a theoretical model which considers the spatial distribution of the laser beam, the interaction time between the laser beam and the workpiece, the absorption coefficient and thermal properties of the material. They reported a good agreement between their results and the theoretical predictions. It was found that the theoretical model successfully predicts the cut quality parameters such as kerf width, the angle of the cut surfaces and the transmitted energy loss through the kerf. Moreover, it was suggested that a different material removal mechanism is involved in the laser cutting of GFRP. Finally, it was reported that as the cutting speed increases the kerf width and the kerf angle decrease.

In 2010 Groke and Emmelmann [67] have investigated the influence of laser cutting parameters on the quality of carbon fibre reinforced plastic (CFRP) parts. Their challenge was to apply a CO_2 laser beam and a fibre laser to cut this material and achieve a small HAZ. A large HAZ is a result of the large difference between the decomposition temperatures of resin and fibre material (i.e. the decomposition temperature of carbon fibre is about 3000° K and that of epoxy resin is about 550° K). It was found that both the HAZ size and the kerf width decrease significantly with high cutting speeds and small energy inputs. Additionally, they demonstrated that both the CO_2 and the fibre laser beam sources are applicable for the LBC of CFRP forming high quality parts. However, it was found that when processing CFRP laminates with thickness between 1 and 7 mm the CO_2 laser has an advantage when compared to the fibre laser due to the higher absorption of the 10.6 μm wavelength, by the material.

A study of the possibilities of using a high quality CO_2 laser to cut 3 mm thick samples of CFRP in plates form was presented by Riveiro et al. [68]. They investigated the influence of different processing parameters such as the pulse frequency, the pulse energy, the duty cycle, and type, and pressure of the assist gas on the cut quality. They evaluated the quality of the cuts in terms of kerf width, perpendicularity of cut kerf, delaminating degree, and extension of the heat affected zone. It was reported that an adequate selection of values for the processing parameters allowed good quality cuts to be obtained.

The thermal damage caused during laser cutting of aramid fibre/epoxy laminates was investigated by Dillio et al [69]. They examined samples cut with a 500 W CO_2 CW laser using different parameters by both optical and scanning electron microscopy. It was reported that cracks were detected in plies with the fibre direction at 90° to the cutting direction. They developed a model to relate the material damage to the cutting parameters.

Bamforth et al. [70] have investigated CO_2 laser cutting of nylon textiles with the aim of optimizing the edge quality. It was reported that nylon textiles can be cut using either a CW or a pulsed CO_2 laser. They optimised the process with the aid of a procedure referred to as 3D finite difference technique. It was mentioned that the edge quality can be significantly better when using the pulsed cutting mode.

2.10.3 Laser cutting of wood and its composites

Some investigations have been done to determine interactive effects of laser parameters on the quality of the final parts made from different woods and wood-composites. Yet, laser cutting of wood and its composite materials has not been widely accepted by the wood industry. At present, most lasers for cutting wood are used to fabricate some items of furniture in mass production to reduce the cutting cost. In fact, cutting wood and wood-composites by means of a laser beam is a complicated process, as it involves an exothermic chemical reaction and it is influenced by several uncontrollable factors such as: composition, density, moisture, thermal conductivity and internal bond strength. In comparison with industrial reports, laser cutting of different

wood based materials has received more attention in the academic literature; yet, in comparison with the cutting of metals and plastics few articles have been published on the laser cutting of woods and wood-composites. In the following section some articles related to the CO_2 laser cutting of woods and wood-composite materials will be summarized.

N. Yusoff et al. [71] have studied the CO_2 laser cutting of Malaysian light hardwood. They succeeded in developing a relationship between the processing parameters and the types of wood with different properties, specifying the optimum cutting conditions. Also, they have presented guidelines for cutting a wide range of Malaysian wood. It was reported that moisture content reduced the cutting efficiency due to the fact that water is readily absorbs the CO_2 laser radiation. It was also shown that the use of an inert gas such as nitrogen can be beneficial and results in a final product with better quality. However, they said that this hypothesis still needs to be proven and that the cost incurred still need to be identified before the approach can be justified.

Hattri [72] has attempted to compare the different types of lasers in the processing of wood. He concluded that the CO_2 laser is the most suitable laser due to the fact that the CO_2 laser produces a higher energy density more easily than the YAG laser when interacting with wood.

Barnekov et al. [73] have concluded that the factors affecting the ability of lasers to cut wood may be generally classified into three categories: the characteristics of the laser beam, the equipment and process variables and the properties of the workpiece. They have reported that most lasers for cutting wood have powers ranged from 200 to 800 W. They have stated that for maximum efficiency, the proper combination of cutting speed and laser power will depend on the workpiece thickness, density and the desired kerf width. Also, they have found that more power is required to cut wet wood than is required for dry wood if the cutting speed is held constant.

Another study was carried out by Barnekov et al. [74] on the laser cutting of wood composites. They have found that the optimal focus position is at the surface, using laser power from 400 to 500 W and a cutting speed of 20 in/min. Moreover, they used

compressed air with a nozzle diameter of 0.05 in. Finally, they reported that these preliminary results suggest that further research on the laser cutting of wood needs to be carried out.

Both Khan et al. [75] and Mukherjee et al. [76] have carried out studies on the laser cutting of timber wood. Both addressed the significance of investigating the LBC parameters such as laser power, cutting speed, nozzle design and variation in shielding gas velocity and their effect on the quality of the cut sections.

Lum et al. [77] have reported on the optimal cutting conditions for the CO_2 laser cutting of MDF. They found that the average kerf width reduces with increasing cutting speeds. It was presented that the composition of the MDF, including the additives such as the bindings, the bonding agent, the tar etc, is also likely to cause variations in cutting speed. In addition, they reported that no significant reduction in the kerf width was found when varying the shielding gas type or pressure. Furthermore, they mentioned that increasing the gas pressure did not improve Ra values. However, Ra values increase as the cutting speed increases. Finally, they pointed out that the maximum cutting speed for each thickness is independent of any increase in the gas pressure or type. Therefore it would be more economical to use compressed air rather than nitrogen to laser cut MDF.

Ng et al. [78] have continued their investigation to estimate the variation in the power distribution with different cutting speeds, material thicknesses and pulse ratios. They succeeded in developing a test procedure to determine primary power losses when performing CW or pulsed mode laser cutting of MDF.

Letellier and Ramos [79] have reported that when cutting MDF boards with thicknesses greater than 8 mm and keeping the focal position fixed at the surface, the result is that the kerfs have curved sides. This side curvature increases as the MDF board becomes thicker. Accordingly, they varied the focal position and beam velocity in order to investigate their effect on the shape of side kerfs. They suggested a focal position for each board thickness and process parameter combinations. Also, they succeeded in determining the optimal cutting conditions by combining the plot of the focal position against the board thickness for minimum side kerf with the plot of the cutting speed against the board thickness at a fixed laser power.

2.10.4 Laser cutting of ceramic and glass materials

Laser cutting of thick ceramic samples by carefully controlling the fracturing of an irradiated area has been studied by Tsai and Chen [80]. They focused the Nd-YAG laser to scribe a groove-crack on the surface of a substrate and then an unfocused CO_2 laser is used to induce thermal stress. They developed a model to predict the cut geometry and stress levels in the cut region. They succeeded in presenting the effect of the cutting parameters on the cut geometry.

Ji et al. [81] have presented a laser crack-free cutting method for Al_2O_3 ceramics by a single-pass process. They could produce both straight and curved profiles. It was found that to achieve crack-free cuts the process parameters must be as follows: the cutting speed must be between 0.23 and 0.42 mm/s, when the laser head moves with a speed of 3 mm/s, the piercing time must be between 0.1 and 0.5 s, the piercing pitch must be between 0.03 and 0.05 mm. The power must reach a peak of 3500 W and the cycle duty must be less than 30%. It was concluded that these results demonstrated that the laser crack-free cutting technique is a promising method to achieve complex profiles in ceramic materials.

CO_2 laser cutting of thick ceramic tiles with thicknesses between 8.5 mm and 9.2 mm has been investigated by Black and Chua [82]. They used a combination of different cutting speeds to cut the tiles in order to determine the necessary cutting parameters for various tile geometries. They also looked into the effects on cutting of using various shield gases. Multipass cutting and underwater cutting were performed to examine their effects on the thermal load during the processing. It was demonstrated that the most critical factor arising from the use of the CO_2 laser to cut ceramic tiles is crack damage, which is caused by a high temperature gradient within the substrate. It was concluded that a reduction of process-induced crack formation is vital for the commercial use of lasers in cutting ceramic tiles.

In another report Commercially-available ceramic tiles were cut using a CO_2 laser cutting machine, with the object of producing a laser beam machining (LBM) database that would contain the essential parameter information for successful processing. This was carried out by Black et al. [83]. They investigated various laser cutting parameters

that would produce cuts in ceramic tiles, but which require minimal post-treatment. They also examined the effects of various shield gases, of multi-pass cutting and of underwater cutting. The effects of these parameters have been described above.

Pulsed CO_2 laser cutting of Si3N4 engineering ceramics has been studied by Hong et al. [84]. They developed a model to investigate the effect of the cut front shape on the absorption of the laser beam. It was shown that "crack-free" cutting, the length of micro-cracks being limited to the grain size, could be obtained by using a high-speed and multi-pass feed cutting process.

The effects of process parameters on the quality achieved during laser cutting of alumina were presented by Wee et al. [85]. The effects of the interaction time, irradiance and assist gas pressure on the quality output variables such as striation angle, striation wavelength and the distance of clearly defined striations were studied. It was observed that the inclination of the striation is most affected by the interaction time, with assist gas pressure having a secondary effect and irradiance playing a minor role. Also, it was reported that the striation wavelength and upper and lower striation lengths are most influenced by the interaction time and irradiance, both causing longer wavelengths.

Grabowski et al. [86] have studied the laser cutting of a AlSi-alloy/SiC_p composite by modelling the kerf geometry. They used a numerical model which describes the inhomogeneous optical and thermo physical properties of the AlSi-alloy/SiC_p composite. It was found that increasing the laser beam scanning speed increases the slope of the cutting front.

Hong and Lijum [87] have investigated the laser cutting of SiN_4 ceramics. Their aim was to achieve crack-free cuts in this engineering ceramic with high efficiency by using a mechanical chopper Q-switched pulse CO_2 laser with optimised process parameters. It was found that the pulse duration should be short to reduce undesirable thermal effects during laser cutting. Moreover, they reported that those undesirable thermal effects can be reduced even more by using a high cutting speed and multiple passes.

Boutinguiza et al. [88] have investigated the CO_2 laser cutting of slate. They studied the influence of some process parameters (average power and assist gas

pressure) on the geometry and quality of the cut. It was shown that the CO_2 laser is a feasible tool for the successful cutting of slate. Also, it was confirmed that the mechanism of the CO_2 laser cutting of slate tiles is similar to that of metals. It was stated that the use of oxygen as an assist gas leads to a slight increase in cutting speed. Finally, it was found that tiles with a thickness of up to 13 mm can be cut with an acceptable cutting speed at a laser power of 1200 W.

A dual-laser-beam method was proposed by Jiao and Wang [89] to cut glass substrates to improve the cutting quality. They used a focused CO_2-laser beam to scribe a straight line on the substrate and then an unfocused CO_2-laser beam was used to irradiate the scribing line to generate a tensile stress and separate the different parts of the substrate. They used finite-element-method (FEM) software ANSYS to calculate the temperature distribution and the resulting thermal stress field. It was concluded that a glass substrate can be divided along chosen path with this dual-laser beams system and the cutting quality is improved compared with cutting using an unfocused laser beam alone.

A comparison of experimental results using high-power CO_2 and diode lasers under roughly equivalent experimental conditions has been presented by Crouse et al. [90]. It was found that the multimode diode laser produces a higher penetration rate when compared with the CO_2 laser under equivalent experimental conditions.

The literature review has shown that there is a lack of information regarding the CO_2 laser cutting of some standard engineering materials such as some polymeric, wood, MDF and GFRP etc. Therefore, the challenge of this research is to explore the laser cutting of some engineering materials with the aim of achieving information about the relationship between the process parameters and the quality characteristics as well as optimizing the process for these engineering materials.

2.11 Modelling and Optimisation Techniques in Common Laser Beam Processing

Generally, the quality of a laser cut, in terms of different quality features, is directly affected by laser cutting input parameters during laser cutting operating. Therefore, laser cutting is a multi-input multi-output process. Traditionally, to achieve the desired cut quality a great deal of time and cost are expended by a trial-and-error method to obtain optimal cutting conditions through a combination of the various cutting process input parameters. Modelling in LBC is one of the methods by which these obstacles can be eliminated and assist the scientist to get a better understanding of this complex process. A mathematical model of a manufacturing process is the relationship between input and output parameters in terms of mathematical equations. On the basis of their origin, models can be divided in three categories e.g. experimental or empirical models, analytical models, and artificial intelligence based models. Complexity in laser cutting process has forced researchers to find optimal or near optimal machining conditions by using a suitable optimisation technique based on a given optimisation criteria. A large number of techniques have been developed by researchers to solve these types of multi-objective optimisation problems.

The literature related to modelling and optimisation of laser beam processing is mainly using statistical DOE such as Taguchi method and RSM. Several analytical methods based on different solution methodologies, such as numerical solution, have also been examined related to laser beam processing. Some researchers concentrated on modelling and optimisation of laser beam processing through artificial intelligence based techniques such as artificial neural network (ANN) and fuzzy logic (FL). The subsequent subsections are a summary of some work carried out by different authors to model common laser processing techniques using these modelling/optimisations approaches.

2.11.1 Laser cutting process

2.11.1.1 Design of experiments

The application of Taguchi method to investigate the quality of the cut edge of stainless steel with different thicknesses has been carried out by Yilbas el al. [18]. It was

found that the oxygen gas pressure is the most significant factor on the waviness and flatness and its contribution is over 60%.

Cadorette and Walker [25] have conducted a study based on central composite design to explore the performance of new laser cutting system. They included the following as input parameters: fees rate, power, frequency and gas pressure and the out put responses were: surface roughness. Their results revealed that this laser system does not guarantee production of cut quality at ≤ 18 μm. They reported that the study space (i.e. factors ranges) should be expanded at levels settings not included in the original range. Therefore, it is very important to make sure that the study space is wide enough to reveal the influence of the factors on the responses, in the same time not too wide at which the model cannot be developed.

Rajaram et al. [28] have used regression analysis to develop models that describe the effect of the independent process parameters on laser cut quality of 4130 steel. They reported that the optimal cut quality is obtained by keeping kerf width, HAZ and surface roughness at minimum. It was reported that regression models predictions are in good agreement with the experimental results.

An experimental programme based on wedge-shaped workpiece was carried out to provide an understanding of the relationship between laser cutting parameters and cut surface quality [40]. Based on factorial experiment, cutting speed and assist gas were found to be significant parameters in determining average surface roughness. It was reported that the parameters which should be optimised in laser cutting include the cutting speed (maximised), the kerf width (minimised), HAZ (minimised) and surface roughness (minimised).

Choudhury and Shirley [49] have applied RSM to develop a model to relate the input laser cutting parameters (laser power, cutting speed and compressed air pressure) on laser cutting quality (HAZ and surface roughness) of three different polymeric materials PP, PC and PMMA. It was found that the predictive models for HAZ and surface roughness are well modelled by the linear function of the input parameters.

Kurt et al. [51] have employed the ANOVA and regression analysis to assess the effect of the process parameters (gas pressure, cutting speed and laser power) on the

dimensional accuracy and surface roughness for engineering plastics. They reported that the relationship can be used to optimise the process to get the optimum surface quality and roughness values.

Bahr et al. [53] have out lined the process parameters that have to be examined in order to get optimal cutting conditions. Also, they mentioned that an optimal result of the cutting process is a surface of optical quality without any deterioration of the bulk plastic material realized in a rather low cutting time.

Dissimilar full depth laser-butt welding of low carbon steel and austenitic steel AISI 316 was investigated by Ruggiero et al. [91] using CW 1.5 kW CO_2 laser. The effect of laser power, welding speed and focal point position on the weld-bead geometry (i.e. weld-bead area, upper width, lower width, and middle width,) and on the operating cost C was investigated using RSM. It wa indicated that the proposed models predict the responses adequately within the limits of welding parameters being used. The regression equations were used to find optimum welding conditions for the desired geometric criteria.

Dubey and Yadava [92] have applied Taguchi method and principal component analysis for multi-objective optimisation of pulsed Nd-YAG LBC of nickel-based superalloy (SUPERNI 718) sheet. They investigated three quality characteristics kerf width, kerf deviation (along the length of cut) and kerf taper. The process input parameters considered are assist gas pressure, pulse width, pulse frequency, and cutting speed. They presented the percentage of contribution of each factor on the quality characteristics mentioned earlier. It was reported that the responses at predicted optimum parameter level are in good agreement with the results of confirmation experiments conducted for verification tests.

Dubey and Yadava [93] have presented a hybrid approach of Taguchi method and RSM for the multi-response to optimise laser cutting process of thin sheets of magnetic material using a pulsed Nd-YAG. The approach first uses the Taguchi quality loss function to find the optimum level of input cutting parameters such as assist gas pressure, pulse width, pulse frequency and cutting speed. The optimum input parameter values are further used as the central values in the RSM to develop and optimise the

second-order response model. The two quality characteristics kerf width and material removal rate have been selected for simultaneous optimisation. It was found that a considerable improvement in both quality characteristics when the hybrid approach is used, as compared to the results of a single approach.

A parameter optimisation of the kerf quality characteristics during pulsed Nd-YAG laser cutting of nickel based superalloy has been investigated by Sharma et al. [94]. The kerf quality characteristics considered are kerf width, kerf taper and kerf deviation. The essential process input parameters were identified as oxygen pressure, pulse width, pulse frequency and cutting speed. They applied Taguchi quality design concept for conducting the experiments for both straight and curved cut profiles. It was indicated that the optimum input parameter levels suggested for curved cut profiles are entirely different from straight cut profiles except kerf width.

A factorial analysis has been carried out by Yilbas [95] to identify the main effects and interaction effects of the LBC parameters on the kerf size variations and thermal efficiency. It was reported that the laser power and oxygen pressure has significant effect on the percentage of kerf width variation. It was found that the thermal efficiency improved at low power intensities and high cutting speed.

A hybrid optimisation approach for the determination of the optimum laser cutting process parameters which minimise the kerf width, kerf taper, and kerf deviation together during pulsed Nd:YAG laser cutting of a thin sheet of nickel-based superalloy SUPERNI 718 has been introduced by Raghavendra and Vinod [96]. They used a higher resolution based L_{27} orthogonal array for conducting the experiments. They applied DOE results in grey relational analysis. The significant parameters were obtained by performing analysis of variance (ANOVA). It was reported that the application of the hybrid approach for straight cuts has reduced kerf width.

Dubey and Yadava [97] have applied a hybrid approach of Taguchi method and principal component analysis for multi-objective optimisation of pulsed Nd-YAG laser beam cutting of nickel-based superalloy (SUPERNI 718) sheet to achieve better cut qualities. The three-quality characteristics kerf width, kerf deviation and kerf taper have been considered for simultaneous optimisation. The input parameters considered are

assist gas pressure, pulse width, pulse frequency, and cutting speed. The results of multi-objective optimisation include the prediction of optimum input parameter level and their relative significance on multiple quality characteristics. It was confirmed that the responses at predicted optimum parameter level are in good agreement with the results of confirmation experiments.

Another study performed by Dubey and Yadava [98] on the optimisation of two kerf qualities namely: kerf deviation and kerf width simultaneously by using Taguchi quality loss function during pulsed Nd-YAG laser beam cutting of 0.9 mm thick aluminium alloy sheet. It was found that the assist gas pressure and pulse frequency are affecting the kerf quality significantly. They achieved a considerable improvement in kerf quality.

Lim et al. [99] have presented the cutting characteristics and optimal cutting conditions in a high speed feeding type laser cutting machine by using Taguchi method. They considered cutting speed, laser power, laser output duty and assistant gas pressure as adjustment parameters. Also, they performed analysis of variance in order to evaluate the effect of adjustment parameters on the surface roughness of the sheet metal. They highlighted the effect of the process parameters on the surface roughness. Finally, they reported the optimal cutting condition which minimises the surface roughness.

Mathew et al. [100] have presented parametric studies on pulsed Nd-YAG laser cutting of carbon fibre reinforced plastic composites. They applied RSM to develop models to predict the HAZ and taper of the cut surface. The process parameters they considered are: cutting speed, pulse energy, pulse duration and gas pressure. It was reported that the predictions finds and the experimental measured data are in agreement.

Cicala et al. [101] have factorial design to optimise the CO_2 laser cutting processes of polymettacrylate. Their main objectives were to identify which factors are statistically important, to build a quantitative model relating the important factors to the response functions, to optimise these response functions and particularly the material removal rate, the kerf walls parallelism deviation and the specific energy consumption. It was concluded that the obtained results allow the selection of laser cutting optimal parameters.

A statistical analysis of the laser cutting of wood based on RSM has been performed by Castaneda et al. [102]. They used this statistical tool to investigate the significant process parameters by considering parameters interactions. The investigated parameters are laser power, focal position, cutting speed, gas pressure, number of passes and cutting direction. The responses are kerf depth, mass removal and specific energy consumption. It was reported that the majority of these process characteristic are significantly affected by the structure of the wood. It was mentioned that the direction of cut was the most significant factor in all responses analysed. They highlighted the significant factors and their interactions. They managed to obtain optimal cutting conditions for both cutting directions. Finally, it was found that the process would be more efficient when applying the energy of the laser in multiple passes.

McMillin and Harry [103] have studied the laser cutting of southern pine using factorial experiment. They explored the effect of moisture content, specific gravity, direction of cut, and wood thickness on the quality of the cut and speed of the process. It was reported that the direction of the cut also has an important effect on cutting results. They determined the optimal conditions for cutting various thicknesses of this wood.

Castaneda et al. [104] have presented data on statistical analysis of the multiple-pass laser cutting of dry and wet pine wood using DOE. They mentioned that the anisotropic nature of wood means that yield and cut quality need to be analysed both parallel and perpendicular to the wood fibre. Additionally, they investigated laser power, focal plane position, cutting speed, gas pressure and number of passes. They compared the results against a range of process responses that define the process efficiency (kerf depth, mass removal, specific energy consumption) and quality of the cut section (heat affected zone - HAZ, kerf width, edge surface roughness, and perpendicularity). It was concluded that the majority of these responses are significantly affected by direction of cut and wood moisture content.

The optimisation of laser cutting of thin Al_2O_3 ceramic layers using DOE approach has been attempted by Huehnlein et al. [105]. They mentioned that DOE allows to separate the most important influencing factors on the targeted cutting process, to clarify their interaction, to reduce the overall amount of parameter sets that need to be examined

and to identify the optimised parameter regions. By using both, a CW 500 W fibre laser and a 200 W CO_2 laser, they optimised and compared the cutting of thin Al_2O_3 ceramic substrate layers applying commercial DOE software. It was demonstrated that DOE has the potential to optimise laser material processes.

A statistical model based on multivariate regression is introduced by Wee et al. [85] to determine the parameters affecting cut quality. They investigated the effects of interaction time, irradiance and assist gas pressure on striation wavelength, striation angle and the depth of separation line during laser cutting of ceramics. It was found that the model predictions are in good agreement with the experimental results. It was concluded that these models can be used for optimizing cut quality, but striation formation cannot be eliminated altogether.

2.11.1.2 Artificial intelligence & genetic algorithm

Dhupal et al. [106] have performed an experiment based five level central composite design. They studied the effects of laser turning process parameters i.e. lamp current, pulse frequency, pulse width, cutting speed (revolution per minute, rpm) and assist gas pressure on the quality of the laser turned micro-grooves. They created a predictive model for laser turning process parameters using a feed-forward ANN technique utilized the experimental observation data based on RSM. The optimisation problem has been constructed based on RSM and solved using multi-objective genetic algorithm (GA). It was mentioned that the neural network coupled with genetic algorithm can be effectively utilized to find the optimum parameter value for a specific laser micro-turning condition in ceramic materials. It was listed the optimal process parameter settings as lamp current of 19 A, pulse frequency of 3.2 kHz, pulse width of 6% duty cycle, cutting speed as 22 rpm and assist air pressure of 0.13 N/mm^2 for achieving the predicted minimum deviation of upper width of −0.0101 mm, lower width 0.0098 mm and depth −0.0069 mm of laser turned micro-grooves.

Yilbas et al. [43] have investigated CO_2 laser cutting of the wedge surfaces and normal surfaces of mild steel to classify the striation patterns of the cut surfaces. It was

observed from the neural network output that the normal pattern of striation is dominant over other patterns. It was mentioned that the cutting quality improves for a specific laser output power setting.

An experimental design is employed by Guo et al. [107] to reduce the number of tests and collect experimental training and test sets. Then they developed ANN approach to describe quantitatively the relationship between cutting quality and cutting parameters in the non-vertical laser cutting situation. They used a quality point system to evaluate the cutting result of thin sheet quantitatively. It was shown that the calculated "quality point" using ANN is quite closely in accord with the actual cutting result. Finally, it was concluded that the ANN is very successful technique for optimizing parameters, predicting cutting results and deducing new cutting information.

Casalino et al. [108] have proposed a model based on fuzzy logic to help planner obtaining the acceptable operable condition when laser cutting of new part with different piece geometry and surface quality. They evaluated the quality of the cut on the basis of 5 criteria namely: frequency of striation, width of the heat affected zone, roughness of the cut, width of the cutting path. It was stated that the model can be used for quality inspection through an automated system that merges the expertise of cutting operators with the mathematical model's accuracy. They claimed that a practiced operator is no longer necessary. Finally, it was mentioned that the model can be extended to other laser cutting processes.

Laser cutting parameters optimisation based on artificial neural network (ANN) has been carried out by Dixin et al. [109]. The ANN approach has been developed to describe quantitatively the relationship between cutting quality and cutting parameters in a non-vertical cutting situation. It was found that the calculated quality point using ANN is well agreed with the actual cutting results. It was mentioned that ANN is very successful for optimizing, predicting cutting results and deducing new cutting conditions.

A multiple regression analysis and an artificial neural network (ANN) were employed by Tsai et al. [110] to build a predicting model for cutting Quad Flat Non-lead (QFN) packages by using a Diode Pumped Solid State Laser. The predicting model

includes three input variables namely: the current, the frequency and the cutting speed. The cutting qualities are (depths of the cutting line, widths HAZ and cutting line for epoxy and for copper-compounded epoxy). It was shown that the ANN model has the predicting ability to estimate the laser-cutting qualities of QFN packages. Finally, a genetic algorithm (GA) is applied to find the optimal cutting parameters that lead to least HAZ width and fast cutting speed with complete cutting. It was reported that the optimal setting are current of 29 A, frequency of 2.7 kHz and cutting speed of 3.49 mm/s.

2.11.2 Laser welding process

2.11.2.1 Design of experiments

Benyounis et al. [111] have developed models using RSM to investigate the effect of welding parameters in SAW (welding current, arc voltage and welding speed) on the impact strength at two testing temperatures of 50 °C and 27 °C. The aim was to predict and optimise the impact strength of the spiral-welded joints. It was observed that the welding current was the most significant factor associated with the impact strength, then the welding speed, whereas the welding voltage has no significant effect within the factors domain investigated. They listed the optimal welding conditions that would lead to acceptable impact strength and improve the process productivity.

The production of strong and stiff, aluminium-titanium, multi-layered composites (laminates) by explosive welding was undertaken by Ege et al. [112]. The study was performed using RSM to investigate the mechanical behaviour of the laminates with changes in two characteristic variables; abundance of interfaces and volume percentage of the more ductile component. Eighteen laminates were produced and then one-step welding of these laminates was carried out by explosive-introduced pressuring. Yield strength, ultimate tensile strength and elongation were the responses under consideration. A second-order model was fitted to define the relationship between the yield strength and the two variables. It was reported that the mechanical properties of the laminates depend strongly on the relative amounts of the components, but only weakly

on the abundance of the interface within the selected operability region. It was also mentioned, that with the aid of the developed model it is possible to fabricate laminates that are tailored to strength, density and load specifications.

Allen et al. [113] have proposed a model based on central composite design with the alpha parameter set equal to 2, for robotic gas metal arc welding of sheet metal of 409-gauge, stainless steel. The six factors controlled in this study were: wire feed speed, weld travel speed, arc voltage, contact-tube-to-work distance, root opening and offset. The objective was to minimise the weld cycle time by maximizing welding speed, while maintaining predictable weld quality over a range of worst-case processing conditions. The optimal welding conditions for this type of material with a lap joint were reported and confirmed by experimental tests. The effect of the process parameters was presented graphically.

Raghukandan [114] has conducted experiments to clad low carbon steel and copper plates using nitroglycerine explosive (2500 m/s detonation velocity). The aim was to adopt RSM to relate the bond and shear strength of the clad to four process factors (flyer thickness, loading ratio, angle of inclination and stand-off distance). Mathematical models were developed and the effect of process parameters on the responses was discussed. It was found that the flyer thickness, the loading ratio and the angle of inclination have significant contribution to the interfacial morphology of explosive clad.

V. Murugan and Gunaraj [115] have implemented RSM to correlate the angular distortion in GMAW of structural steel plate (IS: 2062) to the process parameters, namely: time gap between successive passes, number of passes and wire feed rate. The main and interaction effects of the process parameters were analysed and presented. It was found that the number of passes had a strong effect on the response, therefore, to control the angular distortion in practice the number of passes has to be monitored carefully. Moreover, it was demonstrated that all the process parameters have a negative effect on the angular distortion.

Benyounis et al. [116] have studied the effect of CO_2 laser welding parameters (laser power, welding speed and focus position) on the impact strength and NTS of butt joints made of medium carbon steel plates. Two mathematical models were developed

using RSM to describe the influence of the process parameters on the two responses. The main, quadratic and interaction effects of the process parameters on the two responses were determined quantitatively and presented graphically. It was reported that the welding speed is the main factor affecting the two responses; it was found that decreasing the welding speed from its highest level to lowest level would result in increasing both responses by 89.3% and 76.45% respectively. Laser power and focal point position have also strong effect on both responses investigated.

Benyounis et al. [117] have done another work to predict the residual stress for CO_2 laser butt-welding joints of AISI304 stainless steel plates. The investigation is carried out using RSM to develop models in terms of the process input parameters mentioned earlier in [59] to predict the principal residual stress and its direction. It was observed that the travel speed and laser power were the main factors affecting the behaviour of the maximum residual stress. It was recommended to use the developed models to find the optimal welding conditions to obtain the welded joint with a minimum distortion.

Olabi et al. [118] have established the relationship between the CO_2 laser welding parameters (laser power, welding speed and focus position) and the residual stress magnitude and distribution using RSM for butt joint welded components. The base material was AISI304 stainless steel plates with 3 mm thickness. Incremental hole drilling procedure with the standard seven increments was followed to measure the residual stress magnitude and distribution at three locations, on HAZ, 10 mm and 20 mm from weld centreline repetitively. Twenty one models were developed to describe the residual stress behaviour. A procedure of four steps was presented to use the developed models in order to predict the residual stress magnitude at the proposed welding conditions and at a given position. Also, the effect of the process parameters on residual stress behaviour has been determined quantitatively and presented graphically.

Benyounis et al. [119] have developed a mathematical model using RSM to relate the failure load to the laser welding parameters namely: laser power, welding speed and focal position. The effect of the process parameters on the failure load and the tensile-shear strength of the lap joint made of AISI304 with 1 mm thickness have been

investigated. It was found that the main factor affecting the joint strength is the welding speed and the other two factors are slightly affecting the joint strength.

Koganti et al. [120] have employed a full factorial design to define the optimum weld MIG process parameters for non-treatable 5754 aluminium alloys. The effects of weld process parameters on the lap joint failure load (tensile-shear strength) and weld penetration were investigated. The process parameters were: power input (torch speed, voltage, current, wire feed rate), pulse frequency and gas flow rate. The joint strengths and weld penetration were measured for various operating ranges of weld factors. It was indicated that the power input and the gas flow rate were the two significant factors based on lap shear load to failure and weld penetration data. It was reported also, that the lower the power input, the lower the shear load to failure and depth of penetration and vice versa. The optimum factor settings for higher joint strength were high power input and high gas flow rate.

Multi-response optimisation of CO_2 laser-welding process of austenitic stainless steel was investigated by Benyounis et al. [121]. The relationships between the laser-welding parameters (laser power, welding speed and focal point position) and the three responses (tensile strength, impact strength and the joint-operating cost) were established using RSM. They mentioned that the optimal welding conditions were identified in order to increase the productivity and minimise the total operating cost. They reported that the parameters effect was determined and the optimal welding combinations were tabulated.

Sampath [122] has presented an innovative constrains-based approach that proved quite efficient in developing a specification for consumable solid-wire electrodes for GMAW of HSLA-80 and HSLA-100 steels that meet or exceed the US Navy requirements. Initially, he converted the US Navy requirements into a set of constraints which related the chemical composition of steels to certain metallurgical characteristics. Subsequently, a 2^3 factorial design was used to develop a batch of welding electrodes in order to evaluate their performance. Among the eight electrodes used, it was shown that two electrodes met or exceeded ER-100s requirements, while one electrode met or

exceeded ER-120s requirements. It was concluded that the use of this approach greatly reduced the risk inherent in developing electrode specifications.

Pine et al. [123] have presented an experimental and numerical study to determine the torsional stiffness, elastic limit and ultimate strength of spot welded, adhesively bonded and weld-bonded box sections. They investigated a variety of factors, namely: joining technique, sheet thickness, steel strength, section area, section design and end weld using factorial design techniques to determine their effects on the torsional properties of box sections. The authors have concluded that the joining technique, section area and section thickness were the main factors which have the greatest effect on the torsional stiffness of the box sections. It was found that the torsional stiffness can be improved without substantial weight gain by changing the joining technique from 50 mm pitch spot welds to adhesive bonding, increasing the section area and to a lesser extent, changing the section design. Furthermore, the steel strength was the most important factor in determining the elastic limit and ultimate strength.

2.11.2.2 Artificial intelligence & genetic algorithm

Lightfoot et al. [124] have used ANN to develop a model to study the FCAW process factors affecting the distortion of 6 – 8 mm thick D and DH grade steel plates. A sensitivity analysis was carried out, which highlighted a number of apparently key factors that influenced distortion. It was proven that the carbon content played a key role in the amount of distortion produced by the welding process. They found that an increase in the carbon content was beneficial in reducing thin plate distortion caused by welding. Also, they identified a number of distortion-related factors, such as carbon content, YS/TS ratio and rolling treatment. It was concluded that these factors can be controlled to reduce the distortion in 6-8 mm thick plates.

Olabi et al. [125] have employed the back propagation artificial neural network and the Taguchi approach to find out the optimum levels of the welding speed, the laser power and the focal position for CO_2 laser welding of medium carbon steel. They managed to find the optimal welding setting that would lead to the desired weld joint. It

was reported that the authors do not see any drawbacks to the use of this approach for investigating other keyhole laser welding applications.

Sterjovski et al. [126] have applied the ANN models to predict the mechanical properties of steels in various applications, namely: impact strength of quenched and tempered pressure vessel steel exposed to multiple postweld heat treatment cycles, the hardness of the simulated HAZ in pipeline and lap fitting steel after in-service welding and the hot ductility and hot strength of various microalloyed steel over the temperature range for stand or slab straightening in continuous casting process. It was found that the three ANN models successfully predicted the mechanical properties. It was also shown that ANNs could successfully predict multiple mechanical properties and the result of the sensitivity analysis were in agreement with both findings of the experimental investigation and reported results in the literature. Furthermore, it was mentioned that the use of ANNs resulted in large economic benefits for organisations through minimizing the need for expensive experimental investigation and/or inspection of steels used in various applications.

Christensen et al. [127] have developed a multilayer feed forward network for modelling and online adjustment of GMAW process parameters to guarantee a certain degree of quality. In this study, butt joint welding with full penetration of standard steel S135 with 3 mm thickness was carried out. The process parameters were; wire feed speed, voltage, welding speed and gap width while the network inputs were back bead width and back bead height. In open loop control strategy, it has been demonstrated that use of the model to provide high quality welding is feasible and the network training was straightforward and effective. Whereas, in the closed loop experiments a single input and single output control scheme was investigated, it was shown that it was applicable for adaptive control of GMAW with some limitations.

Okuyucu et al. [128] developed a model using ANN for the analysis and simulation of the correlation between friction stir welding (FSW) parameters of aluminium plates and mechanical properties of the welded joint. The process parameters consist of weld speed and tool rotation speed verses the output mechanical properties of weld joint, namely: tensile strength, yield strength, elongation, hardness of WZ and hardness of

HAZ. Good performance of the ANN model was achieved and the model can be used to calculate mechanical properties of the welded plates as a function of process parameters. Also, it was found that the correlation between the measured and predicted values of tensile strength, hardness of HAZ and hardness of weld metal were better than those of elongation and yield strength.

2.11.3 Laser drilling process

2.11.3.1 Design of experiments

Tam et al. [129] have reported the use of the Taguchi technique of experimental design in optimizing the process parameters for drilling deep-holes in 25 mm thick nickel-based superalloy, Inconel 718. They explored the effects of five process parameters (pulse energy, pulse duration, pulse shape, focal position, and assist gas pressure). Their primary response under study was the drilling time. It was predicted that a minimum drilling time of 31.51 s is needed to drill a hole with pulse energy of 30.0 J, pulse duration of 1.8 ms, a "treble" pulse shape, a focal position of 0.0 mm and an oxygen pressure of 0.35 MPa. It was reported that the confirmation experiments have produced results that lay within the 95% confidence interval.

Bandyopadhyay et al. [130] have reported the use of Taguchi design to study the effects of the process variables (pulse energy, pulse repetition rate, pulse duration, focal position, nozzle standoff, type of gas and gas pressure of the assist gas) on the quality of the drilled holes and determine optimum processing conditions. Their goal was to achieve minimum taper in the drilled hole. It was indicated that optimal laser parameters lead to very significant improvements hole-quality.

Kamalu and Byrd [131] have applied statistical design of laser drilling to study the process performance by measuring laser-drilled hole diameters under a varity of parametric combinations. It was found that the effect of focal position has the more significant effect on the hole diameter than the energy input. It was shown that the combination of accurate high speed measurement of laser drilling performance and the statistical design of laser drilling experiments is essential for the optimisation of laser percussion drilling parameters for a given manufacturing application.

Masmiati and Philip [132] have used Taguchi method to stress the important factors that might affect the drilling process of different polymers. They studied the effects of pulses, standoff distance on the circularity of the hole, spatter thickness, hole taper and material removal rate. It was stated that a specified hole diameter optimal parameters setting should be used in order to achieve less hole taper, greater circularity, less spatter formation and high removal rate.

2.11.3.2 Artificial intelligence & genetic algorithm

The neural network has been used to model Nd:YAG laser percussion drilling of 2.5 thick stainless steel 304 by Ghoreish and Nakhjavani [133]. Approximate experimental models of the process have been developed by the neural network according to the results of the experiments. Then the optimum input parameters (peak power, pulse time, pulse frequency, number of pulses, gas pressure and focal plane position) were specified using the genetic algorithm (GA) method. The output parameters include the hole entrance diameter, circularity of entrance and exit holes, hole exit diameter and taper angle of the hole. It was found that this method is reliable and economical and also confirms the qualitative results of the previous studies.

Karazi et al [134] have developed four models to predict the width and depth of micro-channels formed in glass by CO_2 laser. They built a DOE model using the power, pulse repetition frequency, and traverse speed as input parameters. Three models were developed using ANN separately for both micro-channel width and depth prediction. They compared the performance of these ANN models and DOE model. It was demonstrated that two of the ANN models showed greater average percentage error than the DOE model. While, the other ANN model showed an improved predictive capability that was approximately twice as good as that provided from the DOE model.

Optimizing the laser percussion drilling by combining the neural network method with the genetic algorithm has been investigated by Nakhjavani and Ghoreish [135]. First, optimum input parameters of the process were obtained in order to optimise every single output parameter (response) of the process regardless of their effect on each other (single criterion optimisation). Then, optimum input parameters were obtained in order

to optimise the effect of all output parameters in a multi-criteria manner. ANN method was employed to develop an experimental model of the process according to the experimental results. Then optimum input parameters (peak power, pulse width, pulse frequency, number of pulses, assist gas pressure, and focal plane position) were specified by using the genetic algorithm. The responses are: hole entrance diameter, circularity of hole entrance and hole exit, and hole taper. It was found that this hybrid technique can used to adjust input parameters of the process in multi-criteria optimisation mode and determine the optima drilling setting.

In conclusion, the optimisation techniques mentioned above are suitable for modelling and optimizing different laser processing techniques. The application of these techniques to mathematically model and optimise the laser cutting process for some highly demanding engineering materials to discover the optimal cutting combinations is important. Also, it was found from the review that the DOE is the most widespread technique in this area therefore; it will be used in this research.

CHAPTER III
DESIGN OF EXPERIMENT

3- EXPERIMENTAL DESIGN

3.1 Why Design of Experiments

Previously, the experiments used to be carried out by changing one-factor-at-a-time, this type of experimental approach required enormous number of runs to find out the effect of one factor. This experimental approach is no longer followed as it is expensive and takes longer time. Another disadvantage is that the factors interaction cannot be detected when using this approach. Therefore, other techniques, which overcome these obstacles, have to replace it, such as DOE, ANN etc [136 and137]. A good literature review on the techniques used in optimizing certain manufacturing process and the selection of the appropriate technique has been outlined by Benyounis and Olabi [138]. For these reasons, a DOE approach has been selected to be implemented herein. In fact, there are many designs among DOE as mentioned in [138]. Two level factorial design and Taguchi method are the common designs, which have the less number of runs to study a process with multifactor and multi-responses such as laser cutting. However, the quadratic effect of each factor cannot be determined using 2-level FD due to the limitation of this design as a screen design. In contrast, some of the interactions between the factors affecting the process cannot be determined using Taguchi method due to the aliased structures, which means not all the interaction effects can be estimated [139]. On the other hand, RSM is able to find out all the factor's effects and their interactions. Eq 2.1 below consists of three capital-sigma notations. The first summation term is representing the main factor effects, the second term is standing for the quadratic effects and the third term is representing the two factor interaction effects. Therefore, RSM was chosen by implementing Box-Behnken design, which is a three level design and it is able to investigate the process with a relatively small number of runs as compared with the central composite design [139 and 140]. This design characterizes with its operative region and study region are the same, which would lead to investigate each factor over its whole range. In fact, this is a competitive advantage for this design over the central composite design [141].

$$y = b_o + \sum b_i \chi_i + \sum b_{ii} \chi_{ii}^2 + \sum b_{ij} \chi_i \chi_j + \varepsilon \quad (3.1)$$

3.2 Response Surface Methodology (RSM)

DOE method was introduced by Sir R. A. Fisher in the early 1920's. Fisher developed a method to carry out agricultural experiments in which the effects of properties, such as fertiliser, sunshine and rain on a crop were determined. Since the 1920's DOE method has been applied across a wide range of disciplines. A number of different DOE methods have since been developed, including factorial experiments and Response Surface Methodology techniques, such as the Central Composite Design and the Box-Behnken Design. The method selected for a particular experiment depends on considerations such as the objectives of the experiment, the number of factors being investigated and the funds available [142].

Engineers often search for the conditions, which would optimise the process of interest. The optimum could be either a minimum or a maximum of a particular function in terms of the process input parameters. RSM is one of the optimisation techniques currently in use to explain the performance of the laser cutting process.

RSM is a set of mathematical and statistical techniques that are useful for modelling and predicting the response of interest affected by several input variables with the aim of optimizing this response [139 and 143]. RSM also specifies the relationships among one or more measured responses and the essential controllable input factors [140]. If all independent variables are measurable and can be repeated with negligible error, the response surface can be expressed by:

$$y = f(x_1, x_2, \ldots x_k) \quad (3.2)$$

Where: k is the number of independent variables

To optimise the response "y", it is necessary to find an appropriate approximation for the true functional relationship between the independent variables and the response surface. Usually a second order polynomial Eq.3.1 is used in RSM.

3.3 Box-Behnken Design (BBD)

One of the most popular RSM designs is BBDs, which are based on three level of each factor. These designs developed by Box and Behnken in 1960 [144]. They are constructed by first combining two-level factorial designs with incomplete block designs and then a specified number of centre points are being added. Fig. 3.1 presents a schematic diagram for BBD for three factors.

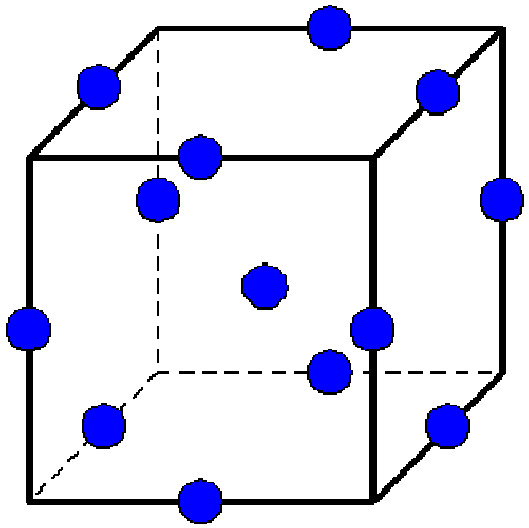

Fig. 3.1: A schematic diagram for BBD of three factors [145].

3.3 Advantages of BBD

1. Has specific positioning of design points.
2. This design has 3 levels for each factor.
3. Created for estimating a quadratic model.
4. Provides strong coefficient estimates near the centre of the design space, but weaker at the corners of the cube, because there weren't any design points.
5. Sensitive to missing data and a bad run.
6. Region of interest and region of operability are nearly the same.

3.4 Applying RSM Step-by-Step

In order to carry out any RSM problem it is usually considered in sequential steps. Hence the following steps are performed in order to develop a mathematical model in the case of laser cutting:

1. **Determining the essential process input parameters.**

These essential parameters may define from the past literatures or by conducting a preliminary study (i.e. screening study) based on factorial design. In this research the process parameters were determined from the past literatures. The process input parameters are: laser power, cutting speed, focal point position, gas pressure and nozzle diameter.

2. **Finding the limits of each factor.**

In order to find the range of each parameter, trial laser cut runs were performed by varying one of the process parameters at-a-time to find out the range of each parameter. Full cut, keeping the kerf width, cutting edge striations and dross to a minimum; were the criteria of selecting the working ranges.

3. **Development of design matrix**

In the current research the design matrix for each experiment was developed using Design-Expert V7 statistical software. For the three, four and five factors the total numbers of runs are: 17, 29 and 46 respectively. Also, these experimental runs are enough to estimate the coefficients in Eq.3.1.

4. **Performing the experiment**

The laser cutting experiments were accomplished according to the design matrix and in a random order to avoid any systematic error in the experiment.

5. Measuring the responses

All responses, mentioned earlier in chapter one, were measured and at least three to five measurements were recorded for response in all experiment. The average of at least three to five recorded measurements is calculated and used to develop the model.

6. Development of mathematical model

The functional relationship, as an example for three factors, representing any response of interest can be expressed as y = f (A, B, C) and Eq. 3.1 becomes as follows:

$$Y = b_o + b_1 A + b_2 B + b_3 C + b_{11} A^2 + b_{22} B^2 + b_{33} C^2 + b_{12} AB + b_{13} AC + b_{23} BC \qquad (3.3)$$

7. Estimation of the coefficients

Regression analysis is applied to estimate the values of the coefficients in Eq. 3.3. However, the computer software was used to estimate the coefficients for all responses of all experiment.

8. Testing the adequacy of the developed models

The analysis of variance (ANOVA) was used to test the adequacy of the models developed. The statistical significance of the models developed and of each term in regression equation was examined using the sequential F-test, lack-of-fit test and other adequacy measures (i.e. R^2, Adj- R^2, Pred. R^2 and Adeq. Precision ratio) using the same software to obtain the best fit. The Prob.>F (sometimes it called p-value) of the model and of each term in the model can be computed by means of ANOVA. If the Prob.> F of the model and of each term in the model does not exceed the level of significance (say α= 0.05) then the model may be considered adequate within the confidence interval of (1- α). For the lack-of-fit test, the lack of fit could be considered insignificant if the Prob.>F of the lack of fit exceeds the level of significance. Table 3.1 below is a summary of the ANOVA table [139 and 140].

Table 3.1: ANOVA table for full model:

Source	SS	df	MS	$F_{cal.}$- Value	p-value or Prob > F
Model	SS_M	p	Each SS divided by its df	Each MS divided by MS_R	From table or software library
A	SS_a	1			
B	SS_b	1			
C	SS_c	1			
AB	SS_{ab}	1			
AC	SS_{ac}	1			
BC	SS_{bc}	1			
A^2	SS_{aa}	1			
B^2	SS_{bb}	1			
C^2	SS_{cc}	1			
Residual	SS_R	N-p-1			-
Lack of Fit	SS_{lof}	$N - p - n_0$			From table
Pure Error	SS_E	$n_{0 - 1}$			-
Cor Total	SS_T	N - 1	-	-	-

Where:

P: Number of coefficients in the model.
N: Total number of runs.
n_0: Number of centre points.
df: Degree of freedom.
MS: Mean square.

9. Model reduction

The complete mathematical model shown in Eq. 3.3 normally contains terms which are not significant that need to be eliminated (i.e. terms with p-value greater than α). This elimination can be done manually or automatically by choosing one of the selection procedure provided by the software.

10. Development of the final reduced model

At this stage the final reduced model as determined by applying the above steps can be build up. This model contains only the significant terms and the terms that are necessary to maintain hierarchically. Also, reduced quadratic ANOVA table can be produced.

11. Post analysis

By using the adequate model predicting the response within the factors ranges is possible. Further, illustrating the factors effects on certain responses is possible though drawing some plots such as contours and perturbation. In addition, finding the optimal laser cutting conditions which could optimise the process and lead to the desired cut quality is feasible using the developed model.

3.5 Optimisation

3.5.1 Desirability approach

The desirability method has some advantages such as simplicity, availability in the commercial software and provides flexibility in weighting and giving importance for individual response for these reasons it is recommended. Solving such multiple response optimisation problems using this technique consist of using a technique for combining multiple responses into a dimension less measure performance called as overall desirability function. The desirability approach consists of transforming of each estimated response, Y_i, into a unit less utilities bounded by $0 < d_i < 1$, where a higher d_i value indicates that response value Y_i is more desirable, if $d_i = 0$ this means a completely undesired response or vice versa when $d_i = 1$ [146]. In the current work the individual desirability for each response d_i was calculated using Eqs.3.4-3.7. The shape of the desirability function can be changed for each goal by the weight field 'wt_i'. Weights are used to give added emphasis to the upper/lower bounds or to emphasize the target value. Weights could be ranged between 0.1 and 10; weight greater than one gives more emphasis to the goal, while weight less than one gives less emphasis to the goal. With weight value of one, this will make the d_i's vary from zero to one in a linear mode. In the desirability objective function (D), each response can be assigned an importance (r), relative to the other responses. Importance varies from the least important a value of 1(+), to the most important a value of 5(+++++). If the varying degrees of importance are assigned to the different responses, the overall objective function is shown below Eq.3.8. Where n is the number of responses in the measure and T_i is the target value of i^{th} response [141].

- *For goal of maximum, the desirability will define by:*

$$d_i = \begin{cases} 0 & , \quad Y_i \le Low_i \\ \left(\dfrac{Y_i - Low_i}{High_i - Low_i} \right)^{wt_i} & , \quad Low_i \langle Y_i \langle High_i \\ 1 & , \quad Y_i \ge High_i \end{cases} \tag{3.4}$$

- For goal of minimum, the desirability will define by:

$$d_i = \begin{cases} 1 & , \quad Y_i \le Low_i \\ \left(\dfrac{High_i - Y_i}{High_i - Low_i} \right)^{wt_i} & , \quad Low_i \langle Y_i \langle High_i \\ 0 & , \quad Y_i \ge High_i \end{cases} \tag{3.5}$$

- *For goal as a target, the desirability will define by:*

$$d_i = \begin{cases} \left(\dfrac{Y_i - Low_i}{T_i - Low_i} \right)^{wt_{1i}} & , \quad Low_i \langle Y_i \langle T_i \\ \left(\dfrac{Y_i - High_i}{T_i - High_i} \right)^{wt_{2i}} & , \quad T_i \langle Y_i \langle High_i \\ 0 & , \quad Otherwise \end{cases} \tag{3.6}$$

- *For goal within range, the desirability will define by:*

$$d_i = \begin{cases} 1 & , \quad Low_i \langle Y_i \langle High_i \\ 0 & , \quad Otherwise \end{cases} \tag{3.7}$$

$$D = \left(d_1^{r_1} \times d_2^{r_2} \times \ldots \times d_n^{r_n}\right)^{\frac{1}{\sum r_i}} = \left(\prod_{i=1}^{n} d_i^{r_i}\right)^{\frac{1}{\sum r_i}} \quad (3.8)$$

3.5.2 Optimisation approach in Design-Expert software

The optimisation part in Design-expert software V7 searches for a combination of factor levels that simultaneously satisfy the requirements placed (i.e. optimisation criteria) on each one of the responses and process factors (i.e. multiple response optimisation). Numerical and graphical optimisation methods were used in this work by choosing the desired goals for each factor and response. As mentioned earlier the numerical optimisation process involves combining the goals into an overall desirability function (D). The numerical optimisation feature in the design expert software package finds a point or more in the factors domain that would maximise this objective function. In the graphical optimisation with multiple responses, the software defines regions where requirements simultaneously meet the proposed criteria. Superimposing or overlaying critical response contours on a contour plot. Then, visual search for the best compromise becomes possible. In case of dealing with many responses, it is recommended to do numerical optimisation first; otherwise it could be impossible to uncover a feasible region. The graphical optimisation displays the area of feasible response values in the factor space. Regions that do not fit the optimisation criteria are shaded [141].

CHAPTER IV
EXPERIMENTAL WORK

4. EXPERIMENTAL WORK

This chapter describes the material specifications, the experimental procedures followed and the equipment used in the current research.

4.1 Materials

Five standard materials have been for CO_2 laser cutting. These materials were selected due to their applicability to different industries; the objective of this research is to provide information on their cutting input and output performance. The chosen materials are: medical grade stainless steel AISI316, ultra-high molecular weight polyethylene (UHMWPE), medium density fibre board (MDF), polymethyl-methacrylate (PMMA) and glass fibre reinforced plastic (GFRP). These materials are commonly used for different engineering applications such as automotive, simple structural components, pharmaceutical equipment, power plants etc. The detailed specifications of these materials are outlined in the following subsections.

4.1.1 Stainless steel (AISI316L)

AISI 316 is an austenitic stainless steel containing molybdenum, which increases general corrosion resistance, improves resistance to pitting from chloride ion solutions, and provides increased strength at elevated temperatures. Grade 316 has a variety of applications in different industries, such as, food preparation equipment particularly in chloride environments, chemical containers, laboratory benches and equipment, artificial knee and hip joints in bio-medical applications [147, 148 and 149]. Medical grade AISI316L stainless steel in sheet form was used as a workpiece material. The sheet dimensions were 500 x 500 mm and 2 mm thick. The chemical composition and the mechanical properties of this grade are presented in Table 4.1 and Table 4.2 respectively. The spark analyser shown in Fig. 4.1 was used to analyse the chemical composition with the aid of DIA 2000SE software for data management. An average of five measurements was calculated as shown in Table 4.1.

Table 4.1: Typical chemical composite of AISI316 (W%).

Element	C	Si	Mn	P	S	Cr
W%	0.002	0.028	1.142	0.001	0.001	19.7626
Element	Ni	W	Mo	V	Co	Fe
W%	9.200	0.214	2.04	0.155	0.450	Bal.

Table 4.2: Mechanical properties of AISI316.

Property	Value	Unit
Modulus of elasticity	196	GPa
Tensile strength (annealed)	573	MPa
Yield strength (annealed)	236	MPa
Elongation (annealed)	55	%

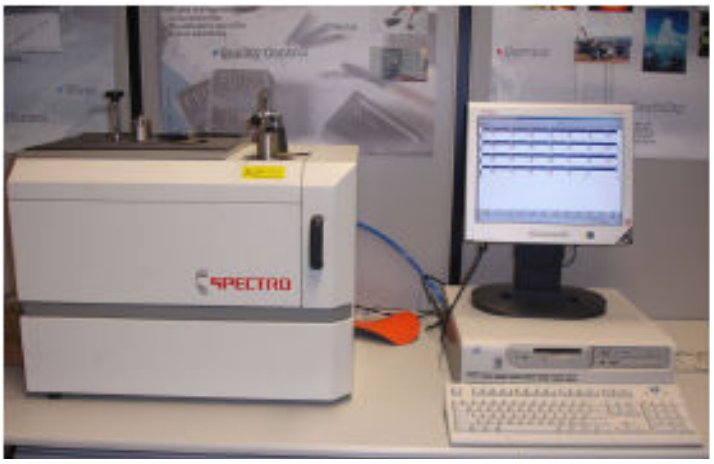

Fig. 4.1: Photograph showing the spark analyser.

4.1.2 Ultra-high molecular weight polyethylene (UHMWPE).

Ultra high molecular weight polyethylene (UHMWPE), also know as high-performance polyethylene is one of the thermoplastic polyethylene. It has the highest impact strength of any thermoplastic currently produced, and consequently, UHMWPE is utilised in many applications [150]. For example, it has been used in clinical applications for over 40 years as a successful biomaterial for hip, knee, and most recently (since the 1980s), for spine implants [151]. It is also used in the fabrication of hydraulic seals, bearings and artificial joints. It is best suited for medium mechanical duties in water, oil hydraulics, pneumatics, and un-lubricated applications [150]. UHMWPE supplied in sheet form with dimensions of 500 x 500 mm and three

thicknesses 6, 8 and 10 mm was used as a substrate for laser cutting. Material, mechanical and thermal properties of this material are presented in Table 4.3.

Table 4.3: Material, mechanical and thermal properties of UHMWPE.

Property	**Units**	**Test Method**	**UHMWPE**
Density	Kg/m^3	ISO 1183	930
Tensile Yield Strength	MPa	ISO 527	17
Tensile Modulus	MPa	ISO 527	700
Impact strength (charpy) at 23°C	kJ/m^2	ISO179	No break
Notched strength (charpy) at 23°C	kJ/m^2	ISO11542-2	≥ 80
Ball indentation hardness	N/mm^2	ISO 2039-1	30-35
Melting temperature	°C	ISO 3146	135-138
Thermal Conductivity	W/(m*K)	ISO 52612	0.4

4.1.3 Polymethyl-methacrylate (PMMA).

Polymethyl-methacrylate (PMMA) is a transparent thermoplastic, often used as a light or shatter-resistant alternative to glass. PMMA is an economical alternative to polycarbonate (PC) when extreme strength is not necessary. Additionally, PMMA does not contain the potentially harmful compounds found in polycarbonate. It is often preferred because of its low cost, moderate properties, easy handling and processing. In fact, PMMA is a versatile material and has been used for a wide range of applications, for example, CDs, toys, boxes, device housings and electronics. PMMA has many applications in medical implantations such as cements for fixing hip and joint prostheses, and replacement intraocular lenses in the eye. PMMA is also used for constructing domestic and commercial aquariums. Occasionally, due to safety and light weight, PMMA is used as an alternative for glass in cars. Moreover, PMMA is used in the sign industry and in modern furniture [152, 153 and154]. The material, mechanical, and thermal properties of this material are illustrated in Table 4.4. PMMA, used for the workpiece, came in sheet form with dimensions of 500 x 500 mm and thicknesses of 2, 4, 6 and 8 mm.

Table 4.4: Material, mechanical and thermal properties of PMMA.

Property	Units	Test Method	PMMA
Density	Kg/m^3	ISO 1183	1180
Tensile Yield Strength	MPa	ISO 527	70
Tensile Modulus	MPa	ISO 527	3300
Impact strength (charpy) at 23°C	kJ/m^2	ISO179	15
Notched strength (charpy) at 23°C	kJ/m^2	ISO11542-2	1.5
Ball indentation hardness	MPa	ISO 2039-1	185
Vicat-softening point	°C	ISO 306	100
Thermal Conductivity	W/(m*K)	ISO 52612	0.19

4.1.4 Medium density fibreboard (MDF)

MDF is an engineered product characterised with great structural integrity, higher dimensional stability and greater flexibility in terms of shaping. Mass-production of this wood composite product commenced in the 1980s. Due to the fact that MDF has no grain, it can be cut, drilled, machined and filed without damaging the surface. However, MDF can be dangerous to use if the correct safety precautions are not taken as it contains a substance called urea formaldehyde, which if released, may cause irritation to the eyes and lungs. MDF panels are suitable for many interior construction and industrial applications. Also, MDF products are increasingly utilised in conventional wood applications that require fungal and insect resistance. MDF is used extensively in factory-assembled and ready-to-assemble furniture, as well as cabinets, drawer fronts, moulding, and counter tops. In addition to this, MDF is replacing thin plywood and wet-process hardboard in the production of moulded and flush door-skins [155, 156 and157]. The specifications of the MDF materials used in this work are listed in Table 4.5. MDF panels supplied in sheet form with dimensions of 500 x 500 mm with three thicknesses of 4, 6 and 9 mm are used as workpiece.

Table 4.5: Properties of MDF panels.

Property	Units	MDF
Density	Kg/m^3	745
Internal bond strength	MPa	> 0.9
Moisture content	%	5-7
Thermal Conductivity	W/(m*K)	0.1-0.2

4.1.5 Glass fibre reinforced plastics (GFRP)

Glass fibre-reinforced plastic (GFRP), also known as, glass-reinforced plastic, is a composite material made of a plastic matrix reinforced by fine glass fibres. GFRP has several advantages including high strength to weight ratio, high fracture toughness and excellent corrosion and thermal resistances. Currently, GFRP becomes an economic alternative to other materials in highly corrosive industrial applications. Furthermore, ongoing research has ensured that GFRP now has a combination of properties such as high specific strength, high specific stiffness and a light weight, that makes it attractive for aircraft and aerospace applications. Actually, GFRP is a promising material for many other applications, including boats, automobiles, water tanks, roofing and pipes [158 and 159]. The properties of the GFRP sheet utilised in this research are listed in Table 4.6. A 3 mm thick GFRP provided in sheet form with dimensions of 900 x 450 mm was used as a workpiece.

Table 4.6: Mechanical properties of GFRP.

Material	**Tensile strength (MPa)**	**Flexural strength, (MPa)**	**Elongation, %**	**Density (kg/m^3)**
Fibre, EMC450	133	175	2.1	-
Resin, polyester	47	90	2.2	1100

4.2 Specimen Design

The specimen geometry is shown in Fig 4.2. The basic geometry was chosen as a 50 mm by 50 mm square, cut in one pass with a 5mm external lead-in. A 50 mm internal slot was cut diagonally through the specimen to maximise the length, while minimising material usage. It was necessary to have an internal slot to maintain dimensional stability for kerf geometry measurements. The laser cut directions are shown in Fig. 4.2.

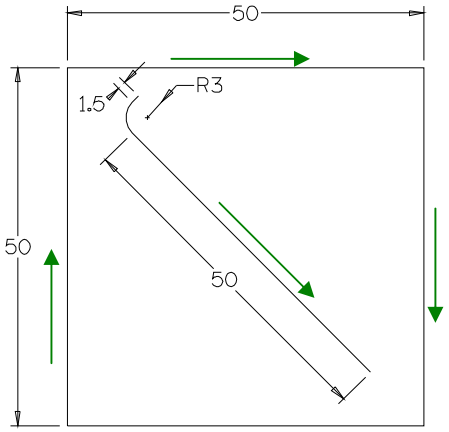

Fig. 4.2: Specimen geometry and laser cutting direction, dimensions in mm.

4.3 Laser cutting machine

The laser used is a Rofin DC 015 industrial CO_2 slab laser which operates at 1.5 kW output power with a wavelength of 10.6 μm and a linear polarised beam angled at 45°. This laser is a high frequency excited, diffusion cooled CO_2 gas laser, designed for materials processing on an industrial scale, e.g. cutting, welding, hardening, engraving, marking, and cladding. The laser machine at Dublin City University shown in Fig. 4.3 is provided by Mechtronic Industries, which supply the Rofin laser with motion table and control software. The machine type is MTI 0505 Scientific, incorporated with two Mannesman Rexroth precision machine tables with a resolution of 0.00125 mm, to provide XY motion of 50 x 50 cm. A speed controller is provided to control the speed from 1 mm/min to 5000 mm/min in 1 mm steps. This laser machine is equipped with a power supply, computer rack, controller terminal, water chiller, air compressor and fume extraction system. The beam delivery system in this machine accepts both 127 and 190 mm FL high pressure lenses. The beam delivery system has a high pressure nozzle assembly with four thumbscrew adjusters to centre the assist gas around the beam, and replaceable copper nozzles which allow a stand-off distance between material and workpiece of 1 mm at 50% shoe height. The lens assembly allows ±10 mm lens focal position, relative to the tip via a micrometer movement which is operated manually by a rotating drum. The gas used for the operation is a Premix laser gas. It contains a 94%

mixture of carbon dioxide, helium, nitrogen and xenon, plus 6% of potential hazardous carbon monoxide. The laser gas bottle contains 1500 standard litres. The specifications of this machine are presented in Table 4.7 [160 and161].

Fig. 4.3: Photograph of the laser machine and its units.

Table 4.7: Laser machine specifications.

Voltage	3x230/400 V, at 50 or 60 Hz
Max current consumption	38-45A
Stability	±2% (cooling water ΔT ≤±1K)
Beam Quality factor	k>0.9
Width	26 µs-CW
Laser gas	Rofin-Sinar special-Premix
Consumption	<0.15 l/h
Laser gas exchange intervals	72 h
Mode	semiautomatic
Cooling water	Demineralized water
Minimal flow rate	≥4000 l/h
Supply pressure	6 bars
temperature	20 C
Refrigeration Capacity	≥24 kW
Laser head	L=1700mm W=800mm H=853mm
Control Cabinet	W=800 D=600 H=1900
Head weight	500kg
Cabinet weight	570kg

4.4 Laser cutting

In this research, as mentioned earlier, five materials with different thicknesses were investigated. As reported by many authors, to avail form the whole range of each factor Box-Behnken design was choosing. The experiments were designed based on a three level Box-Behnken design with full replication [139 and 140]. Trial laser cut runs were performed by varying one of the process factors at-a-time to determine the range of each factor. These trial runs were performed for all materials and thicknesses. The criteria for selecting the working ranges were full cut while keeping the following to a minimum: the kerf width, cutting edge striations and dross. For all materials the main experiment was performed as per the design matrices in a random order to avoid any systematic error. A CW 1.5 kW CO_2 Rofin laser and a focusing lens with focal length of 127 mm were used to perform the cut. For safety reasons, only the trained technician was allowed to operate the laser machine under the student instructions. All other experimental measurements and analysis were carried out by the author.

4.4.1 Laser cutting of AISI 316L stainless steel

For AISI316L laser power, cutting speed, focal point position, nitrogen pressure and nozzle diameter are the process input parameters. The stand-off distance is kept constant at 0.5 mm. Table 4.8 shows the LBC parameters and experimental design levels used. As recommended in [19, 24 and 34] nitrogen gas was used as an assist gas to ensure a brighter and smoother cut surface with smaller kerf. The specimens were cut from the plate for each condition according to Table 4.9.

Table 4.8: Process variables and experimental design levels for AISI 316.

Parameter	Code	Unit	-1	0	+1
Laser power	A	kW	1	1.25	1.5
Cutting speed	B	mm/min	1000	2000	3000
Focal point position	C	mm	-4	-3	-2
Gas pressure	D	Bar	10	12.5	15
Nozzle diameter*	E	mm	1	1.5	2

* Categorical factor.

Table 4.9: Design matrix for AISI 316.

Std	Run	A, kW	B, mm/min	C, mm	D, bar	E, mm	Std	Run	A, kW	B, mm/min	C, mm	D, bar	E, mm
1	21	1	1000	-3	12.5	1.5	24	**36**	1.25	3000	-2	12.5	1.5
2	33	1.5	1000	-3	12.5	1.5	25	**3**	1	2000	-3	10	1.5
3	41	1	3000	-3	12.5	1.5	26	**46**	1.5	2000	-3	10	1.5
4	45	1.5	3000	-3	12.5	1.5	27	**4**	1	2000	-3	15	1.5
5	40	1.25	2000	-4	10	1.5	28	**28**	1.5	2000	-3	15	1.5
6	23	1.25	2000	-2	10	1.5	29	**38**	1.25	2000	-4	12.5	1
7	5	1.25	2000	-4	15	1.5	30	**29**	1.25	2000	-2	12.5	1
8	25	1.25	2000	-2	15	1.5	31	**27**	1.25	2000	-4	12.5	2
9	2	1.25	1000	-3	12.5	1	32	**11**	1.25	2000	-2	12.5	2
10	34	1.25	3000	-3	12.5	1	33	**13**	1	2000	-3	12.5	1
11	1	1.25	1000	-3	12.5	2	34	**16**	1.5	2000	-3	12.5	1
12	19	1.25	3000	-3	12.5	2	35	**37**	1	2000	-3	12.5	2
13	17	1	2000	-4	12.5	1.5	36	**42**	1.5	2000	-3	12.5	2
14	24	1.5	2000	-4	12.5	1.5	37	**10**	1.25	1000	-3	10	1.5
15	18	1	2000	-2	12.5	1.5	38	**9**	1.25	3000	-3	10	1.5
16	8	1.5	2000	-2	12.5	1.5	39	**14**	1.25	1000	-3	15	1.5
17	7	1.25	2000	-3	10	1	40	**26**	1.25	3000	-3	15	1.5
18	6	1.25	2000	-3	15	1	41	**43**	1.25	2000	-3	12.5	1.5
19	15	1.25	2000	-3	10	2	42	**35**	1.25	2000	-3	12.5	1.5
20	12	1.25	2000	-3	15	2	43	**32**	1.25	2000	-3	12.5	1.5
21	39	1.25	1000	-4	12.5	1.5	44	**22**	1.25	2000	-3	12.5	1.5
22	30	1.25	3000	-4	12.5	1.5	45	**31**	1.25	2000	-3	12.5	1.5
23	20	1.25	1000	-2	12.5	1.5	46	**44**	1.25	2000	-3	12.5	1.5

4.4.2 Laser cutting of UHMWPE

In this case, laser power, cutting speed and focal point position are the laser beam cutting LBC process input parameters. Table 4.10 shows the LBC parameters and experimental design levels used for the three thicknesses (6, 8 and 10mm). For this experiment, the stand-off distance and the nozzle diameter were kept constant at 0.5 mm and 1.5 mm respectively. It was noted during the trial experiments for this material that the use of an air pressure above or below the selected threshold for each thickness did not lead to a full cut. Below this threshold the air pressure was not sufficient to perform the cut and above it the cooling effect of the compressed air was found to obstruct the progression of the cut. Air is normally used as an assist gas when cutting plastics as mentioned in [48 and 58] and to reduce the gas cost if another inert gas is used. As a result, compressed air was supplied coaxially as an assist gas with a constant pressure of 3 bar for 6 mm thick and 2 bar for 8 and 10 mm thick UHMWPE. The specimens were cut from the plates for each condition according to Tables 4.11- 4.13.

Table 4.10: Process variables and experimental design levels for UHMWPE.

Parameter	**Code**	**Unit**	**Levels**								
			-1			**0**			**+1**		
			Thickness, mm			**Thickness, mm**			**Thickness, mm**		
			6	**8**	**10**	**6**	**8**	**10**	**6**	**8**	**10**
Laser power	A	kW	800	900	1100	1050	1150	1275	1300	1400	1450
Cutting speed	B	mm/min	1000	800	700	1375	1100	925	1750	1400	1150
Focal point position	C	mm	-4	-6	-7	-2.5	-4.5	-5.5	-1	-3	-4

Table 4.11: Design matrix for 6 mm thick UHMWPE.

Std	Run	Factors		
		A, W	B, mm/min	C, mm
1	10	800	1000	-2.5
2	13	1300	1000	-2.5
3	15	800	1750	-2.5
4	3	1300	1750	-2.5
5	7	800	1375	-4
6	8	1300	1375	-4
7	5	800	1375	-1
8	2	1300	1375	-1
9	6	1050	1000	-4
10	4	1050	1750	-4
11	12	1050	1000	-1
12	11	1050	1750	-1
13	14	1050	1375	-2.5
14	16	1050	1375	-2.5
15	17	1050	1375	-2.5
16	9	1050	1375	-2.5
17	1	1050	1375	-2.5

Table 4.12: Design matrix for 8 mm thick UHMWPE.

Std	Run	Factors		
		A, W	B, mm/min	C, mm
1	13	900	800	-4.5
2	1	1400	800	-4.5
3	17	900	1400	-4.5
4	3	1400	1400	-4.5
5	4	900	1100	-6
6	8	1400	1100	-6
7	9	900	1100	-3
8	11	1400	1100	-3
9	5	1150	800	-6
10	10	1150	1400	-6
11	7	1150	800	-3
12	15	1150	1400	-3
13	2	1150	1100	-4.5
14	6	1150	1100	-4.5
15	14	1150	1100	-4.5
16	16	1150	1100	-4.5
17	12	1150	1100	-4.5

Table 4.13: Design matrix for 10 mm thick UHMWPE.

Std	Run	Factors		
		A, W	B, mm/min	C, mm
1	12	1100	700	-5.5
2	9	1450	700	-5.5
3	2	1100	1150	-5.5
4	16	1450	1150	-5.5
5	14	1100	925	-7
6	6	1450	925	-7
7	8	1100	925	-4
8	10	1450	925	-4
9	4	1275	700	-7
10	3	1275	1150	-7
11	11	1275	700	-4
12	17	1275	1150	-4
13	15	1275	925	-5.5
14	1	1275	925	-5.5
15	5	1275	925	-5.5
16	13	1275	925	-5.5
17	7	1275	925	-5.5

4.4.3 Laser cutting of PMMA

For this material, four process parameters were considered namely: laser power, cutting speed, air pressure and focal point position. Table 4.14 shows the process input parameters and experimental design levels used for the four thicknesses (2, 4, 6 and 8 mm). Similarly, for this material the stand-off distance and the nozzle diameter were kept constant at 0.5 mm and 1.5 mm respectively. As reported in [48 and 58], compressed air is usually used as an assist gas when cutting PMMA and also, to reduce the operating cost. For these two reasons the compressed air was supplied coaxially to assist the cutting process. The specimens were cut from the plate for each condition according to Tables 4.15-4.18.

Table 4.14: Process variables and experimental design levels for PMMA.

Parameter	Levels											
	-1				0				+1			
	Thickness, mm				Thickness, mm				Thickness, mm			
	2	4	6	8	2	4	6	8	2	4	6	8
A, kW	100	200	350	450	225	350	525	625	350	500	700	800
B, mm/min	1500	1200	1000	800	3250	3100	2300	2000	5000	5000	3600	3200
C, bar	0.5	0.5	0.5	0.5	1	1.25	1.75	1.75	1.5	2	3	3
D, mm	-3	-4	-5	-6	-2	-3	-3.5	-4.5	-1	-2	-2	-3

Table 4.15: Design matrix for 2 mm thick PMMA.

Std	Run	Factors			
		A, W	B, mm/min	C, bar	D, mm
1	17	100	1500	1	-2
2	29	350	1500	1	-2
3	11	100	5000	1	-2
4	20	350	5000	1	-2
5	9	225	3250	0.5	-3
6	22	225	3250	1.5	-3
7	24	225	3250	0.5	-1
8	25	225	3250	1.5	-1
9	19	100	3250	1	-3
10	14	350	3250	1	-3
11	16	100	3250	1	-1
12	2	350	3250	1	-1
13	4	225	1500	0.5	-2
14	18	225	5000	0.5	-2
15	1	225	1500	1.5	-2
16	15	225	5000	1.5	-2
17	26	100	3250	0.5	-2
18	3	350	3250	0.5	-2
19	6	100	3250	1.5	-2
20	12	350	3250	1.5	-2
21	27	225	1500	1	-3
22	8	225	5000	1	-3
23	21	225	1500	1	-1
24	10	225	5000	1	-1
25	13	225	3250	1	-2
26	5	225	3250	1	-2
27	28	225	3250	1	-2
28	7	225	3250	1	-2
29	23	225	3250	1	-2

Table 4.16: Design matrix for 4 mm thick PMMA.

Std	Run	Factors			
		A, W	B, mm/min	C, bar	D, mm
1	9	200	1200	1.25	-3
2	13	500	1200	1.25	-3
3	26	200	5000	1.25	-3
4	23	500	5000	1.25	-3
5	6	350	3100	0.5	-4
6	11	350	3100	2	-4
7	5	350	3100	0.5	-2
8	14	350	3100	2	-2
9	8	200	3100	1.25	-4
10	15	500	3100	1.25	-4
11	29	200	3100	1.25	-2
12	21	500	3100	1.25	-2
13	10	350	1200	0.5	-3
14	25	350	5000	0.5	-3
15	4	350	1200	2	-3
16	19	350	5000	2	-3
17	16	200	3100	0.5	-3
18	24	500	3100	0.5	-3
19	7	200	3100	2	-3
20	12	500	3100	2	-3
21	28	350	1200	1.25	-4
22	2	350	5000	1.25	-4
23	18	350	1200	1.25	-2
24	1	350	5000	1.25	-2
25	20	350	3100	1.25	-3
26	3	350	3100	1.25	-3
27	17	350	3100	1.25	-3
28	22	350	3100	1.25	-3
29	27	350	3100	1.25	-3

Table 4.17: Design matrix for 6 mm thick PMMA.

Std	Run	Factors			
		A, W	B, mm/min	C, bar	D, mm
1	12	350	1000	1.75	-3.5
2	28	700	1000	1.75	-3.5
3	20	350	3600	1.75	-3.5
4	1	700	3600	1.75	-3.5
5	14	525	2300	0.5	-5
6	13	525	2300	3	-5
7	26	525	2300	0.5	-2
8	6	525	2300	3	-2
9	22	350	2300	1.75	-5
10	9	700	2300	1.75	-5
11	8	350	2300	1.75	-2
12	23	700	2300	1.75	-2
13	27	525	1000	0.5	-3.5
14	21	525	3600	0.5	-3.5
15	15	525	1000	3	-3.5
16	10	525	3600	3	-3.5
17	29	350	2300	0.5	-3.5
18	7	700	2300	0.5	-3.5
19	25	350	2300	3	-3.5
20	18	700	2300	3	-3.5
21	5	525	1000	1.75	-5
22	19	525	3600	1.75	-5
23	2	525	1000	1.75	-2
24	24	525	3600	1.75	-2
25	17	525	2300	1.75	-3.5
26	11	525	2300	1.75	-3.5
27	16	525	2300	1.75	-3.5
28	3	525	2300	1.75	-3.5
29	4	525	2300	1.75	-3.5

Table 4.18: Design matrix for 8 mm thick PMMA.

Std	Run	Factors			
		A, W	B, mm/min	C, bar	D, mm
1	27	450	800	1.75	-4.5
2	7	800	800	1.75	-4.5
3	5	450	3200	1.75	-4.5
4	24	800	3200	1.75	-4.5
5	17	625	2000	0.5	-6
6	18	625	2000	3	-6
7	26	625	2000	0.5	-3
8	8	625	2000	3	-3
9	3	450	2000	1.75	-6
10	9	800	2000	1.75	-6
11	20	450	2000	1.75	-3
12	29	800	2000	1.75	-3
13	1	625	800	0.5	-4.5
14	23	625	3200	0.5	-4.5
15	15	625	800	3	-4.5
16	12	625	3200	3	-4.5
17	11	450	2000	0.5	-4.5
18	22	800	2000	0.5	-4.5
19	13	450	2000	3	-4.5
20	28	800	2000	3	-4.5
21	4	625	800	1.75	-6
22	10	625	3200	1.75	-6
23	6	625	800	1.75	-3
24	25	625	3200	1.75	-3
25	21	625	2000	1.75	-4.5
26	14	625	2000	1.75	-4.5
27	19	625	2000	1.75	-4.5
28	16	625	2000	1.75	-4.5
29	2	625	2000	1.75	-4.5

4.4.4 Laser cutting of MDF

For this material, four process parameters were controlled namely: laser power, cutting speed, air pressure and focal point position. Table 4.19 shows the process input parameters and experimental design levels used for the three thicknesses (4, 6 and 9 mm). Dry panels of MDF wood composite in sheet form were used as a workpiece material. The sheet dimensions were 500 x 500 mm with thicknesses of 4, 6 and 9 mm. Fig. 4.4 shows the location of the focal plane relative to the upper surface for 6 mm MDF board. Among the trial laser cut runs, no significant difference was noted in terms of kerf width, roughness values and edge burn between the samples processed using nitrogen and the samples processed using compressed air. Also, it was reported in [74 and 77] that there is no significant reduction in the kerf width when using either compressed air or nitrogen. Importantly, compressed air is cheaper than nitrogen. Therefore, compressed air was supplied coaxially as an assist gas with different pressures. The nozzle used has a conical shape with nozzle diameter of 1.5 mm and the stand-off distance was kept constant at 0.5 mm. Specimens were cut from the panel for each condition according to the values shown in Tables 4.20-4.22.

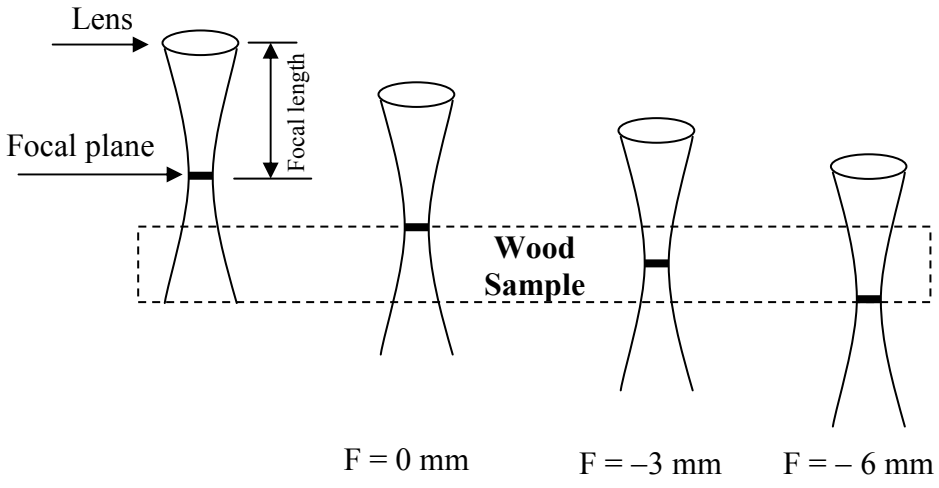

Fig. 4.4: Schematic plot showing the location of the focus of the beam relative to the upper surface.

Table 4.19: Process variables and experimental design levels.

Parameter	Code	Unit	Levels								
			-1			0			+1		
			Thickness, mm			Thickness, mm			Thickness, mm		
			4	6	9	4	6	9	4	6	9
Laser power	A	W	150	270	375	275	385	487.5	400	500	600
Cutting speed	B	mm/min	2000	2000	2000	3500	3500	3500	5000	5000	5000
Air pressure	C	bar	3	4	4	4.5	5.5	6	6	7	8
Focal point position	D	mm	-4	-6	-7	-2	-3	-3.5	0	0	0

Table 4.20: Design matrix for 4 mm thick MDF.

Std	Run	Factors			
		A, W	B, mm/min	C, bar	D, mm
1	25	150	2000	4.5	-2
2	13	400	2000	4.5	-2
3	1	150	5000	4.5	-2
4	14	400	5000	4.5	-2
5	24	275	3500	3	-4
6	8	275	3500	6	-4
7	22	275	3500	3	0
8	23	275	3500	6	0
9	17	150	3500	4.5	-4
10	28	400	3500	4.5	-4
11	27	150	3500	4.5	0
12	3	400	3500	4.5	0
13	29	275	2000	3	-2
14	11	275	5000	3	-2
15	16	275	2000	6	-2
16	6	275	5000	6	-2
17	12	150	3500	3	-2
18	20	400	3500	3	-2
19	5	150	3500	6	-2
20	9	400	3500	6	-2
21	26	275	2000	4.5	-4
22	19	275	5000	4.5	-4
23	4	275	2000	4.5	0
24	18	275	5000	4.5	0
25	15	275	3500	4.5	-2
26	2	275	3500	4.5	-2
27	21	275	3500	4.5	-2
28	10	275	3500	4.5	-2
29	7	275	3500	4.5	-2

Table 4.21: Design matrix for 6 mm thick MDF.

Std	Run	Factors			
		A, W	B, mm/min	C, bar	D, mm
1	25	270	2000	5.5	-3.0
2	28	500	2000	5.5	-3.0
3	19	270	5000	5.5	-3.0
4	24	500	5000	5.5	-3.0
5	3	385	3500	4	-6.0
6	14	385	3500	7	-6.0
7	23	385	3500	4	0.0
8	5	385	3500	7	0.0
9	10	270	3500	5.5	-6.0
10	9	500	3500	5.5	-6.0
11	26	270	3500	5.5	0.0
12	22	500	3500	5.5	0.0
13	20	385	2000	4	-3.0
14	15	385	5000	4	-3.0
15	17	385	2000	7	-3.0
16	11	385	5000	7	-3.0
17	12	270	3500	4	-3.0
18	1	500	3500	4	-3.0
19	27	270	3500	7	-3.0
20	21	500	3500	7	-3.0
21	4	385	2000	5.5	-6.0
22	13	385	5000	5.5	-6.0
23	18	385	2000	5.5	0.0
24	6	385	5000	5.5	0.0
25	8	385	3500	5.5	-3.0
26	16	385	3500	5.5	-3.0
27	2	385	3500	5.5	-3.0
28	7	385	3500	5.5	-3.0
29	29	385	3500	5.5	-3.0

Table 4.22: Design matrix for 9 mm thick MDF.

Std	Run	Factors			
		A, W	B, mm/min	C, bar	D, mm
1	15	375	2000	6	-3.5
2	25	600	2000	6	-3.5
3	7	375	5000	6	-3.5
4	19	600	5000	6	-3.5
5	13	487.5	3500	4	-7.0
6	1	487.5	3500	8	-7.0
7	18	487.5	3500	4	0.0
8	5	487.5	3500	8	0.0
9	28	375	3500	6	-7.0
10	26	600	3500	6	-7.0
11	10	375	3500	6	0.0
12	20	600	3500	6	0.0
13	12	487.5	2000	4	-3.5
14	9	487.5	5000	4	-3.5
15	17	487.5	2000	8	-3.5
16	6	487.5	5000	8	-3.5
17	3	375	3500	4	-3.5
18	23	600	3500	4	-3.5
19	22	375	3500	8	-3.5
20	29	600	3500	8	-3.5
21	4	487.5	2000	6	-7.0
22	11	487.5	5000	6	-7.0
23	2	487.5	2000	6	0.0
24	21	487.5	5000	6	0.0
25	16	487.5	3500	6	-3.5
26	27	487.5	3500	6	-3.5
27	14	487.5	3500	6	-3.5
28	8	487.5	3500	6	-3.5
29	24	487.5	3500	6	-3.5

4.4.5 Laser cutting of GFRP

Regarding GFRP, four process parameters were controlled laser power, cutting speed, air pressure and focal point position. Table 4.23 shows the process input parameters and experimental design levels used for 3 mm thick GFRP. GFRP composite material in sheet form was used as a workpiece material. A conical shape nozzle was used with nozzle diameter of 1.5 mm and the stand-off distance was maintained at a constant value of 0.5 mm. During the trial cut runs it was found that argon was the most suitable inert gas and leads to good quality cut with less edge burning and minimum HAZ, kerf and roughness value. Therefore, argon gas was supplied coaxially as an assist gas. Specimens were cut from the panel for each condition in Table 4.24.

Table 4.23: Process variables and experimental design levels for GFRP.

Parameter	Code	Unit	-1	0	+1
Laser power	A	kW	500	900	1300
Cutting speed	B	mm/min	2000	3500	5000
Argon pressure	C	bar	2	3	4
Focal point position	D	mm	-3	-1.5	0

Table 4.24: Design matrix for 3 mm thick GFRP.

Std	Run	Factors			
		A, W	B, mm/min	C, bar	D, mm
1	24	500	2000	3	-1.5
2	18	1300	2000	3	-1.5
3	27	500	5000	3	-1.5
4	17	1300	5000	3	-1.5
5	5	900	3500	2	-3
6	3	900	3500	4	-3
7	21	900	3500	2	0
8	13	900	3500	4	0
9	14	500	3500	3	-3
10	26	1300	3500	3	-3
11	1	500	3500	3	0
12	2	1300	3500	3	0
13	19	900	2000	2	-1.5
14	9	900	5000	2	-1.5
15	6	900	2000	4	-1.5
16	7	900	5000	4	-1.5
17	8	500	3500	2	-1.5
18	15	1300	3500	2	-1.5
19	12	500	3500	4	-1.5
20	23	1300	3500	4	-1.5
21	10	900	2000	3	-3
22	16	900	5000	3	-3
23	11	900	2000	3	0
24	22	900	5000	3	0
25	25	900	3500	3	-1.5
26	4	900	3500	3	-1.5
27	20	900	3500	3	-1.5
28	29	900	3500	3	-1.5
29	28	900	3500	3	-1.5

4.5 Measurements of the Quality Characterises (Responses)

The quality characteristics in laser cutting have been highlighted by Pietro and Yao [27] as follows: kerf width, cut edge squareness, inner side slope of the kerf, HAZ extent, dross appearance and surface roughness. In this research, five different quality features were considered to characterise the quality of the cut. Firstly, kerf width was considered; this refers to the width of the slot that is formed during through-thickness cutting. The kerf is not generally symmetrical however, it is usually found to be wider at the top or bottom surface, depending on the focusing optics of the beam. As mentioned earlier, the focus position can alter the beam diameter at the upper and lower surface which may have an effect on the upper and lower kerf widths. Therefore, two kerf widths were measured namely: the upper kerf width and the lower kerf width. The ratio between these two kerf widths is of great importance as it represents the cut edge squareness and inner side slope. In this work the ratio between the two kerf widths was calculated for all specimens. Ideally, it should be as close as possible to one to ensure edge perpendicularity. Moreover, surface roughness and striation are of extra importance in laser cutting and the arithmetic average roughness parameter, Ra, was found to be a reliable parameter for characterising the profile [27]. Furthermore, it is known that surface roughness affects fatigue life, corrosion, friction and thermal conductivity of parts [51]. Consequently, in this work Ra values were considered as a quality feature. The HAZ was taken into consideration as a quality feature in some cases only, as it is not possible to measure it for some materials.

4.5.1 Measurements of kerf widths

The upper and the lower kerf widths were measured using a Mitutoyo optical microscope with attached digital micrometer. This microscope has an accuracy of 0.000 mm allows measurement in both the x-axis and y-axis directions, see Fig. 4.5. The average of at least five results of each kerf width was calculated for each sample for all materials and recorded for further analysis. As some of the materials under investigation were translucent it was necessary to apply ink to the samples as shown in Fig. 4.6 to provide sufficient contrast to accurately identify the edge of the kerf. Both the upper and

lower kerf width measurements were carried out for the internal, diagonal cut. Five measurements were taken, centred on the midpoint of the diagonal cut and spaced approximately 5 mm apart. No measurements were taken from the areas at the start and end of the cut in order to eliminate the effect of the acceleration and deceleration of the machine table on the cutting speed. In each case the results were recorded and the average was calculated for further analysis. The ratio of the average upper and lower kerf widths was calculated to approximate the degree of taper of the cut, with a ratio of 1 indicating a plane parallel cut.

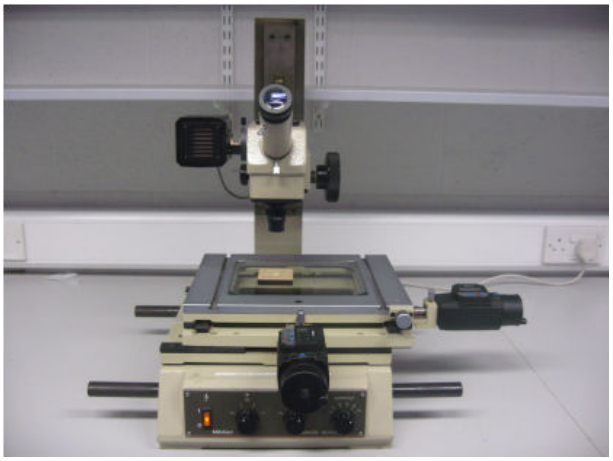

Fig. 4.5: Photograph showing the microscope used to measure the kerf width and HAZ.

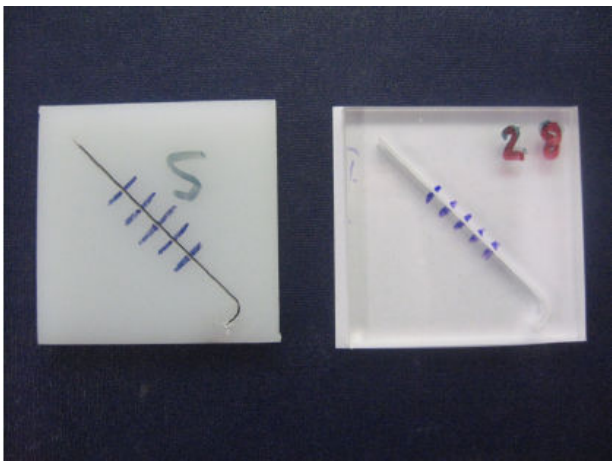

Fig. 4.6: Photograph showing the ink applied to specimen surface for kerf measurement.

4.5.2 Measurements of surface roughness

The arithmetic average roughness parameter, Ra, values were measured using a surface roughness tester model TR-200 shown in Fig. 4.7(a). Pietro and Yao [27] have concluded that the measurements of Ra can only be recorded soon after performing the cut. As a result of these findings, the surface roughness test was carried out straight after the laser cutting process. Five consistent surface roughness values for each specimen were measured at the centre of the cut surface as presented in Fig. 4.7(b and c) and an average was calculated for each specimen. Then, the average value was recorded for each specimen for all materials.

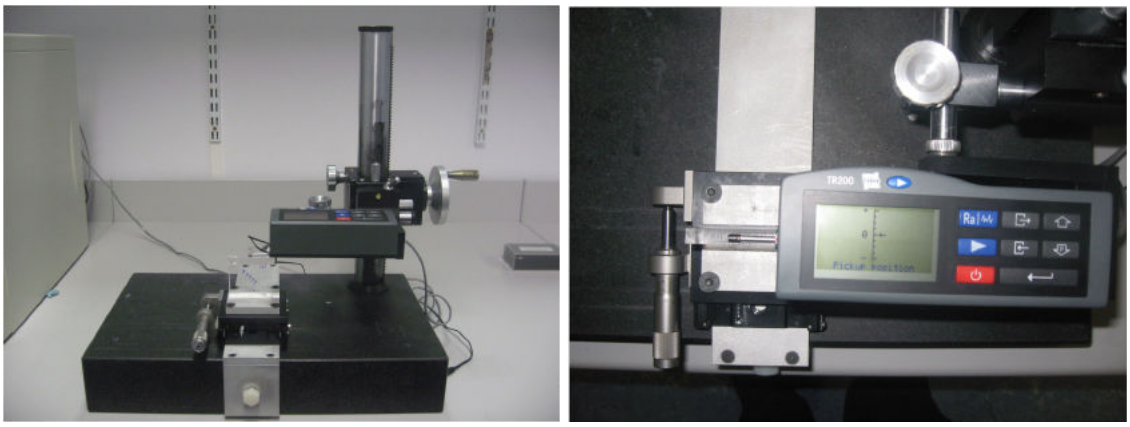

(a) (b)

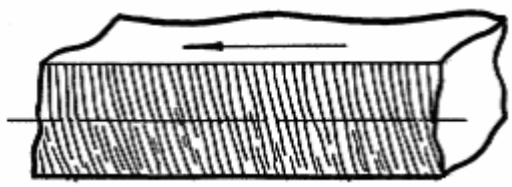

(c)

Fig. 4.7: Photograph showing (a) the surface roughness tester TR-200 and (b) pick up position and (c) line of measuring Ra.

4.5.3 Measurements of heat-affected zone

The heat-affected zone was measured on the top side of the specimen as shown in Fig. 4.8 using the Mitutoyo optical microscope described earlier. In the case of PMMA, the scanning electron microscope SEM shown in Fig. 4.9 was used to measure the HAZ extent. However, the measurement of HAZ was unachievable in some cases (e.g. AISI316, UHMWPE and MDF) due to the small size of HAZ making measurement unclear, or its values too close to each other, which in turn does not facilitate model development as the best fit is the mean of these values. In the cases where the HAZ extent was measured an average of at least three measurements was calculated for each sample.

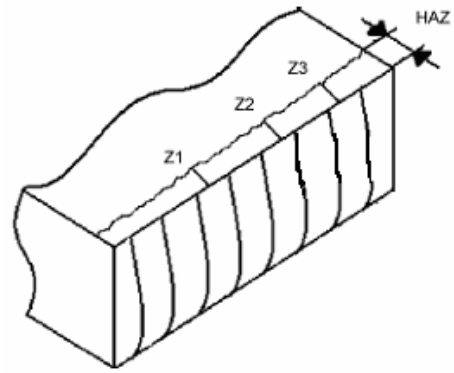

Fig. 4.8: Schematic diagram showing the HAZ extent.

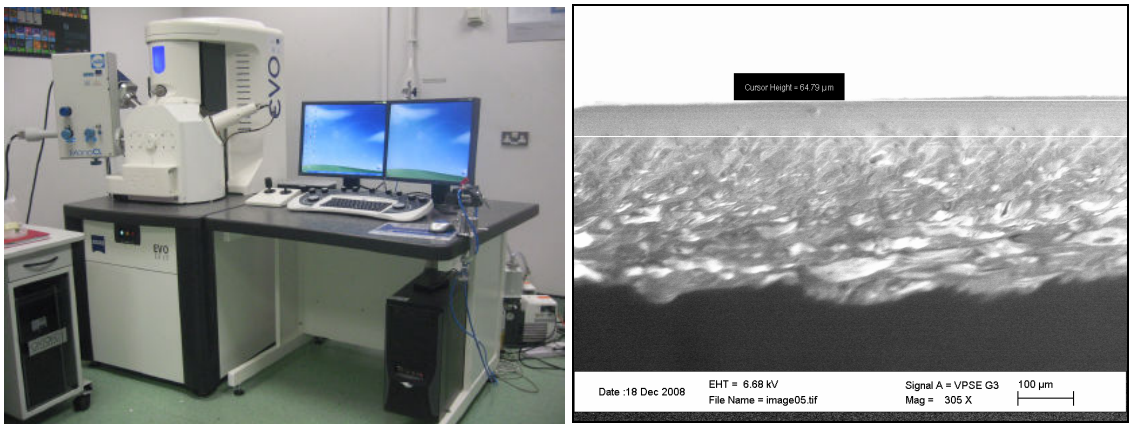

(a) (b)

Fig. 4.9: Photograph showing (a) the SEM and (b) micrograph of HAZ extent for 2 mm PMMA.

4.5 Estimation of operating cost

Laser cutting operating costs can be estimated as cutting per hour or per unit length. The laser system used in this work utilised CO_2 using a static volume of laser gases of approximately 7.5 litres every 72 hours. For this laser system with 1.5 kW maximum output power the operating costs generally falls into the categories listed in Tables 4.25-4.27. The operating cost calculation does not account for any unscheduled breakdowns and maintenance, such as a breakdown in the table motion controller or PC hard disc replacement.

4.5.1 Operating cost when compressed nitrogen gas is used

The total approximated operating cost per hour as a function of process parameters can be estimated by $2.654+1.376xP + 9.60x10^{-3}xF$. While the total approximated operating cost per unit length of the cut is given by Eq. 4.1, assuming 85% utilisation. Eq. 4.2 was used to calculate the cutting cost per meter for all samples.

Table 4.25: Operating costs break down when nitrogen is used.

Element of cost	Calculations	Cutting cost €/hr
Laser electrical power	(20.88 kVA)(0.8 pf)(€ 0.12359/kWhr)x(P/1.5)	1.376xP
Chiller electrical power	(11.52 kVA)(0.8 pf)(€ 0.12359/kWhr)	1.139
Motion controller power	(4.8 kVA)(0.8 pf)(€ 0.12359/kWhr)	0.475
Exhaust system power	(0.9 kWhr)(€ 0.12359/kWhr)	0.111
Laser gas LASPUR208	{(€1043.93/ bottle)/(1500liter/bottle)}x 7.5Liter/72hr	0.072
Gas bottle rental	(€181.37/720hr)	0.252
Chiller additives	(€284.80/year)/(8760 hr/year)	0.033
Compressed nitrogen	€9.60 x 10^{-3}/liter x F[litre/hr]	$9.60x10^{-3}xF$
Nozzle tip	(€7.20/200hr)	0.036
Exhaust system filters	(€5/100hr)	0.05
Focus lens	(€186/lens)/(1000hr)	0.186
Maintenance labour (with overhead)	(12 hr/2000hrs operation)(€50/hr)	0.30
Total operation cost per hour		$2.654+1.376xP +9.60 x10^{-3}xF$

$$\text{Cutting cost[Euro/m]} = \frac{2.654 + 1.376 \times \text{P [kW]} + 9.60\,\text{x}10^{-3} \times \text{F[l/hr]}}{(0.85) \times \text{S[mm/min][60min/hr][m/1000mm]}} \tag{4.1}$$

$$\text{cutting cost[Euro/m]} = \frac{2.654 + 1.376 \times \text{P} + 9.60\text{x}10^{-3} \times \text{F}}{0.051 \times \text{S}} \tag{4.2}$$

Where

P: used out put power in kW.
F: flow rate in l/hr.
S: cutting speed in mm/min.

At pressures above 1, 0.89 and 1.05 bar the compressed nitrogen, compressed air and compressed argon will flow in a supersonic manner. Note that these pressure values are independent of nozzle diameter. At pressure values above these thresholds the flow rate in [l/hr] of these fluids through a nozzle can be easily calculated from Eq. 4.3 [4].

$$\text{Flow Rate [l/hr]} = \text{F} = 492 \times d^2 \left(p_g + 1 \right) \tag{4.3}$$

where:

d: Nozzle diameter [mm].

P_g: Nozzle supply pressure [bar].

4.5.2 Operating cost when compressed air is used

The total approximated operating cost per hour as a function of process parameters can be estimated by 2.654+1.376xP +1.3718x10^{-5}xF. While the total approximated operating cost per unit length of the cut is given by Eq. 4.4 assuming 85% utilisation. Eq. 4.5 was used to calculate the cutting cost per meter for all samples.

Table 4.26: Operating costs break down when compressed air is used.

Element of cost	Calculations	Cutting cost €/hr
Laser electrical power	(20.88 kVA)(0.8 pf)(€ 0.12359/kWhr)x(P/1.5)	1.376xP
Chiller electrical power	(11.52 kVA)(0.8 pf)(€ 0.12359/kWhr)	1.139
Motion controller power	(4.8 kVA)(0.8 pf)(€ 0.12359/kWhr)	0.475
Exhaust system power	(0.9 kWhr)(€ 0.12359/kWhr)	0.111
Laser gas LASPUR208	{(€1043.93/ bottle)/(1500litre/bottle)}x 7.5Liter/72hr	0.072
Gas bottle rental	(€181.37/720hr)	0.252
Chiller additives	(€284.80/year)/(8760 hr/year)	0.033
Compressed air	(0.111 kW/m^3)(€0.12359/kWhr)x(m^3/1000liter)	$1.3718x10^{-5}$ [€/l] x F[l/hr]
Nozzle tip	(€7.20/200hr)	0.036
Exhaust system filters	(€5/100hr)	0.05
Focus lens	(€186/lens)/(1000hr)	0.186
Maintenance labour (with overhead)	(12 hr/2000hrs operation)(€50/hr)	0.30
Total operation cost per hour		$2.654+1.376xP+1.3718x10^{-5}xF$

$$\text{Cutting cost[Euro/m]} = \frac{2.654 + 1.376 \times \text{P[kW]} + 1.3718x10^{-5} \times \text{F[l/hr]}}{(0.85) \times \text{S[mm/min][60min/hr][m/1000mm]}} \tag{4.4}$$

$$\text{Cutting cost[Euro/m]} = \frac{2.654 + 1.376 \times \text{P} + 1.3718x10^{-5} \times \text{F}}{0.051 \times \text{S}} \tag{4.5}$$

4.5.3 Operating cost when compressed argon is used

The total approximated operating cost per hour as a function of process parameters can be estimated by $2.654+1.376xP + 12.174x10^{-5}xF$. While the total approximated operating cost per unit length of the cut is given by Eq. 4.6 assuming 85% utilisation. Eq. 4.7 was used to calculate the cutting cost per meter for all samples.

Table 4.27: Operating costs break down when compressed Argon is used.

Element of cost	Calculations	Cutting cost €/hr
Laser electrical power	(20.88 kVA)(0.8 pf)(€ 0.12359/kWhr)x(P/1.5)	1.376xP
Chiller electrical power	(11.52 kVA)(0.8 pf)(€ 0.12359/kWhr)	1.139
Motion controller power	(4.8 kVA)(0.8 pf)(€ 0.12359/kWhr)	0.475
Exhaust system power	(0.9 kWhr)(€ 0.12359/kWhr)	0.111
Laser gas LASPUR208	{(€1043.93/ bottle)/(1500liter/bottle)}x 7.5Liter/72hr	0.072
Gas bottle rental	(€181.37/720hr)	0.252
Chiller additives	(€284.80/year)/(8760 hr/year)	0.033
Compressed argon	€12.174 x 10^{-3}/liter x F[litre/hr]	12.174 x10^{-3}xF
Nozzle tip	(€7.20/200hr)	0.036
Exhaust system filters	(€5/100hr)	0.05
Focus lens	(€186/lens)/(1000hr)	0.186
Maintenance labour (with overhead)	(12 hr/2000hrs operation)(€50/hr)	0.30
Total operation cost per hour		2.654+1.376xP +12.174x10^{-3}xF

$$\text{Cutting cost[Euro/m]} = \frac{2.654 + 1.376 \times \text{P[kW]} + 12.174\ \text{x}10^{-3} \times \text{F[l/hr]}}{(0.85) \times \text{S[mm/min][60min/hr][m/1000mm]}} \tag{4.6}$$

$$\text{cutting cost[Euro/m]} = \frac{2.654 + 1.376 \times \text{P} + 12.174\ \text{x}10^{-3} \times \text{F}}{0.051 \times \text{S}} \tag{4.7}$$

4.5.4 Method of showing error in measurements

Two readings measured using the same measurement instrument may not be exactly the same. This difference is called a variation in the measurements or it is commonly termed as “error”. The error in measurements is a mathematical way to show the uncertainty in the measurement. It is the difference between the result of the measurement and the true value of what one is measuring.

There are several ways to express the error in measurement such as absolute error, relative error and the percentage error etc. In this work, the percentage error has been

utilised to show the error between the experimentally measured "actual" value and the value obtained by the mathematical model or the "predicted" value. The percentage error can be calculated using Eq. 4.8. In order to minimise the error in the measurements several steps were considered in this work. All the measuring instruments were calibrated and were chosen to have the highest possible level of precision. Also, all readings were repeated at least three times and an average value was calculated for each condition. Finally, the measurements of all the responses were carried out immediately after the laser cutting operation in the same environment.

$$\text{Percentage error} = \left(\frac{\text{Actual value - Predicted value}}{\text{Actual value}} \right) \times 100 \tag{4.8}$$

4.6 Visual Basic Program

Visual basic (VB) is a computer programming system introduced by Microsoft in 1999. VB was originally created to make it easier to write programs for the Windows computer operating system. The basis of VB is an earlier programming language called BASIC that was invented by Dartmouth College professors John Kemeny and Thomas Kurtz. VB is considered a relatively easy programming language to learn and use because of its graphical development features. Also, the programmer can put together an application using the components provided within VB itself. In VB windows are created by using drag-and-drop techniques. A tool is used to place controls (e.g. text boxes, buttons, etc.) in the window. VB can create executables (i.e. EXE files) [162 and 163].

VB was used to write a programme so that all the developed models build together in one database. By using this software one can predict the quality features for a given material and thickness at selected values of the LBC process parameters, see Fig. 4.10.

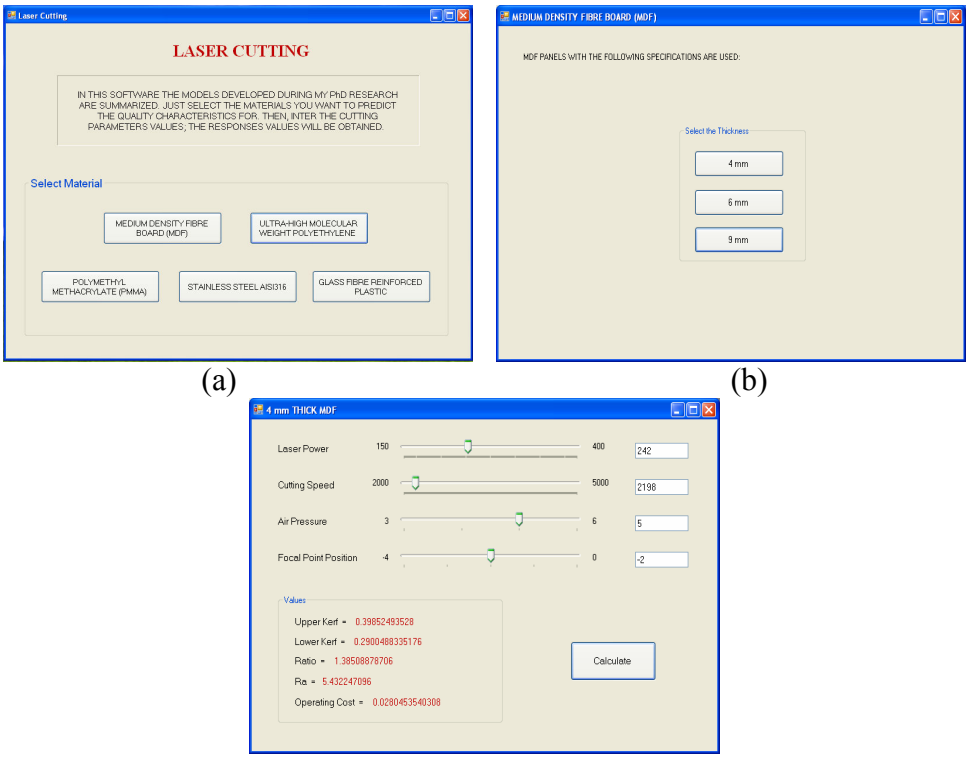

Fig. 4.8: Visual basic windows for MDF, (a) Select material, (b) material specification and thickness selection and (c) inter parameters values and calculate responses.

CHAPTER V
RESULTS AND DISCUSSION

5. RESULTS AND DISCUSSION

In this chapter, the results for all materials studied in this work are presented, in terms of the analysis of variance (ANOVA) of each response, and the validation experiments. Also, the effects of laser beam cutting parameters on each of the quality characteristics are explained and discussed. Furthermore, the operating cost is estimated for each material and discussed to establish the effect of LBC process factors on it.

5.1 Stainless Steel (AISI 316L)

For this material, five responses were considered namely: the upper kerf, the lower kerf, the ratio between the upper to the lower kerfs, the surface roughness and the operating cost. The equipment and procedures described earlier in chapter 4 were used to determine and record these responses. An average of at least three consistent measurements of both kerf widths and the surface roughness were recorded for all the 46 runs presented previously in Table 4.9. The ratio of the upper kerf to the lower kerf was calculated for each run using the averaged data for both the upper and the lower kerfs. The average values of the measured responses are listed in Table 5.1. All experimentally recorded responses are presented in appendix A. The operating cost was estimated using Eq. 4.2 and Eq. 4.3 and the estimated operating cost for each experiment is presented in Table 5.1.

5.1.1 Development of the mathematical models for (AISI316L)

Design expert software V7 was used to analyse the measured responses. The fit summary output indicates that for all responses, the quadratic models are statistically recommended for further analysis as they have the maximum predicted and adjusted R^2 [141]. The test for significance of the regression models, the test for significance on individual model coefficients and the lack of fit test were performed using the same statistical package for all responses. By selecting the step-wise regression method, the insignificant model terms can be automatically eliminated. The resulting ANOVA tables (Tables 5.2 to 5.6) for the reduced quadratic models outline the analysis of variance for

each response and illustrate the significant model terms. The same tables show also the other adequacy measures R^2, Adjusted R^2 and Predicted R^2.

Table 5.1: Average of experimentally measured responses for AISI316L.

No.	Upper kerf, mm	Lower kerf, mm	Ratio	Ra, μm	Operating cost, €/m
1	0.296	0.203	1.461	0.792	2.8921
2	0.325	0.227	1.435	0.732	2.9056
3	0.222	0.147	1.512	1.648	0.9640
4	0.241	0.216	1.119	0.804	0.9685
5	0.263	0.183	1.435	1.735	1.1890
6	0.221	0.224	0.988	0.394	1.1890
7	0.293	0.218	1.348	2.161	1.7099
8	0.265	0.157	1.688	0.693	1.7099
9	0.300	0.233	1.288	0.967	1.3360
10	0.194	0.145	1.341	0.734	0.4453
11	0.321	0.191	1.685	0.870	5.0868
12	0.223	0.167	1.337	0.814	1.6956
13	0.264	0.184	1.430	1.633	1.4461
14	0.307	0.212	1.450	0.910	1.4528
15	0.196	0.206	0.952	0.665	1.4461
16	0.231	0.245	0.940	0.409	1.4528
17	0.196	0.147	1.333	0.556	0.5522
18	0.264	0.209	1.265	0.610	0.7838
19	0.254	0.171	1.488	0.633	2.0803
20	0.289	0.190	1.521	0.490	3.0065
21	0.321	0.246	1.304	0.733	2.8988
22	0.250	0.182	1.371	1.039	0.9663
23	0.309	0.258	1.199	0.781	2.8988
24	0.180	0.173	1.042	0.578	0.9663
25	0.197	0.162	1.216	1.033	1.1856
26	0.235	0.188	1.246	0.481	1.1923
27	0.251	0.155	1.625	0.835	1.7065
28	0.314	0.192	1.634	0.449	1.7133
29	0.268	0.182	1.470	0.942	0.6680
30	0.242	0.216	1.122	0.620	0.6680
31	0.305	0.200	1.523	0.582	2.5434
32	0.263	0.230	1.145	0.744	2.5434
33	0.237	0.171	1.384	0.755	0.6646
34	0.281	0.186	1.511	0.634	0.6714
35	0.272	0.197	1.377	0.697	2.5400
36	0.303	0.186	1.630	0.522	2.5468
37	0.315	0.180	1.750	1.211	2.3779
38	0.211	0.174	1.213	0.743	0.7926
39	0.350	0.246	1.419	0.883	3.4198
40	0.264	0.159	1.659	0.479	1.1399
41	0.325	0.168	1.935	0.757	1.4494
42	0.312	0.167	1.863	0.613	1.4494
43	0.289	0.161	1.797	0.561	1.4494
44	0.301	0.174	1.735	0.694	1.4494
45	0.302	0.171	1.763	0.601	1.4494
46	0.297	0.193	1.539	0.683	1.4494

The entire adequacy measures are close to 1, which are in reasonable agreement and indicate adequate models [138, 139 and 140]. The adequate precision compares the range of the predicted value at the design points to the average prediction error. In all cases the values of adequate precision ratios are dramatically greater than 4. An adequate precision ratio above 4 indicates that the model is adequate [141]. An adequate model means that the reduced model has successfully passed all the required statistical tests and can be used to predict the responses or to optimise the process etc.

Table 5.2: ANOVA table for upper kerf width reduced quadratic model.

Source	Sum of Squares	DF	Mean Square	F Value	Prob > F	
Model	0.0741	11	0.0067	31.060	< 0.0001	Significant
A	0.0057	1	0.0057	26.297	< 0.0001	
B	0.0353	1	0.0353	162.761	< 0.0001	
C	0.0083	1	0.0083	38.202	< 0.0001	
D	0.0100	1	0.0100	46.132	< 0.0001	
E	0.0076	2	0.0038	17.493	< 0.0001	
BC	0.0008	1	0.0008	3.835	0.0584	
A^2	0.0050	1	0.0050	23.150	< 0.0001	
B^2	0.0011	1	0.0011	5.203	0.0289	
C^2	0.0048	1	0.0048	22.195	< 0.0001	
D^2	0.0047	1	0.0047	21.465	< 0.0001	
Residual	0.0074	34	0.0002			
Lack of Fit	0.0066	29	0.0002	1.469	0.3583	Not Sig.
Pure Error	0.0008	5	0.0002			
Cor Total	0.0814	45				
$R^2 = 0.910$			Pred $R^2 = 0.839$			
Adj $R^2 = 0.880$			Adeq Precision = 20.808			

For the upper kerf model the analysis of variance indicates that the main effect of all the following factors, quadratic effect of laser power (A^2), cutting speed (B^2), focal position (C^2) and nitrogen pressure (D^2) are the most significant model terms associated with this response. However, the interaction effect between cutting speed and nitrogen pressure (BC) is also affecting this response. While, for the lower kerf model, the analysis indicates that the main effect of all factors, the quadratic effect of (A^2), (B^2), (C^2) and the interaction effect between (AE), (BD), (BE), (CD) and (DE) are the significant model terms. The analysis demonstrates that the cutting speed has the main role on the lower kerf width, then the laser power. For the ratio model, the analysis

demonstrates that, the main effect of all the following factors, the quadratic effect of (A^2), (B^2), (C^2), (D^2) and the interaction effect between (BD) and (CD) are the significant model terms. All the findings for the kerf width are in agreement with the results reported in [15, 19, 21 and 24]. Then, for the roughness model, it is evident from the analysis that the main effect of the laser power (A), the cutting speed (B), the focal point position (C), the nitrogen pressure (D), the quadratic effects of the cutting speed (B^2), the focal position (C^2) and the nitrogen pressure (D^2) are the significant terms. However, the cutting speed is the factor which has the most significant effect on the roughness a finding which agrees with [28]. The focal position and laser power also affect the roughness notably. All the above findings are in agreement with the results found in [39]. Finally, for the operating cost model the results demonstrate that the main effect of the laser power (A), the cutting speed (B), the nitrogen pressure (D), the nozzle diameter (E), the interaction effects of laser power with nitrogen pressure (AD), laser power with nozzle diameter (AE), nitrogen pressure with nozzle diameter (DE), the quadratic effect of cutting speed (B^2) and nitrogen pressure (D^2) are the significant model terms related to operating cost. The final mathematical models in terms of actual factors as determined by design expert software are shown in Eqs. 5.1 – 5.15.

Table 5.3: ANOVA table for lower kerf width reduced quadratic model.

Source	Sum of Squares	DF	Mean Square	F Value	Prob > F	
Model	0.0323	17	0.0019	9.711	< 0.0001	Significant
A	0.0032	1	0.0032	16.378	0.0004	
B	0.0111	1	0.0111	56.578	< 0.0001	
C	0.0006	1	0.0006	3.197	0.0846	
D	0.0006	1	0.0006	3.050	0.0917	
E	0.0003	2	0.0001	0.726	0.4929	
AE	0.0011	2	0.0006	2.872	0.0733	
BD	0.0016	1	0.0016	8.322	0.0075	
BE	0.0010	2	0.0005	2.683	0.0859	
CD	0.0026	1	0.0026	13.046	0.0012	
DE	0.0015	2	0.0008	3.926	0.0314	
A^2	0.0008	1	0.0008	3.951	0.0567	
B^2	0.0020	1	0.0020	10.486	0.0031	
C^2	0.0079	1	0.0079	40.47176	< 0.0001	
Residual	0.0055	28	0.000195			
Lack of Fit	0.004871	23	0.000212	1.758863	0.2768	Not Sig.
Pure Error	0.000602	5	0.00012			
Cor Total	0.037744	45				
$R^2 = 0.855$			Pred $R^2 = 0.542$			
Adj $R^2 = 0.767$			Adeq Precision = 12.065			

Table 5.4: ANOVA table for ratio reduced quadratic model.

Source	Sum of Squares	DF	Mean Square	F Value	Prob > F	
Model	1.9997	12	0.1666	9.091	< 0.0001	Significant
A	0.0000	1	0.0000	0.000	0.9861	
B	0.0560	1	0.0560	3.057	0.0897	
C	0.3178	1	0.3178	17.339	0.0002	
D	0.1387	1	0.1387	7.568	0.0096	
E	0.2862	2	0.1431	7.806	0.0017	
BD	0.1507	1	0.1507	8.223	0.0072	
CD	0.1547	1	0.1547	8.442	0.0065	
A^2	0.3558	1	0.3558	19.408	0.0001	
B^2	0.2954	1	0.2954	16.118	0.0003	
C^2	0.9395	1	0.9395	51.256	< 0.0001	
D^2	0.1395	1	0.1395	7.610	0.0094	
Residual	0.6049	33	0.0183			
Lack of Fit	0.5138	28	0.0184	1.007827	0.5597	Not Sig.
Pure Error	0.0910	5	0.018209			
Cor Total	2.604571	45				
$R^2 = 0.855$			Pred $R^2 = 0.511$			
Adj $R^2 = 0.683$			Adeq Precision = 12.300			

Table 5.5: ANOVA table for roughness reduced quadratic model.

Source	Sum of Squares	DF	Mean Square	F Value	Prob > F	
Model	4.1410	7	0.5916	17.8507	< 0.0001	Significant
A	0.2806	1	0.2806	8.4681	0.0060	
B	1.2778	1	1.2778	38.5585	< 0.0001	
C	0.9195	1	0.9195	27.7462	< 0.0001	
D	0.0735	1	0.0735	2.2188	0.1446	
B^2	1.5248	1	1.5248	46.0097	< 0.0001	
C^2	0.1089	1	0.1089	3.2856	0.0778	
D^2	0.2081	1	0.2081	6.2789	0.0166	
Residual	1.2593	38	0.0331			
Lack of Fit	1.2331	33	0.0374	7.1325	0.0184	Not Sig. at α=0.01
Pure Error	0.0262	5	0.0052			
Cor Total	5.4004	45				
$R^2 = 0.767$			Pred $R^2 = 0.635$			
Adj $R^2 = 0.734$			Adeq Precision = 16.956			

Table 5.6: ANOVA table for operating cost reduced quadratic model.

Source	Sum of Squares	DF	Mean Square	F Value	Prob > F	
Model	12.884206	12	1.0737	15774705.83	< 0.0001	Significant
A	0.000105	1	0.0001	1542.23	< 0.0001	
B	4.827796	1	4.8278	70930617.16	< 0.0001	
D	0.525086	1	0.5251	7714639.87	< 0.0001	
E	7.256601	2	3.6283	53307470.27	< 0.0001	
AD	0.000001	1	0.0000	10.97	0.0022	
AE	0.000016	2	0.0000	117.16	< 0.0001	
DE	0.000095	2	0.0000	698.08	< 0.0001	
B^2	0.204422	1	0.2044	3003398.42	< 0.0001	
D^2	0.002628	1	0.0026	38618.03	< 0.0001	
Residual	0.000002	33	6.81E-08			
Cor Total	12.884209	45				
$R^2 = 0.855$			Pred $R^2 = 0.511$			
Adj $R^2 = 0.683$			Adeq Precision = 12.300			

The mathematical models for nozzle diameter of 1 mm are as follows:

$$\begin{aligned}\text{Upper Kerf} = {} & -1.27254 + 1.03467 * \text{Laser power} - 4.47361E\text{-}005 * \text{Cutting speed} \\ & -0.13479 * \text{Focal position} + 0.10236 * \text{Nitrogen pressure} \\ & -1.44167E\text{-}005 * \text{Cutting speed} * \text{Focal position} - 0.38367 * \text{Laser power}^2 \\ & -1.13681E\text{-}008 * \text{Cutting speed}^2 - 0.023479 * \text{Focal position}^2 \\ & -3.69444E\text{-}003 * \text{Nitrogen pressure}^2 \end{aligned} \quad (5.1)$$

$$\begin{aligned}\text{Lower Kerf} = {} & 0.81013 - 0.33202 * \text{Laser power} - 2.14646E\text{-}006 * \text{Cutting speed} \\ & + 0.30630 * \text{Focal position} - 1.76667E\text{-}003 * \text{Nitrogen pressure} \\ & - 8.06667E\text{-}006 * \text{Cutting speed} * \text{Nitrogen pressure} \\ & - 0.010100 * \text{Focal position} * \text{Nitrogen pressure} \\ & + 0.14481 * \text{Laser power}^2 + 1.47449E\text{-}008 * \text{Cutting speed}^2 \\ & + 0.028967 * \text{Focal position}^2 \end{aligned} \quad (5.2)$$

$$\begin{aligned}\text{Ratio} = {} & -12.12985 + 8.07832 * \text{Laser power} - 2.93788E\text{-}004 * \text{Cutting speed} \\ & - 3.09299 * \text{Focal position} + 0.62368 * \text{Nitrogen pressure} \\ & + 7.76458E\text{-}005 * \text{Cutting speed} * \text{Nitrogen pressure} \\ & + 0.078674 * \text{Focal position} * \text{Nitrogen pressure} \\ & - 3.23038 * \text{Laser power}^2 - 1.83990E\text{-}007 * \text{Cutting speed}^2 \\ & - 0.32810 * \text{Focal position}^2 - 0.020228 * \text{Nitrogen pressure}^2 \end{aligned} \quad (5.3)$$

$$Ra = 6.52117 - 0.52975 * \text{Laser power} - 1.28860E\text{-}003 * \text{Cutting speed} + 0.39008 * \text{Focal position} - 0.60755 * \text{Nitrogen pressure} + 3.92802E\text{-}007 * \text{Cutting speed}^2 + 0.10497 * \text{Focal position}^2 + 0.023217 * \text{Nitrogen pressure}^2 \quad (5.4)$$

$$\text{Ln(Operating cost)} = -0.048359 + 0.028837 * \text{Laser power} - 1.12461E\text{-}003 * \text{Cutting speed} + 0.13613 * \text{Nitrogen pressure} - 6.91362E\text{-}004 * \text{Laser power} * \text{Nitrogen pressure} + 1.43825E\text{-}007 * \text{Cutting speed}^2 - 2.60941E\text{-}003 * \text{Nitrogen pressure}^2 \quad (5.5)$$

The mathematical models for nozzle diameter of 1.5 mm are as follows:

$$\text{Upper Kerf} = -1.23634 + 1.03467 * \text{Laser power} - 4.47361E\text{-}005 * \text{Cutting speed} - 0.13479 * \text{Focal position} + 0.10236 * \text{Nitrogen pressure} - 1.44167E\text{-}005 * \text{Cutting speed} * \text{Focal position} - 0.38367 * \text{Laser power}^2 - 1.13681E\text{-}008 * \text{Cutting speed}^2 - 0.023479 * \text{Focal position}^2 - 3.69444E\text{-}003 * \text{Nitrogen pressure}^2 \quad (5.6)$$

$$\text{Lower Kerf} = 0.86483 - 0.28769 * \text{Laser power} + 1.61035E\text{-}005 * \text{Cutting speed} + 0.30630 * \text{Focal position} - 0.013622 * \text{Nitrogen pressure} - 8.06667E\text{-}006 * \text{Cutting speed} * \text{Nitrogen pressure} - 0.010100 * \text{Focal position} * \text{Nitrogen pressure} + 0.14481 * \text{Laser power}^2 + 1.47449E\text{-}008 * \text{Cutting speed}^2 + 0.028967 * \text{Focal position}^2 \quad (5.7)$$

$$\text{Ratio} = -11.9074 + 8.07832 * \text{Laser power} - 2.93788E\text{-}004 * \text{Cutting speed} - 3.09299 * \text{Focal position} + 0.62368 * \text{Nitrogen pressure} + 7.76458E\text{-}005 * \text{Cutting speed} * \text{Nitrogen pressure} + 0.078674 * \text{Focal position} * \text{Nitrogen pressure} - 3.23038 * \text{Laser power}^2 - 1.83990E\text{-}007 * \text{Cutting speed}^2 - 0.32810 * \text{Focal position}^2 - 0.020228 * \text{Nitrogen pressure}^2 \quad (5.8)$$

$$Ra = 6.52117 - 0.52975 * \text{Laser power} - 1.28860E\text{-}003 * \text{Cutting speed} + 0.39008 * \text{Focal position} - 0.60755 * \text{Nitrogen pressure} + 3.92802E\text{-}007 * \text{Cutting speed}^2 + 0.10497 * \text{Focal position}^2 + 0.023217 * \text{Nitrogen pressure}^2 \quad (5.9)$$

$$\text{Ln(Operating cost)} = +0.70636 + 0.018053 * \text{Laser power} - 1.12461E\text{-}003 * \text{Cutting speed} + 0.13877 * \text{Nitrogen pressure} - 6.91362E\text{-}004 * \text{Laser power} * \text{Nitrogen pressure} + 1.43825E\text{-}007 * \text{Cutting speed}^2 - 2.60941E\text{-}003 * \text{Nitrogen pressure}^2 \quad (5.10)$$

The mathematical models for nozzle diameter of 2 mm are as follows:

$$\text{Upper Kerf} = -1.24154 + 1.03467 * \text{Laser power} - 4.47361E\text{-}005 * \text{Cutting speed} - 0.13479 * \text{Focal position} + 0.10236 * \text{Nitrogen pressure} - 1.44167E\text{-}005 * \text{Cutting speed} * \text{Focal position} - 0.38367 * \text{Laser power}^2 - 1.13681E\text{-}008 * \text{Cutting speed}^2 - 0.023479 * \text{Focal position}^2 - 3.69444E\text{-}003 * \text{Nitrogen pressure}^2 \quad (5.11)$$

$$\text{Lower Kerf} = 0.92446 - 0.38535 * \text{Laser power} - 3.00202E\text{-}005 * \text{Cutting speed} + 0.30630 * \text{Focal position} - 0.010300 * \text{Nitrogen pressure} - 8.06667E\text{-}006 * \text{Cutting speed} * \text{Nitrogen pressure} - 0.010100 * \text{Focal position} * \text{Nitrogen pressure} + 0.14481 * \text{Laser power}^2 + 1.47449E\text{-}008 * \text{Cutting speed}^2 + 0.028967 * \text{Focal position}^2 \quad (5.12)$$

$$\text{Ratio} = -12.0057 + 8.07832 * \text{Laser power} - 2.93788E\text{-}004 * \text{Cutting speed} - 3.09299 * \text{Focal position} + 0.62368 * \text{Nitrogen pressure} + 7.76458E\text{-}005 * \text{Cutting speed} * \text{Nitrogen pressure} + 0.078674 * \text{Focal position} * \text{Nitrogen pressure} - 3.23038 * \text{Laser power}^2 - 1.83990E\text{-}007 * \text{Cutting speed}^2 - 0.32810 * \text{Focal position}^2 - 0.020228 * \text{Nitrogen pressure}^2 \quad (5.13)$$

$$\text{Ra} = 6.52117 - 0.52975 * \text{Laser power} - 1.28860E\text{-}003 * \text{Cutting speed} + 0.39008 * \text{Focal position} - 0.60755 * \text{Nitrogen pressure} + 3.92802E\text{-}007 * \text{Cutting speed}^2 + 0.10497 * \text{Focal position}^2 + 0.023217 * \text{Nitrogen pressure}^2 \quad (5.14)$$

$$\text{Ln(Operating cost)} = +1.26155 + 0.013946 * \text{Laser power} - 1.12461E\text{-}003 * \text{Cutting speed} + 0.13975 * \text{Nitrogen pressure} - 6.91362E\text{-}004 * \text{Laser power} * \text{Nitrogen pressure} + 1.43825E\text{-}007 * \text{Cutting speed}^2 - 2.60941E\text{-}003 * \text{Nitrogen pressure}^2 \quad (5.15)$$

5.1.2 Validation of the models.

Fig 5.1 shows the relationship between the actual and predicted values of upper kerf, lower kerf, ratio, roughness and operating cost respectively. These plots indicate that the developed models are satisfactory since the residuals in prediction of each response are small and scattered randomly and tend to be close to the diagonal line. Furthermore, to confirm the adequacy of the developed models, three confirmation experiments were carried out using new randomly selected test conditions, each within the experiment range defined earlier in chapter 4. Using the point prediction option in the software, the values of all responses of the validation experiments were predicted using the previous developed models and compared with the experimentally measured responses values for these confirmation experiments. Table 5.7 summarises the experimental conditions, actual experimental values, predicted values and percentages of error in prediction. It is evident that the models can adequately describe the responses within the ranges considered as the maximum error percent in prediction is 9.292% which is in good agreement. All the percentages of error are in agreement with the values reported in [115 and 136].

Table 5.7: Confirmation experiments for AISI 316L.

Exp. No.	A	B	C	D	E		Upper kerf	Lower kerf	ratio	R_a	Cost
1	1	3000	-3	12.5	1	Actual	0.159	0.138	1.152	1.582	0.4431
						Predicted	0.167	0.145	1.104	1.469	0.4432
						Error %	-5.036	-5.179	4.210	7.164	-0.0247
2	1.5	1000	-3	12.5	1	Actual	0.286	0.237	1.207	0.704	1.3428
						Predicted	0.299	0.248	1.223	0.639	1.3431
						Error %	-4.431	-4.703	-1.364	9.292	-0.024
3	1.5	1000	-3	15	2	Actual	0.317	0.261	1.215	0.773	6.0197
						Predicted	0.332	0.238	1.120	0.716	6.0207
						Error %	-4.600	8.884	7.788	7.387	-0.016

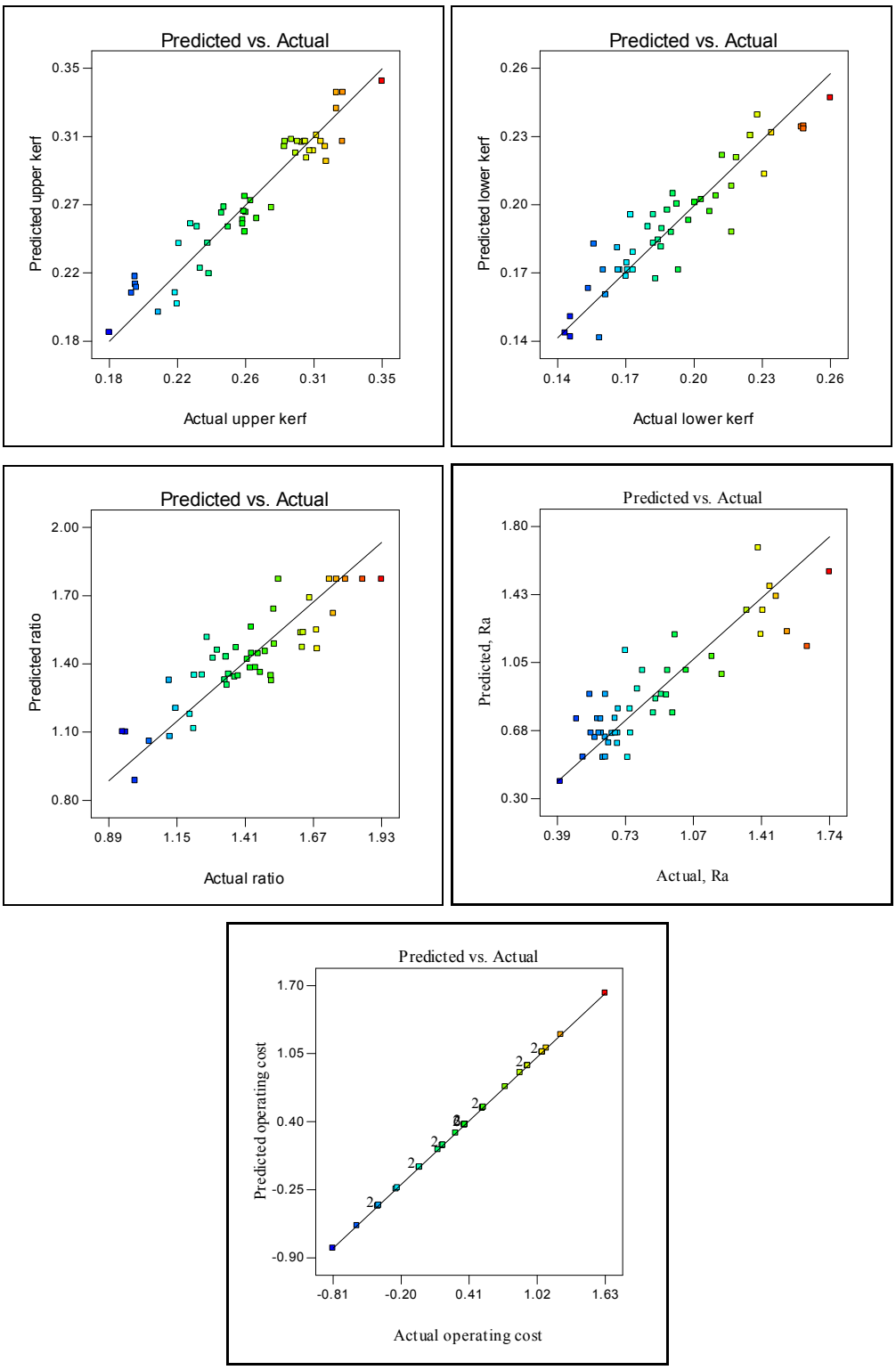

Fig. 5.1: Scatter diagram showing the relationship between the actual and predicted values for each response.

5.1.3 Effect of process parameters on the responses

5.1.3.1 Upper kerf

The perturbation plot for the upper kerf width is shown in Fig. 5.2. The perturbation plot helps to compare the effect of all the factors at a particular point in the design space. This type of display does not show the effect of interactions. The lines represent the behaviours of each factor while holding the others constant (i.e. centre point by default). In the case of more than one factor this type of display could be used to find those factors that most affect the response. It is evident from Fig. 5.2 that the upper kerf width increases as the laser power and gas pressure increase, which agrees with [13, 15, 16 and 21], yet above the centre values of both factors the upper kerf becomes stable. However, the upper kerf width sharply decreases as the cutting speed increases. This is in a good agreement with [14, 15 and 21]. In the case of the focal point position, it is notable that as the focal position increases up to the centre point (C = -3 mm) the upper kerf slightly increases, but, as the focal point increases beyond this point the upper kerf begins to decrease.

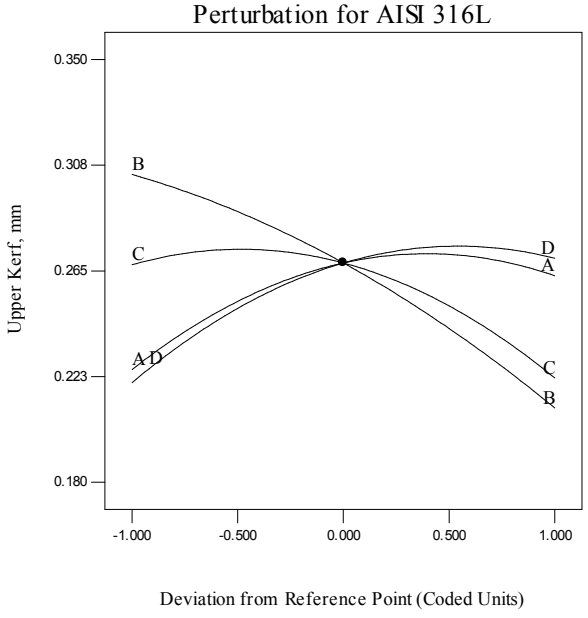

Fig. 5.2: Perturbation plot showing the effect of process parameters on upper kerf width.

Table 5.8 presents the overall percentage change in the upper kerf width as a result of changing each factor from its lowest value to its highest value while keeping the other factor at their centre values. It is evident from Table 5.8 that the cutting speed is the main factor influencing the upper kerf width, this result agrees with the results found in [18 and 21]. Fig. 5.3 is a contour graph demonstrating the effect of both laser power and cutting speed on the upper kerf width at two nozzle diameters 1 and 1.5 mm. In fact, all the investigated LBC parameters are found to affect the upper kerf, and this outcome agrees with [19 and 44].

Table 5.8: Percentage change in upper kerf as each factor increases.

Factor	Percentage change in upper kerf, %
Laser power	Increases by 16.75
Cutting speed	Decreases by 30.92
Focal position	Decreases by 17.01
Nitrogen pressure	Increases by 22.72
Nozzle diameter	Increases by 11.56

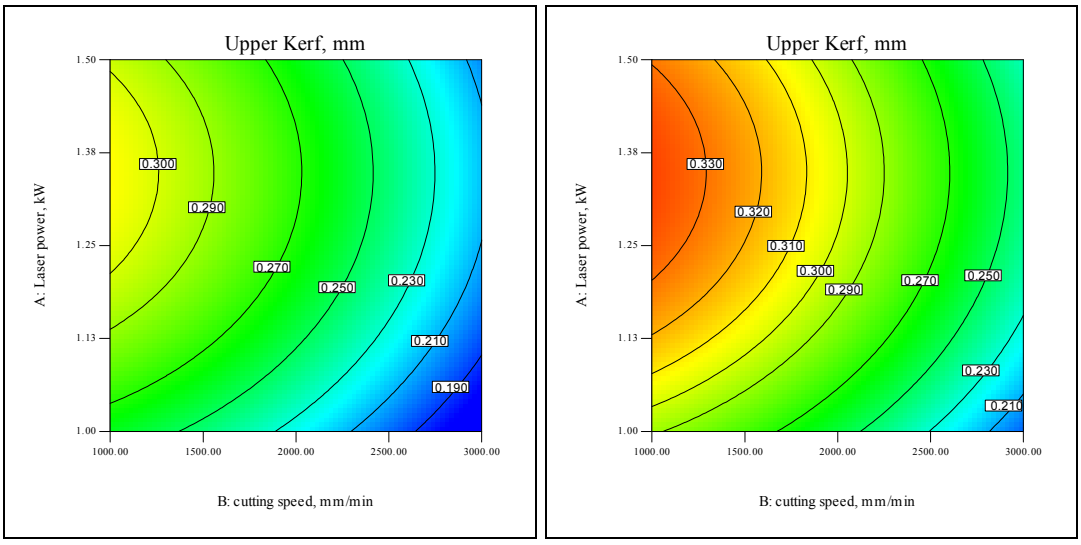

(a) (b)

Fig. 5.3: Contours plot showing the effect of laser power and cutting speed on the upper kerf width at different nozzle diameters (a) 1 mm and (b) 1.5 mm.

5.1.3.2 Lower kerf

It is clear from Fig. 5.4 that the lower kerf width increases as the laser power and the gas pressure increase. However, this response decreases with the increase in the focal point position up to the midpoint (i.e. -3 mm) and then starts to increase as the focal point position increases from -3 mm towards -2 mm. This incident could be related to the interaction between the gas pressure and the focal point position, which will be discussed later. Also, the lower kerf decreases as the cutting speed increases this is in agreement with findings reported in [21].

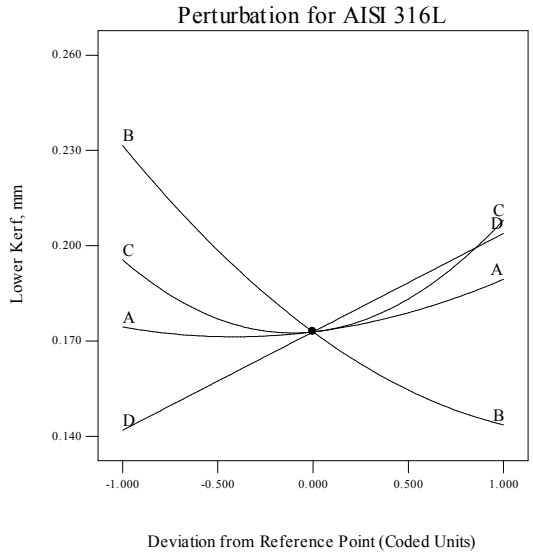

Fig. 5.4: Perturbation plot showing the effect of process parameters on lower kerf width.

Fig. 5.5 demonstrates the interaction effect between the cutting speed and nitrogen pressure on the lower kerf width. It is clear that at low cutting speeds below 2100 mm/min a smaller lower kerf width of 0.170 mm could be obtained if the lowest nitrogen pressure of 10 bar is used. On the other hand, at higher cutting speeds above 2100 mm/min the smallest lower kerf width of 0.14 mm could be produced if the highest nitrogen pressure of 15 bar was supplied. At cutting speeds of about 2100 mm/min both levels of nitrogen pressure have the same effect on the lower kerf width. Fig. 5.6 shows the interaction effect between the focal point position and the nitrogen pressure. It is evident that the use of wider laser beam (i.e. focal position of - 4 mm) leads to a small

lower kerf width of 0.17 only if the lowest gas pressure of 10 bar is applied. On the other hand, using a narrower laser beam (i.e. focal position of - 2 mm) results in a small lower kerf width only when the highest nitrogen pressure of 15 bar is applied. However, the nitrogen pressure would have the same effect on the lower kerf width if a focal point position just above -3 mm was employed. Dilthey et al. [24] have reported that exact adjustment of focal position and gas jet is essential, which support the above findings. It is clear from the interaction graph shown in Fig. 5.7 that when using a nozzle diameter of 1.5 mm there is no significant difference between the lower kerf width values produced by supplying either level of nitrogen pressures. It is evident from Table 5.9 that the nitrogen pressure and cutting speed are the main factors influencing the lower kerf width.

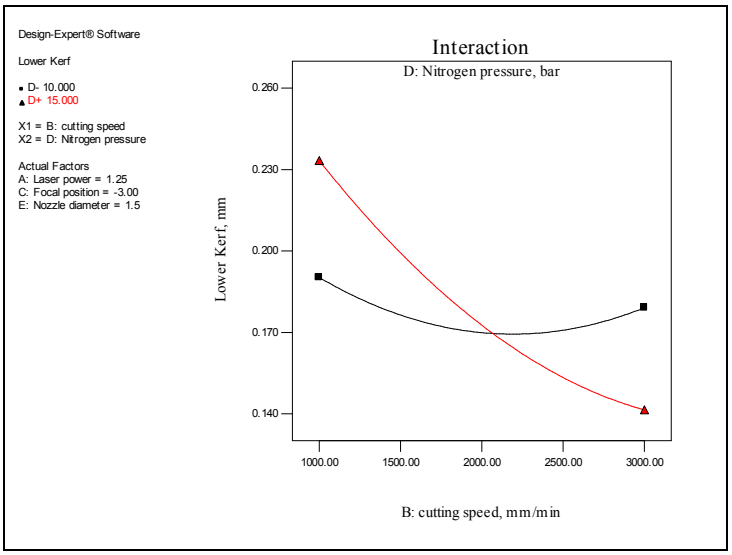

Fig. 5.5: Interaction plot showing the interaction between the cutting speed and the nitrogen pressure on the lower kerf.

Table 5.9: Percentage change in lower kerf as each factor increases.

Factor	Percentage change in lower kerf, %
Laser power	Increases by 8.60
Cutting speed	Decreases by 38.00
Focal position	Increases by 6.39
Nitrogen pressure	Increases by 43.71
Nozzle diameter	Increases by 3.09

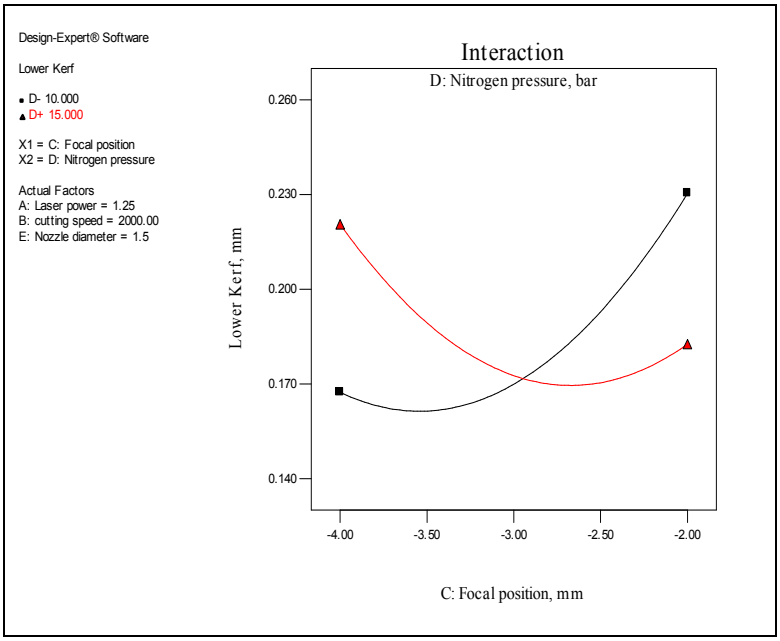

Fig. 5.6: Interaction plot showing the interaction between the focal position and the nitrogen pressure on the lower kerf.

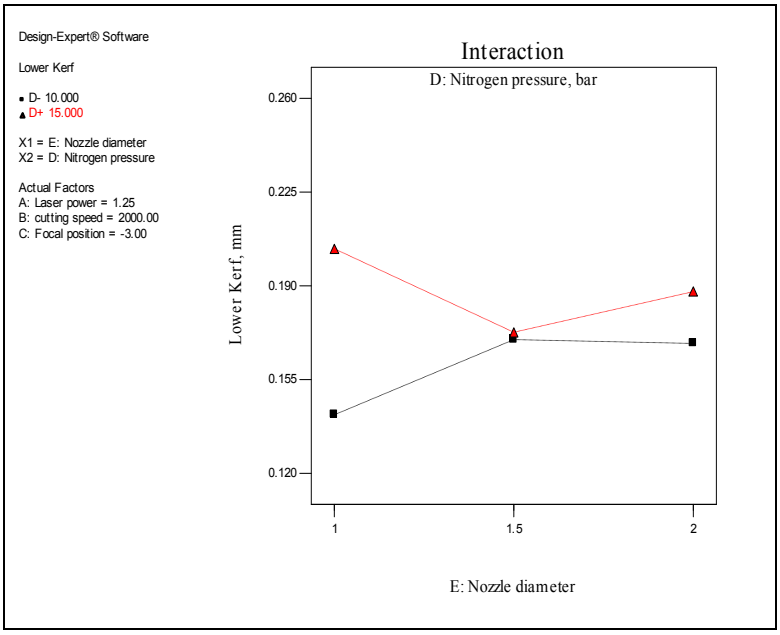

Fig. 5.7: Interaction plot showing the interaction between the nozzle diameter and the nitrogen pressure on the lower kerf.

5.1.3.3 Ratio

Fig. 5.7 is an interaction plot showing the influence of cutting speed and nitrogen pressure on the ratio. It is apparent that by using cutting speeds below 1520 mm/min the ratio would be less (close to one) if the highest nitrogen pressure of 15 bar was supplied. Above this value of cutting speed the ratio would be less if the lowest nitrogen pressure of 10 bar was used. The same trend was noticed as the nozzle diameter changed. From the interaction graph shown in Fig. 5.8 it is obvious that by using focal position below -3.48 mm the ratio would be close to one if the highest nitrogen pressure of 15 bar was used. Above -3.48 the ratio would be close to one as the lowest nitrogen pressure of 10 bar was used. It is evident from Table 5.10 that the focal position and nitrogen pressure are the main factors influencing the ratio. These findings are in fair agreement with results reported in [18 and 37]. The results show that the range of the ratio lays between 0.94 and 1.93 for AISI316L. Therefore, a target ratio of one in this case will be a desirable goal when searching for the optimal condition to obtain a square cut edge. The optimised conditions that would lead to a square cut edge are: laser power of 1.5 kW, cutting speed of 1650 mm/min, focal point position of -2 mm, nitrogen pressure of 11.4 bar and nozzle diameter of 1.5 mm.

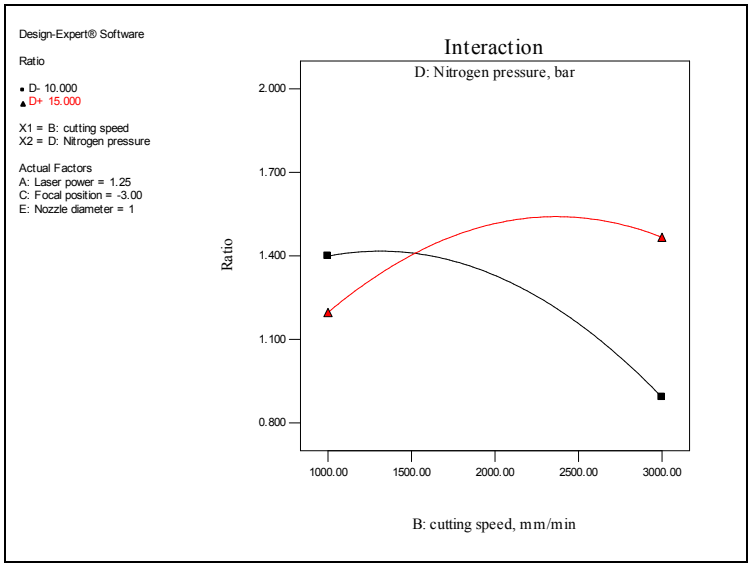

Fig. 5.7: Interaction plot showing the interaction between the cutting speed and the nitrogen pressure on the ratio.

Table 5.10: Percentage change in ratio as each factor increases.

Factor	Percentage change in ratio, %
Laser power	Increases by 0.09
Cutting speed	Decreases by 8.31
Focal position	Decreases by 20.69
Nitrogen pressure	Increases by 14.00
Nozzle diameter	Increases by 8.02

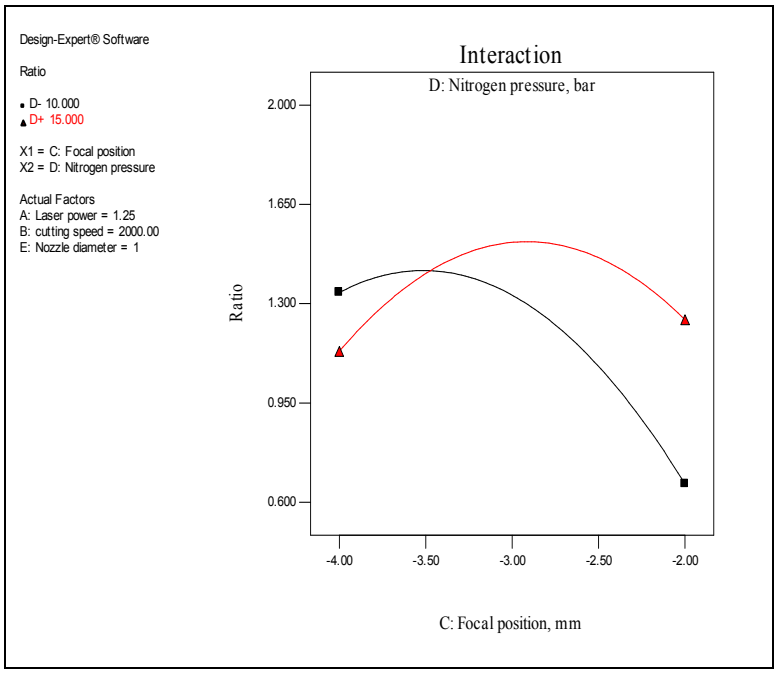

Fig. 5.8: Interaction plot showing the interaction between the focal position and the nitrogen pressure on the ratio.

5.1.3.4 Surface roughness

Fig. 5.9 is a perturbation plot showing the effect of all laser cutting parameters on the roughness of the cut surface. It is evident from the results that the Ra value decreases as the laser power, focal point position and nitrogen pressure increase; these finding are in agreement with [39] and disagree with [40]. However, the Ra value starts to rise as the nitrogen pressure increases above 13.4 bar as can be seen in Fig. 5.9. Moreover, the roughness decreases slightly as the cutting speed increases up to 1505 mm/min, which agrees with [40]. Between 1505 – 1740 mm/min the surface roughness values become

stable, and then they remarkably increase as the cutting speed increases above 1740 mm/min, which disagrees with [40]. The results confirm that the nozzle diameter has no significant effect on the roughness of the cut surface in contrast to the apparent results in Fig. 5.9. It is clear from Table 5.11 that the cutting speed, focal position and laser power are the main factors influencing the cut surface roughness.

Table 5.11: Percentage change in roughness as each factor increases.

Factor	Percentage change in R_a, %
Laser power	Decreases by 33.39
Cutting speed	Increases by 73.31
Focal position	Decreases by 47.68
Nitrogen pressure	Decreases by 15.52
Nozzle diameter	No effect

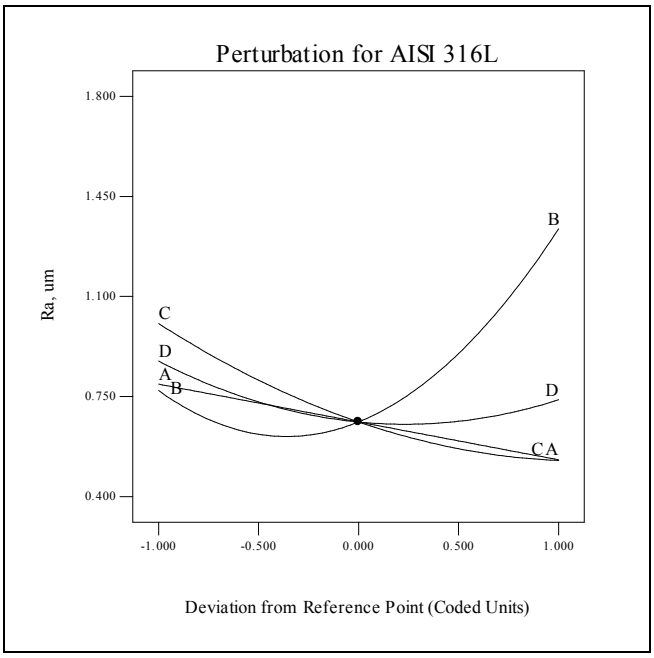

Fig. 5.9: Perturbation plot showing the effect of process parameters on roughness.

5.1.3.5 Operating cost

The perturbation plot would help to compare the effect of all the factors at a particular point in the design space. It is evident from Fig. 5.10, that in the case of cutting speed, steep curvatures indicate that the responses are too sensitive to this factor. Also, Fig. 5.10a-c demonstrates the importance of the nozzle diameter with respect to the operating cost, while the steep slopes in the case of laser power and nitrogen pressure indicate that the operating cost is less sensitive to these factors. In addition, the results indicate that as the laser power, nitrogen pressure and nozzle diameter increase the operating cost increases too. On the other hand, as the cutting speed increases the operating cost decreases sharply. These results are logical because more electrical power will be consumed as the laser power increases. Also, more gas will be consumed as both the nitrogen pressure and the nozzle diameter increase. However, the cost will decrease as the cutting speed increases due to the fact that the cutting will be performed in less time, and consequently, less electrical power and nitrogen gas will be consumed. Fig. 5.10 is a perturbation plot illustrating the above findings. It is apparent that nozzle diameter, cutting speed and nitrogen pressure are the key factors affecting the operating cost. Moreover, these changes in the operating cost in terms of percentages are presented in Table 5.12 as each factor increases from its lowest level to its highest level. It is clear that the focal position has no effect on the operating cost.

On balance, it is evident from the above results for AISI316L that all the process parameters considered in this research affect the quality features some way. Furthermore, in some cases these parameters may interact in such a way that it becomes to hard too find the best cutting conditions which lead to the desired quality features. Therefore, an overall optimisation should be performed for this investigation which would account for the minimisation of the surface roughness, kerf widths and operating cost etc, or the maximisation of the cut edge squareness. It is notable that the main factors affecting the operating cost are: nozzle diameter, cutting speed, nitrogen pressure and minor effect of laser power.

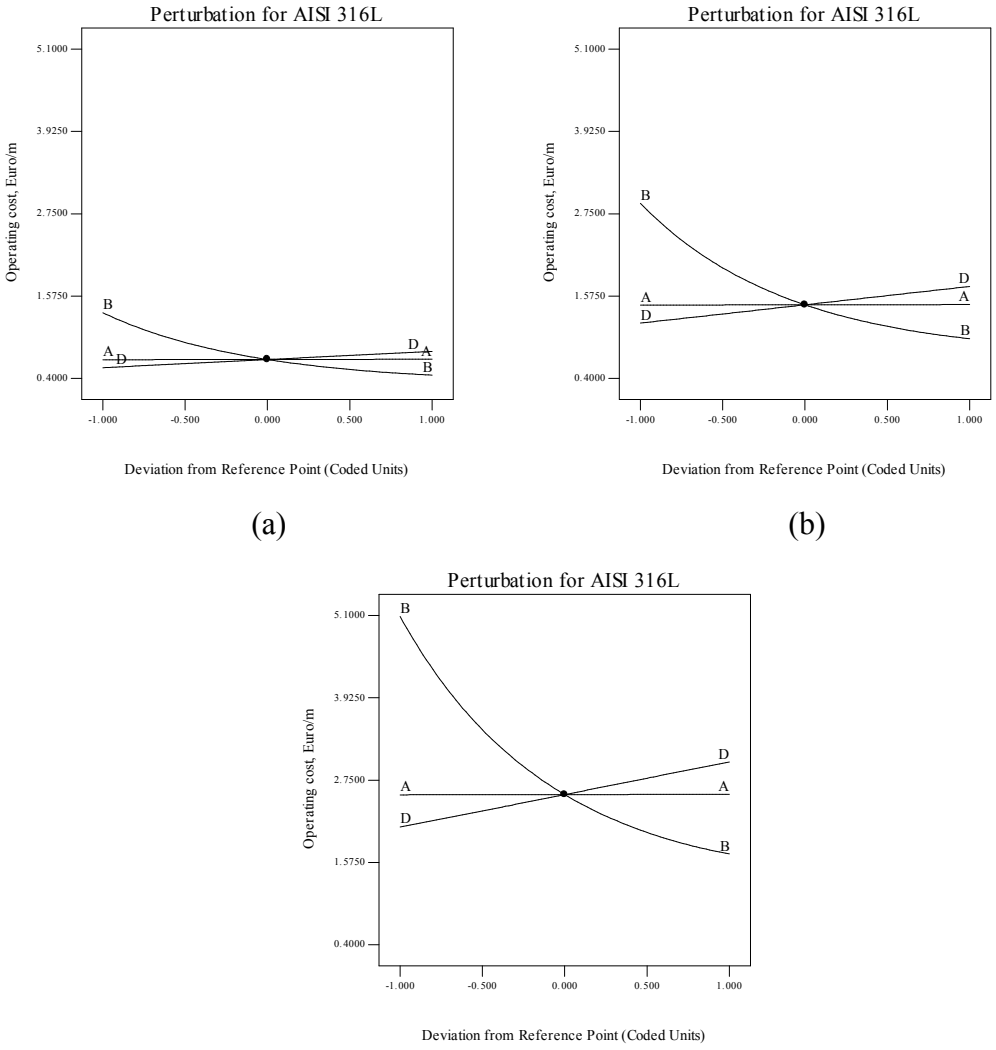

Fig. 5.10: Perturbation plot illustrating the effect of process factors on operating cost at different nozzle diameters (a) 1 mm, (b) 1.5 mm and (c) 2 mm.

Table 5.12: Percentage change in cost as each factor increases.

Factor	Percentage change in cost, %
Laser power	Increases by 1.01
Cutting speed	Decreases by 66.67
Focal position	No effect
Nitrogen pressure	Increases by 41.92
Nozzle diameter	Increases by 280.59

5.2 Ultra High Molecular Weight Polyethylene (UHMWPE)

For this material, the same five responses were considered namely: upper kerf, lower kerf, ratio between upper to lower kerfs, surface roughness and operating cost. In fact, three thicknesses were studied 6, 8 and 10mm. The apparatus and procedures illustrated previously in chapter 4 were utilised to evaluate these responses. An average of at least five consistent measurements of both kerf widths and surface roughness were recorded for all 51 runs shown in Tables 4.11-4.13 for the three thicknesses. The ratio of the upper kerf to the lower kerf was calculated for each run using the averaged data. The average values of the measured responses are listed in Tables 5.7-5.9. All experimentally evaluated responses are presented in appendix B. The operating cost was estimated using Eq. 4.5 and Eq. 4.3 and the estimated operating cost for each experiment is presented in Tables 5.13 – 5.15.

Table 5.13: Experimentally evaluated responses for thickness 6 mm UHMWPE.

Std	Run	Responses				
		Upper kerf, mm	Lower kerf, mm	Ratio	Ra, μm	Cost, €/m
1	10	0.516	1.242	0.416	2.233	0.0748
2	13	0.570	1.361	0.419	1.603	0.0883
3	15	0.420	0.866	0.485	2.339	0.0428
4	3	0.461	1.321	0.349	2.054	0.0505
5	7	0.649	1.047	0.620	2.645	0.0544
6	8	0.680	1.291	0.527	2.178	0.0642
7	5	0.274	1.154	0.238	2.867	0.0544
8	2	0.317	1.470	0.216	2.475	0.0642
9	6	0.718	1.263	0.569	2.274	0.0816
10	4	0.628	1.147	0.548	2.876	0.0466
11	12	0.344	1.351	0.255	2.089	0.0816
12	11	0.273	1.228	0.222	2.640	0.0466
13	14	0.509	1.320	0.385	1.561	0.0593
14	16	0.498	1.355	0.367	1.933	0.0593
15	17	0.500	1.333	0.375	1.718	0.0593
16	9	0.483	1.333	0.363	1.601	0.0593
17	1	0.490	1.339	0.366	1.682	0.0593

Table 5.14: Experimentally evaluated responses for thickness 8 mm UHMWPE.

Std	Run	Responses				
		Upper kerf, mm	Lower kerf, mm	Ratio	Ra, μm	Cost, €/m
1	13	0.574	1.368	0.420	2.313	0.0973
2	1	0.662	1.423	0.465	1.683	0.1141
3	17	0.519	0.862	0.601	2.399	0.0556
4	3	0.561	1.413	0.397	2.104	0.0652
5	4	0.755	1.000	0.756	2.705	0.0707
6	8	0.774	1.288	0.601	2.298	0.0830
7	9	0.408	1.294	0.315	2.987	0.0707
8	11	0.445	1.528	0.291	2.595	0.0830
9	5	0.776	1.238	0.627	2.398	0.1057
10	10	0.756	1.016	0.744	2.766	0.0604
11	7	0.470	1.484	0.316	2.158	0.1057
12	15	0.379	1.333	0.284	2.720	0.0604
13	2	0.600	1.370	0.438	1.681	0.0769
14	6	0.578	1.372	0.421	1.933	0.0769
15	14	0.583	1.387	0.420	1.798	0.0769
16	16	0.593	1.362	0.435	1.701	0.0769
17	12	0.586	1.370	0.427	1.762	0.0769

Table 5.15: Experimentally evaluated responses for thickness 10 mm UHMWPE.

Std	Run	Responses				
		Upper kerf, mm	Lower kerf, mm	Ratio	Ra, μm	Cost, €/m
1	12	0.730	1.443	0.506	2.376	0.1189
2	9	0.736	1.593	0.462	1.798	0.1324
3	2	0.688	0.927	0.742	2.950	0.0724
4	16	0.706	1.676	0.421	2.344	0.0806
5	14	0.851	1.226	0.694	3.521	0.0900
6	6	0.878	1.459	0.602	2.912	0.1002
7	8	0.554	1.418	0.391	3.438	0.0900
8	10	0.580	1.659	0.349	3.059	0.1002
9	4	0.874	1.392	0.628	2.949	0.1256
10	3	0.846	1.193	0.709	3.427	0.0765
11	11	0.580	1.601	0.362	2.875	0.1256
12	17	0.543	1.281	0.424	3.370	0.0765
13	15	0.716	1.476	0.485	2.178	0.0951
14	1	0.715	1.473	0.485	2.330	0.0951
15	5	0.719	1.526	0.471	2.243	0.0951
16	13	0.690	1.463	0.471	2.147	0.0951
17	7	0.704	1.476	0.477	2.215	0.0951

5.2.1 Development of the mathematical models for UHMWPE

The test for significance of the regression models, the test for significance on each of the model coefficients and the lack of fit test were carried out. Step-wise regression methods were selected to identify the significant model terms automatically, the resultant ANOVA tables for the reduced quadratic models summarise the analysis of variance of each response and show the significant model terms. For this material, there are fifteen ANOVA tables, too much to present. Therefore, the most important data was extracted from these tables and is shown in Table 5.16. This table also shows the other adequacy measures R^2, Adjusted R^2 and predicted R^2. The entire adequacy measures are close to 1, which are in reasonable agreement and indicate adequate models. These adequacy measures are in good agreement to measures obtained in [121].

Table 5.16: Abstracted ANOVA Tables for all reduced quadratic models of UHMWPE.

Thickness	Response	SS_M	DF	Lack of Fit	Prob. >F Model	R^2	Adj- R^2	Pre- R^2
6	Upper kerf	0.29	13	Not Sig.	< 0.0001 (Sig.)	0.9951	0.9940	0.9916
	Lower kerf	0.31	6	Not Sig.	< 0.0001 (Sig.)	0.9697	0.9515	0.8569
	Ratio	0.24	7	Not Sig.	< 0.0001 (Sig.)	0.9950	0.9911	0.9741
	Ra	2.836	6	Not Sig.	< 0.0001 (Sig.)	0.9126	0.8602	0.7168
	Cost	0.003	4	-	< 0.0001 (Sig.)	0.9999	0.9998	0.9995
8	Upper kerf	0.25	4	Not Sig.	< 0.0001 (Sig.)	0.9895	0.9859	0.9757
	Lower kerf	0.51	7	Not Sig.	< 0.0001 (Sig.)	0.9884	0.9794	0.9144
	Ratio	0.35	9	Not Sig.	< 0.0001 (Sig.)	0.9987	0.9970	0.9897
	Ra	2.68	5	Not Sig.	< 0.0001 (Sig.)	0.9166	0.8787	0.7689
	Cost	0.005	4	-	< 0.0001 (Sig.)	0.9999	0.999	0.9995
10	Upper kerf	0.18	3	Not Sig.	< 0.0001 (Sig.)	0.9951	0.9940	0.9932
	Lower kerf	0.50	4	Not Sig.	< 0.0001 (Sig.)	0.8882	0.8510	0.7243
	Ratio	0.22	5	Not Sig.*	< 0.0001 (Sig.)	0.9567	0.9371	0.8298
	Ra	4.69	6	Not Sig.	< 0.0001 (Sig.)	0.9921	0.9874	0.9742
	Cost	0.005	4	-	< 0.0001 (Sig.)	0.9999	0.9999	0.9998

* Not Significant at $\alpha = 0.001$.

5.2.1.1 Analysis of variance for 6 mm thick UHMWPE model.

The analysis of variance of the 6 mm thick model indicates that, for the upper kerf model, the main effect of all the factors are the most significant model terms associated with this response. While, for the lower kerf model, the analysis indicates that the main effect of all factors, the quadratic effect of laser power (A^2), cutting speed (B^2) and

interaction effect between laser power with cutting speed (AB) are the significant model terms. Then, for the ratio model the analysis demonstrated that the main effect of all the following factors, the quadratic effect of laser power (A^2), cutting speed (B^2), and the interaction effect between laser power with cutting speed (AB) and laser power with focal position (AC) are the significant model terms. For the roughness model the analysis shows that the main and the quadratic effects of all factors are the significant model terms. Finally, for the cost model the ANOVA results confirm that the main effect of laser power (A), cutting speed (B), interaction effect between laser power with cutting speed (AB) and quadratic effect of cutting speed are the important model terms associated with the operating cost model. The final mathematical models in terms of actual factors as determined by design expert software are shown below Eqs. 5.16 – 5.20:

$$\text{Upper kerf} = 0.26423 + 8.41000E\text{-}005 * \text{Laser power} - 1.22267E\text{-}004 * \text{Cutting speed} - 0.12228 * \text{Focal position} \quad (5.16)$$

$$\text{Lower kerf} = 0.21041 + 1.82204E\text{-}003 * \text{Laser power} + 1.55536E\text{-}004 * \text{Cutting speed} + 0.037950 * \text{Focal position} + 8.93867E\text{-}007 * \text{Laser power} * \text{Cutting speed} - 1.18324E\text{-}006 * \text{Laser power}^2 - 4.77174E\text{-}007 * \text{Cutting speed}^2 \quad (5.17)$$

$$\text{Ratio} = 0.31284 - 3.00566E\text{-}004 * \text{Laser power} - 6.42746E\text{-}005 * \text{Cutting speed} - 0.16109 * \text{Focal position} - 3.69797E\text{-}007 * \text{Laser power} * \text{Cutting speed} + 4.76135E\text{-}005 * \text{Laser power} * \text{Focal position} + 3.82953E\text{-}007 * \text{Laser power}^2 + 1.57950E\text{-}007 * \text{Cutting speed}^2 \quad (5.18)$$

$$\text{Ra} = 9.32682 - 8.10304E\text{-}003 * \text{Laser power} - 2.23609E\text{-}003 * \text{Cutting speed} + 1.40210 * \text{Focal position} + 3.43664E\text{-}006 * \text{Laser power}^2 + 1.02037E\text{-}006 * \text{Cutting speed}^2 + 0.27877 * \text{Focal position}^2 \quad (5.19)$$

$$\text{Operating cost} = 0.14379 + 4.16094E\text{-}005 * \text{Laser power} - 1.23628E\text{-}004 * \text{Cutting speed} - 1.54174E\text{-}008 * \text{Laser power} * \text{Cutting speed} + 3.38949E\text{-}008 * \text{Cutting speed}^2 \quad (5.20)$$

5.2.1.2 Analysis of variance for 8 mm thick UHMWPE model.

The analysis of variance of the 8 mm thick model demonstrates that, for the upper kerf model, the main effect of all the factors and interaction effect between cutting speed with focal position (BC) are the most significant model terms associated with upper kerf width. For the lower kerf model, the analysis shows that the main effect of all factors, the quadratic effect of laser power (A^2), cutting speed (B^2) and focal position (C^2) and interaction effect between laser power with cutting speed (AB) are the significant model terms in this case. Regarding the ratio model the analysis demonstrates that, the main, the quadratic and the interaction effects of all factors are the significant model terms. For the roughness model, the analysis indicates that the main effect of all factors and the quadratic effect of laser power (A^2) and focal position (C^2) are the significant model terms. At last, for the cost model the results reveal that the main effect of laser power (A), cutting speed (B), interaction effect between laser power with cutting speed (AB) and quadratic effect of cutting speed are the important model terms associated with the operating cost model. The final mathematical models in terms of actual factors, as determined by design expert software, are shown below Eqs 5.21 – 5.25:

$$\text{Upper kerf} = 0.28788 + 9.32000E\text{-}005 * \text{Laser power} - 2.87083E\text{-}004 * \text{Cutting speed} - 0.070450 * \text{Focal position} - 3.90000E\text{-}005 * \text{Cutting speed} * \text{Focal position} \quad (5.21)$$

$$\text{Lower kerf} = 1.42244 + 5.12015E\text{-}004 * \text{Laser power} - 8.64961E\text{-}004 * \text{Cutting speed} - 0.095873 * \text{Focal position} + 1.65267E\text{-}006 * \text{Laser power} * \text{Cutting speed} - 7.67760E\text{-}007 * \text{Laser power}^2 - 6.38722E\text{-}007 * \text{Cutting speed}^2 - 0.020816 * \text{Focal position}^2 \quad (5.22)$$

$$\text{Ratio} = -0.025316 + 3.97060E\text{-}004 * \text{Laser power} + 1.24032E\text{-}004 * \text{Cutting speed} + 0.033892 * \text{Focal position} - 8.34475E\text{-}007 * \text{Laser power} * \text{Cutting speed} + 8.67107E\text{-}005 * \text{Laser power} * \text{Focal position} - 8.26412E\text{-}005 * \text{Cutting speed} * \text{Focal position} + 3.22777E\text{-}007 * \text{Laser power}^2 + 2.48208E\text{-}007 * \text{Cutting speed}^2 + 0.018824 * \text{Focal position}^2 \quad (5.23)$$

$$Ra = 13.22115 - 9.99691E\text{-}003 * \text{Laser power} + 5.98833E\text{-}004 * \text{Cutting speed} + 2.56056 * \text{Focal position} + 3.97192E\text{-}006 * \text{Laser power}^2 + 0.28180 * \text{Focal position}^2 \quad (5.24)$$

$$\text{Operating cost} = 0.18315 + 5.20117E\text{-}005 * \text{Laser power} - 1.98785E\text{-}004 * \text{Cutting speed} - 2.40896E\text{-}008 * \text{Laser power} * \text{Cutting speed} + 6.86327E\text{-}008 * \text{Cutting speed}^2 \quad (5.25)$$

5.2.1.3 Analysis of variance for 10 mm thick UHMWPE model.

The analysis of variance of the 10 mm thick model reveals that, for the upper kerf model, the main effect of all the factors are the most significant model terms associated with this response. While, for the lower kerf model the analysis shows that the main effect of all factors and interaction effect between laser power and cutting speed (AB) are the major model terms. For the ratio model the analysis exhibits that, the main effect of all factors, the quadratic effect of cutting speed (B^2) and the interaction effect between laser power and cutting speed (AB) are the significant model terms. Then, for the roughness model the analysis indicates that the main effect of all factors and the interaction effect between laser power and cutting speed (AC) and the quadratic effect of laser power (A^2) and focal position (C^2) are the significant model terms. Finally, for the cost model the results reveal that the main effect of laser power (A), cutting speed (B), interaction effect between laser power with cutting speed (AB) and quadratic effect of cutting speed are the most important model terms associated with the operating cost model. The final mathematical models in terms of actual factors, as determined by design expert software, are shown below Eqs 5.26 – 5.30:

$$\text{Upper kerf} = 0.16689 + 5.48571E\text{-}005 * \text{Laser power} - 7.67778E\text{-}005 * \text{Cutting speed} - 0.099350 * \text{Focal position} \quad (5.26)$$

$$\text{Lower kerf} = 5.46361 - 2.53356E\text{-}003 * \text{Laser power} - 5.37308E\text{-}003 * \text{Cutting speed} + 0.057400 * \text{Focal position} + 3.79937E\text{-}006 * \text{Laser power} * \text{Cutting speed} \quad (5.27)$$

$$\text{Ratio} = -1.13392 + 1.27256E\text{-}003 * \text{Laser power} + 9.67550E\text{-}004 * \text{Cutting speed} - 0.092199 * \text{Focal position} - 1.76063E\text{-}006 * \text{Laser power} * \text{Cutting speed} + 7.91773E\text{-}007 * \text{Cutting speed}^2 \quad (5.28)$$

$$\text{Ra} = 19.65596 - 9.71989E\text{-}003 * \text{Laser power} + 1.16189E\text{-}003 * \text{Cutting speed} + 4.11779 * \text{Focal position} + 2.19810E\text{-}004 * \text{Laser power} * \text{Focal position} + 3.67725E\text{-}006 * \text{Laser power}^2 + 0.40034 * \text{Focal position}^2 \quad (5.29)$$

$$\text{Operating cost} = 0.21924 + 6.10875E\text{-}005 * \text{Laser power} - 2.84949E\text{-}004 * \text{Cutting speed} - 3.35160E\text{-}008 * \text{Laser power} * \text{Cutting speed} + 1.18084E\text{-}007 * \text{Cutting speed}^2 \quad (5.30)$$

5.2.2 Validation of the developed models of UHMWPE

The validity of the models developed for 6 mm UHMWPE can be drawn from Fig. 5.11, which presents the relationship between the measured and predicted values of the investigated responses. These scatter diagrams indicate that the above mathematical models show excellent agreement between the measured and estimated values of the above mentioned responses. The same trends have been found for the other two thicknesses as presented in Figs. 5.12-5.13. In order to verify the adequacy of the developed models furthermore, two confirmation experiments for each thickness were carried out using new test conditions. These experiments are taken from the optimisation results which are within the investigated range. By using the point prediction option in the software, all the responses values can be predicted by substituting these conditions into the previous developed models. Table 5.17 presents the experimental conditions, the actual experimental values, the predicted values and the percentages of error for all thicknesses. It is clear that all the percentage error values for all the five responses, are within reasonable agreement with the values achieved in [119 and 136], and therefore, it would strongly suggest that the models are valid.

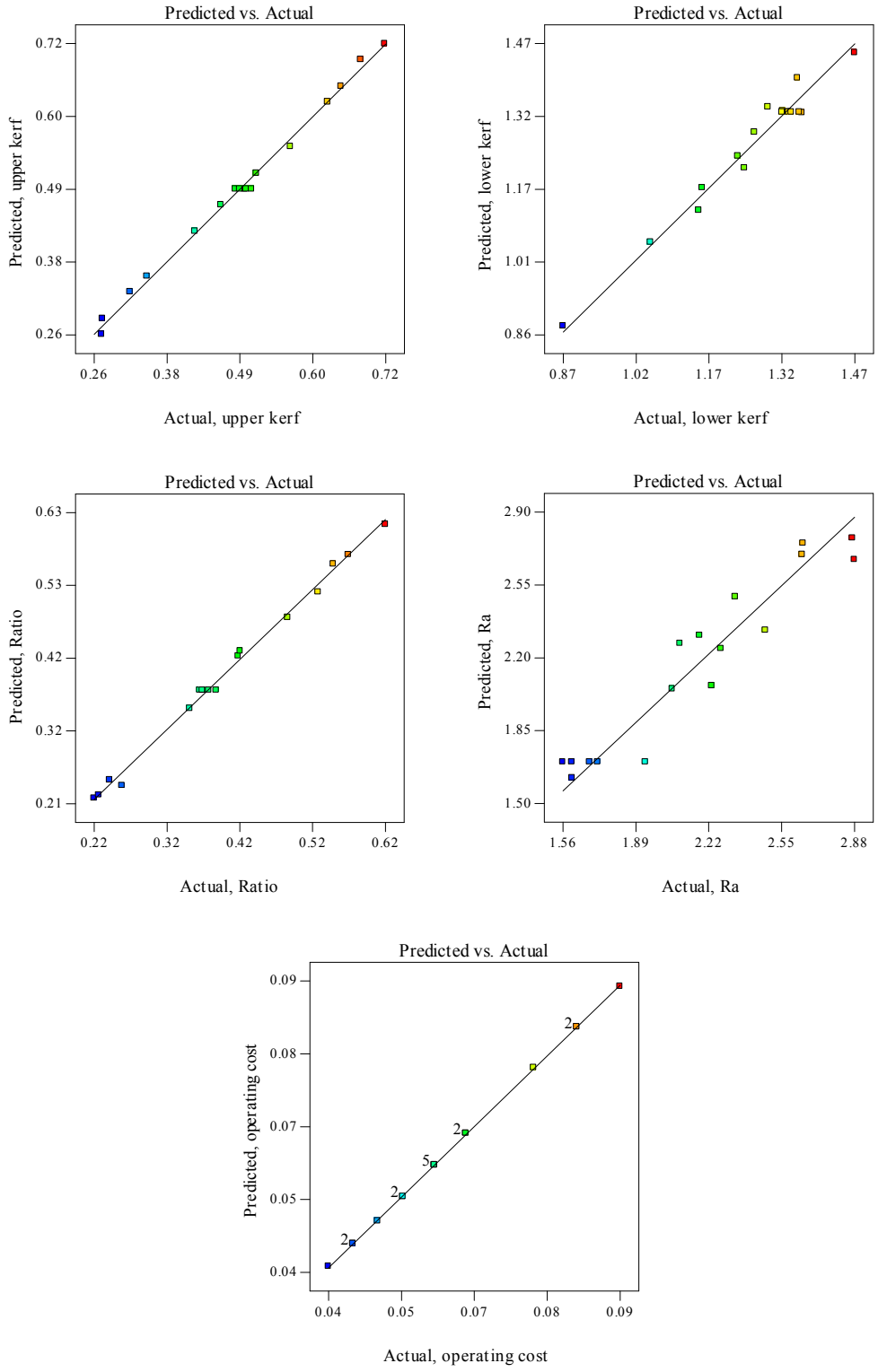

Fig. 5.11: Scatter diagram showing the relationship between the actual and predicted values for each response for 6 mm thick UHMWPE.

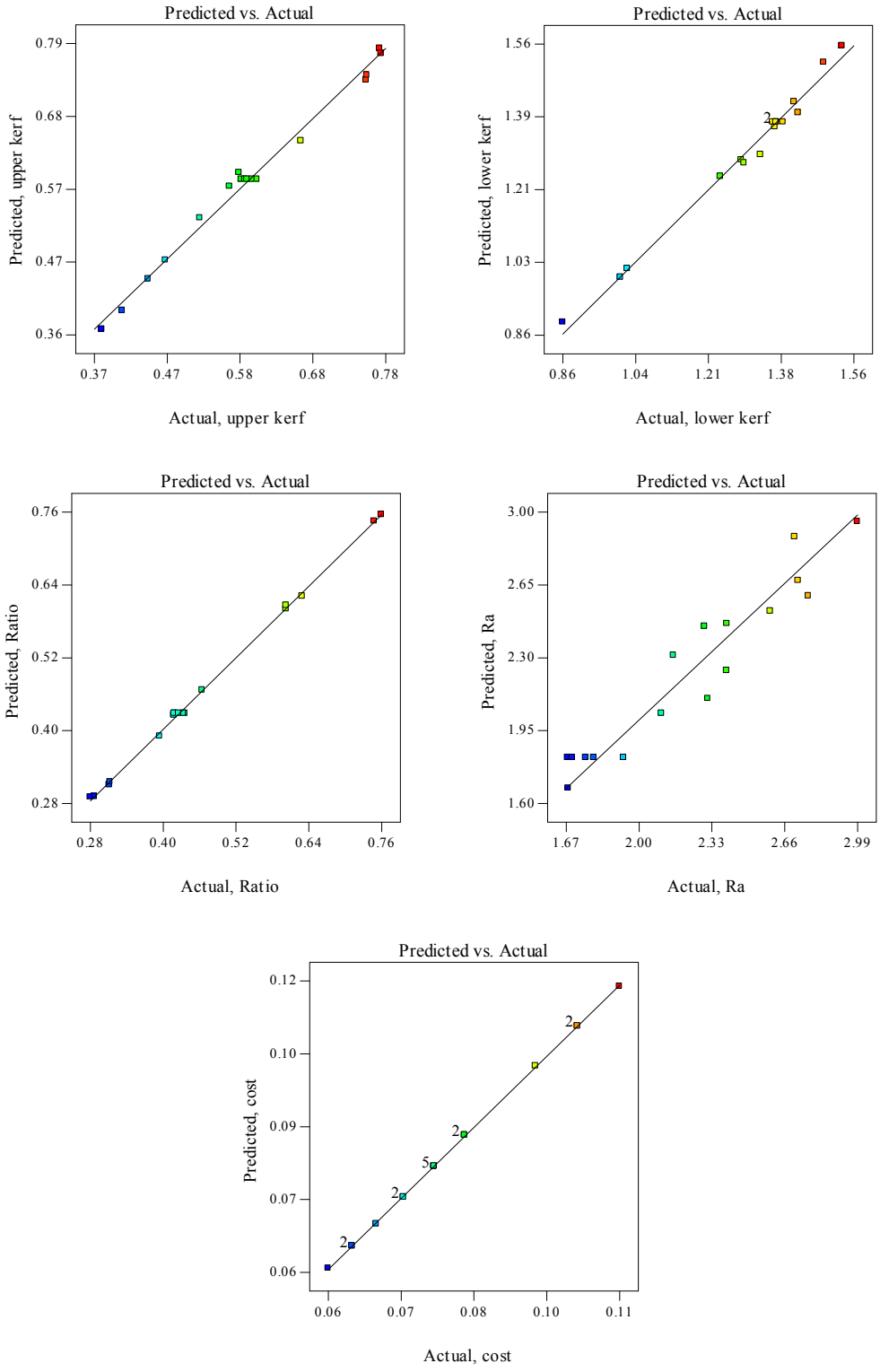

Fig. 5.12: Scatter diagram showing the relationship between the actual and predicted values for each response for 8 mm thick UHMWPE.

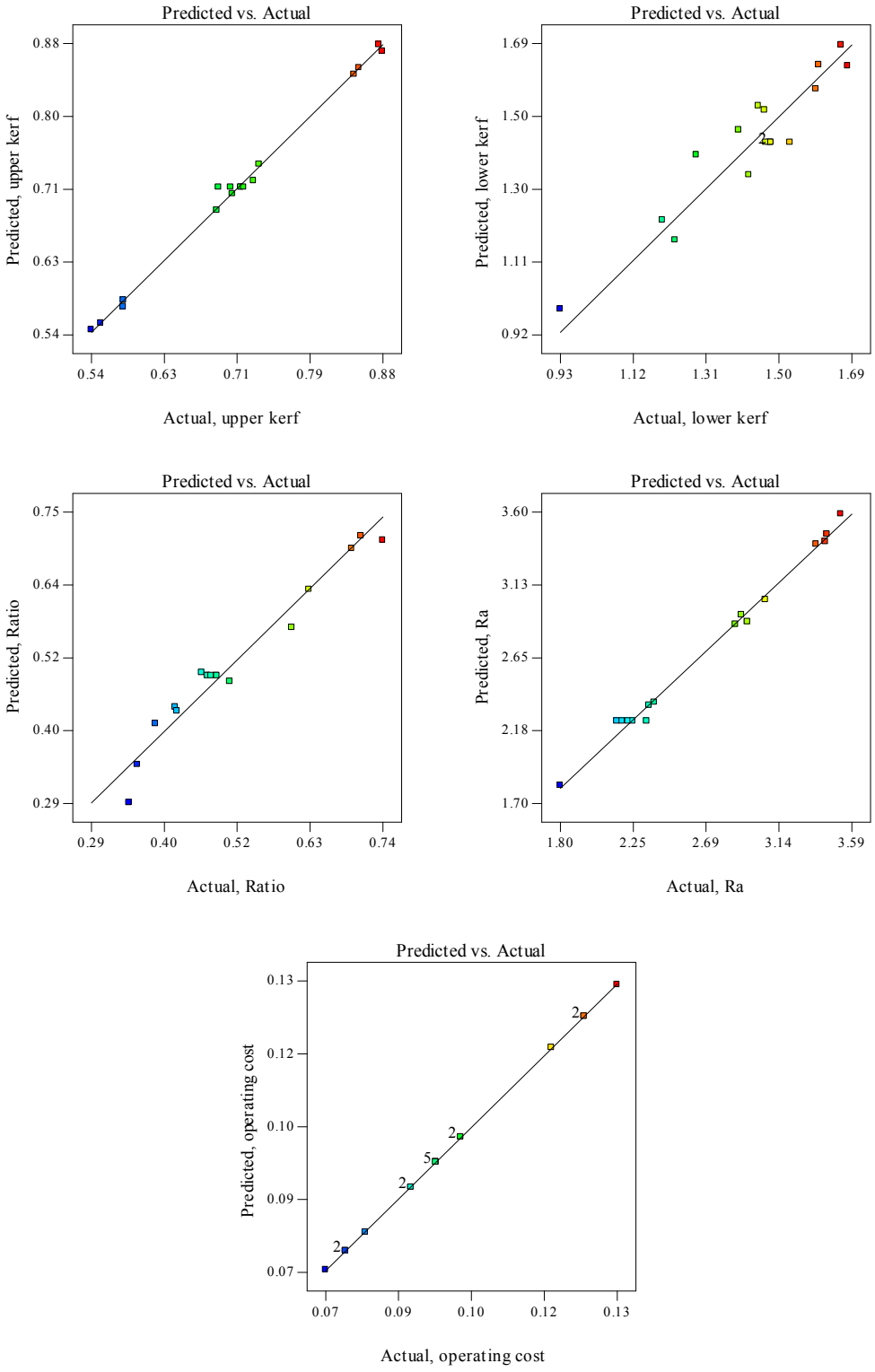

Fig. 5.13: Scatter diagram showing the relationship between the actual and predicted values for each response for 10 mm thick UHMWPE.

Table 5.17: Confirmation experiments for UHMWPE.

Thickness	Exp. No.	Factors			Values	Responses				
		A	B	C		Upper kerf	Lower kerf	Ratio	Roughness	Cost
6	1	1261.7	1000	-3.24	Actual	0.634	1.450	0.437	1.774	0.0876
					Predicted	0.644	1.309	0.498	1.743	0.0871
					Error %	-1.577	9.749	-13.927	1.747	0.571
	2	800	1750	-1.35	Actual	0.267	0.879	0.303	2.590	0.0429
					Predicted	0.283	0.922	0.337	2.869	0.0429
					Error %	-6.072	-4.868	-11.053	-10.755	0.000
8	1	1312.8	800	-5.48	Actual	0.792	1.406	0.563	1.801	0.1112
					Predicted	0.738	1.307	0.552	1.853	0.111
					Error %	6.795	7.054	1.967	-2.864	0.180
	2	900	1400	-4.5	Actual	0.572	0.904	0.633	2.167	0.0556
					Predicted	0.533	0.891	0.600	2.463	0.0558
					Error %	6.883	1.416	5.262	-13.649	-0.360
10	1	1450	700	-6.31	Actual	0.810	1.619	0.500	2.147	0.1324
					Predicted	0.819	1.523	0.571	2.050	0.1322
					Error %	-1.161	5.930	-14.186	4.518	0.151
	2	1100	1150	-5.5	Actual	0.705	0.921	0.766	2.560	0.0724
					Predicted	0.685	0.988	0.706	2.882	0.0725
					Error %	2.809	-7.321	7.783	-12.587	-0.138

5.2.3 Effect of process factors on the responses for UHMWPE

5.2.3.1 Upper kerf

It is evident from Fig. 5.14 that the focal point position has the most important effect on the upper kerf, and then the laser power and cutting speed. However, the upper kerf increases as the focal position and cutting speed decreases while it increases as the laser power increases. This is due to the fact that when a defocused beam is being used the laser power spreads on the surface onto a wider area; as the beam becomes wider at the top of the specimen, causing the upper kerf to increase. Also, when using slow cutting speeds especially at high laser power, more heat is introduced to the specimen, and thus, more materials melt and are ejected causing the upper kerf to increase. In the case of laser power effect, the upper kerf would increase as a consequence of increased laser power due to the increase in the heat input. These results are in good agreement with the results obtained by Caiazzo et al. [48]. The percentage change in the upper kerf as a result of changing each factor from its lowest value to its highest value while keeping the other factors at their centre values are as follows (the percentages are for 6 mm, 8 mm and 10 mm thick respectively): (i) Changing focal position would result in a decrease of 54.64%, 44.78% and 34.61%. (ii) Changing the cutting speed would result in a decrease of 17.11%, 10.75% and 4.74%. (iii) Changing the laser power would result in an increase of 8.96%, 8.23% and 2.73%. Figure 5.15 contour plots show the effect of focal position and cutting speed on the upper kerf for the three thicknesses.

5.2.3.2 Lower kerf

It is apparent from Fig. 5.16 that all three factors have a major effect on the lower kerf. The order of importance is as follows; laser power, cutting speed and focal position. However, upper kerf increases as the laser power and focal position increase while it decreases as the cutting speed increases. Caiazzo et al. [48] have reported the same observations. This is due to the fact that when a defocused beam is being used the laser power spreads on the bottom surface over a wider area; as the beam becomes wider at the bottom of the specimen the lower kerf increases.

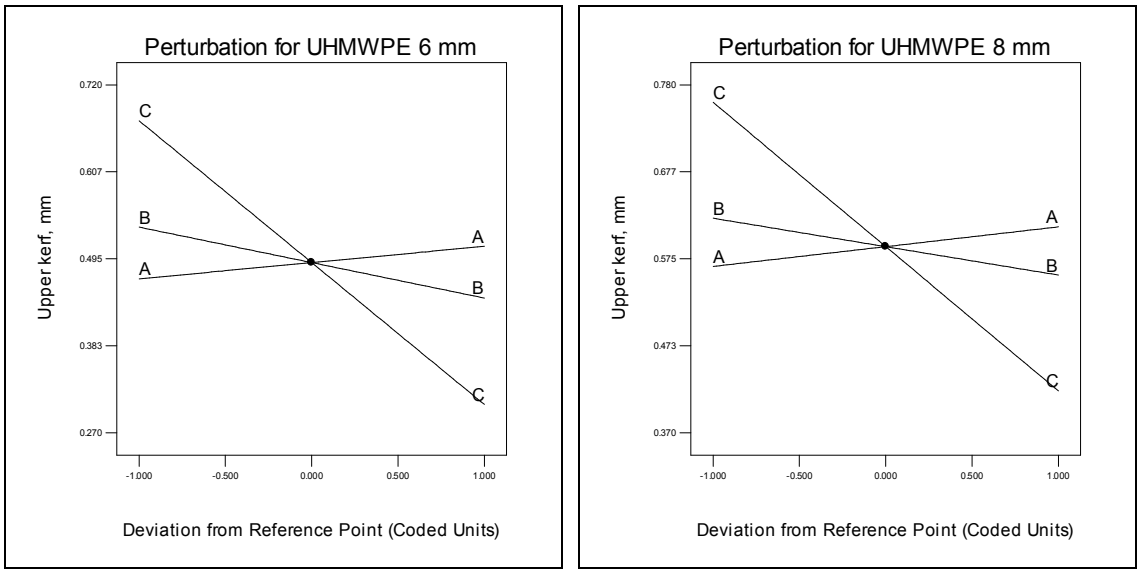

(a) (b)

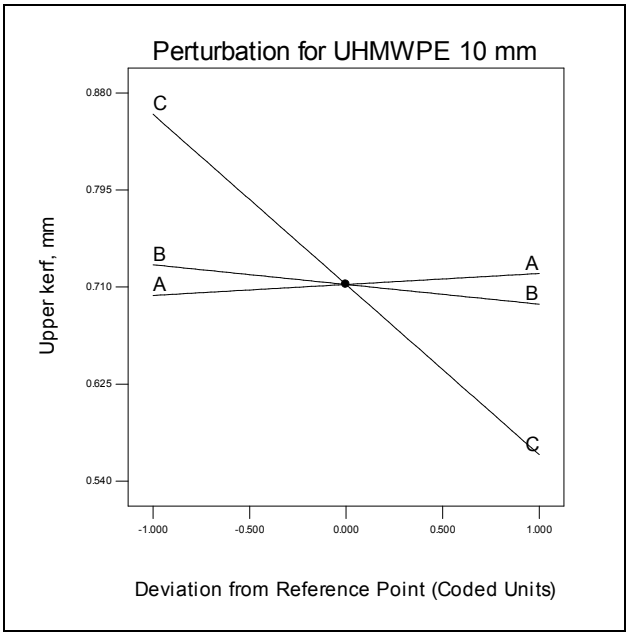

(c)

Fig. 5.14: Perturbation plots illustrating the effect of each factor on the upper kerf for the (a) 6 mm thick, (b) 8 mm thick and (c) 10 mm thick.

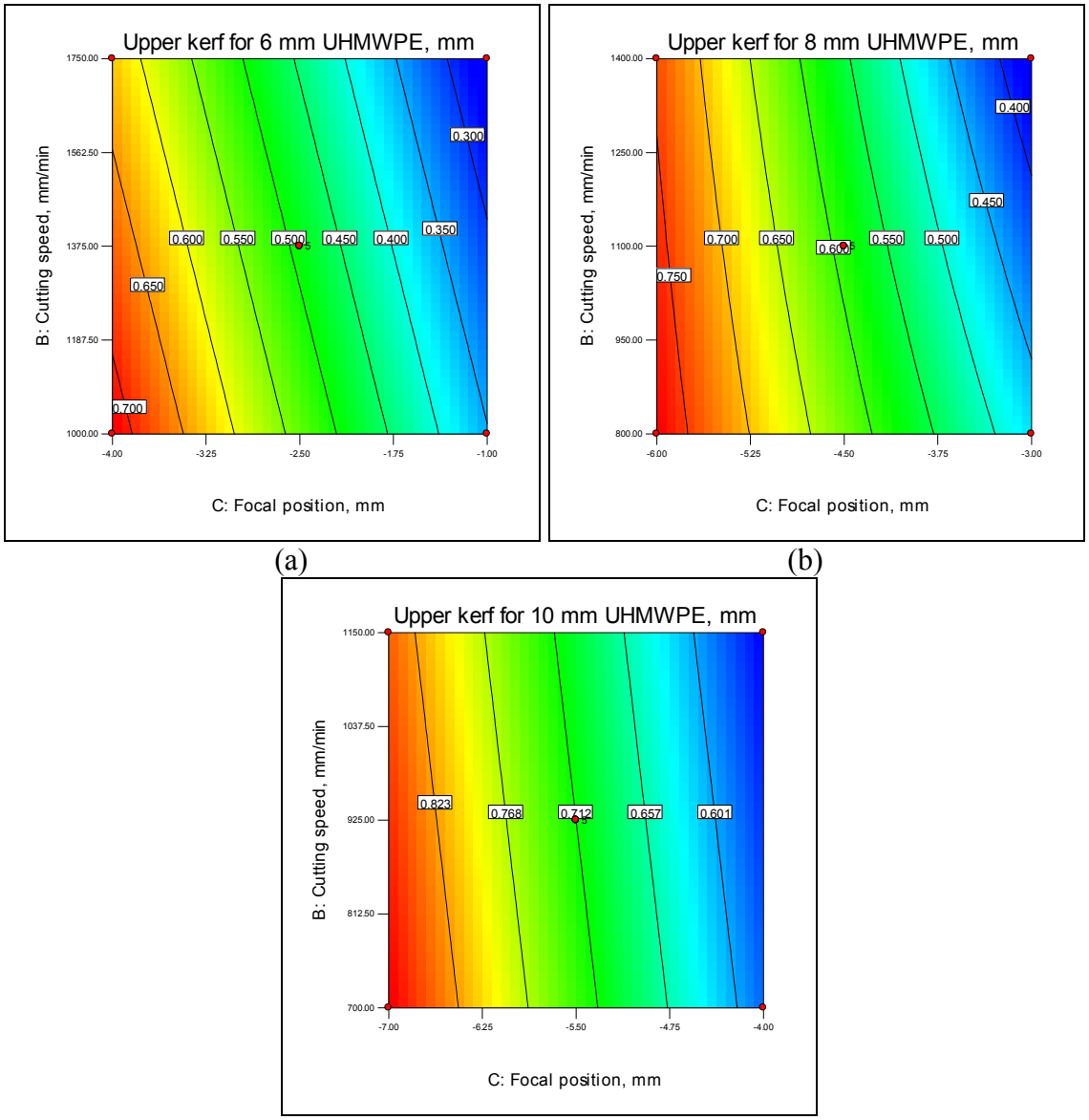

(a) (b)

(c)

Fig. 5.15: Contour plots showing the effect of focal position and cutting speed on the upper kerf for the (a) 6 mm thick, (b) 8 mm thick and (c) 10 mm thick.

Also, by using slow cutting speeds more heat would be transferred to the specimen, and consequently, more materials would melt and be ejected causing the lower kerf to increase. Remarked, in the case of laser power effect, the lower kerf would increase as the laser power increased due to the increase of heat input, which is a consequence of raising the beam power. The percentage change in the lower kerf as a result of changing each factor from its lowest value to its highest value whilst

maintaining the other factors at their centre values are as follows (the percentages are for 6 mm, 8 mm and 10 mm thick respectively): (i) Changing focal position would result in an increase of 8.97%, 23.10% and 12.83%. (ii) Changing the cutting speed would result in a decrease of 12.20%, 15.56% and 15.38%. (iii) Changing the laser power would result in an increase of 25.49%, 23.84% and 27.32%. The Fig. 5.17 contour plots present the effect of cutting speed and laser power on the lower kerf for the three thicknesses.

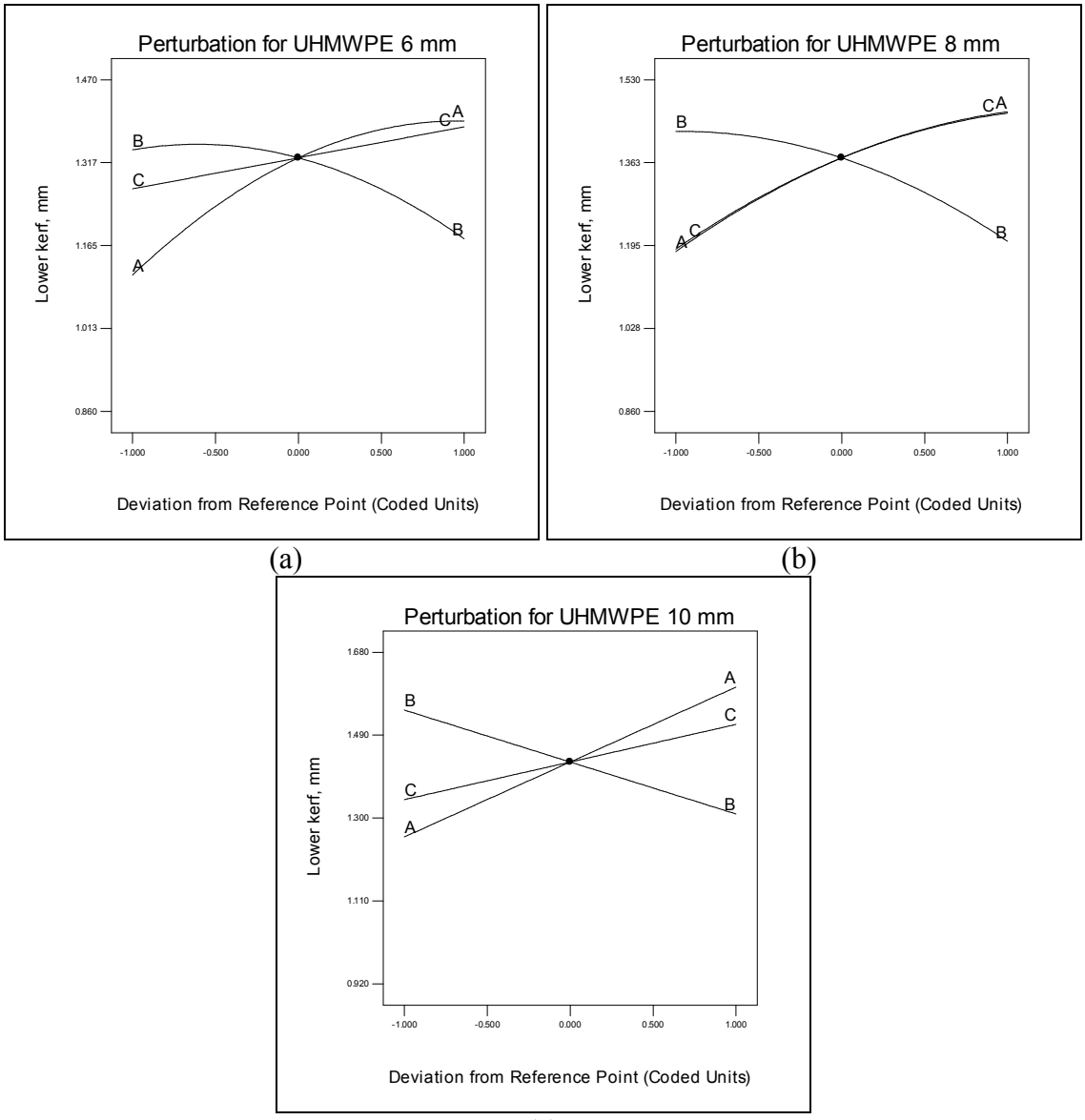

(a) (b)

(c)

Fig. 5.16: Perturbation plots illustrating the effect of each factor on the lower kerf for the (a) 6 mm thick, (b) 8 mm thick and (c) 10 mm thick.

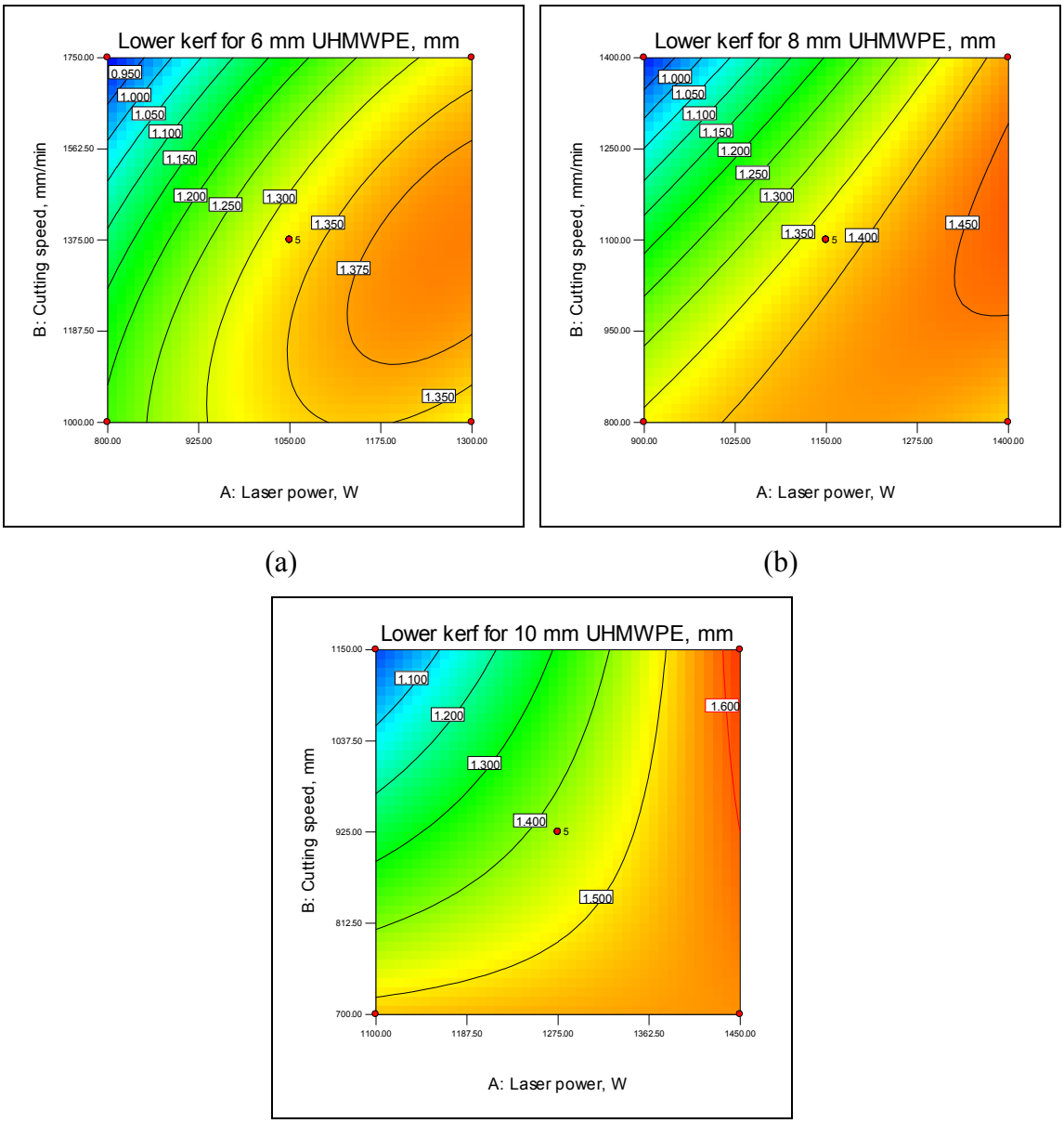

(a) (b)

(c)

Fig. 5.17: Contour plots showing the effect of cutting speed and laser power on the lower kerf for the (a) 6 mm thick, (b) 8 mm thick and (c) 10 mm thick.

5.2.3.3 Ratio of the upper kerf to the lower kerf

It is obvious from Fig. 5.18 that the focal point position has the main impact on the ratio between the upper kerf and the lower kerf and then, in order of importance, the laser power and cutting speed. In the case of cutting speed effect, the ratio would increase as the cutting speed increased; this increase is higher for the thicker UHMWPE and becomes insignificant for the thinner UHMWPE. The percentage change in the ratio as a result of manipulating each factor from its lowest value to its highest value while keeping the other factors at their centre levels are as follows (the percentages are for 6 mm, 8 mm and 10 mm respectively): (i) Changing focal position would result in a decrease of 61.70%, 57.53% and 43.91%. (ii) Changing laser power would result in a decrease of 14.46%, 17.19% and 22.49%. (iii) Changing the cutting speed would result in an increase of 3.39%, 11.60% and 17.24%. Fig. 5.19 demonstrates the interaction effect between the laser power and cutting speed on the ratio between the upper kerf and lower kerf. It is clear from Fig. 5.19a-c that using the highest cutting speed with low laser power would result in reduced operating costs. Higher ratio value would be achieved in comparison with the case of applying lowest cutting speeds, yet this is valid only up to certain thresholds of laser power, which are around 1000 W, 1250 W and 1380 W for the thicknesses of 6 mm, 8 mm and 10 mm respectively. Above these thresholds higher values of ratios can be obtained only if the slowest cutting speed is being applied, of course in conjunction with higher laser power levels, but these would increase the operating cost. These results support the results reported by Caiazzo et al. [48] because the high cutting speeds are not at all times associated with good cutting efficiency. The results indicate that the range of the ratio falls within 0.216 to 0.756 for all thicknesses of UHMWPE. As the results for this material demonstrate, it is not possible to obtain ratio values equal to 1, which would lead to a plane-parallel cut faces. Therefore, maximising the ratio in this case is a desirable criterion while searching for the optimal cutting conditions.

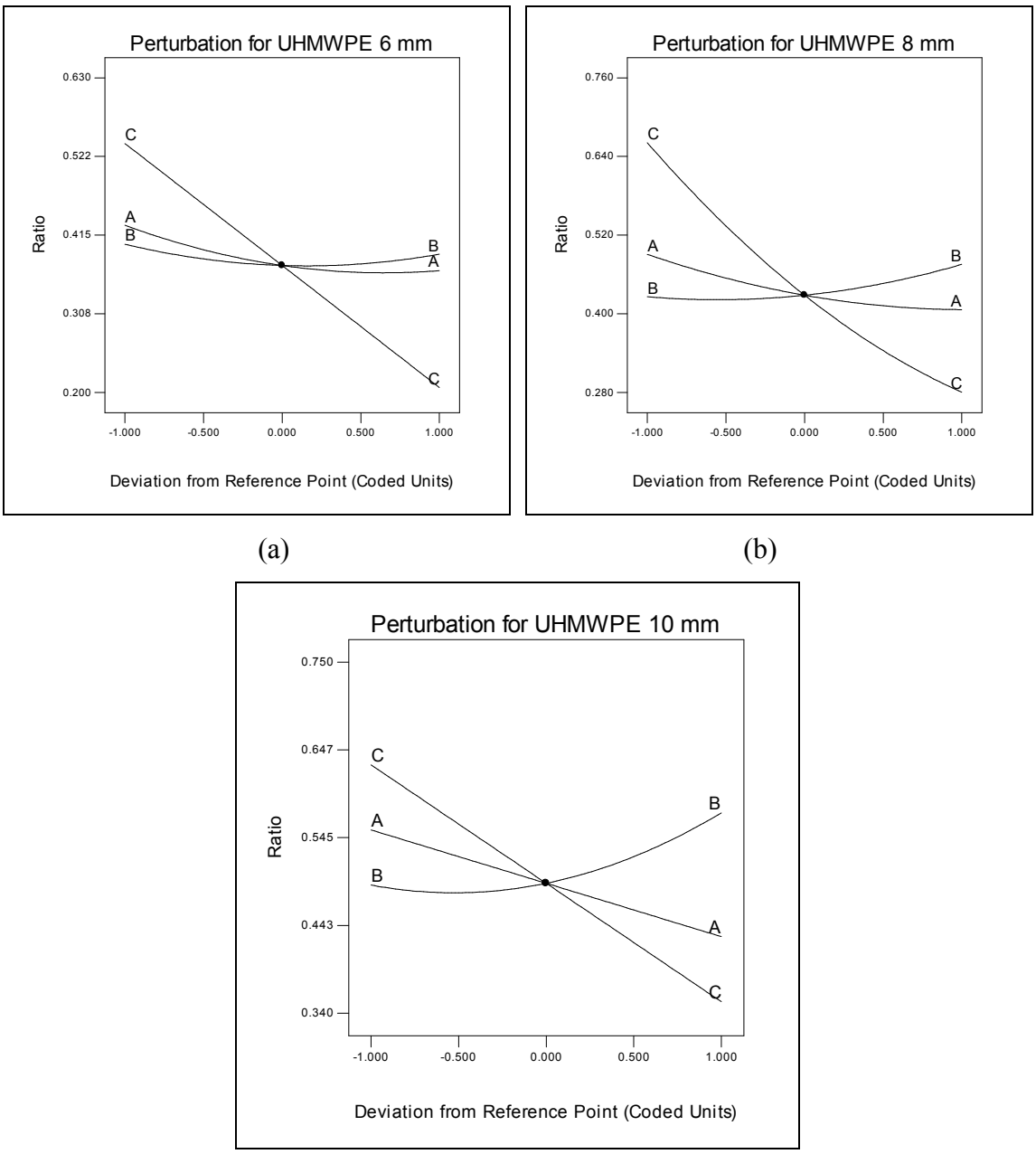

Fig. 5.18: Perturbation plots illustrating the effect of each factor on the ratio between kerfs for the (a) 6 mm thick, (b) 8 mm thick and (c) 10 mm thick.

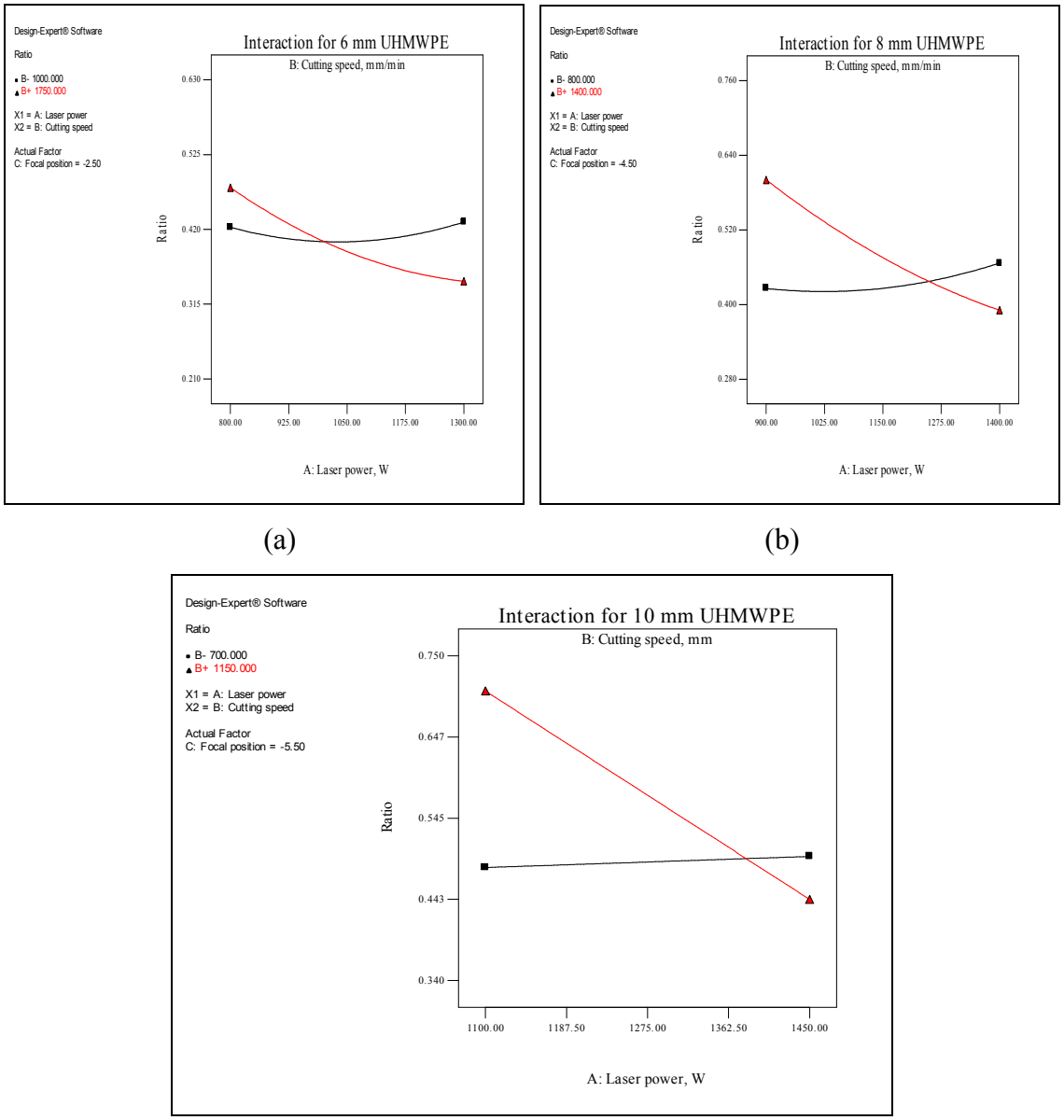

Fig. 5.19: Interaction graph illustrating the interaction effect between cutting speed and laser power on the ratio for the (a) 6 mm thick, (b) 8 mm thick and (c) 10 mm thick.

5.2.3.4 Roughness

It is clear from Fig. 5.20 that all the three factors have a major effect on the roughness of the cut surface; the same has been outlined in [48] and [49]. The results show that the roughness is inversely proportional to laser power which is in agreement with the results reported in [49 and 50]. Also, it was found that the roughness is proportional to cutting speed, which is in agreement with the result reported in [50] and disagrees with results reported in [49]. However, this disagreement may be due to the differences in the properties of the plastic material. In the case of focal point position, the roughness decreases as the focal position increases up to a certain point (when the focal position is approximately half of the thickness) and then it starts to increase. Therefore, when the focal point is located at the centre of the material to be cut, the roughness would be a minimum value given that all the other factors are at their centre levels. The percentage changes in the roughness as a result of changing each factor from its lowest value to its highest value whilst maintaining the other factors at their centre values are as follows (the percentages are for 6 mm, 8 mm and 10 mm thick respectively): (i) Changing cutting speed would result in an increase of 26.24%, 21.90% and 26.47%. (ii) Changing the laser power would result in a decrease of 20.75%, 18.86% and 20.72%. (iii) Changing the focal point position from its lowers level to its centre level would result in a decrease of 26.57%, 24.71% and 28.90%. However, by changing the focal point position from its centre level to its highest level would result in an increase of 37.64%, 36.84% and 39.89%. The Fig. 5.21 contour plots present the effect of cutting speed and laser power on the roughness for the 10 mm thick UHMWPE at three levels of focal position. It is clear that when C = -5.5 mm (Fig. 5.21-b) the roughness would be less in comparison with the Ra values obtained using the same levels of laser power and cutting speed but using C = -7 mm and C = -4 mm as in Fig. 5.21 a and c. Therefore an optimisation is necessary to find out the exact location of the focal point to achieve the minimum roughness.

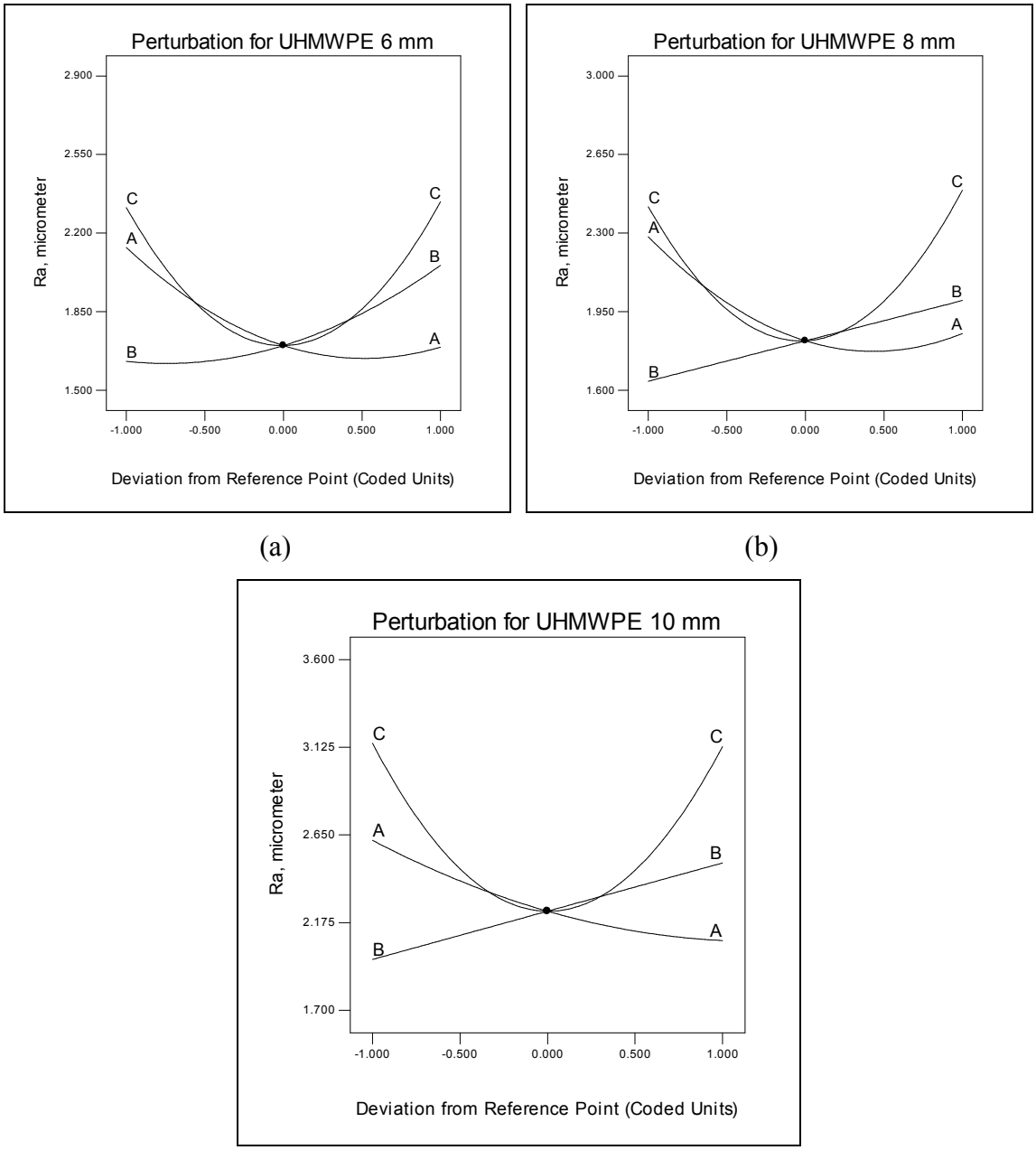

Fig. 5.20: Perturbation plots illustrating the effect of each factor on the roughness for (a) 6 mm thick, (b) 8 mm thick and (c) 10 mm thick.

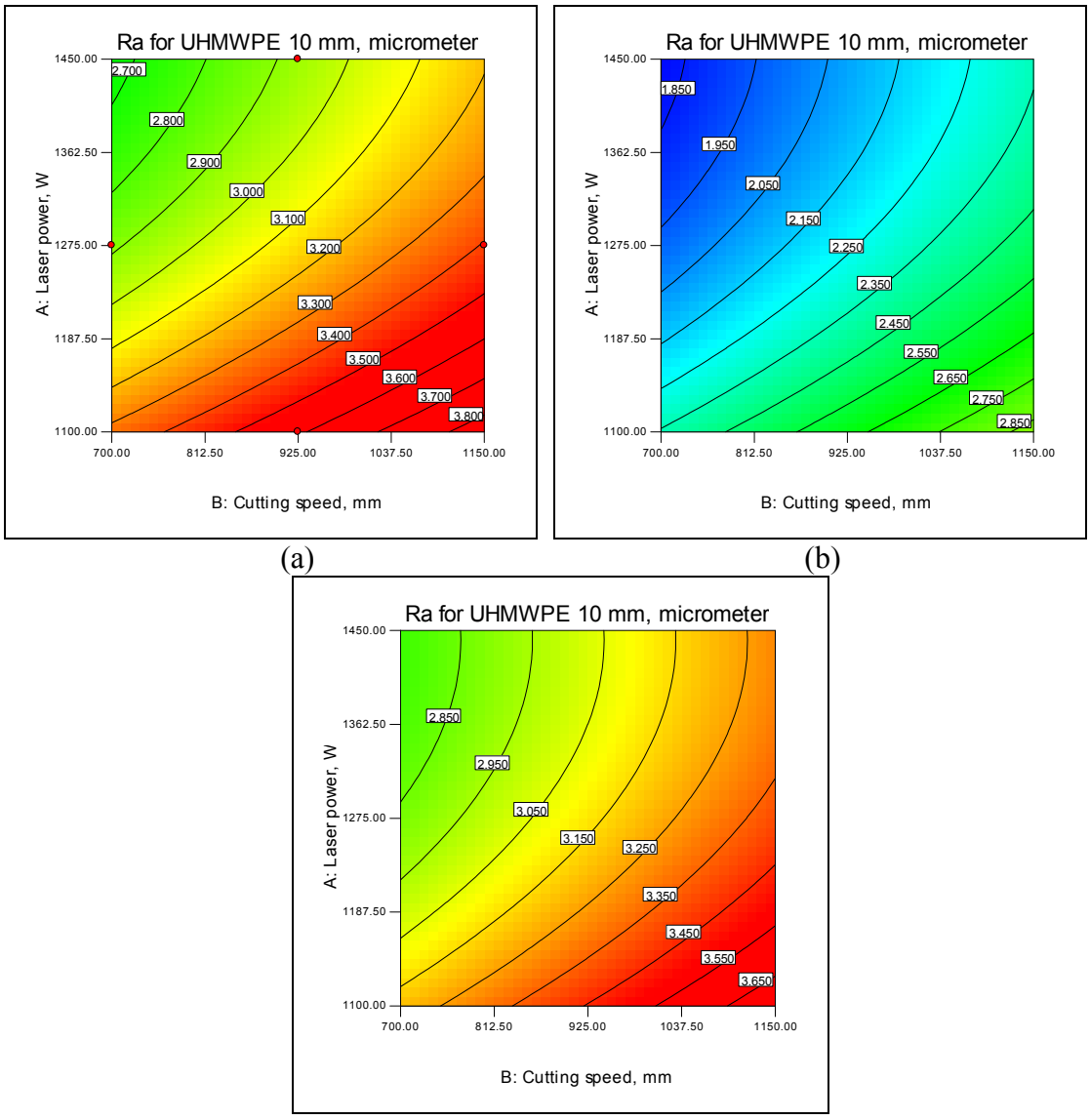

Fig. 5.21: Contour plots shows the effect of cutting speed and laser power on the roughness for 10 mm thick UHMWPE at three levels of focal position. (a) F = -7 mm, (b) F = -5.5 mm and (c) F = -4 mm.

5.2.3.5 Operating cost

It is evident from the results that the cutting speed and laser power have a strong effect on the operating cost as shown in Fig. 5.22. However, the laser power has a positive effect on the operating cost and the cutting speed has a negative effect. It is obvious from the perturbation plots shown in Fig. 5.22 that the operating cost is more

sensitive to the cutting speed. The results indicate that increasing the cutting speed from its lowest value to highest value would result in reducing the operating cost by 42.86%, 42.86% and 39.13% for the three thicknesses respectively. This is due to the fact that using faster cutting speeds leads to decreased cutting time resulting in a reduction in the operating cost. The results indicate that increasing the laser power from its lowest value to highest value would result in increasing the operating cost by 18.82%, 18.10% and 11.73% for the three thicknesses respectively. This increase in the operating cost as the laser power increase is due to the consumption of more electrical power as higher laser power is used.

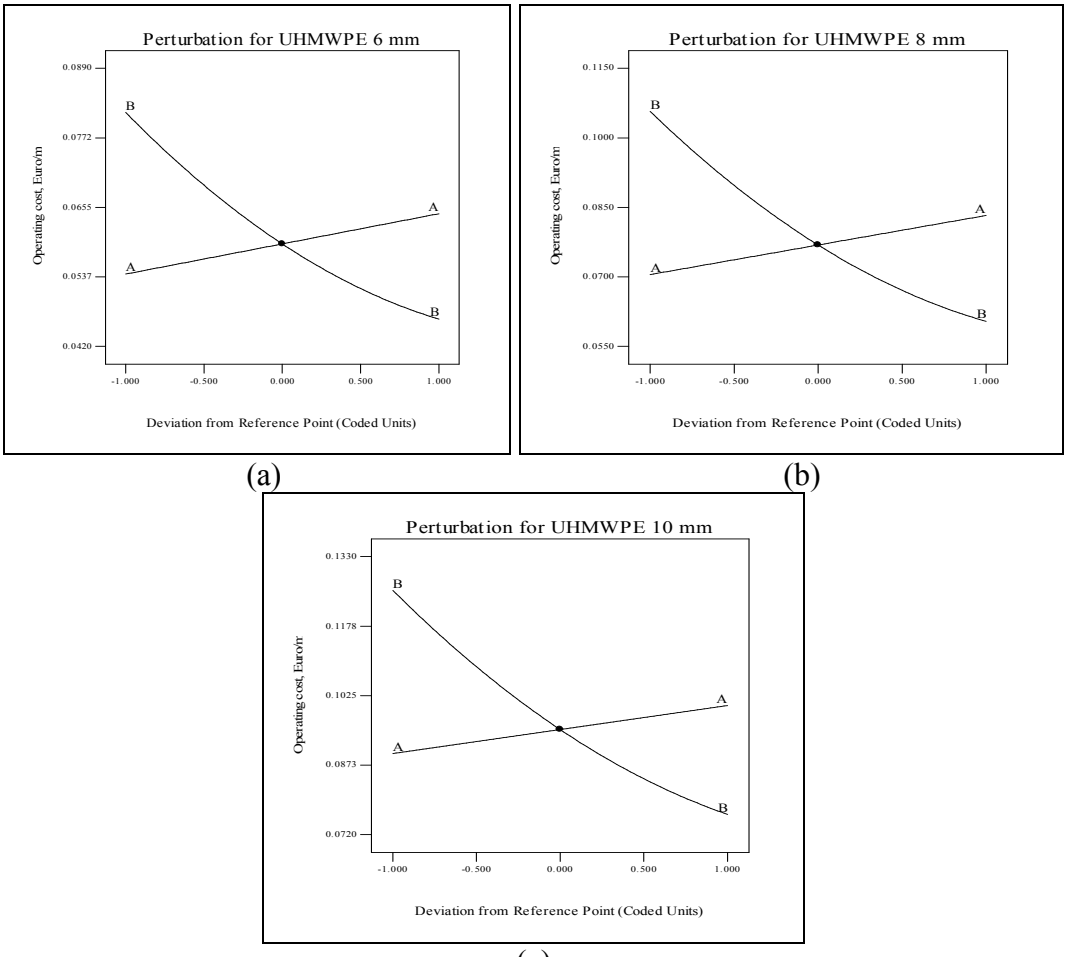

Fig. 5.22: Perturbation plots illustrating the effect of each factor on the operating cost for (a) 6 mm thick, (b) 8 mm thick and (c) 10 mm thick.

Depending on the end-user's requirements for cutting UHMWPE, there may be a trade-off between quality of the cutting operation and the cost of the cutting operation. Thus, an optimisation of the LBC process for this polymeric material is crucial.

5.3 Polymethyl-Methacrylate (PMMA)

For this polymeric material PMMA, six responses were considered namely: upper kerf, lower kerf, ratio between upper and lower kerfs, surface roughness, operating cost and HAZ (the HAZ was successfully modelled for two thicknesses only). In fact, four thicknesses were studied 2, 4, 6 and 8mm. The equipments illustrated previously in chapter 4 were employed to assess these responses. An average of at least five steady measurements for both kerf widths, surface roughness and HAZ were recorded for all 29 runs shown in Tables 4.15-4.18 for the four thicknesses. The ratio of the upper kerf to the lower kerf was calculated for each run using the averaged data. The average values of the measured responses are listed in Tables 5.18 – 5.21. The complete experimentally evaluated responses are presented in appendix C. The operating cost was estimated using Eq. 4.5 and Eq. 4.3 and the estimated operating cost for each experiment is presented in Tables 5.18 – 5.21.

5.3.1 Development of the mathematical models for PMMA

The test for significance of the regression models, test for significance on each model coefficients and the lack of fit test were carried out. Step-wise regression methods were selected to select the significant model terms automatically, the resultant ANOVA tables for the reduced quadratic models summarise the analysis of variance of each response and show the significant model terms. For this material, there are twenty two ANOVA tables. The most important results were extracted and are shown in Table 5.22. Therefore, these tables were abstracted to show only the most important information as shown in Table 5.22. This table also shows the other adequacy measures R^2, Adjusted R^2 and predicted R^2. The entire adequacy measures are close to 1, which are in reasonable agreement and indicate adequate models. These adequacy measures are in good agreement in comparison to the similar ones obtained in [115 and 138].

Table 5.18: Average of Experimentally measured responses for 2 mm PMMA.

No	Upper kerf	Lower kerf	Ratio	R_a	HAZ	Cost
1	0.593	0.233	2.545	4.011	0.042	0.0369
2	0.752	0.233	3.220	1.280	0.050	0.0414
3	0.708	0.212	3.342	5.390	0.035	0.0111
4	0.430	0.222	1.934	6.083	0.039	0.0124
5	0.448	0.205	2.192	1.752	0.041	0.0180
6	0.732	0.173	4.223	3.254	0.032	0.0181
7	0.751	0.259	2.897	2.104	0.053	0.0180
8	0.361	0.178	2.029	2.617	0.023	0.0181
9	0.444	0.266	1.671	5.517	0.022	0.0170
10	0.653	0.232	2.810	2.388	0.045	0.0191
11	0.576	0.194	2.977	3.563	0.025	0.0170
12	0.606	0.220	2.756	2.543	0.047	0.0191
13	0.557	0.182	3.056	0.867	0.067	0.0390
14	0.475	0.142	3.338	4.764	0.051	0.0117
15	0.574	0.233	2.460	2.440	0.034	0.0392
16	0.504	0.157	3.220	5.323	0.039	0.0118
17	0.572	0.233	2.459	2.532	0.031	0.0170
18	0.731	0.252	2.902	0.959	0.045	0.0191
19	0.665	0.231	2.885	4.301	0.029	0.0171
20	0.435	0.267	1.627	3.801	0.035	0.0191
21	0.442	0.245	1.802	1.474	0.056	0.0391
22	0.533	0.220	2.424	5.872	0.036	0.0117
23	0.542	0.231	2.351	1.547	0.065	0.0391
24	0.565	0.236	2.394	5.593	0.041	0.0117
25	0.590	0.217	2.714	4.251	0.041	0.0181
26	0.577	0.222	2.601	4.337	0.043	0.0181
27	0.593	0.233	2.545	3.938	0.047	0.0181
28	0.752	0.233	3.220	4.192	0.042	0.0181
29	0.708	0.212	3.342	3.797	0.045	0.0181

Table 5.19: Average of Experimentally measured responses for 4 mm PMMA.

No.	Upper kerf	Lower kerf	Ratio	R_a	Cost
1	0.692	0.278	2.488	1.845	0.0484
2	0.770	0.337	2.285	1.262	0.0552
3	0.628	0.173	3.626	7.050	0.0116
4	0.731	0.257	2.850	6.050	0.0132
5	0.916	0.211	4.341	1.377	0.0200
6	0.821	0.202	4.069	4.111	0.0201
7	0.672	0.307	2.185	1.188	0.0200
8	0.527	0.310	1.699	4.674	0.0201
9	0.765	0.164	4.663	2.656	0.0187
10	0.873	0.244	3.580	2.228	0.0214
11	0.545	0.216	2.530	4.883	0.0187
12	0.608	0.357	1.700	2.877	0.0214
13	0.778	0.279	2.790	0.943	0.0516
14	0.785	0.241	3.259	2.849	0.0124
15	0.746	0.256	2.918	1.148	0.0520
16	0.677	0.234	2.895	8.486	0.0125
17	0.658	0.181	3.637	1.719	0.0187
18	0.815	0.263	3.093	0.942	0.0213
19	0.675	0.196	3.440	3.098	0.0188
20	0.771	0.267	2.887	2.747	0.0214
21	0.895	0.287	3.121	1.074	0.0518
22	0.829	0.202	4.110	5.606	0.0124
23	0.688	0.362	1.901	0.684	0.0518
24	0.593	0.275	2.156	7.555	0.0124
25	0.682	0.247	2.766	1.626	0.0200
26	0.696	0.244	2.856	1.345	0.0200
27	0.718	0.237	3.030	1.689	0.0200
28	0.697	0.234	2.973	1.468	0.0200
29	0.696	0.231	3.017	1.469	0.0200

Table 5.20: Average of Experimentally measured responses for 6 mm PMMA.

No	Upper kerf	Lower kerf	Ratio	R_a	HAZ	Cost
1	0.820	0.314	2.551	2.606	0.045	0.0623
2	0.929	0.414	2.221	1.875	0.054	0.0717
3	0.745	0.187	3.968	5.992	0.026	0.0173
4	0.772	0.341	2.234	4.296	0.035	0.0199
5	1.043	0.235	4.019	0.227	0.037	0.0290
6	0.929	0.262	3.698	2.943	0.034	0.0293
7	0.680	0.442	1.542	0.447	0.046	0.0290
8	0.700	0.291	2.426	3.043	0.039	0.0293
9	0.955	0.188	5.582	2.291	0.029	0.0271
10	1.033	0.234	4.343	1.747	0.039	0.0312
11	0.586	0.327	1.878	2.840	0.034	0.0271
12	0.618	0.461	1.349	1.713	0.051	0.0312
13	0.868	0.400	2.207	1.371	0.043	0.0667
14	0.631	0.298	2.113	1.556	0.038	0.0185
15	0.890	0.388	2.463	2.161	0.039	0.0674
16	0.693	0.275	2.444	6.787	0.028	0.0187
17	0.760	0.268	2.796	1.539	0.038	0.0269
18	0.857	0.398	2.132	0.455	0.041	0.0310
19	0.729	0.236	3.077	3.865	0.032	0.0272
20	0.833	0.333	2.542	3.443	0.039	0.0314
21	1.039	0.281	3.669	1.371	0.042	0.0670
22	1.011	0.198	4.937	4.721	0.030	0.0186
23	0.681	0.538	1.225	2.170	0.045	0.0670
24	0.588	0.330	1.699	3.008	0.032	0.0186
25	0.837	0.383	2.205	1.291	0.039	0.0291
26	0.836	0.373	2.236	1.327	0.041	0.0291
27	0.794	0.391	2.057	1.572	0.038	0.0291
28	0.830	0.381	2.227	1.400	0.041	0.0291
29	0.771	0.388	2.005	1.376	0.042	0.0291

Table 5.21: Average of Experimentally measured responses for 8 mm PMMA.

No	Upper kerf	Lower kerf	Ratio	R_a	Cost
1	1.023	0.530	1.928	1.212	0.0812
2	1.047	0.635	1.649	0.829	0.0931
3	0.915	0.217	4.220	4.922	0.0203
4	0.972	0.387	2.511	3.621	0.0233
5	1.105	0.343	3.225	0.979	0.0347
6	1.117	0.259	4.308	1.408	0.0350
7	0.790	0.455	1.738	0.914	0.0347
8	0.802	0.471	1.704	2.987	0.0350
9	1.127	0.241	4.679	1.129	0.0325
10	1.158	0.325	3.562	1.007	0.0372
11	0.743	0.380	1.952	2.265	0.0325
12	0.781	0.540	1.447	1.269	0.0372
13	1.006	0.584	1.723	0.777	0.0867
14	0.940	0.336	2.797	1.140	0.0217
15	1.011	0.556	1.818	1.138	0.0876
16	0.978	0.292	3.346	6.861	0.0219
17	1.011	0.334	3.032	0.912	0.0323
18	0.986	0.483	2.041	0.619	0.0370
19	0.970	0.335	2.891	1.561	0.0327
20	1.025	0.493	2.078	1.207	0.0374
21	1.172	0.387	3.032	0.947	0.0872
22	1.111	0.228	4.863	2.259	0.0218
23	0.860	0.664	1.296	2.691	0.0872
24	0.711	0.333	2.134	8.447	0.0218
25	0.962	0.417	2.307	0.978	0.0349
26	0.972	0.417	2.329	0.959	0.0349
27	0.968	0.413	2.343	0.990	0.0349
28	0.975	0.418	2.329	1.155	0.0349
29	0.976	0.420	2.325	0.937	0.0349

Table 5.22: Extracted ANOVA Tables for all reduced quadratic models of PMMA.

Thickness	Response	SS_M	DF	Lack of Fit	Prob. >F Model	R^2	Adj- R^2	Pre- R^2
2	Upper kerf	0.28	3	Not Sig.	< 0.0001 (Sig.)	0.9263	0.9174	0.9174
	Lower kerf	0.028	7	Not Sig.	< 0.0001 (Sig.)	0.9367	0.9155	0.8755
	Ratio	8.41	7	Not Sig.	< 0.0001 (Sig.)	0.9249	0.8998	0.8099
	HAZ	0.003	8	Not Sig.	< 0.0001 (Sig.)	0.8179	0.7450	0.5557
	Ra	64.13	8	Not Sig.	< 0.0001 (Sig.)	0.9359	0.9102	0.8424
	Cost	4.6	7	-	< 0.0001 (Sig.)	0.9999	0.9999	0.9999
4	Upper kerf	0.24	6	Not Sig.	< 0.0001 (Sig.)	0.9294	0.9102	0.8686
	Lower kerf	0.067	6	Not Sig.	< 0.0001 (Sig.)	0.9261	0.9059	0.8498
	Ratio	14.38	6	Not Sig.	< 0.0001 (Sig.)	0.9284	0.9089	0.8678
	Ra	9.44	9	Not Sig.	< 0.0001 (Sig.)	0.9537	0.9318	0.8616
	Cost	6.55	7	-	< 0.0001 (Sig.)	0.9999	0.9999	0.9999
6	Upper kerf	0.46	3	Not Sig.	< 0.0001 (Sig.)	0.9030	0.8914	0.8694
	Lower kerf	0.2	10	Not Sig.	< 0.0001 (Sig.)	0.9541	0.9285	0.8291
	Ratio	29.50	8	Not Sig.	< 0.0001 (Sig.)	0.9323	0.9052	0.8130
	HAZ	0.001	4	Not Sig.	< 0.0001 (Sig.)	0.8270	0.7982	0.7410
	Ra	66.83	10	Not Sig.	< 0.0001 (Sig.)	0.9830	0.9736	0.9345
	Cost	0.008	5	-	< 0.0001 (Sig.)	0.9997	0.9996	0.9990
8	Upper kerf	0.40	7	Not Sig.	< 0.0001 (Sig.)	0.9822	0.9762	0.9614
	Lower kerf	0.38	10	Not Sig.	< 0.0001 (Sig.)	0.9919	0.9874	0.9732
	Ratio	25.86	10	Not Sig.	< 0.0001 (Sig.)	0.9843	0.9756	0.9798
	Ra	3.51	7	Not Sig.	< 0.0001 (Sig.)	0.9096	0.8795	0.8104
	Cost	6.17	7	-	< 0.0001 (Sig.)	0.9999	0.9999	0.9999

5.3.1.1 Analysis of variance for 2 mm thick PMMA model

ANOVA results for the 2 mm PMMA model confirm that, for the upper kerf model, the main effect laser power (A), cutting speed (B) and focal point position (D) are the most significant model terms associated with this response. Whilst, for the lower kerf model, the analysis indicates that the main effect of all factors, the quadratic effect of laser power (A^2), air pressure (C^2) and focal position (D^2) are the significant model terms. In the case, of the ratio model, the analysis demonstrates that the main effect of laser power (A), air pressure (C), focal position (C), the quadratic effect of laser power (A^2), air pressure (C^2), focal position (C^2) and the interaction effect between laser power and focal position (AD) are the significant model terms. Then, for the HAZ model the ANOVA results indicate that the main effect of all factors, the quadratic effect of laser power (A^2), cutting speed (B^2), the interaction effect of cutting speed and air pressure

(BC) as well as air pressure and focal position (CD) were the most important factors. For the roughness model the analysis demonstrates that the main effect of all factors and the quadratic effects of air pressure (C^2), focal position (D^2), interaction effects of laser power and cutting speed (AB) and laser power and focal position (AD) are the important model terms. Finally, for the cost model the ANOVA results confirm that the main effect of laser power (A), cutting speed (B), air pressure (C), interaction effect between laser power with air pressure (AC) and quadratic effects of laser power (A^2), cutting speed (B^2) and air pressure (C^2) are the significant model terms associated with the operating cost model. However, the operating cost values were transformed using the natural log as recommended by the software (i.e. the Box Cox plot on the Diagnostics button will provide the suitable transform function) in order to reduce the range between the response value to ensure model development. The final mathematical models in terms of actual factors as determined by design expert software are shown below Eqs. 5.31 – 5.36:

$$\text{Upper kerf} = 0.25624 + 2.70933E\text{-}004 * \text{Laser power} - 1.32286E\text{-}005 * \text{Cutting speed} - 0.14823 * \text{Focal position} \quad (5.31)$$

$$\text{Lower kerf} = 0.10562 + 8.69947E\text{-}004 * \text{Laser power} - 7.61905E\text{-}006 * \text{Cutting speed} + 0.15703 * \text{Gas pressure} + 0.058454 * \text{Focal position} - 1.24048E\text{-}006 * \text{Laser power}^2 - 0.082630 * \text{Gas pressure}^2 + 0.014143 * \text{Focal position}^2 \quad (5.32)$$

$$\text{Ratio} = 2.11723 - 5.67959E\text{-}003 * \text{Laser power} - 1.94070 * \text{Gas pressure} - 1.64621 * \text{Focal position} + 1.93528E\text{-}003 * \text{Laser power} * \text{Focal position} + 1.47086E\text{-}005 * \text{Laser power}^2 + 0.99402 * \text{Gas pressure}^2 - 0.13160 * \text{Focal position}^2 \quad (5.33)$$

$$\text{HAZ} = 0.10619 + 2.33159E\text{-}004 * \text{Laser power} - 2.56585E\text{-}005 * \text{Cutting speed} - 0.056757 * \text{Gas pressure} + 0.011933 * \text{Focal position} + 6.17143E\text{-}006 * \text{Cutting speed} * \text{Gas pressure} - 0.010300 * \text{Gas pressure} * \text{Focal position} - 4.02873E\text{-}007 * \text{Laser power}^2 + 2.45881E\text{-}009 * \text{Cutting speed}^2 \quad (5.34)$$

$$Ra = -5.53043 - 9.78811E\text{-}003 * \text{Laser power} + 1.38848E\text{-}004 * \text{Cutting speed} + 9.95657 * \text{Gas pressure} - 3.63285 * \text{Focal position} + 3.91314E\text{-}006 * \text{Laser power} * \text{Cutting speed} + 4.21800E\text{-}003 * \text{Laser power} * \text{Focal position} - 4.24855 * \text{Gas pressure}^2 - 0.62326 * \text{Focal position}^2 \quad (5.35)$$

$$\text{Ln(Operating cost)} = -2.41992 + 5.10041E\text{-}004 * \text{Laser power} - 7.07363E\text{-}004 * \text{Cutting speed} + 5.62980E\text{-}003 * \text{Gas pressure} - 2.33884E\text{-}006 * \text{Laser power} * \text{Gas pressure} - 1.05787E\text{-}007 * \text{Laser power}^2 + 5.59032E\text{-}008 * \text{Cutting speed}^2 - 1.29100E\text{-}005 * \text{Gas pressure}^2 \quad (5.36)$$

5.3.1.2 Analysis of variance for 4 mm thick PMMA model

The results for the 4 mm thick PMMA model show that, for the upper kerf model, the main effects of all factors, quadratic effects of cutting speed (B^2) and air pressure (C^2) are the most important model terms. For the lower kerf model, the ANOVA indicates that the main effect of laser power (A), cutting speed (B), air pressure (C), the quadratic effect of cutting speed (B^2), focal position (D^2) and the interaction effect of laser power and focal position are the significant model terms. Then, for the ratio model the analysis demonstrates that the main effects of all factors, quadratic effects of cutting speed (B^2) and air pressure (C^2) are the most significant model terms. While, regarding the roughness model, the analysis demonstrates that the main effect of all factors and the quadratic effects of laser power (A^2), cutting speed (B^2), focal position (D^2) and the interaction effects of cutting speed with both the air pressure (BC) and focal position (BD) are the important model terms. Finally, for the cost model, the results show that the main effect of laser power (A), cutting speed (B), air pressure (C), interaction effect between laser power with air pressure (AC) and quadratic effects of laser power (A^2), cutting speed (B^2) and air pressure (C^2) are the significant model terms associated with the operating cost model. For the roughness and operating cost models the responses values were transformed using the square root and natural log functions respectively to

facilitate the models development as recommended by the software. The final mathematical models in terms of actual factors as determined by design expert software are shown below Eqs. 5.37 – 5.41:

$$\text{Upper kerf} = 0.45909 + 3.36556E\text{-}004 * \text{Laser power} - 5.61241E\text{-}005 * \text{Cutting speed} - 0.16904 * \text{Gas pressure} - 0.12223 * \text{Focal position} + 6.75035E\text{-}009 * \text{Cutting speed}^2 + 0.049589 * \text{Gas pressure}^2 \quad (5.37)$$

$$\text{Lower kerf} = 0.46407 + 5.96667E\text{-}004 * \text{Laser power} - 6.28651E\text{-}005 * \text{Cutting speed} + 0.13076 * \text{Focal position} + 1.03000E\text{-}004 * \text{Laser power} * \text{Focal position} + 7.18962E\text{-}009 * \text{Cutting speed}^2 + 0.020605 * \text{Focal position}^2 \quad (5.38)$$

$$\text{Ratio} = 0.49089 - 2.21691E\text{-}003 * \text{Laser power} + 4.90262E\text{-}004 * \text{Cutting speed} - 0.83599 * \text{Gas pressure} - 0.97612 * \text{Focal position} - 5.50737E\text{-}008 * \text{Cutting speed}^2 + 0.27227 * \text{Gas pressure}^2 \quad (5.39)$$

$$\text{Sqrt(Ra)} = 4.51557 - 8.05840E\text{-}003 * \text{Laser power} - 2.33910E\text{-}004 * \text{Cutting speed} - 0.12422 * \text{Gas pressure} + 1.33711 * \text{Focal position} + 1.97310E\text{-}004 * \text{Cutting speed} * \text{Gas pressure} + 7.76448E\text{-}005 * \text{Cutting speed} * \text{Focal position} + 1.03023E\text{-}005 * \text{Laser power}^2 + 9.52540E\text{-}008 * \text{Cutting speed}^2 + 0.24899 * \text{Focal position}^2 \quad (5.40)$$

$$\text{Ln(Operating cost)} = -2.28902 + 5.03425E\text{-}004 * \text{Laser power} - 7.80055E\text{-}004 * \text{Cutting speed} + 5.55748E\text{-}003 * \text{Gas pressure} - 2.08859E\text{-}006 * \text{Laser power} * \text{Gas pressure} - 9.44236E\text{-}008 * \text{Laser power}^2 + 6.52417E\text{-}008 * \text{Cutting speed}^2 - 1.15297E\text{-}005 * \text{Gas pressure}^2 \quad (5.41)$$

5.3.1.3 Analysis of variance for 6 mm thick PMMA model

For the upper kerf model, the results for the 6 mm thick PMMA model show that the main effects of laser power (A), cutting speed (B) and focal point position (D) are the most significant model terms. For the lower kerf model, the ANOVA indicates that the main effect of all parameters, the quadratic effect of laser power (B^2), air pressure

(C^2), focal position (D^2) and the interaction effect of focal position with laser power, cutting speed and air pressure (AD), (BD) and (CD) respectively are the significant model terms. In the case of the ratio model, the analysis confirms that the main effects of all factors, quadratic effects of laser power (A^2), focal position (D^2), the two way interaction between laser power with cutting speed (AB) and also between air pressure and focal position (CD) are the most significant model terms. For the HAZ model the results indicate that the linear model is significant because the main effects of all parameters are significant model terms. For, the roughness model the analysis reveals that the main effects of all factors and the quadratic effects of laser power (A^2), cutting speed (B^2), air pressure (C^2), the interaction effects of laser power with cutting speed (AB) also cutting speed with both air pressure (BC) and focal position (BD) are the important model terms. At last, for the cost model, the results illustrate that the main effect of laser power (A), cutting speed (B), air pressure (C), interaction effect between laser power with air pressure (AC) and quadratic effect of cutting speed (B^2) and air pressure (C^2) are the significant model terms associated with the operating cost model. The final mathematical models in terms of actual factors as determined by design expert software are shown below Eqs. 5.42 – 5.47:

$$\text{Upper kerf} = 0.39355 + 2.13333E\text{-}004 * \text{Laser power} - 5.03974E\text{-}005 * \text{Cutting speed} - 0.11980 * \text{Focal position} \quad (5.42)$$

$$\begin{aligned}\text{Lower kerf} = {} & 0.012917 + 2.13715E\text{-}003 * \text{Laser power} - 1.01128E\text{-}004 * \text{Cutting speed} \\ & - 0.035807 * \text{Gas pressure} - 0.016189 * \text{Focal position} \\ & + 8.47619E\text{-}005 * \text{Laser power} * \text{Focal position} \\ & - 1.59744E\text{-}005 * \text{Cutting speed} * \text{Focal position} \\ & - 0.023840 * \text{Gas pressure} * \text{Focal position} - 1.45288E\text{-}006 \\ & * \text{Laser power}^2 - 0.018509 * \text{Gas pressure}^2 \\ & - 0.015031 * \text{Focal position}^2 \end{aligned} \quad (5.43)$$

$$\begin{aligned}\text{Ratio} = {} & 4.33860 - 0.013903 * \text{Laser power} + 1.00592E\text{-}003 * \text{Cutting speed} \\ & + 0.68480 * \text{Gas pressure} + 0.84811 * \text{Focal position} \\ & - 1.54226E\text{-}006 * \text{Laser power} * \text{Cutting speed} \\ & + 0.16061 * \text{Gas pressure} * \text{Focal position} + 1.43367E\text{-}005 *\end{aligned}$$

Laser power^2 +0.28934 * Focal position^2 (5.44)

HAZ = 0.047 + 2.61905E-005 * Laser power - 5.08974E-006 * Cutting speed
-2.16000E-003 * Gas pressure + 1.93333E-003 * Focal position (5.45)

Ra = 14.59540 - 0.026988 * Laser power - 4.72825E-003 * Cutting speed
-0.85900 * Gas pressure + 0.73629 * Focal position
-1.06088E-006 * Laser power * Cutting speed
+6.83354E-004 * Cutting speed * Gas pressure
-3.22026E-004 * Cutting speed * Focal position +
2.54857E-005 * Laser power^2+8.50281E-007*
Cutting speed^2 + 0.11347 * Gas pressure^2 (5.46)

Operating cost =0.098347 + 3.08037E-005 * Laser power - 5.19177E-005
*Cutting speed +1.49720E-004 * Gas pressure
- 7.49455E-009 * Laser power * Cutting speed
+ 8.09454E-009 * Cutting speed^2 (5.47)

5.3.1.4 Analysis of variance for 8 mm thick PMMA model

In the case of the upper kerf model for the 8 mm thick PMMA, the results demonstrate that the main effects of all parameters, the quadratic effects of focal position (D^2), the interaction effects between laser power and air pressure (AC), cutting speed and focal position (BD) are the most significant model terms. For the lower kerf model, the ANOVA indicates that the main effect of all parameters, the quadratic effect of laser power (B^2), air pressure (C^2), and the interaction effects of laser power with both cutting speed (AB) and focal position (AD), but also the interaction effects of focal position with both cutting speed (BD) and air pressure (CD) are the significant model terms. For the ratio model, the analysis verifies that the main effects of all factors, quadratic effects of laser power (A^2), focal position (D^2), the two ways interaction between laser power with cutting speed (AB) also between focal position and all the other factors (AD), (BD) and (CD) are the most significant model terms. For the roughness model the analysis reveals that the main of all factors and the quadratic effects of cutting speed (B^2), focal position (C^2), the interaction effects of air pressure

and focal position (CD) are the important model terms. Finally, for the cost model the results illustrate that the main effect of laser power (A), cutting speed (B), air pressure (C), interaction effect between laser power with air pressure (AC) and quadratic effect of laser power (A^2), cutting speed (B^2) and air pressure (C^2) are the significant model terms associated with the operating cost model. For the roughness and operating cost models the response values were transformed using the inverse and natural log functions respectively to make the models development possible as recommended by the software. The final mathematical models in terms of actual factors as determined by design expert software are shown below Eqs. 5.48 – 5.52:

$$\begin{aligned}\text{Upper kerf} = {} & 0.42498 - 7.52000\text{E-}005 * \text{Laser power} - 8.90833\text{E-}005* \\ & \text{Cutting speed} - 0.053185* \text{Gas pressure} - 0.20411* \text{Focal position} \\ & + 9.21143\text{E-}005 * \text{Laser power} * \text{Gas pressure} - 1.21944\text{E-}005* \\ & \text{Cutting speed} * \text{Focal position} - 0.012412 * \text{Focal position}^2\end{aligned} \quad (5.48)$$

$$\begin{aligned}\text{Lower kerf} = {} & 0.40432 + 5.59143\text{E-}004 * \text{Laser power} - 3.40527\text{E-}004* \\ & \text{Cutting speed} + 0.051227 * \text{Gas pressure} - 0.11415* \\ & \text{Focal position} + 7.80952\text{E-}008 * \text{Laser power}* \\ & \text{Cutting speed} + 7.16190\text{E-}005* \text{Laser power}* \text{Focal position} - \\ & 2.39722\text{E-}005 * \text{Cutting speed} * \text{Focal position} + \\ & 0.013253 * \text{Gas pressure} * \text{Focal position} + 1.88494\text{E-}008* \\ & \text{Cutting speed}^2 - 0.017003 * \text{Focal position}^2\end{aligned} \quad (5.49)$$

$$\begin{aligned}\text{Ratio} = {} & 3.49181 - 2.87308\text{E-}003 * \text{Laser power} + 1.02879\text{E-}003 * \text{Cutting speed} \\ & -0.56389 * \text{Gas pressure} + 1.02127 * \text{Focal position} \\ & -1.70242\text{E-}006 * \text{Laser power} * \text{Cutting speed} \\ & +5.83078\text{E-}004 * \text{Laser power} * \text{Focal position} \\ & -1.37830\text{E-}004 * \text{Cutting speed} * \text{Focal position} \\ & -0.14886 * \text{Gas pressure} * \text{Focal position} + 5.05841\text{E-}006* \\ & \text{Laser power}^2 + 0.17710 * \text{Focal position}^2\end{aligned} \quad (5.50)$$

$$\begin{aligned}1.0/(\text{Roughness}) = {} & - 1.47984 + 7.70112\text{E-}004 * \text{Laser power} \\ & +5.85865\text{E-}004 * \text{Cutting speed} - 0.49928 * \text{Gas pressure} \\ & - 0.92023* \text{Focal position} - 0.059776 * \text{Gas pressure}* \\ & \text{Focal position} - 2.08324\text{E-}007 * \text{Cutting speed}^2 – \\ & 0.10177 * \text{Focal position}^2\end{aligned} \quad (5.51)$$

$$\text{Ln(Operating cost)} = -1.86220 + 4.84293E\text{-}004 * \text{Laser power} - 1.19747E\text{-}003 * \text{Cutting speed} + 5.34717E\text{-}003 * \text{Gas pressure} - 1.66035E\text{-}006 * \text{Laser power} * \text{Gas pressure} - 7.50504E\text{-}008 * \text{Laser power}^2 + 1.54961E\text{-}007 * \text{Cutting speed}^2 - 9.16599E\text{-}006 * \text{Gas pressure}^2 \quad (5.52)$$

5.3.2 Validation of the developed models

The validation of the models developed of the four thicknesses of PMMA can be drawn from Figs. 5.23- 5.26, which present the relationship between the measured and predicted values of the investigated responses. These scatter diagrams indicate that the above mathematical models show excellent agreement between the measured and estimated values of the above mentioned responses. Furthermore, to verify the adequacy of the developed models, two confirmation experiments for each thickness were carried out by using new test conditions. These experiments are taken from the optimisation results which are within the investigated range. Using the point prediction option in the software, all the responses values can be predicted by substituting these conditions into the previous developed models. Table 5.23 presents the experimental conditions, the actual experimental values, the predicted values and the percentage errors for all thicknesses. It is clear that all the values of the percentage errors for all responses are within reasonable agreement, therefore the models are valid. All the percentage errors are in agreement in contrast to the values reported in [111 and 118].

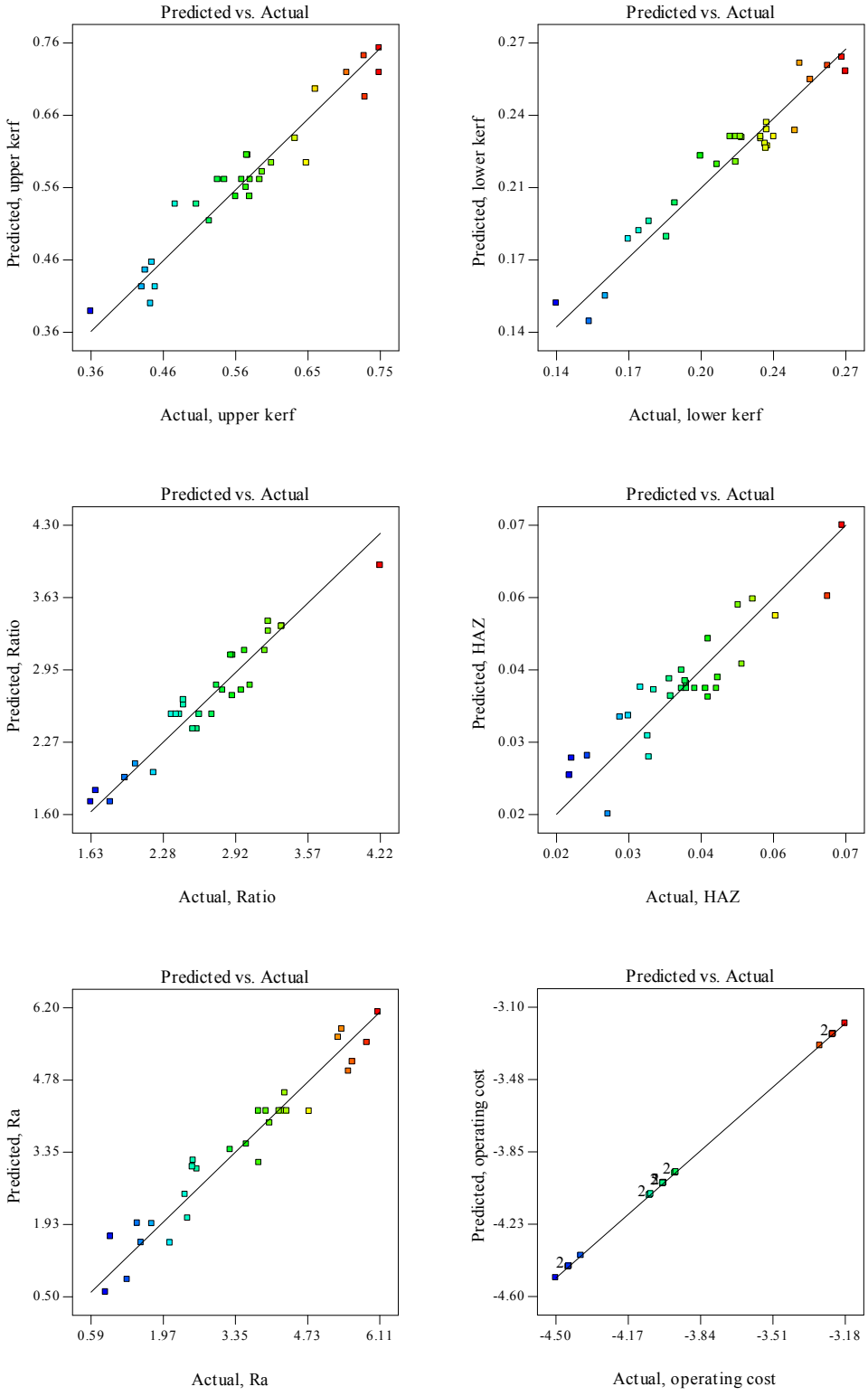

Fig. 5.23: Scatter diagram showing the relationship between the actual and predicted values for each response for 2 mm thick PMMA.

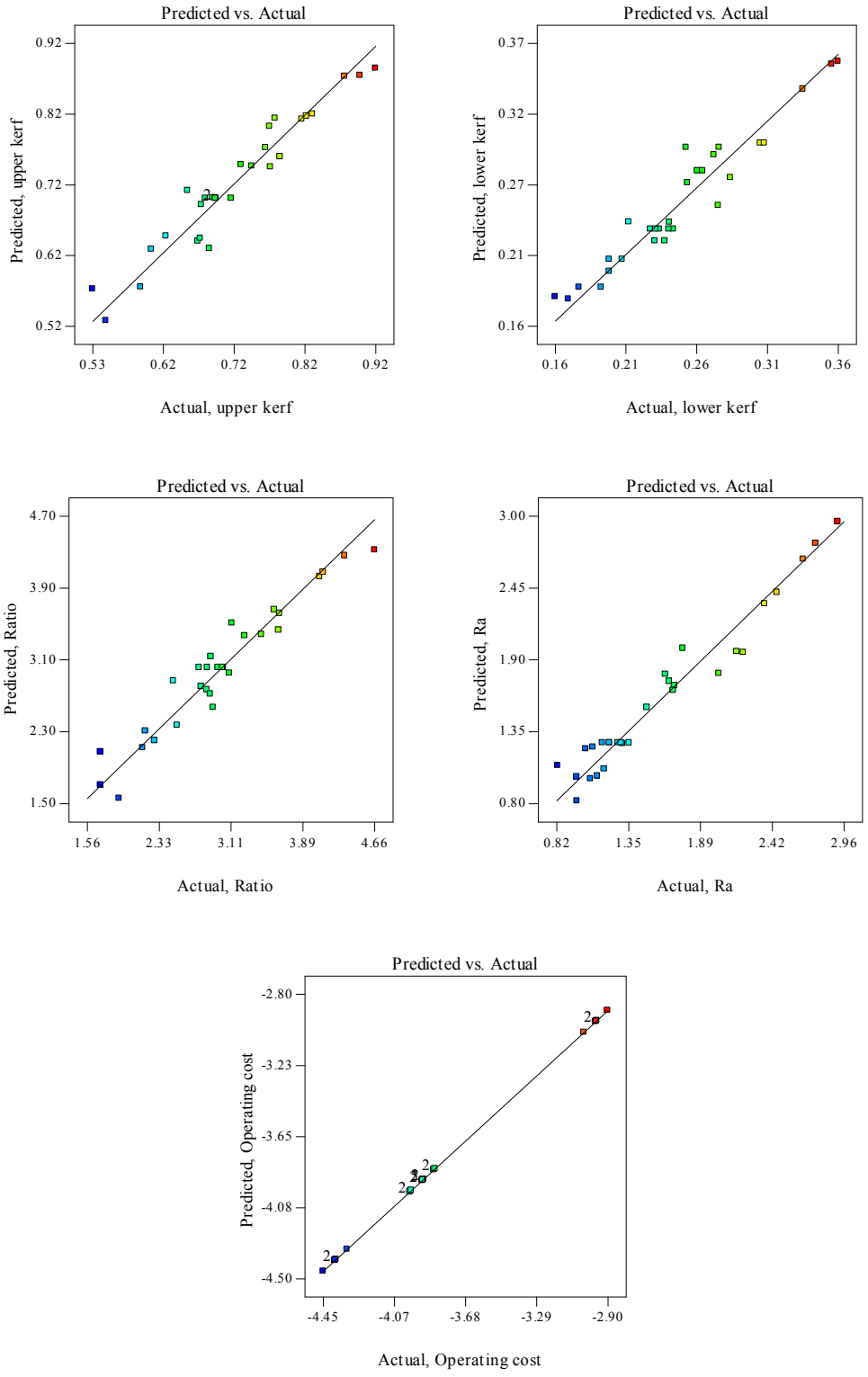

Fig. 5.24: Scatter diagram showing the relationship between the actual and predicted values for each response for 4 mm thick PMMA.

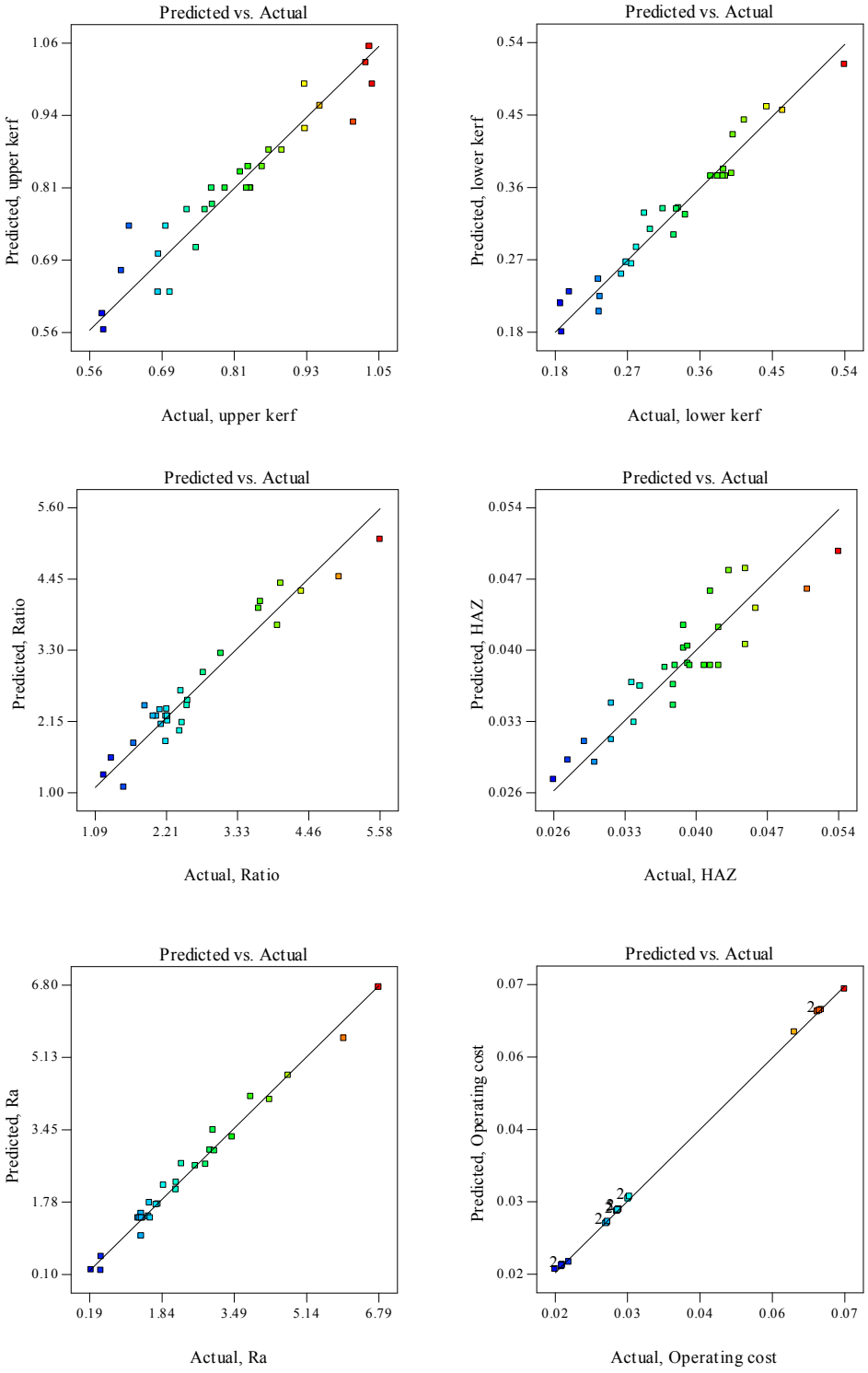

Fig. 5.25: Scatter diagram showing the relationship between the actual and predicted values for each response for 6 mm thick PMMA.

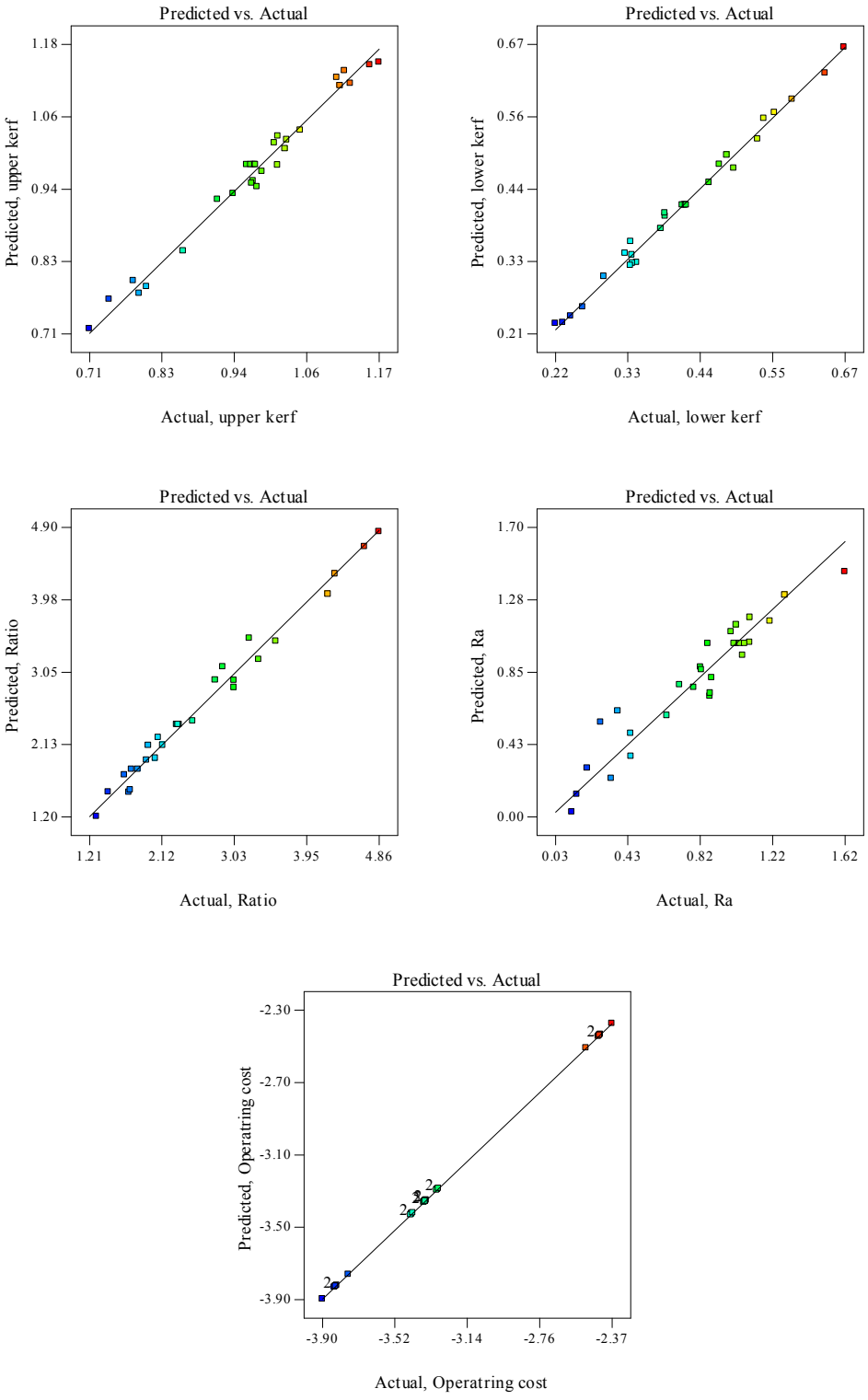

Fig. 5.26: Scatter diagram showing the relationship between the actual and predicted values for each response for 8 mm thick PMMA.

Table 5.23: Confirmation experiments of PMMA.

Thickness	No.	Factors				Values	Responses					
		A	B	C	D		Upper kerf	Lower kerf	Ratio	HAZ	Roughness	Cost
2	1	264.4	1500	0.83	-1	Actual	0.440	0.256	1.719	0.066	0.793	0.0398
						Predicted	0.456	0.267	1.721	0.064	0.867	0.0398
						Error %	-3.636	-4.297	-0.131	3.030	-9.332	0.0000
	2	100	5000	0.5	-1.57	Actual	0.426	0.148	2.878	0.033	3.745	0.0110
						Predicted	0.45	0.143	2.931	0.035	3.563	0.0110
						Error %	-5.634	3.378	-1.828	-6.061	4.865	0.0000
4	1	417.4	1200	1.01	-2.25	Actual	0.682	0.359	1.899	N/A	0.863	0.0532
						Predicted	0.696	0.362	1.699	N/A	0.924	0.0533
						Error %	-2.113	-0.836	10.513	N/A	-7.027	-0.188
	2	200	5000	0.5	-2.55	Actual	0.616	0.207	2.971	N/A	4.417	0.0116
						Predicted	0.654	0.197	3.263	N/A	4.742	0.0116
						Error %	-6.288	5.040	-9.819	N/A	-7.365	0.202
6	1	607.1	2901	0.51	-2.23	Actual	0.592	0.472	1.253	0.046	0.235	0.0237
						Predicted	0.644	0.436	1.098	0.043	0.219	0.0214
						Error %	-8.814	7.798	12.323	6.926	6.781	9.544
	2	350	3600	0.5	-3.54	Actual	0.736	0.221	3.332	0.034	3.347	0.0172
						Predicted	0.711	0.206	3.590	0.03	3.260	0.0178
						Error %	3.444	6.792	-7.739	10.714	2.603	-3.263
8	1	800	1153	0.5	-4.19	Actual	0.923	0.603	1.531	N/A	0.718	0.0642
						Predicted	0.968	0.609	1.618	N/A	0.676	0.0675
						Error %	-4.928	-1.077	-5.694	N/A	5.859	-5.142
	2	450	3200	0.5	-5.14	Actual	1.028	0.240	4.283	N/A	1.924	0.0202
						Predicted	1.022	0.229	4.517	N/A	1.808	0.0202
						Error %	0.537	4.444	-5.455	N/A	6.029	0.0398

5.3.3 Effect of process factors on the responses for PMMA

5.3.3.1 Upper kerf

The results indicate that all the parameters have a significant effect of the upper kerf as shown in Fig. 5.27. It is clear that the focal point position has the main effect on the upper kerf width. It was found that the upper kerf decreases as the focal position increases. The use of wider laser beam would cause the laser power to extent over a greater top surface, which would result in increased upper kerf.. In addition, the cutting speed and the laser power affect the upper kerf as presented in Fig. 5.27. The cutting speed has a negative effect while the laser power has a positive effect. In other words, as the laser power increases the resulting upper kerf becomes larger, especially at low cutting speed. The reason behind this could be explained as follows; as higher laser power and slower speed is applied, the heat input into the specimen accumulates over a longer period of time in the cut zone. Consequently, this will take a longer period of time to dissipate, hence, causing more portions of the PMMA to be vaporized and resulting in larger upper kerf. It was found that the compressed air pressure has a slight effect on the upper kerf. However, the air pressure has no significant effect on the upper kerf for both thicknesses 2 and 6 mm. These results are in good agreement with the results obtained by Berrie and Birkett [56] and Caiazzo et al. [48]. The percentage changes in the upper kerf as a result of changing each factor from its lowest value to its highest value while keeping the other factors at their centre values are presented in Table 5.24. From this table it is evident that the focal point position is the key factor affecting the upper kerf. Then, cutting speed and laser power as mentioned above. The (+) and (–) signs indicate the increase or decrease in the upper kerf (response) value as the factor changes. The Fig. 5.28 contour plots show the effect of focal position and cutting speed on the upper kerf for the four thicknesses. The interaction effect between the laser power and air pressure on the upper kerf for 8 mm thick PMMA is illustrated in Fig. 5.29. It is clear from Fig. 5.29, that at the lowest laser power of 450 W, a smaller upper kerf of 0.95 mm would be obtained if the highest air pressure of 3 bar was supplied. However, this is valid only up to a certain level of laser power of 580 W. At greater laser power

level values a smaller upper kerf width of 0.97 mm would be achieved if the slowest air pressure of 0.5 bar was applied.

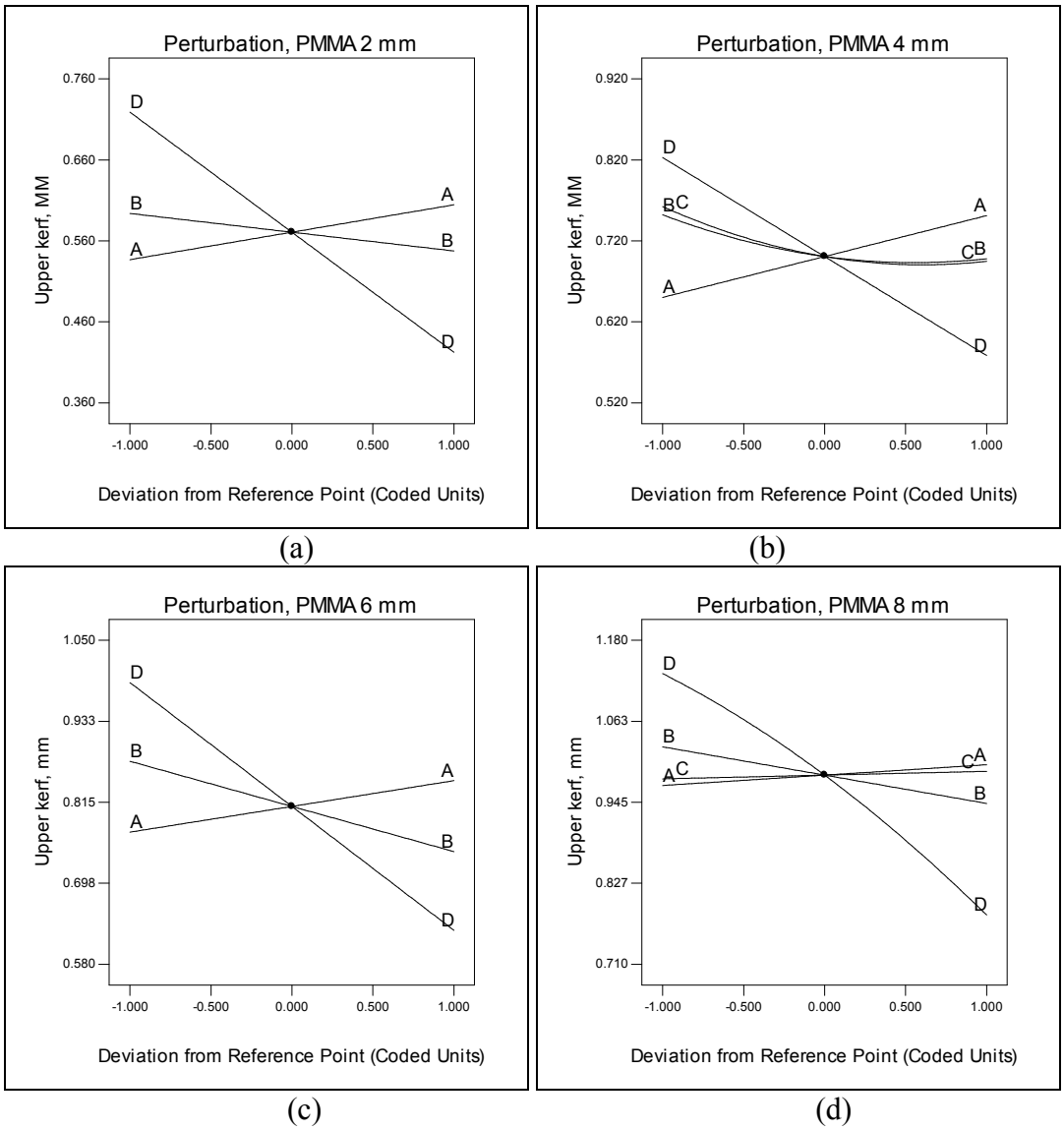

Fig. 5.27: Perturbation plots showing the effect of process parameter on upper kerf for PMMA (a) 2 mm, (b) 4 mm, (c) 6 mm and (d) 8 mm.

Table 5.24: Percentage change in upper kerf as each factor increases for PMMA.

Factor	Percentage change in upper kerf, %			
	2 mm	4 mm	6 mm	8 mm
Laser power	+12.62	+15.53	+9.68	+3.11
Cutting speed	-7.80	-7.21	-14.98	-8.01
Air pressure	0.00	-8.87	0.00	+1.12
Focal position	-41.24	-29.71	-36.35	-30.96

The (+) or (–) signs indicate the increase or decrease in the response value as the factor changes over its range.

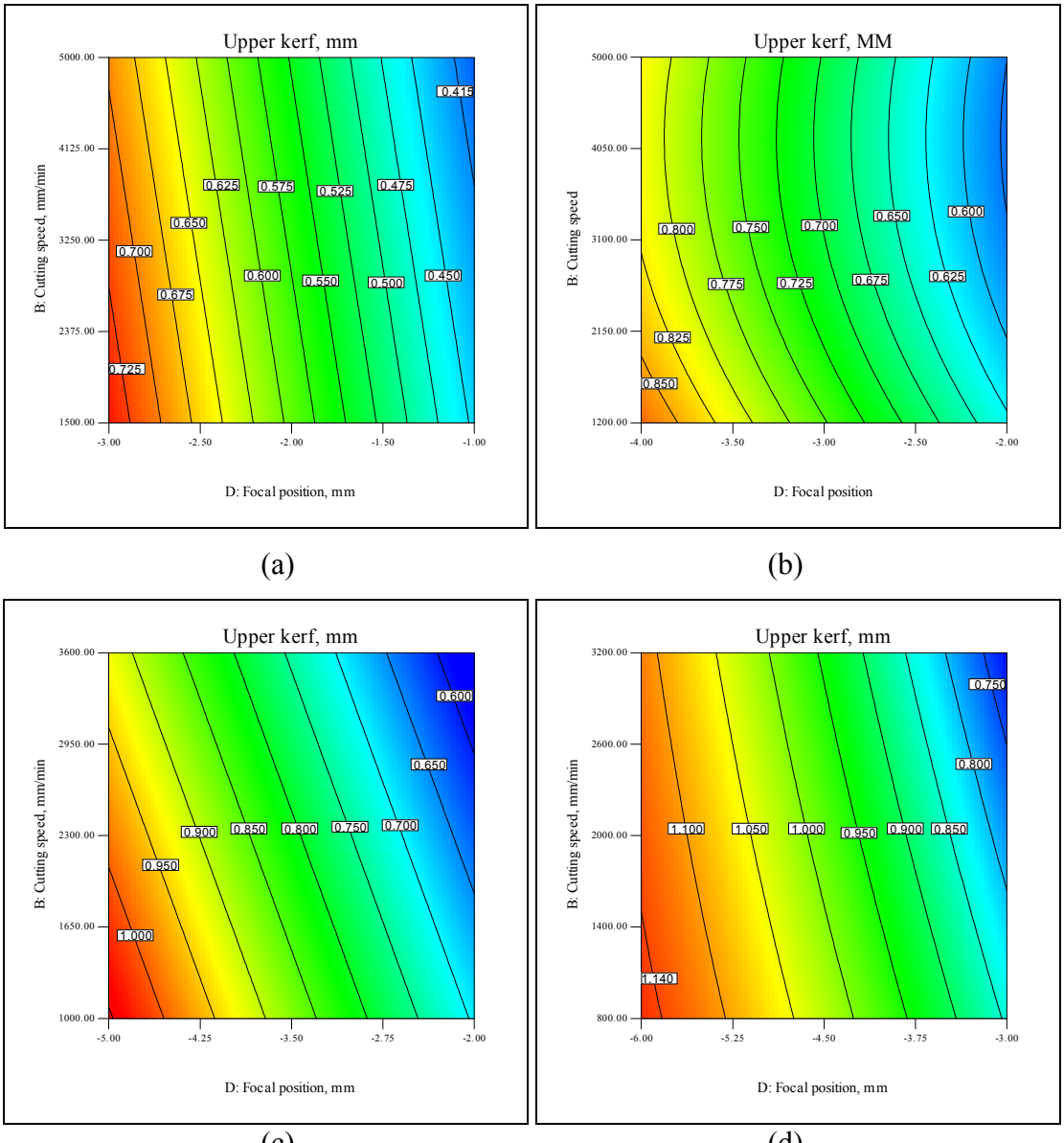

(a) (b)

(c) (d)

Fig. 5.28: Contour plots showing the effect of focal position and cutting speed on the upper kerf for PMMA (a) 2 mm, (b) 4 mm, (c) 6 mm and (d) 8 mm.

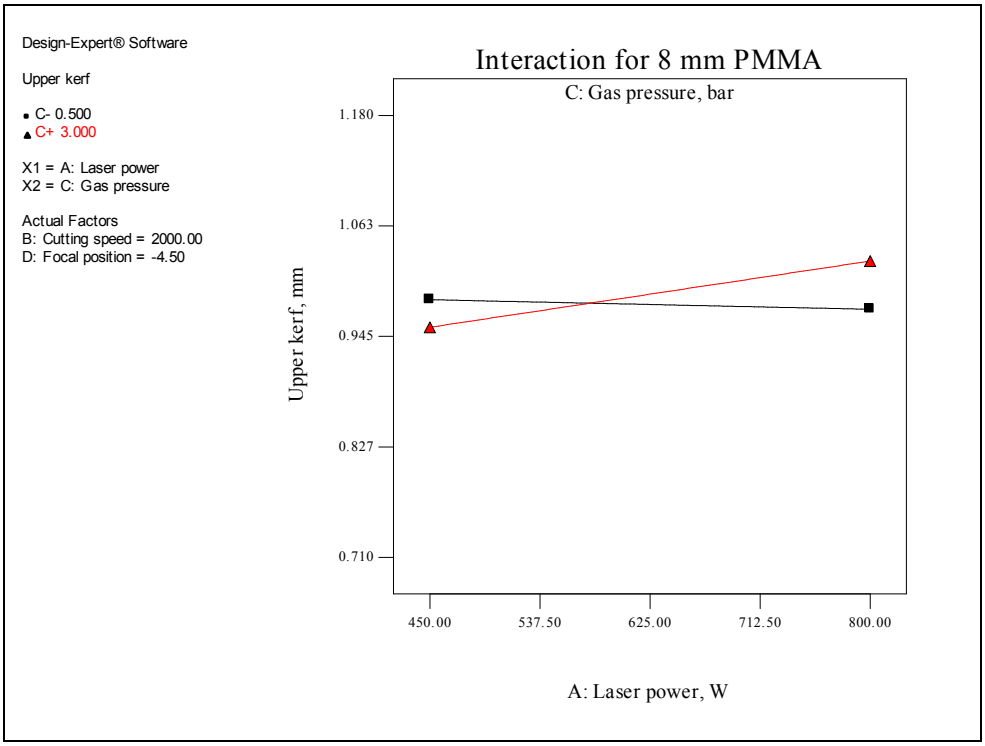

Fig. 5.29: Interaction graph illustrating the interaction effect between laser power and air pressure on the ratio for 8 mm PMMA.

5.3.3.2 Lower kerf

The results demonstrate that all the process parameters investigated have an effect on the lower kerf width as shown in Fig. 5.30. From Fig. 5.30 it is evident that the main factors affecting the lower kerf width are cutting speed, laser power and focal point position. However, the cutting speed has a negative effect, while both laser power and focal point position have positive effect on the lower kerf. So, the lower kerf width decreases as the cutting speed increases and both focal position and laser power decrease. This is could be due to the fact that, as the cutting speed increases, there is considerably less time for laser beam exposure to the workpiece, which reduces the laser beam's capability to evaporate more material, and consequently, a smaller lower kerf would be produced. This fact is more obvious at low laser power. In the case of the focal position effect, as a defocused laser beam is used, which means the focal position will be well beneath the substrate surface, the resulting lower kerf width would be smaller

because the laser beam's power would be spread over less area or vice versa. Figure 5.31 is an interaction graph between the focal point position and the air pressure for 6 mm thick PMMA. It is notable from this figure that by setting the focal point position at – 5 mm a smaller lower kerf of 0.21 mm could be achieved only if the lowest air pressure of 0.5 bar was supplied. However, in the case of setting the focal point position at – 2 mm, a smallest lower kerf width of 0.33 mm could be reached if the highest air pressure of 3 bar was supplied. At a focal position of – 2 mm, it is clear from Fig. 5.31 that there is a significant difference between the values of the two lower kerf widths produced by using 0.5 and 3 bar air pressure, i.e. when compared with the two lower kerf widths produced with the same two air pressure but at focal position of – 5 mm. Generally speaking, it is clear from Table 5.25 that the laser power is the main factor affecting the lower kerf width for all thicknesses. However, the focal position and the cutting speed influence the lower kerf more than the laser power, especially for thicker PMMA.

Table 5.25: Percentage change in lower kerf as each factor increases for PMMA.

Factor	Percentage change in lower kerf, %			
	2 mm	4 mm	6 mm	8 mm
Laser power	+45.98	+45.67	+40.19	+39.77
Cutting speed	-11.06	-23.73	-27.17	-45.50
Air pressure	-3.90	0.00	-11.70	-4.95
Focal position	+1.57	+41.22	+64.15	+61.32

The (+) or (–) signs indicate the increase or decrease in the response value as the factor changes over its range.

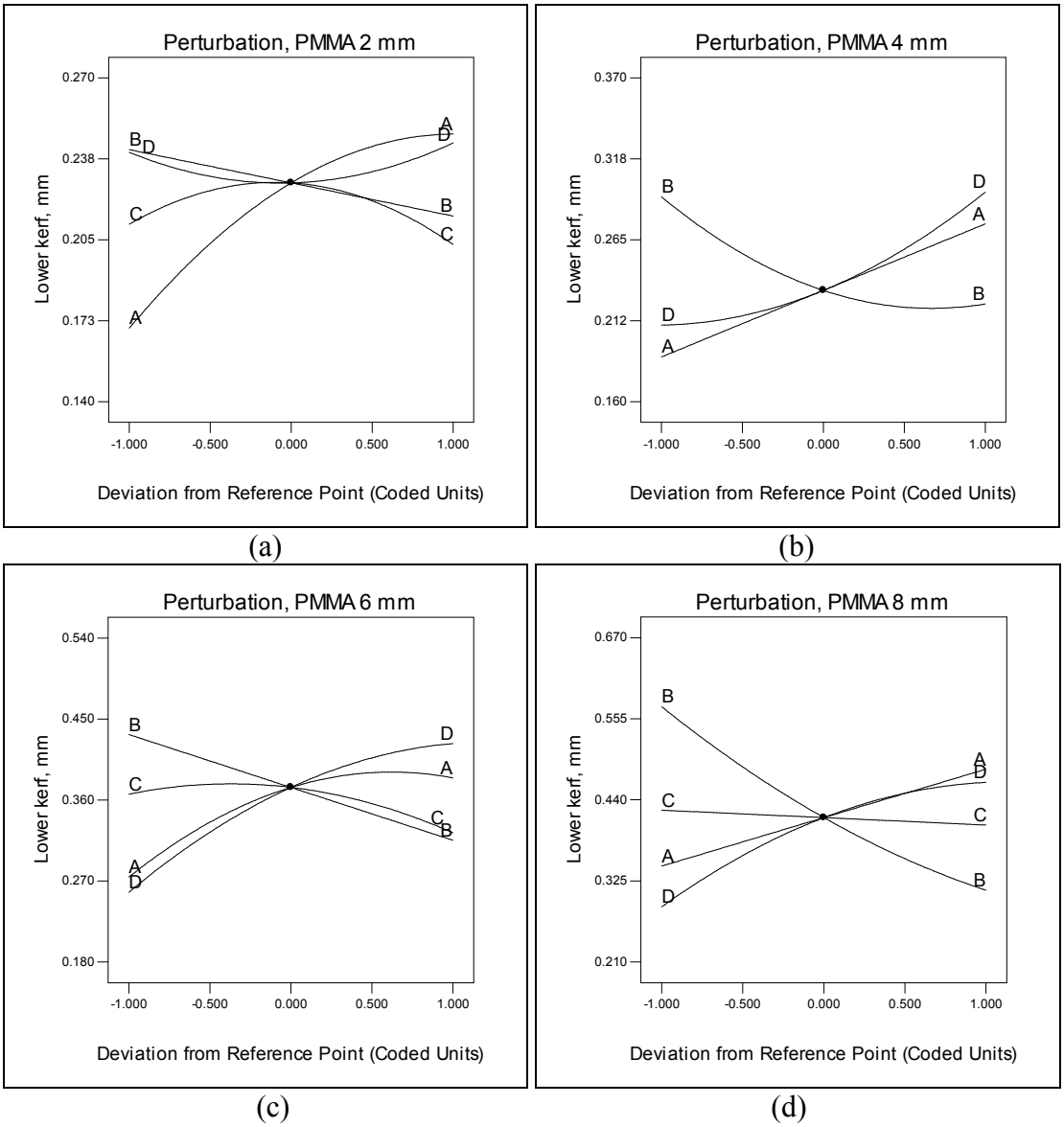

Fig. 5.30: Perturbation plots showing the effect of process parameter on lower kerf for PMMA (a) 2 mm, (b) 4 mm, (c) 6 mm and (d) 8 mm.

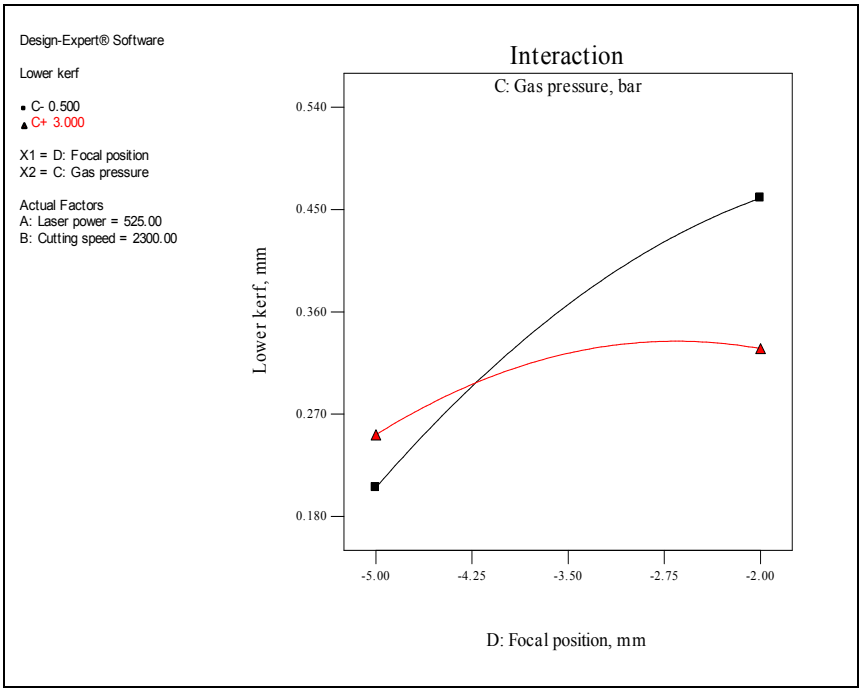

Fig. 5.31: Interaction graph illustrating the interaction effect between focal point position and air pressure on the ratio for 6 mm PMMA.

5.3.3.3 Ratio of the upper kerf to the lower kerf

It clear from Fig. 5.32 that all the parameters investigated have an influence on the ratio between the upper and the lower kerf widths. However, the main factor affecting the ratio is the focal point position followed by cutting speed, laser power and air pressure. Any increase in the focal position or laser power would result in a decrease in this ratio. On the other hand, any increase in the cutting speed or air pressure would lead to an increase in the ratio. The above findings are also clearly demonstrated in Table 5.28. From Table 5.26 it is obvious that as the PMMA sheet becomes thicker the factors have an extra effect on the ratio. This could be related to the fact that as the sheet becomes thicker the chance of getting a tapered cut surface becomes more pronounced. The Fig. 5.33 contour plots demonstrate the effect of laser power and cutting speed on the ratio for 6 and 8 mm thick PMMA. The results indicate that the ratio values fall between 1.22 and 5.58 for all thicknesses. Therefore, minimising the ratio in this case will be a desirable constrain when searching for the optimal condition to achieve nearly parallel sides of the cut surface.

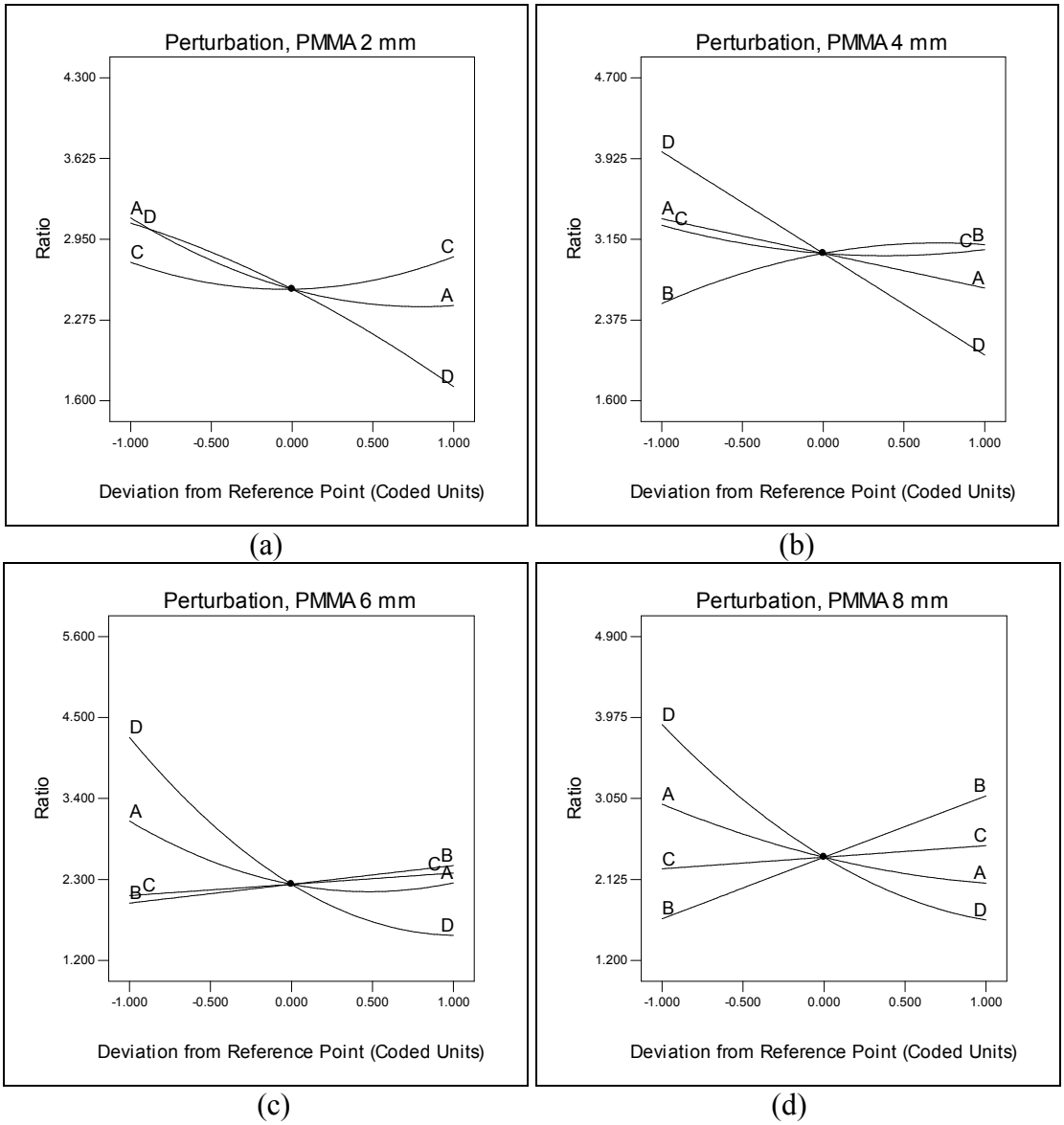

Fig. 5.32: Perturbation plots showing the effect of process parameter on ratio for (a) 2 mm, (b) 4 mm, (c) 6 mm and (d) 8 mm.

Table 5.26: Percentage change in ratio as each factor increases for PMMA.

Factor	Percentage change in ratio, %			
	2 mm	4 mm	6 mm	8 mm
Laser power	-23.42	-19.87	-27.13	-30.24
Cutting speed	0.00	+22.33	+25.79	+83.76
Air pressure	+1.72	7.09	+14.75	+11.80
Focal position	-44.36	-48.92	-63.58	-57.36

The (+) or (–) signs indicate the increase or decrease in the response value as the factor changes over its range.

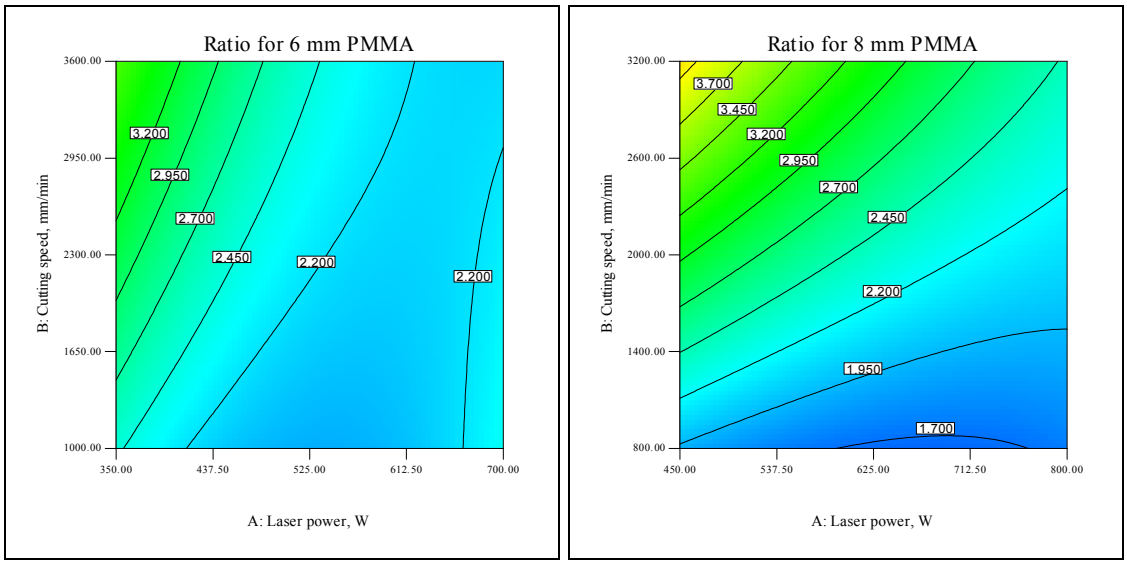

(a) (b)

Fig. 5.33: Contour plots showing the effect of laser power and cutting speed on the ratio for PMMA (a) 6 mm and (b) 8 mm.

5.3.3.4 Heat-affected zone HAZ

For this material the HAZ was successfully modelled only for two thicknesses namely: 2 mm and 6 mm. The results indicate that the dimensions of HAZ are between 0.022 and 0.067 for the two thicknesses. These results are in good agreement with the results reported by Davim et al. [50 and 54]. Figure 5.34 is a perturbation graph showing the effect of the significant laser parameters on the HAZ. It is evident that any increase in the cutting speed and the air pressure would result in a smaller HAZ, whereas any increase in the laser power and the focal position would result in a larger HAZ. These findings are in agreement with the results reported in [49, 50 and 54]. In the same way, the relationship between cutting speed and laser power, discussed earlier, was found to be the same for the case of HAZ. Hence, using faster cutting speeds produce smaller HAZ, especially at low laser power because the heat input becomes less. The HAZ becomes wider when a focused laser beam is used. This is in fact due to the higher power density as a result of using a focused laser beam (i.e. small spot size). Table 5.27 demonstrates that the laser power is the most significant factor influencing the HAZ

which is in agreement with [50 and 54]. Figure 5.35 is an interaction graph between the air pressure and focal position for 2 mm PMMA. It is clear from Fig. 5.35 that by supplying an air pressure of 0.5 bar a smaller HAZ of 0.041 mm could be reached only if the lowest focal position of -3 mm was used. However, in the case of supplying the highest air pressure of 1.5 bar the smallest HAZ of 0.029 mm could be reached if the highest focal position of -1 mm was used. At an air pressure of 1.15 bar it is clear form Fig. 5.35 that a HAZ extent of 0.038 mm can be obtained at either focal positions.

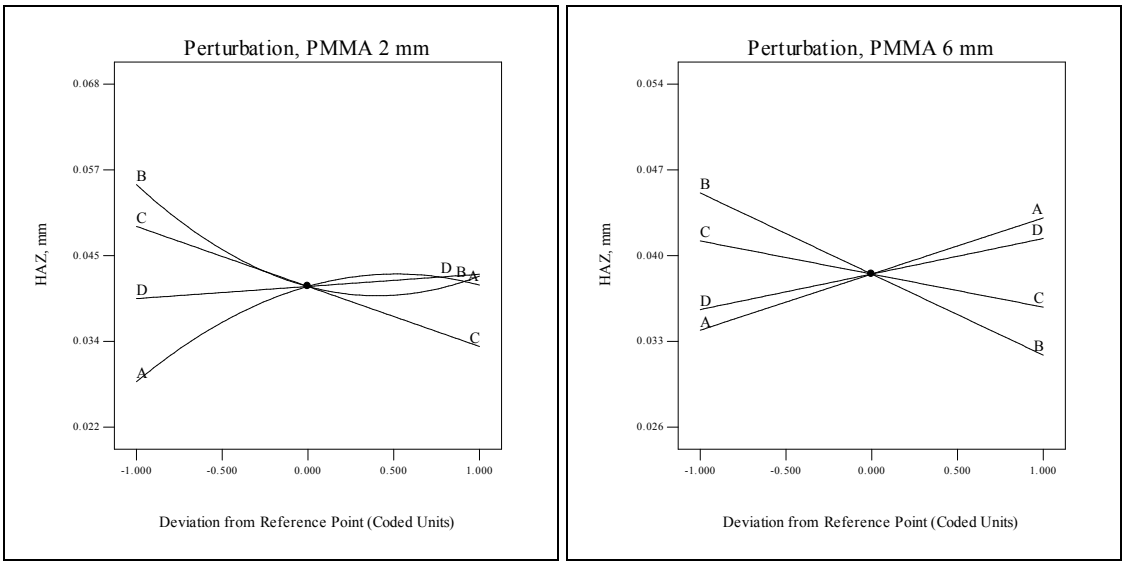

(a) (b)

Fig. 5.34: Perturbation plots showing the effect of process parameter on HAZ for (a) 2 mm and (b) 6 mm.

Table 5.27: Percentage change in HAZ as each factor increases for PMMA.

Factor	Percentage change in HAZ, %	
	2 mm	6 mm
Laser power	+46.16	+37.03
Cutting speed	-22.49	-29.33
Air pressure	-32.91	-13.11
Focal position	+8.33	+16.29

The (+) or (–) signs indicate the increase or decrease in the response value as the factor changes over its range.

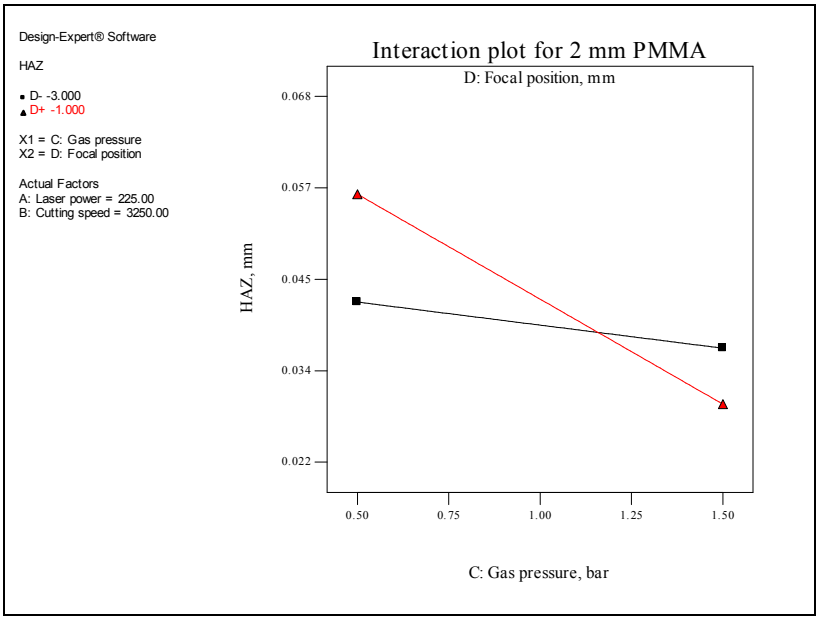

Fig. 5.35: Interaction graph illustrating the interaction effect between air pressure and focal position on the HAZ for 2 mm PMMA.

5.3.3.5 Surface roughness

The results indicate that all the investigated LBC parameters have an effect on the roughness of the cut surface. This result is in agreement with [49 and 50]. It was found that the quality of the cut surface for PMMA is high in comparison with the quality of UHMWPE, a finding which agrees with [50 and 54]. Figure 5.36 is a perturbation graph representing the influence of each factor. According to Fig. 5.36, it is obvious that the roughness values decreases as the thickness of PMMA sheet increases. Moreover, Fig. 5.36 demonstrates that the cutting speed and the air pressure are the most significant factors affecting the Ra values for all thicknesses. However, the laser power also affects the roughness significantly. These results agree well with the results reported by Choudhury and Shirley [49] and Davim et al. [50]. It is noted that the roughness is also affected by the focal position. However, in some cases it has a negligible effect. All the above results are supported by the percentage change of each factor shown in Table 5.28. It is notable, that in some cases, the percentage values are extremely high; this is due to the fact that the lowest value of the Ra is very small in comparison with the highest value.

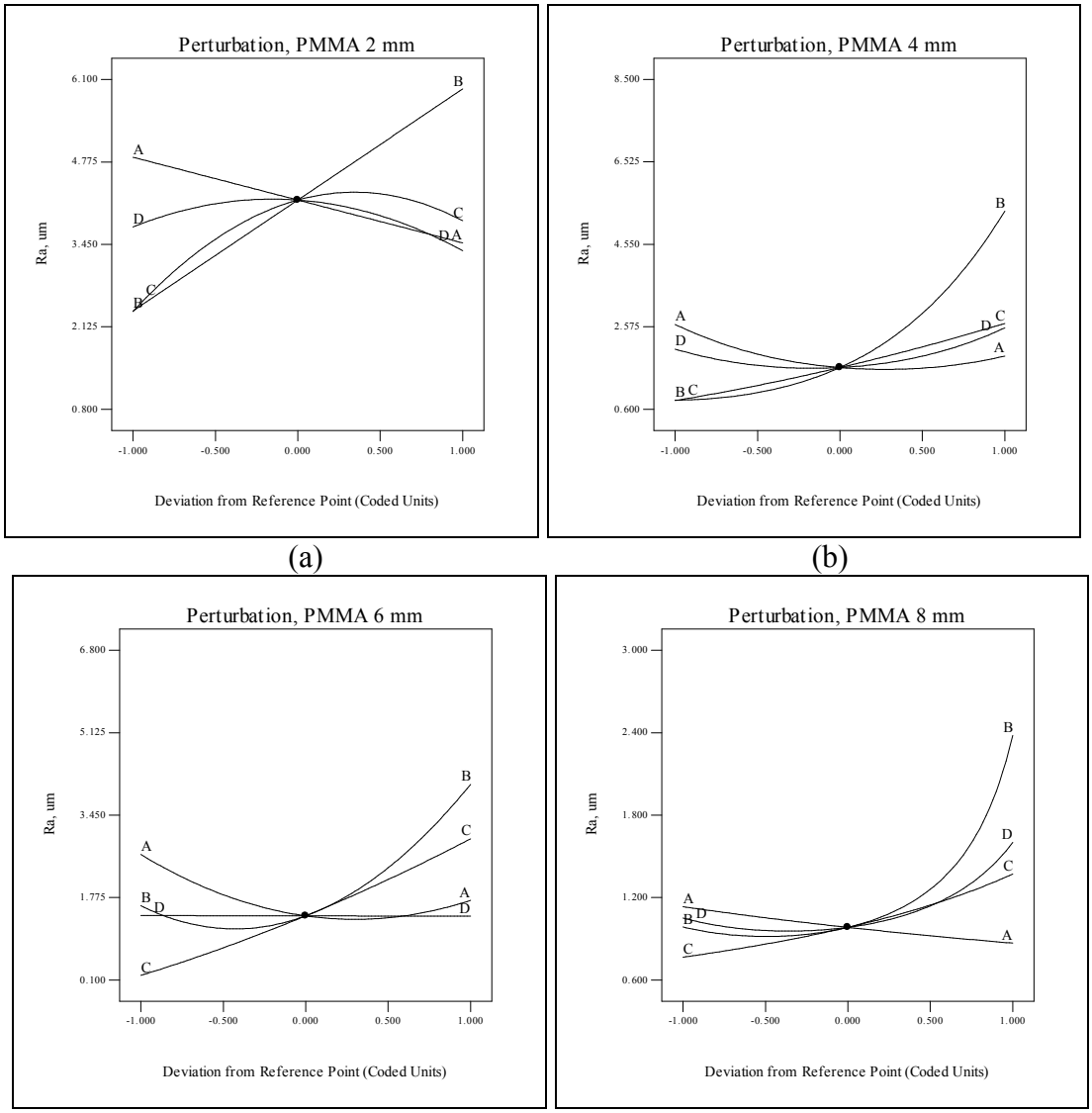

Fig. 5.36: Perturbation plots showing the effect of process parameter on surface roughness for (a) 2 mm, (b) 4 mm, (c) 6 mm and (d) 8 mm.

Table 5.28: Percentage change in R_a as each factor increases for PMMA.

Factor	Percentage change in R_a, %			
	2 mm	4 mm	6 mm	8 mm
Laser power	-28.38	-28.85	-35.23	-23.40
Cutting speed	+149.97	+553.37	+153.59	+141.32
Air pressure	+61.56	+228.91	+1435.36	+78.95
Focal position	10.23	+24.84	+0.93	+52.30

The (+) or (–) signs indicate the increase or decrease in the response value as the factor changes over its range.

Figure 5.37 contours plots represent the effect of the cutting speed and the air pressure on the roughness. It is clear that the Ra values increase sharply as the cutting speed and air pressure reach their highest levels, highlighting the importance of these two factors. Another way of presenting the importance of these two factors on the roughness is illustrated in Fig. 5.38. From this figure it is clear that at a low air pressure of 0.5 bar there is no significant difference in the roughness values produced using both levels of cutting speed. However, at a higher air pressure of 3 bar it is clear that the roughness increases dramatically if the highest cutting speed is used.

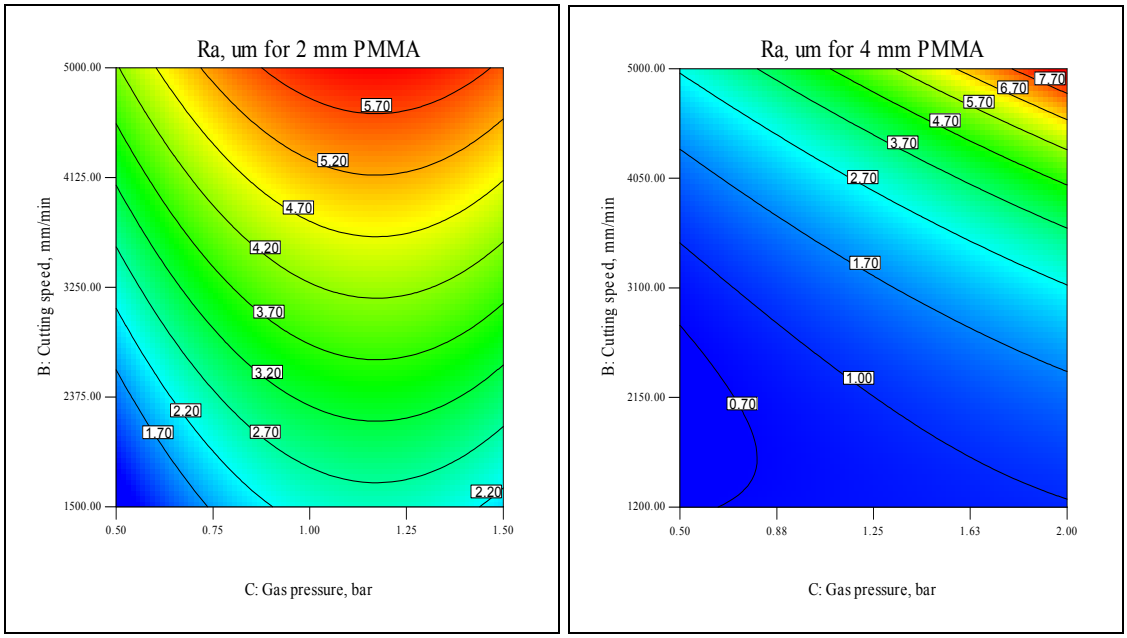

(a) (b)

Fig. 5.37: Contour plots showing the effect of air pressure and cutting speed on the roughness for PMMA (a) 2 mm and (b) 4 mm.

5.3.3.6 Operating cost

In Fig. 5.39a-d it is obvious from the very steep curvature, that the operating cost models for all thicknesses are highly affected by the cutting speed. Also, the steep slopes in the case of laser power and air pressure indicate that the operating cost is less

influenced by these two factors. Additionally the result shows that as the laser power and air pressure increase, so too does the operating cost. On the other hand, as the cutting speed increases the operating cost decreases sharply. These results are logical as discussed previously. Moreover, these changes in the operating cost in terms of percentages are presented in Table 5.29 as each factor increase from its lowest level to its highest level. It is clear that the focal position has no effect on the operating cost.

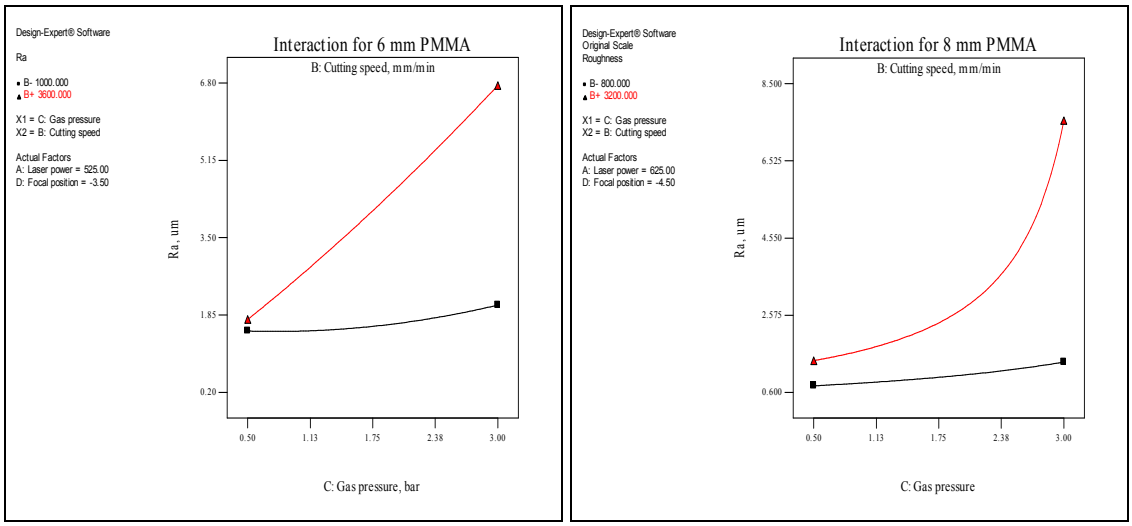

(a) (b)

Fig. 5.38: Interaction graph illustrating the interaction effect between air pressure and cutting speed on the roughness for PMMA (a) 6 mm and (b) 8mm.

Table 5.29: Percentage change in cost as each factor increases for PMMA.

Factor	Percentage change in R_a, %			
	2 mm	4 mm	6 mm	8 mm
Laser power	-12.19	-13.93	-17.74	-14.53
Cutting speed	70.00	76.00	72.22	75.00
Air pressure	-0.51	-0.72	-1.29	-1.08
Focal position	0	0	0	0

The (+) or (–) signs indicate the increase or decrease in the response value as the factor changes over its range.

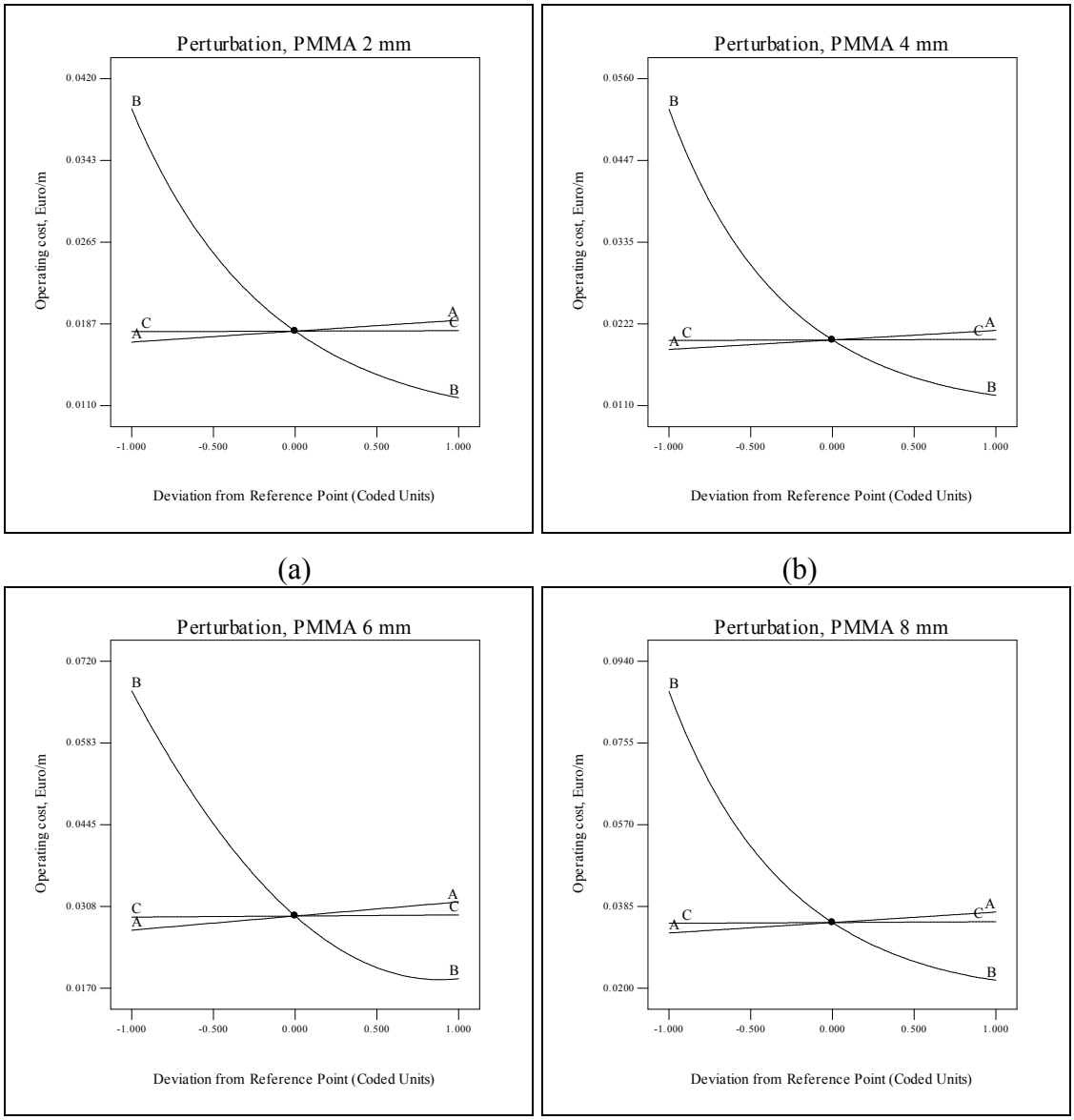

Fig. 5.39: Perturbation plots showing the effect of process parameter on operating cost for (a) 2 mm, (b) 4 mm, (c) 6 mm and (d) 8 mm.

5.4 Medium Density Fibreboard (MDF)

The same responses were investigated for MDF for 3 thicknesses 4, 6 and 9 mm. The same apparatus were used to evaluate these responses. An average of at least five stable measurements for the two kerf widths and surface roughness were recorded for all 29 runs for each thickness shown in Tables 4.20 - 4.22. The ratio of the upper kerf to the lower kerf was calculated for each run using the averaged data. The average values of the measured responses are listed in Tables 5.30 - 5.30. All experimentally evaluated responses are presented in appendix D. The operating cost was estimated using Eq. 4.5 and Eq. 4.3 and the estimated operating cost for each experiment is presented in Tables 5.30 – 5.32.

5.4.1 Development of the mathematical models for MDF

In this case, fifteen ANOVA tables for the reduced quadratics models have been obtained. Same as before the most important values were extracted and shown in Table 5.33. This table shows also the other adequacy measures R^2, Adjusted R^2 and predicted R^2. The entire adequacy measures are close to 1, which are in reasonable agreement and indicate adequate models. The values of adequacy measures are in good form in comparison with the values listed in [121 and 136]. There is one case where the lack-of-fit is significance at both level of significant 1% and 5%. This case is for the ratio model for 9 mm thick MDF, which has a significant lack-of-fit, this may result in the inapplicability of this model at some points in the design space. The developed mathematical models are listed below in terms of actual factors. Eqs 5.53-5.57 are the mathematical models for 4 mm thick MDF, Eqs 5.58-5.62 are the mathematical models for 6 mm thick MDF and Eqs. 5.63-67 are the mathematical models for 9 mm thick MDF. From these mathematical models one can notice the significant factors that would principally affect each response as they appear in its model.

Table 5.30: Experimentally recorded responses for 4 mm thick MDF.

Std	Run	Responses				
		Upper kerf, mm	Lower kerf, mm	Ratio	Ra, μm	Cost €/m
1	25	0.326	0.232	1.404	5.857	0.0289
2	13	0.435	0.363	1.197	3.809	0.0322
3	1	0.267	0.134	1.997	6.877	0.0115
4	14	0.328	0.264	1.241	5.188	0.0129
5	24	0.694	0.246	2.822	5.785	0.0173
6	8	0.625	0.254	2.457	6.615	0.0176
7	22	0.326	0.221	1.472	4.515	0.0173
8	23	0.302	0.224	1.344	5.196	0.0176
9	17	0.633	0.132	4.800	6.860	0.0165
10	28	0.667	0.279	2.390	5.277	0.0184
11	27	0.284	0.123	2.307	5.476	0.0165
12	3	0.356	0.341	1.042	4.298	0.0184
13	29	0.450	0.324	1.388	4.248	0.0303
14	11	0.377	0.244	1.542	6.014	0.0121
15	16	0.420	0.335	1.253	5.827	0.0308
16	6	0.379	0.264	1.436	5.913	0.0123
17	12	0.369	0.128	2.875	5.083	0.0164
18	20	0.443	0.312	1.420	4.216	0.0183
19	5	0.333	0.138	2.423	6.145	0.0166
20	9	0.409	0.301	1.356	5.961	0.0185
21	26	0.680	0.301	2.261	5.663	0.0305
22	19	0.644	0.256	2.516	6.514	0.0122
23	4	0.336	0.356	0.943	4.410	0.0305
24	18	0.335	0.222	1.508	5.495	0.0122
25	15	0.400	0.245	1.631	5.253	0.0175
26	2	0.374	0.252	1.486	5.935	0.0175
27	21	0.417	0.240	1.741	6.339	0.0175
28	10	0.410	0.260	1.575	5.896	0.0175
29	7	0.340	0.255	1.335	6.368	0.0175

Table 5.31: Experimentally recorded responses for 6 mm thick MDF.

Std	Run	Responses				
		Upper kerf, mm	Lower kerf, mm	Ratio	Ra, μm	Cost €/m
1	25	0.529	0.314	1.685	6.891	0.0306
2	28	0.588	0.410	1.435	5.488	0.0337
3	19	0.338	0.142	2.379	8.736	0.0123
4	24	0.401	0.278	1.441	6.961	0.0135
5	3	0.959	0.213	4.512	7.257	0.0183
6	14	0.910	0.235	3.867	8.684	0.0185
7	23	0.327	0.196	1.670	6.567	0.0183
8	5	0.326	0.193	1.684	7.186	0.0185
9	10	0.827	0.107	7.740	8.314	0.0175
10	9	0.983	0.279	3.519	6.906	0.0193
11	26	0.304	0.179	1.703	7.353	0.0175
12	22	0.375	0.221	1.697	5.332	0.0193
13	20	0.556	0.363	1.534	5.719	0.0320
14	15	0.433	0.234	1.851	7.325	0.0128
15	17	0.485	0.372	1.305	6.760	0.0324
16	11	0.533	0.248	2.148	8.071	0.0130
17	12	0.492	0.136	3.618	7.939	0.0174
18	1	0.545	0.297	1.838	5.721	0.0191
19	27	0.539	0.144	3.741	8.295	0.0176
20	21	0.577	0.302	1.909	6.480	0.0194
21	4	0.916	0.325	2.823	6.834	0.0322
22	13	0.840	0.205	4.096	8.757	0.0129
23	18	0.365	0.381	0.957	5.193	0.0322
24	6	0.336	0.202	1.661	7.524	0.0129
25	8	0.560	0.264	2.122	6.922	0.0184
26	16	0.448	0.253	1.772	7.072	0.0184
27	2	0.467	0.253	1.845	6.750	0.0184
28	7	0.569	0.255	2.228	6.620	0.0184
29	29	0.545	0.246	2.219	6.891	0.0184

Table 5.32: Experimentally recorded responses for 9 mm thick MDF.

Std	Run	Responses				
		Upper kerf, mm	Lower kerf, mm	Ratio	Ra, μm	Cost €/m
1	15	0.580	0.338	1.717	8.221	0.0321
2	25	0.659	0.469	1.407	7.802	0.0352
3	7	0.475	0.180	2.646	9.690	0.0128
4	19	0.566	0.275	2.059	8.854	0.0141
5	13	0.935	0.192	4.860	9.459	0.0191
6	1	0.907	0.199	4.555	10.400	0.0194
7	18	0.321	0.224	1.432	6.327	0.0191
8	5	0.306	0.214	1.431	7.343	0.0194
9	28	0.883	0.132	6.679	10.411	0.0184
10	26	1.007	0.259	3.884	9.340	0.0201
11	10	0.294	0.201	1.464	7.258	0.0184
12	20	0.353	0.242	1.459	6.351	0.0201
13	12	0.650	0.432	1.505	7.377	0.0333
14	9	0.532	0.200	2.662	8.674	0.0133
15	17	0.662	0.410	1.616	8.749	0.0339
16	6	0.620	0.202	3.065	9.823	0.0136
17	3	0.646	0.178	3.633	7.521	0.0182
18	23	0.654	0.304	2.152	7.845	0.0199
19	22	0.621	0.176	3.531	9.125	0.0185
20	29	0.669	0.314	2.132	8.321	0.0203
21	4	0.950	0.362	2.626	9.185	0.0336
22	11	1.002	0.140	7.134	10.892	0.0135
23	2	0.358	0.371	0.966	6.231	0.0336
24	21	0.323	0.203	1.593	7.993	0.0135
25	16	0.602	0.200	3.006	8.382	0.0192
26	27	0.630	0.203	3.099	8.835	0.0192
27	14	0.594	0.196	3.036	8.072	0.0192
28	8	0.624	0.213	2.930	8.507	0.0192
29	24	0.642	0.217	2.964	9.099	0.0192

Table 5.33: Extracted ANOVA tables for all reduced quadratic models of MDF.

Thickness, mm	Response	SS-$_{model}$	DF	Lack of Fit	Prob. >F Model	R^2	Adj- R^2	Pre- R^2
4	Upper kerf	0.45	6	Not Sig.	< 0.0001 (Sig.)	0.9648	0.9552	0.9398
	Lower kerf	0.12	7	Not Sig.	< 0.0001 (Sig.)	0.9619	0.9492	0.9492
	Ratio	15.28	7	Not Sig.	< 0.0001 (Sig.)	0.8828	0.8437	0.6318
	Ra	15.21	4	Not Sig.	< 0.0001 (Sig.)	0.7881	0.7528	0.7098
	Cost	0.001131	6	-	< 0.0001 (Sig.)	0.9999	0.9999	0.9997
6	Upper kerf	1.12	7	Not Sig.	< 0.0001 (Sig.)	0.9629	0.9505	0.9294
	Lower kerf	0.16	8	Not Sig.	< 0.0001 (Sig.)	0.9677	0.9548	0.9182
	Ratio	48.75	7	Not Sig.	< 0.0001 (Sig.)	0.9134	0.8845	0.7291
	Ra	25.45	4	Not Sig.	< 0.0001 (Sig.)	0.9324	0.9211	0.8999
	Cost	0.001251	6	-	< 0.0001 (Sig.)	0.9999	0.9999	0.9997
9	Upper kerf	1.18	3	Not Sig.	< 0.0001 (Sig.)	0.9686	0.9648	0.9537
	Lower kerf	0.21	10	Not Sig.	< 0.0001 (Sig.)	0.9849	0.9765	0.9547
	Ratio	1.23	7	Sig.*	< 0.0001 (Sig.)	0.9727	0.9636	0.9274
	Ra	38.12	4	Not Sig.	< 0.0001 (Sig.)	0.9437	0.9343	0.9201
	Cost	0.001365	6	-	< 0.0001 (Sig.)	0.9999	0.9999	0.9998

* Significant at both $\alpha = 0.001$ & 0.05.

The mathematical models for 4 mm thick MDF are:

$$\text{Upper kerf} = 0.25017 + 1.09495E\text{-}003 * \text{Laser power} - 1.76000E\text{-}005 * \text{Cutting speed} - 0.010556 * \text{Gas pressure} + 0.022352 * \text{Focal position} - 1.47398E\text{-}006 * \text{Laser power}^2 + 0.026467 * \text{Focal position}^2 \quad (5.53)$$

$$\text{Lower kerf} = 0.24389 + 1.86812E\text{-}003 * \text{Laser power} - 1.62315E\text{-}004 * \text{Cutting speed} + 7.16167E\text{-}003 * \text{Focal position} + 7.12000E\text{-}005 * \text{Laser power} * \text{Focal position} - 7.40000E\text{-}006 * \text{Cutting speed} * \text{Focal position} - 1.95513E\text{-}006 * \text{Laser power}^2 + 1.68894E\text{-}008 * \text{Cutting speed}^2 \quad (5.54)$$

$$\text{Ratio} = 1.72015 - 0.015787 * \text{Laser power} + 1.16675E\text{-}003 * \text{Cutting speed} - 0.12038 * \text{Focal position} + 1.14466E\text{-}003 * \text{Laser power} * \text{Focal position} + 2.41892E\text{-}005 * \text{Laser power}^2 - 1.52435E\text{-}007 * \text{Cutting speed}^2 + 0.13849 * \text{Focal position}^2 \quad (5.55)$$

$$\text{Ra} = 3.67448 - 5.03233E\text{-}003 * \text{Laser power} + 3.43722E\text{-}004 * \text{Cutting speed} + 0.32197 * \text{Gas pressure} - 0.30512 * \text{Focal position} \quad (5.56)$$

Operating cost = 0.054467 + 1.77300E-005 * Laser power - 1.74530E-005* Cutting speed + 1.95672E-004 * Gas pressure - 2.69804E-009* Laser power* Cutting speed - 2.97761E-008* Cutting speed* Gas pressure +1.74561E-009 * Cutting speed^2 (5.57)

The mathematical models for 6 mm thick MDF are:

Upper kerf = 0.51117 + 3.19855E-004 * Laser power - 3.69854E-005 * Cutting speed - 0.063489* Gas pressure - 0.020067 * Focal position + 1.90444E-005 * Cutting speed * Gas pressure - 1.41116E-008 * Cutting speed^2 + 0.012411 * Focal position^2 (5.58)

Lower kerf = 0.37930 + 1.61830E-003 * Laser power - 2.43702E-004 * Cutting speed +0.026528 * Focal position - 9.42029E-005 * Laser power * Focal position -3.31111E-006 * Cutting speed * Focal position- 1.74746E-006* Laser power^2 + 2.66177E-008 * Cutting speed^2 – 3.59279E-003 * Focal position^2 (5.59)

Ratio = 1.89366 - 0.026826 * Laser power + 2.29084E-003 * Cutting speed – 1.04712 * Focal position + 3.05405E-003 * Laser power* Focal position +3.82434E-005* Laser power^2 - 2.96815E-007* Cutting speed^2 + 0.10100* Focal position^2 (5.60)

Ra = 5.83725 - 7.71029E-003 * Laser power + 5.82711E-004 * Cutting speed +0.27490 * Gas pressure -0.21104 * Focal position (5.61)

Operating cost = 0.055540 + 1.77300E-005 *Laser power - 1.81061E-005* Cutting speed+1.95672E-004 * Gas pressure - 2.69804E-009* Laser power* Cutting speed - 2.97761E-008 * Cutting speed * Gas pressure +1.83892E-009 * Cutting speed^2 (5.62)

The mathematical models for 6 mm thick MDF are:

Upper kerf = 0.23051 + 3.03407E-004 * Laser power - 1.89000E-005* Cutting speed -0.088781* Focal position (5.63)

Lower kerf = 1.29654 - 1.35685E-003 * Laser power - 3.23488E-004 * Cutting speed-0.056743 * Gas pressure + 0.010726 * Focal position - 5.47302E-005* Laser power * Focal position + 2.54286E-006* Cutting speed * Focal position + 1.69508E-006 * Laser power^2 + 3.81126E-008 * Cutting speed^2 +4.67583E-003 * Gas pressure^2 – 1.58340E-003 * Focal position^2 (5.64)

1/(Ratio) = 2.23221 - 1.94771E-003 * Laser power - 5.70715E-004 * Cutting speed +0.14492 * Focal position - 7.94211E-006 * Cutting speed* Focal position+2.54588E-006 * Laser power^2 + 6.43906E-008* Cutting speed^2 +6.27356E-003 * Focal position^2 (5.65)

Ra = 5.04497 - 2.74963E-003 * Laser power + 4.64556E-004 * Cutting speed +0.27329 * Gas pressure - 0.43295 * Focal position (5.66)

Operating cost = 0.056498 + 1.77300E-005* Laser power - 1.86890E-005 *Cutting speed + 1.95672E-004* Gas pressure - 2.69804E-009* Laser power* Cutting speed - 2.97761E-008* Cutting speed* Gas pressure +1.92219E-009 * Cutting speed^2 (5.67)

5.4.2 Validation of the developed models for MDF

In order to verify the adequacy of the developed models, two confirmation experiments for each thickness were carried out using a new set of test conditions. These experiments were randomly selected from the optimisation results, which were within the investigated range. Using the point prediction option in the software, all the response values can be predicted by substituting these conditions into the previous developed models. Table 5.34 presents the experimental condition, the actual experimental values, the predicted values and the percentage errors for all thicknesses. It is clear that all the values of the percentage errors for all the four responses are within reasonable agreement. Therefore, the models are valid. It is apparent from Table 5.34 that the ratio model for thickness 9 mm has the highest percentage error of -17.397% in the second validation experiment, this is due to the fact that this model has a significant lack-of-fit. However, if the predicted ratio is calculated by dividing the predicted upper kerf of

0.299 mm by the predicted lower kerf of 0.207 mm the percentage error would be equal to 5.125 %, which is in excellent agreement. On balance, the ratio model for 9 mm MDF may not be used for predictions, but can still be used to investigate the general influence of the process parameters on the ratio and in the optimisation.

5.4.3 Effect of process factors on the responses for MDF

5.4.3.1 Upper kerf

The perturbation plots for the upper kerfs for all thicknesses are shown in Fig. 5.40. In this graph it is clear that the focal point position is the major factor affecting the upper kerf. The results show that the upper kerf decreases as the focal point position increases and this is logical because the smallest spot size of the laser beam occurs at the surface when the focal point is exactly on the surface, and consequently, the laser power will localise in a narrow area. On the other hand, defocusing the beam below the surface would result in spreading the laser power onto a wider area on the surface, results in a wider upper kerf. The upper kerf is on average 2.5 times wider when using the defocused beam. From the same figure, it is notable that the laser power also affects the upper kerf. The upper kerf would increase as the laser power increased. Finally, it is clear that the upper kerf reduces slightly as the cutting speed and gas pressure increase. These observations are in agreement with Lum et al. [77]. However, the effect of the gas pressure on the average upper kerf reduces as the thickness increases until it disappears for 9 mm thick MDF. Fig. 5.41 shows the interaction effect between the cutting speed and the air pressure on the average upper kerf for 6 mm MDF. Figure 5.41 shows that at slower cutting speeds less than 3337.58 mm/min a narrower upper kerf of 0.50 mm would be achieved using the highest air pressure of 7 bars. Alternatively, the narrowest average upper kerf of 0.40 mm could be obtained using faster cutting speeds above 3337.58 mm/min and an air pressure of 4 bar.

Table 5.34: Confirmation experiments for MDF.

Thickness, mm	Exp. No.	Factors				Values	Responses				
		A, W	B, mm/min	C, bar	D, mm		Upper kerf, mm	Lower kerf, mm	Ratio	Ra, µm	Cost, €/m
4	1	400	2164.51	4.08	-0.29	Actual	0.358	0.407	0.879	3.598	0.0297
						Predicted	0.367	0.4	1	3.809	0.0302
						Error %	-2.629	1.672	-13.758	-5.876	-1.684
	2	150	4999.99	3	-1.72	Actual	0.303	0.136	2.220	5.632	0.0115
						Predicted	0.302	0.124	2.241	6.129	0.0116
						Error %	0.264	9.091	-0.949	-8.832	-0.870
6	1	482.29	2000	6.41	-0.69	Actual	0.369	0.406	0.909	5.120	0.0336
						Predicted	0.392	0.388	1	5.193	0.0335
						Error %	-6.348	4.339	-10.038	-1.418	0.298
	2	270	5000	4	-3.54	Actual	0.441	0.137	3.210	7.629	0.0122
						Predicted	0.413	0.146	3.525	8.515	0.0123
						Error %	6.349	-6.259	-9.827	-11.614	-0.820
9	1	600	2000	4.14	-0.77	Actual	0.416	0.477	0.874	5.358	0.0349
						Predicted	0.444	0.456	1	5.791	0.0348
						Error %	-6.628	4.322	-14.457	-8.089	0.287
	2	375	5000	4	-0.55	Actual	0.322	0.212	1.522	6.788	0.0127
						Predicted	0.299	0.207	1.787	7.67	0.0129
						Error %	7.258	2.266	-17.397	-12.990	-1.575

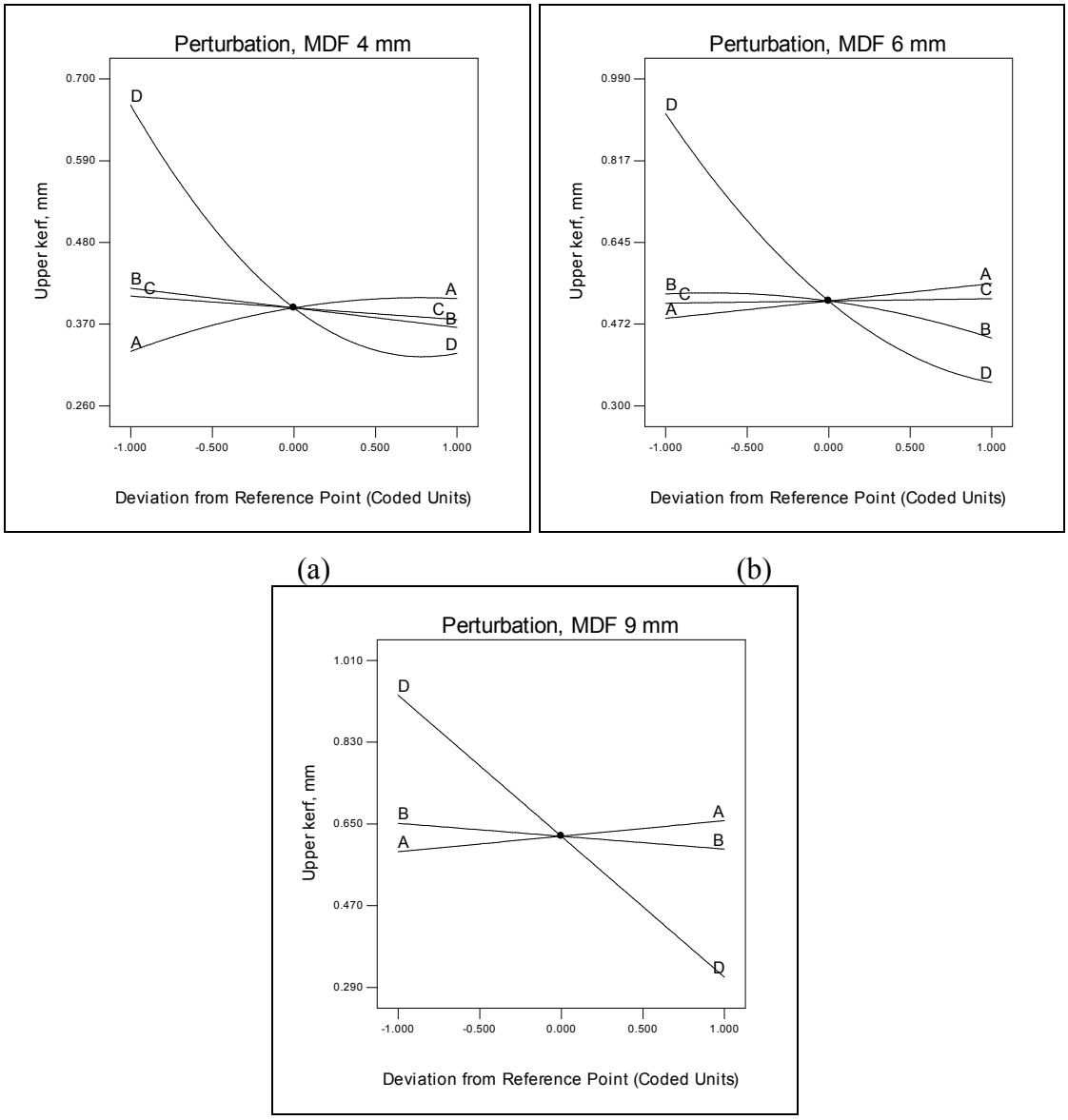

Fig. 5.40: Perturbation plots showing the effect of each factor on the average upper kerf for (a) 4 mm, (b) 6 mm and (c) 9 mm thick MDF.

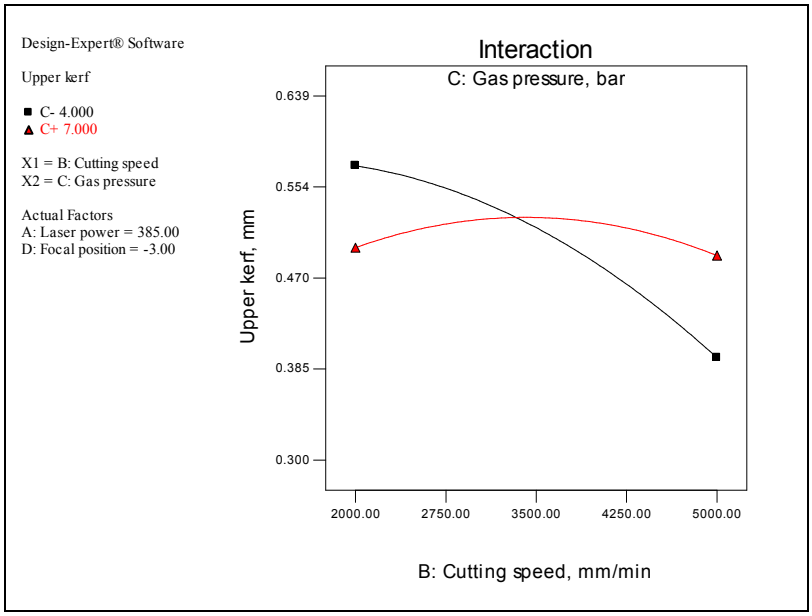

Fig. 5.41: Interaction graph between cutting speed and gas pressure for 6 mm MDF.

5.4.3.2 Lower kerf

The perturbation plots for the average lower kerf widths for all thicknesses are exhibited in Fig. 5.42. In this plot it is obvious that the laser power and the cutting speed are the factors which have the greatest effect on the lower kerf. The results confirm that the lower kerf decreases as the cutting speed increases and this is in agreement with Lum et al. [77]. Also, it was found that the lower kerf increases as the laser power increases and this is in good agreement with results found in the literature. When using the highest laser power the lower kerf is on average 2.21 times wider than that obtained using the lowest laser power. By using the slowest cutting speed, the lower kerf is on average 1.37 times wider than that obtained using the fastest cutting speed. It is evident that the lower kerf changes slightly as the focal point position increases. However, the air pressure has a very minor effect on the average lower kerf for 9 mm thick MDF only. Figure 5.43a-c shows the interaction effect between the cutting speed and the focal point position on the average lower kerf for the three thicknesses. Figure 5.43a-b demonstrates that at slower cutting speeds less than 3337.58 mm/min or 3570.03 mm/min, for 4 or 6 mm thick respectively, a narrower lower kerf would be achieved using focal point position of -4 mm or -6 mm. On the other hand, a narrower average lower kerf could be obtained using

faster cutting speeds above 3337.58 mm/min or 3570.03 mm/min for the same two thicknesses and a focused beam. According to Fig. 5.43c, it is clear that at the slowest cutting speed both focal point positions would lead to the same lower kerf, but as the speed increases a focal position of -7 mm would lead to a narrower lower kerf. It is evident from Fig. 543(a-c) that the effect of the focal point position becomes insignificant when using slow cutting speeds.

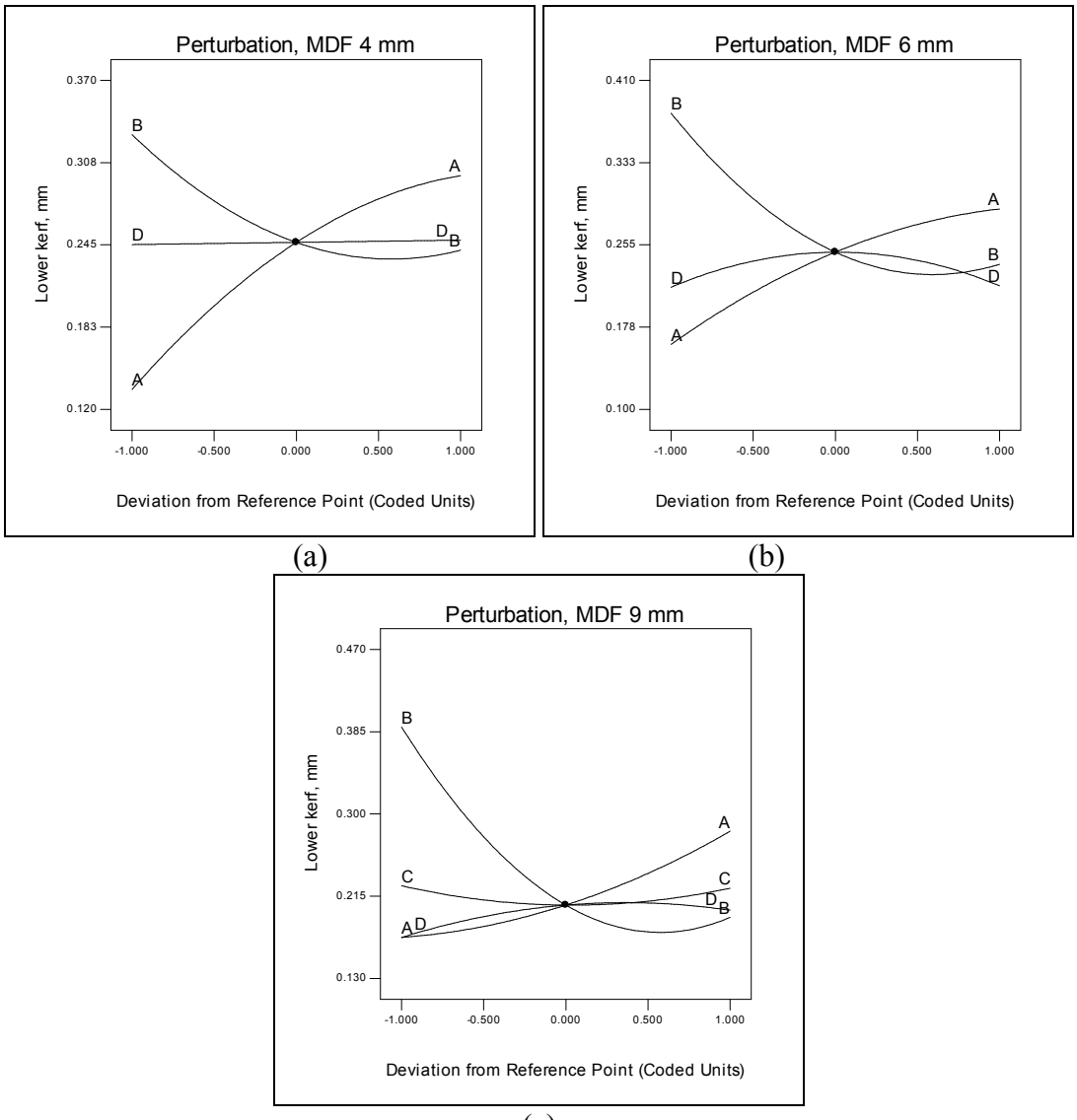

Fig. 5.42: Perturbation plots showing the effect of each factor on the average lower kerf for the (a) 4 mm thick, (b) 6 mm thick and (c) 9 mm thick.

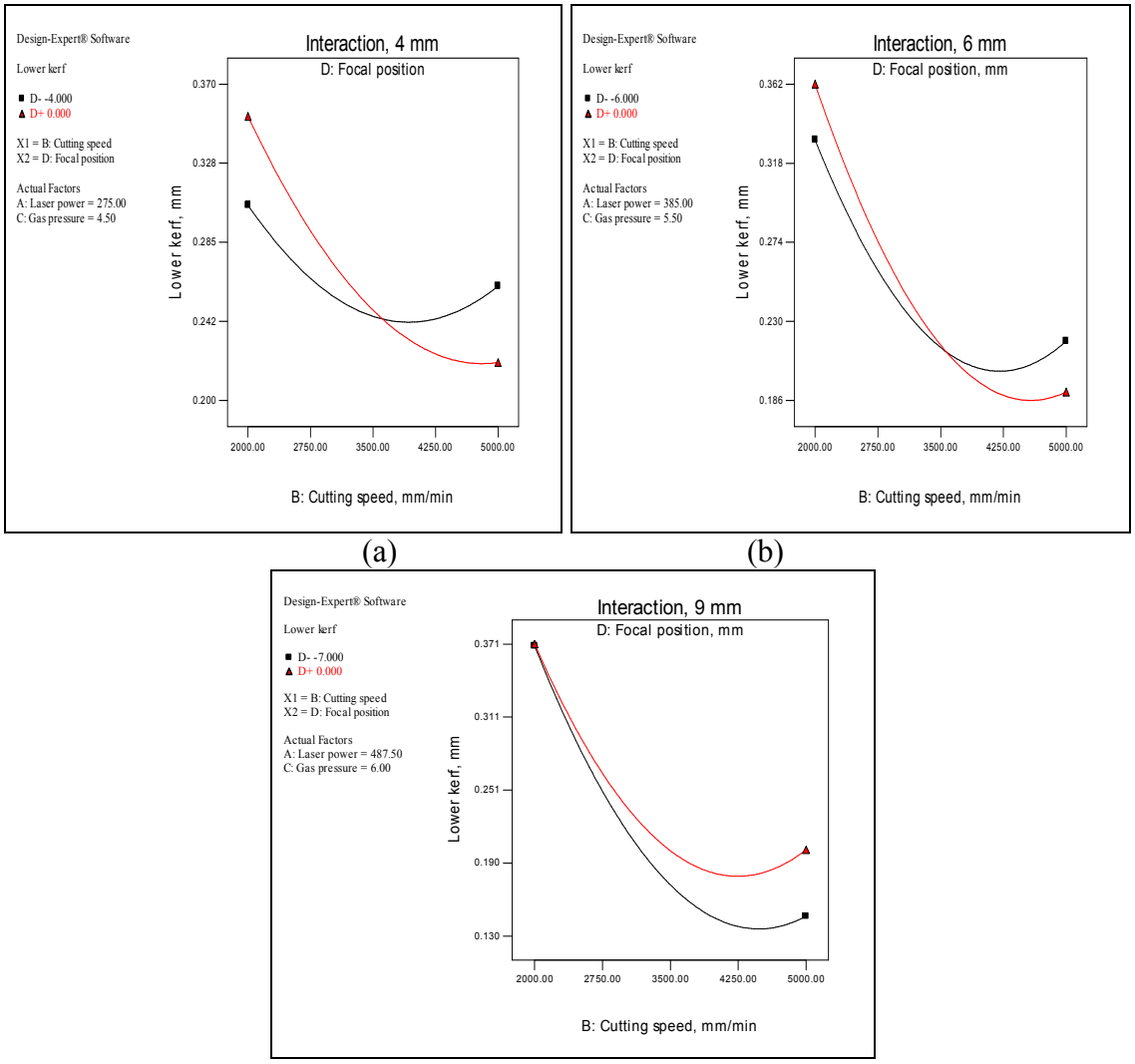

Fig. 5.43: Interaction graph between cutting speed and focal position for the three thicknesses.

5.4.3.3 Ratio between upper kerf to lower kerf

The perturbation plots for the ratio between the upper kerf and the lower kerf for all thicknesses are presented in Fig. 5.44a-c. In this plot it is obvious that the focal position is the most important factor affecting the ratio of the upper kerf to the lower kerf. The results show that the ratio decreases as the focal position increases. It can be seen from Fig. 5.44a-c that the laser power has the second most important effect on the ratio. However, this effect reduces as the thickness increases. In general, the ratio decreases as the laser power increases. Also, it was found that the ratio increases as the

cutting speed increases up to approximately 3875 mm/min, and then it starts to decrease as the cutting speed increases. However, the air pressure has no effect on the ratio for all thicknesses. The Fig. 5.45a-c contour graph shows the effect of the focal point position and the laser power on the ratio for the three thicknesses. Figure 5.45a-b apparently shows the area where the ratio is as close as possible to 1.

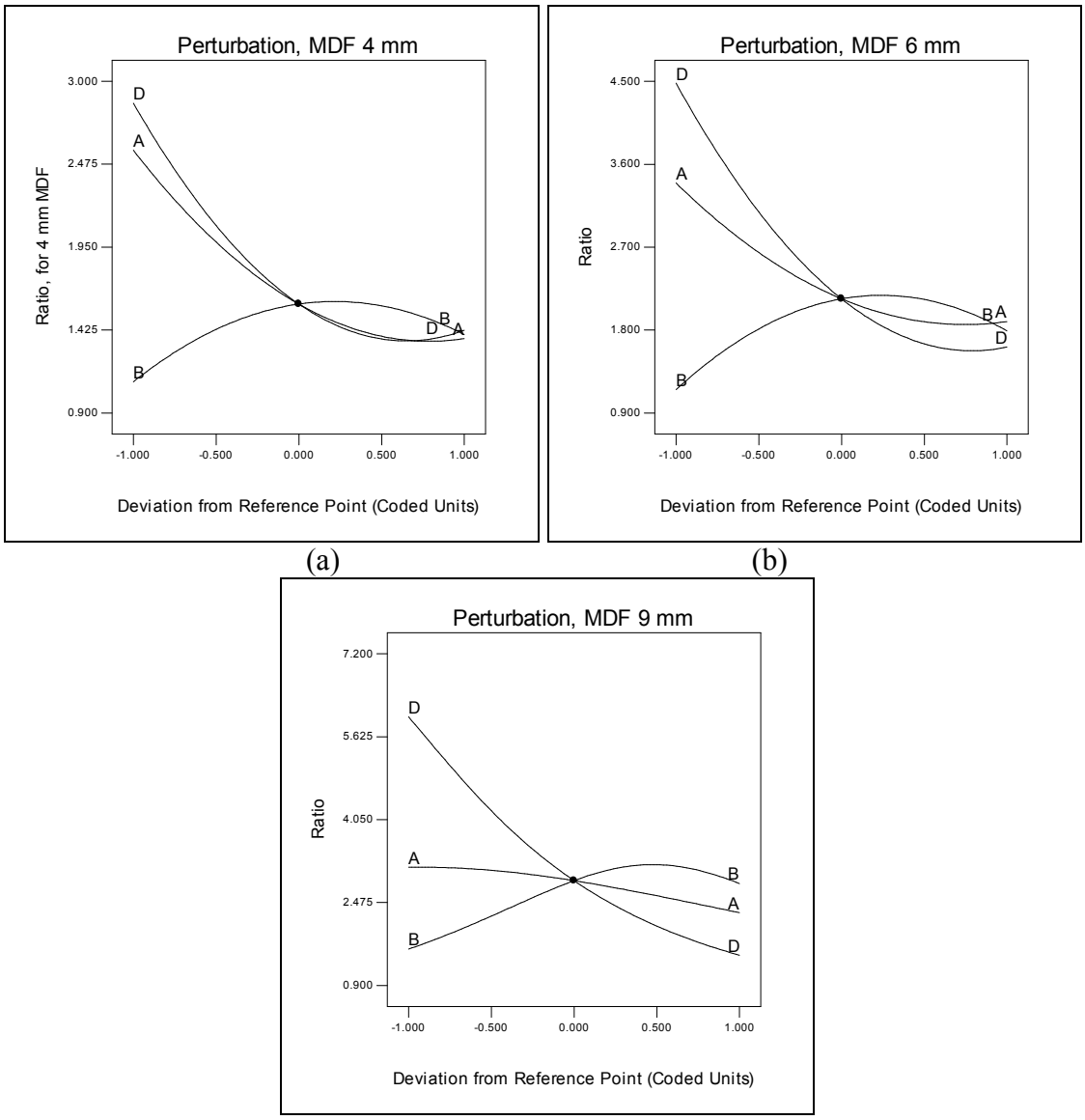

Fig. 5.44: Perturbation plots showing the effect of each factor on the ratio for the (a) 4 mm thick, (b) 6 mm thick and (c) 9 mm thick.

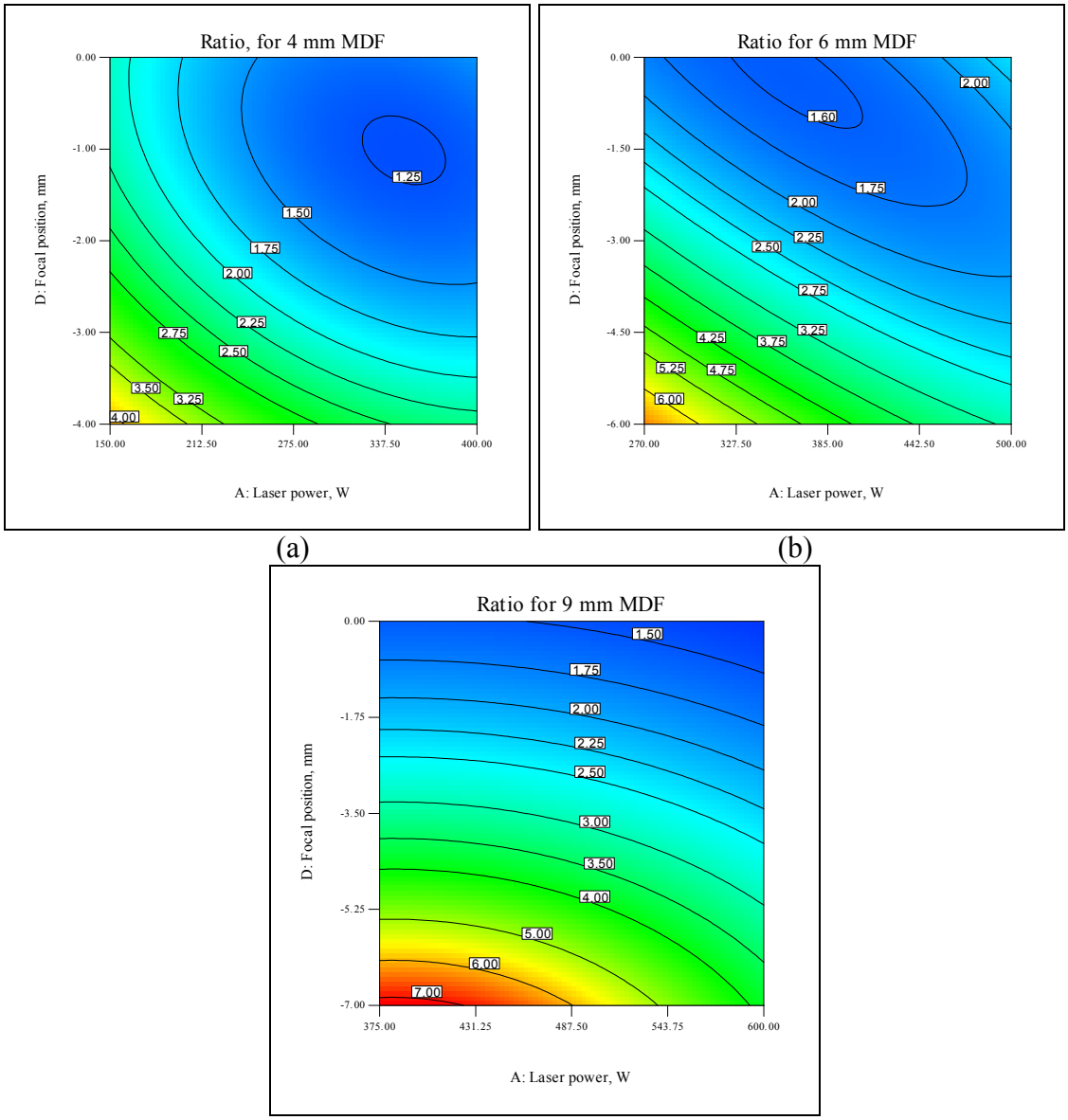

Fig. 5.45: Contours graph showing the effect of focal point position and laser power for the three thicknesses.

5.4.3.4 Roughness

The perturbation graphs for the roughness for all thicknesses are shown in Fig. 5.46a-c. In these graphs it is clear that all the factors significantly affect the roughness. The results show that the roughness decreases as the focal point position and laser power increase and this is in agreement with the results reported by Barnekov et al. [73].

However, the effect of laser power on the roughness of the cut surface reduces as a thicker MDF sheet is considered. The results demonstrate that the roughness value increases as the cutting speed and gas pressure increase.

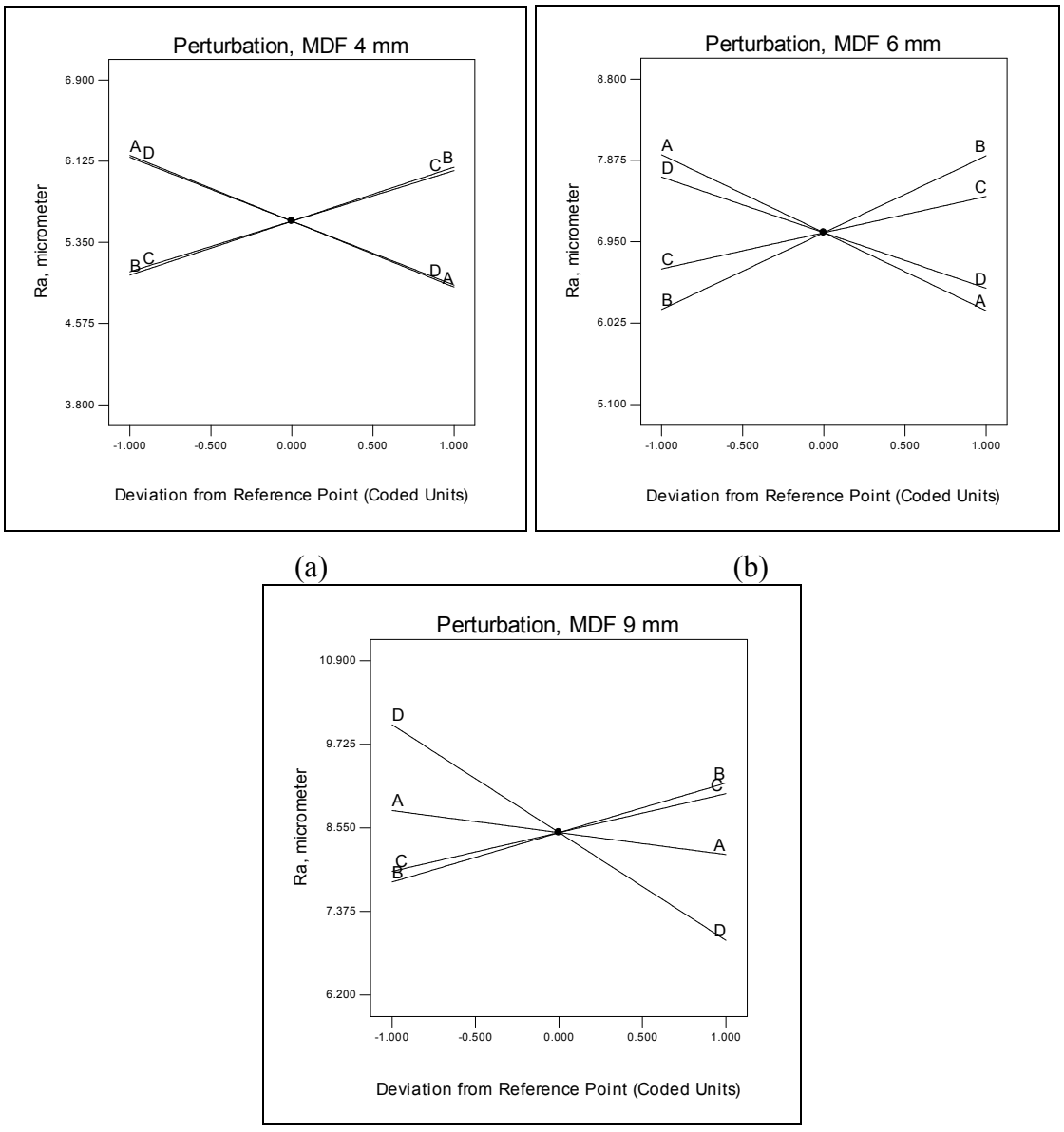

Fig. 5.46: Perturbation plots showing the effect of each factor on the roughness for (a) 4 mm, (b) 6 mm and (c) 9 mm thick MDF.

5.4.3.5 Operating cost

Figure 5.47a-c are the perturbation graphs which show the main factors affecting the operating cost. From these graphs, it is obvious that three factors affect the operating cost. The results confirm that the main factor affecting the cost is the cutting speed because the operating cost reduces considerably as the cutting speed increases. On the other hand, the laser power and the compressed air only slightly affect the operating cost. As both laser power and air pressure increase the operating cost increases.

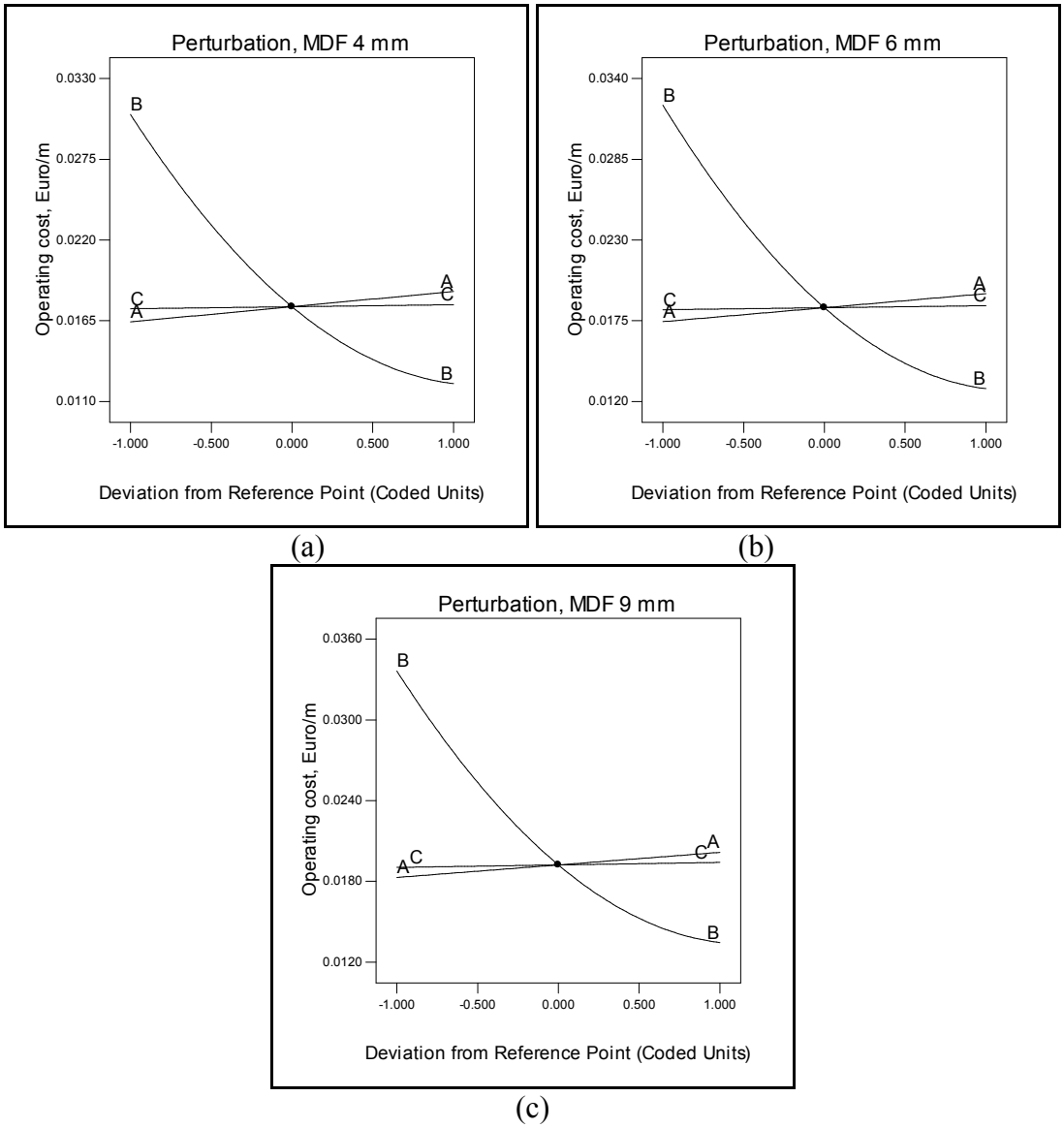

Fig. 5.47: Perturbation plots showing the effect of each factor on the operating cost per meter for the (a) 4 mm, (b) 6 mm and (c) 9 mm thick.

5.5 Glass-Fibre Reinforced Plastic (GFRP)

For this composite material, five responses were successfully measured namely: upper kerf, lower kerf, ratio between upper to lower kerfs, HAZ and operating cost. The equipment and procedures described earlier in chapter 4 were again used to determine and record these responses. An average of at least three consistent measurements of both kerf widths and HAZ were recorded for all the 29 runs presented previously in Table 4.24. The ratio of the upper kerf to the lower kerf was calculated for each run using the averaged data for both the upper and lower kerfs. The average values of the measured responses are listed in Table 5.35. All experimentally recorded responses are presented in appendix E. The operating cost was estimated using Eq. 4.7 and Eq. 4.3 and the estimated operating cost for each experiment is presented in Table 5.35.

5.5.1 Development of the mathematical models for (GFRP)

Design expert software V7 was used to analyse the measured responses. The fit summary output indicates that, for all responses, the quadratic models are statistically recommended for further analysis as they have the maximum predicted and adjusted R^2 [141]. The test for significance of the regression models, the test for significance on individual model coefficients and the lack of fit test were performed using the same statistical package for all responses. By selecting the step-wise regression method, the insignificant model terms can be automatically eliminated. The resulting ANOVA tables (Tables 5.36 to 5.40) for the reduced quadratic models outline the analysis of variance for each response and illustrate the significant model terms. The same tables show also the other adequacy measures R^2, Adjusted R^2 and Predicted R^2. All adequacy measures are close to 1, which are in reasonable agreement and indicate adequate models [116 and 117]. The adequate precision compares the range of the predicted value at the design points to the average prediction error. In all cases the values of adequate precision ratios are significantly greater than 4. An adequate precision ratio above 4 indicates an adequate model [141]. The developed mathematical models are shown in Eqs.5.68 – Eqs. 5.72 in terms of actual factors.

Table 5.35: Experimentally recorded responses for 3 mm thick GFRP.

Std	Run	Responses				
		Upper kerf, mm	Lower kerf, mm	Ratio	HAZ, mm	Cost €/m
1	24	0.413	0.336	1.231	0.078	0.0380
2	18	0.490	0.458	1.071	0.089	0.0488
3	27	0.324	0.298	1.090	0.044	0.0152
4	17	0.430	0.373	1.154	0.047	0.0195
5	5	0.690	0.348	1.982	0.084	0.0241
6	3	0.542	0.296	1.830	0.057	0.0256
7	21	0.356	0.409	0.871	0.082	0.0241
8	13	0.330	0.380	0.870	0.058	0.0256
9	14	0.661	0.247	2.682	0.065	0.0217
10	26	0.560	0.351	1.594	0.090	0.0279
11	1	0.332	0.207	1.602	0.054	0.0217
12	2	0.311	0.390	0.796	0.084	0.0279
13	19	0.388	0.415	0.935	0.078	0.0421
14	9	0.313	0.402	0.778	0.056	0.0168
15	6	0.336	0.439	0.765	0.075	0.0448
16	7	0.361	0.351	1.029	0.044	0.0179
17	8	0.390	0.219	1.783	0.078	0.0210
18	15	0.517	0.415	1.245	0.099	0.0272
19	12	0.418	0.306	1.368	0.060	0.0225
20	23	0.477	0.449	1.062	0.086	0.0287
21	10	0.743	0.324	2.292	0.078	0.0434
22	16	0.556	0.339	1.642	0.046	0.0174
23	11	0.388	0.432	0.899	0.082	0.0434
24	22	0.371	0.397	0.935	0.049	0.0174
25	25	0.347	0.351	0.989	0.064	0.0248
26	4	0.302	0.375	0.805	0.079	0.0248
27	20	0.382	0.365	1.047	0.065	0.0248
28	29	0.365	0.358	1.019	0.060	0.0248
29	28	0.325	0.354	0.920	0.061	0.0248

Table 5.36: ANOVA table for upper kerf width reduced quadratic model for GFRP.

Source	Sum of Squares	DF	Mean Square	F Value	Prob > F	
Model	0.331	5	0.066	20.453	< 0.0001	Significant
A	0.005	1	0.005	1.559	0.2243	
B	0.013	1	0.013	4.157	0.0531	
D	0.231	1	0.231	71.371	< 0.0001	
A^2	0.011	1	0.011	3.525	0.0732	
D^2	0.077	1	0.077	23.685	< 0.0001	
Residual	0.074	23	0.003			
Lack of Fit	0.070	19	0.004	3.712	0.1060	Not Sig.
Pure Error	0.004	4	0.001			
Cor Total	0.405	28				
$R^2 = 0.816$			Pred $R^2 = 0.681$			
Adj $R^2 = 0.777$			Adeq Precision =14.381			

Table 5.37: ANOVA table for lower kerf width reduced quadratic model for GFRP.

Source	Sum of Squares	DF	Mean Square	F Value	Prob > F	
Model	0.091	6	0.015	15.622	< 0.0001	Significant
A	0.057	1	0.057	58.581	< 0.0001	
B	0.005	1	0.005	5.126	0.0338	
D	0.008	1	0.008	8.223	0.0089	
A^2	0.008	1	0.008	8.470	0.0081	
B^2	0.006	1	0.006	6.046	0.0223	
D^2	0.004	1	0.004	4.636	0.0425	
Residual	0.021	22	0.001			
Lack of Fit	0.021	18	0.001	12.287	0.0129	Not Sig.
Pure Error	0.000378	4	0.000094			
Cor Total	0.112	28.00				
$R^2 = 0.810$			Pred $R^2 = 0.649$			
Adj $R^2 = 0.758$			Adeq Precision = 15.629			

Table 5.38: ANOVA table for ratio reduced quadratic model for GFRP.

Source	Sum of Squares	DF	Mean Square	F Value	Prob > F	
Model	5.747	6	0.958	24.786	< 0.0001	Significant
A	0.669	1	0.669	17.310	0.0004	
B	0.027	1	0.027	0.687	0.4163	
D	3.048	1	3.048	78.880	< 0.0001	
BD	0.118	1	0.118	3.053	0.0945	
A^2	0.622	1	0.622	16.105	0.0006	
D^2	1.492	1	1.492	38.605	< 0.0001	
Residual	0.850	22	0.039			
Lack of Fit	0.813	18	0.045	4.836	0.0687	Not Sig.
Pure Error	0.037	4	0.009			
Cor Total	6.597	28				
$R^2 = 0.871$			Pred $R^2 = 0.749$			
Adj $R^2 = 0.836$			Adeq Precision = 17.282			

Table 5.39: ANOVA table for HAZ reduced quadratic model for GFRP.

Source	Sum of Squares	DF	Mean Square	F Value	Prob > F	
Model	0.005	3	0.002	22.971	< 0.0001	Significant
A	0.001	1	0.001	15.496	0.0006	
B	0.003	1	0.003	42.749	< 0.0001	
D	0.001	1	0.001	10.669	0.0032	
Residual	0.002	25	0.000			
Lack of Fit	0.002	21	0.00008	1.259	0.4581	Not Sig.
Pure Error	0.00024	4	0.00006			
Cor Total	0.007	28				
$R^2 = 0.734$			Pred $R^2 = 0.621$			
Adj $R^2 = 0.702$			Adeq Precision = 16.284			

Table 5.40: ANOVA table for operating cost reduced quadratic model for GFRP.

Source	Sum of Squares	DF	Mean Square	F Value	Prob > F	
Model	0.002	6	0.0004015	6492.140	< 0.0001	Significant
A-Laser	0.0001318	1	0.0001318	2132.067	< 0.0001	
B-Cutting	0.002	1	0.0020385	32964.02	< 0.0001	
C-Argon	0.0000079	1	0.0000079	127.822	< 0.0001	
AB	0.0000105	1	0.0000105	169.505	< 0.0001	
BC	0.0000006	1	0.0000006	10.162	0.0043	
B^2	0.00022	1	0.0002195	3549.258	< 0.0001	
Residual	0.0000014	22	0.0000001			
Cor Total	0.00241	28				Not Sig.
$R^2 = 0.999$			Pred $R^2 = 0.998$			
Adj $R^2 = 0.999$			Adeq Precision = 267.620			

Upper kerf = 0.57218 - 4.05984E-004 * Laser power - 2.23148E-005 * Cutting speed +0.048005 * Focal position +2.54019E-007* Laser power^2 +0.046823* Focal position^2 (5.68)

Lower kerf = 0.24754 +5.64113E-004 * Laser power -1.05228E-004* Cutting speed -0.017252 * Focal position -2.18003E-007* Laser power^2+1.30976E-008 * Cutting speed^2 – 0.011469* Focal position^2 (5.69)

Ratio = 2.65577 - 3.96840E-003 * Laser power + 8.31539E-005 * Cutting speed +0.016723 * Focal position + 7.63331E-005 * Cutting speed * Focal position+1.87675E-006 * Laser power^2 + 0.20663* Focal position^2 (5.70)

HAZ = 0.10854 + 2.42708E-005* Laser power -1.07500E-005* Cutting speed - 8.05556E-003* Argon pressure (5.71)

Operating Cost= 0.064484+1.77300E-005 * Laser power-2.28465E-005* Cutting speed +1.73648E-003*Argon pressure-2.69804E-009* Laser power* Cutting speed-2.64247E-007*Cutting speed* Argon pressure +2.48261E-009 * Cutting speed^2 (5.71)

5.5.2 Validation of the developed models for GFRP

The strength of the models developed for 3 mm GFRP can be validated from Fig. 5.48, which presents the relationship between the measured and predicted response values. These scatter diagrams indicate that the mathematical models for GFRP show excellent agreement between the measured and estimated values for all responses considered. With the aim of verifying the adequacy of the developed models furthermore, three confirmation experiments were carried out by using new test conditions. These experiments are taken from the optimisation results which are within the investigated range. By using the point prediction option in the software, all the response values can be predicted by substituting these conditions into the previously developed models. Table 5.41 presents the experimental conditions, the actual experimental values, the predicted values and the percentage errors. It is clear that all the values of percentage error for all the five responses are in agreement with the values reported in [119 and 121]. Therefore, it would strongly suggest that the models are valid.

Table 5.41: Confirmation experiments for GFRP.

Exp. No.	A	B	C	D		Upper kerf	Lower kerf	ratio	HAZ	Cost
1	716.92	4844.97	3.75	-1.05	Actual	0.312	0.337	0.925	0.046	0.0173
					Predicted	0.305	0.343	1.000	0.044	0.0171
					Error %	2.257	-1.788	-8.128	4.348	1.0372
2	746.41	4796.57	3.99	-1.36	Actual	0.306	0.327	0.937	0.047	0.0178
					Predicted	0.325	0.346	1.000	0.043	0.0175
					Error %	-6.131	-5.800	-6.746	9.235	1.900
3	500	5000	2	-0.85	Actual	0.328	0.263	1.246	0.050	0.0147
					Predicted	0.314	0.283	1.367	0.051	0.0153
					Error %	4.173	-7.523	-9.753	-1.629	-3.858

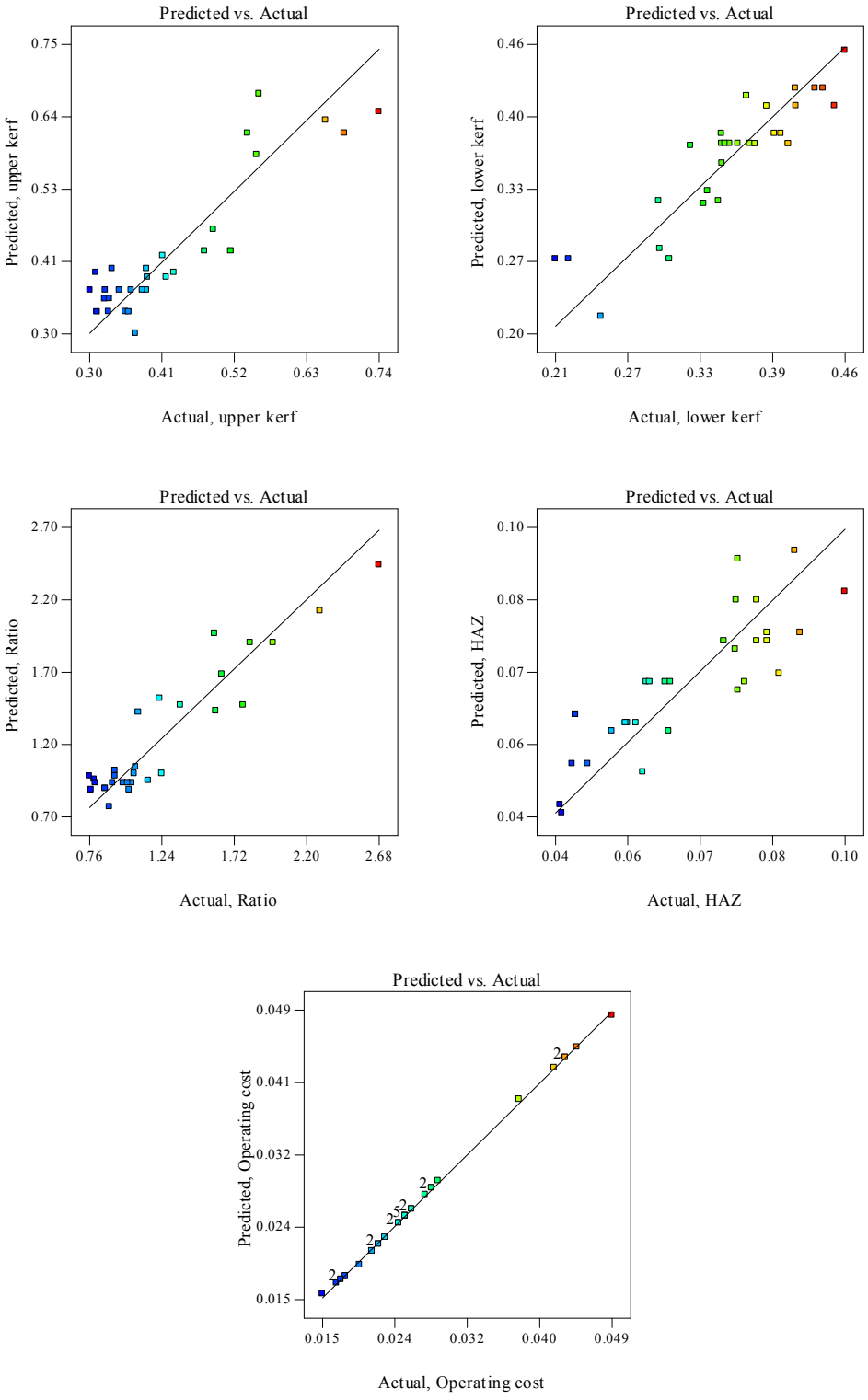

Fig. 5.48: Scatter diagram showing the relationship between the actual and predicted values for each response for GFRP.

5.5.3 Effect of process factors on the responses for GFRP

5.5.3.1 Upper kerf

The results demonstrate that the laser cutting of GFRP is of acceptable quality and depends mainly on the distribution of the fibre along the thickness, which agrees with Caprino et al. [64]. It is evident from Fig. 5.49 that the focal point position has the most important significant effect on the upper kerf for GFRP, followed by the cutting speed and the laser power. However, the upper kerf increases as the focal position and cutting speed decrease, while it increases as the laser power increases. These results are in good agreement with the results reported in [66]. The percentage changes in the upper kerf as a result of changing each factor from its lowest value to its highest value while keeping the other factors at their centre values are as follows: (i) Changing focal position would result in a decrease of 45.34%. (ii) Changing the cutting speed would result in a decrease of 16.68%. (iii) Changing the laser power would result in an increase of 10.57%. It is obvious that the argon pressure has no significant effect on the upper kerf.

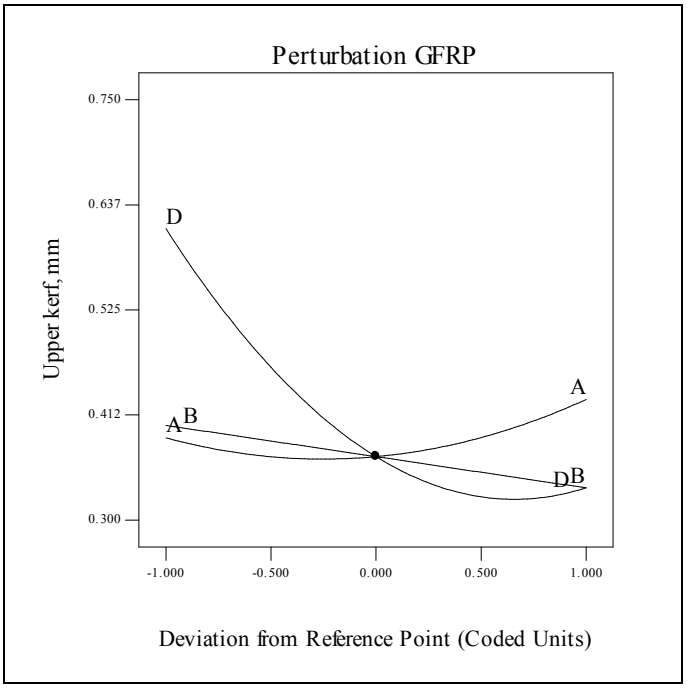

Fig. 5.49: Perturbation plots showing the effect of each factor on the upper kerf for 3mm thick GFRP.

5.5.3.2 Lower kerf

The perturbation plot for the average lower kerf width for GFRP is presented in Fig. 5.50. From Fig. 5.50 it is clear that the laser power is the key factor affecting the lower kerf. The results confirm that the lower kerf decreases as the laser power decreases and this agrees with result found in [66]. When using the highest laser power, the lower kerf is on average 1.51 times wider than that obtained using the lowest laser power. It was found that the cutting speed and focal position have a significant effect on the lower kerf. By using the slowest cutting speed, the lower kerf is on average 1.11 times wider than that obtained using the fastest cutting speed. It is evident that the lower kerf width increases by 1.16 as the focal point position increases from its smallest level to its highest level. However, the air pressure has no significant effect on the average lower kerf for 3 mm thick GFRP.

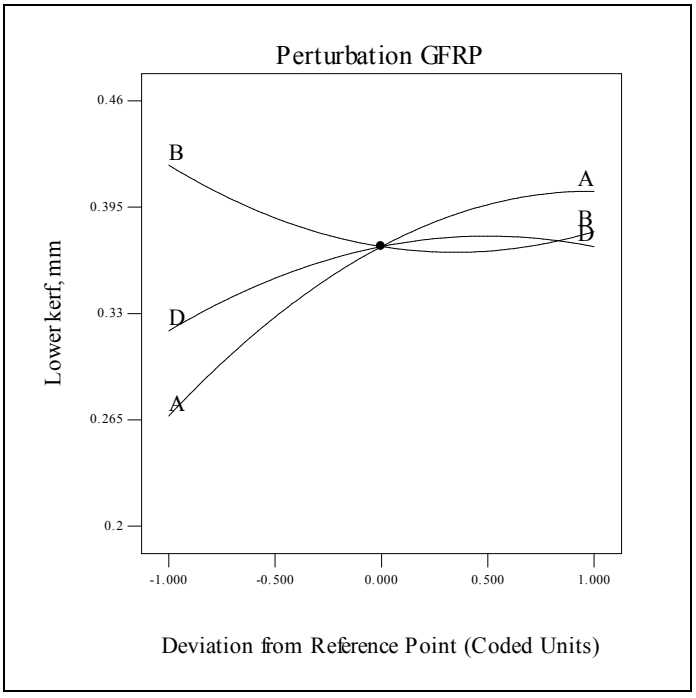

Fig. 5.50: Perturbation plots showing the effect of each factor on the lower kerf for 3mm thick GFRP.

5.5.3.3 Ratio between upper kerf to lower kerf

Figure 5.51 demonstrates that the focal position, the laser power and cutting speed are the laser beam cutting parameters which affect the ratio. It was found that the focal position and laser power are the most important factors influencing the ratio. However, the cutting speed only has a minor effect on the ratio. It is clear that as the focal position and laser power increase the ratio would decrease. It is clear from Fig. 5.51 that a ratio of one is the desirable option in order to obtain a square cut edge. Fig. 5.52 is the interaction plot between the cutting speed and focal position. It is evident that at a focal position of -3 mm a ratio of 1.68 could be obtained if the maximum cutting speed of 5000 mm/min was applied. On the other hand, when the focal position is exactly on the surface of the substrate a ratio of 0.77 could be achieved if the slowest cutting speed of 200 mm/min was used. At a focal position of -1.08 mm a ratio of 0.82 might be obtained by using either maximum or minimum cutting speed.

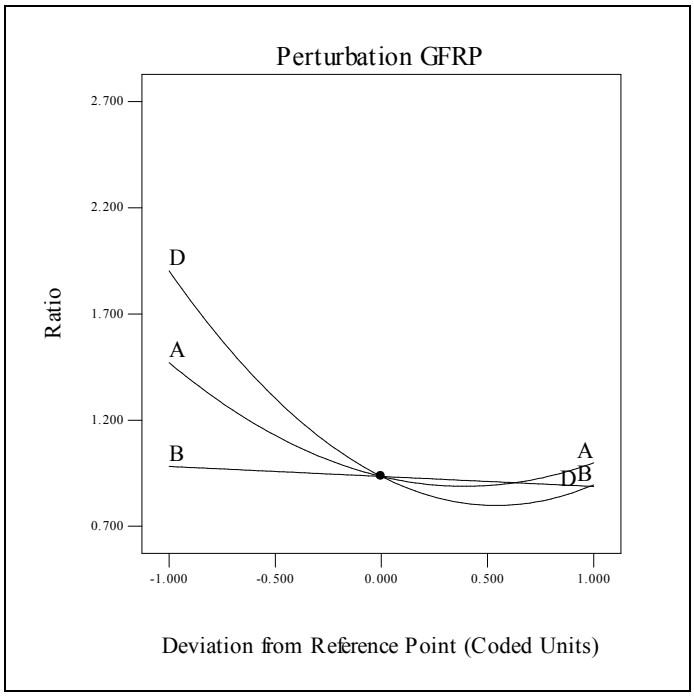

Fig. 5.51: Perturbation plots showing the effect of each factor on the ratio for 3mm thick GFRP.

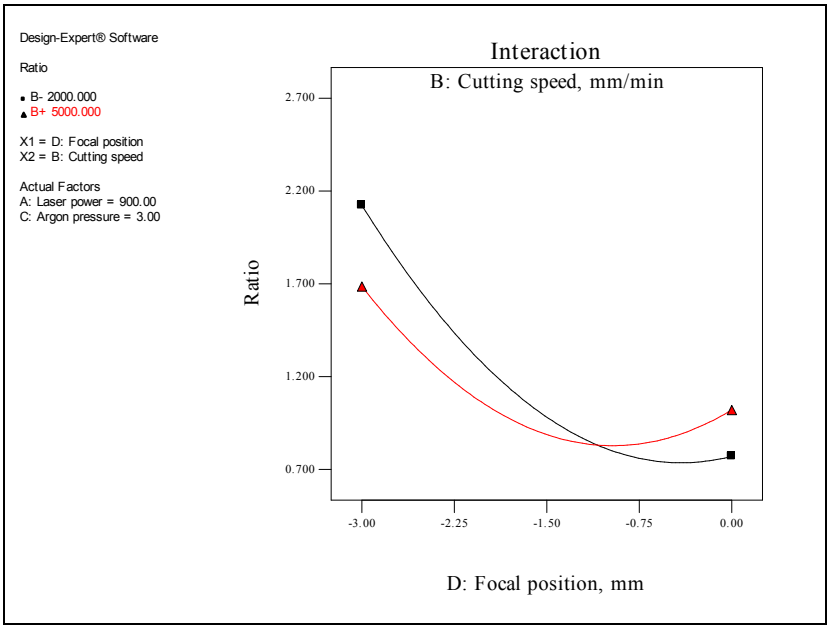

Fig. 5.52: Interaction graph between cutting speed and focal position for 3 mm GFRP.

5.5.3.4 Heat-affected zone HAZ

For this material the HAZ was successfully modelled. The results indicate that the dimensions of HAZ are between 0.044 and 0.099 mm. Fig. 5.53 is a perturbation graph showing the effect of the significant laser parameters on this response. It is evident that any increase in the cutting speed and argon pressure would result in smaller HAZ, whereas any increase in the laser power would lead to a larger HAZ. These findings are in agreement with the results reported in [67]. The heat input plays an important role in the HAZ extent because as the heat input increases the HAZ becomes wider and vice versa. Therefore, any increase in the laser power results in a wider HAZ, especially at slow cutting speeds. In the case of the argon pressure effect, as mentioned above, the HAZ becomes smaller as the argon pressure increases. This could be related to the cooling effect as the argon pressure increases which slows down the burning of the cut edge sides, and consequently, leads to a smaller HAZ. Fig. 5.54 is a contour plot showing the effect of laser power and cutting speed on the HAZ of GFRP. Also, Fig. 5.55 is a contours plot showing the effect of argon pressure and cutting speed on the HAZ extent of GFRP.

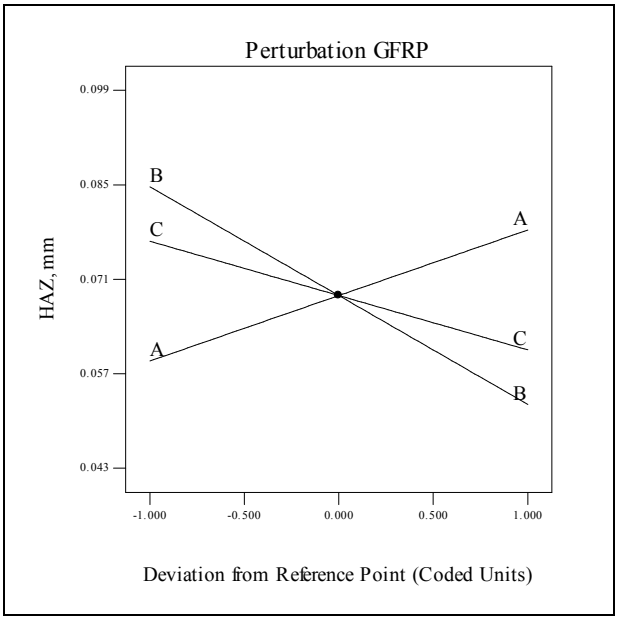

Fig. 5.53: Perturbation plots showing the effect of each factor on the ratio for 3mm thick GFRP.

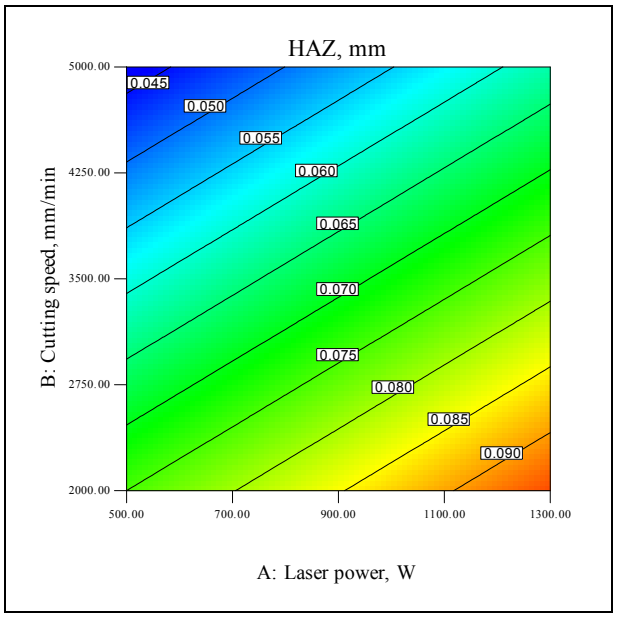

Fig. 5.54: contours plot showing the effect of laser power and cutting speed on the HAZ for 3mm thick GFRP.

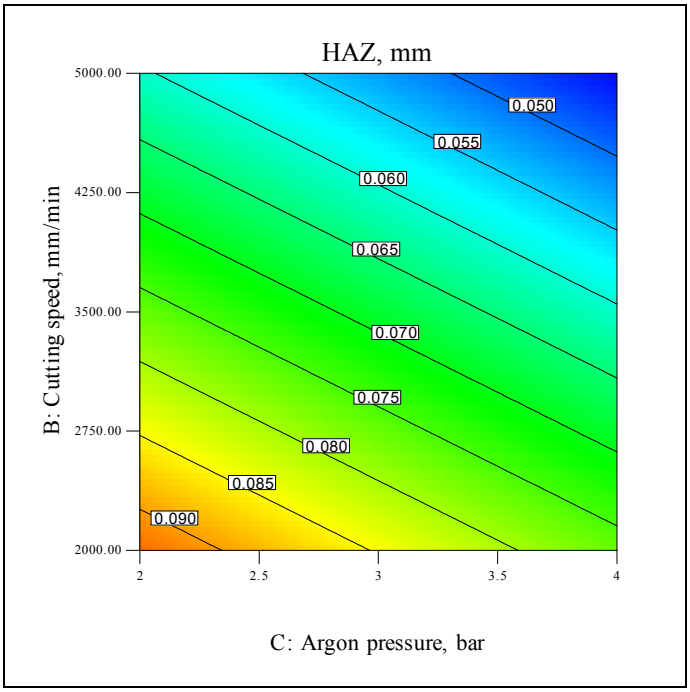

Fig. 5.55: contours plot showing the effect of argon pressure and cutting speed on the HAZ for 3mm thick GFRP.

5.5.3.5 Operating cost

It is evident from the results that the cutting speed, laser power and argon pressure have a strong effect on the operating cost as shown in Fig. 5.55. However, the laser power and argon pressure have a positive effect on the operating cost and the cutting speed has a negative effect. It is obvious from Fig. 5.55 and the 3D plots shown in Fig. 5.56 that the operating cost is more sensitive to the cutting speed than the other factors.

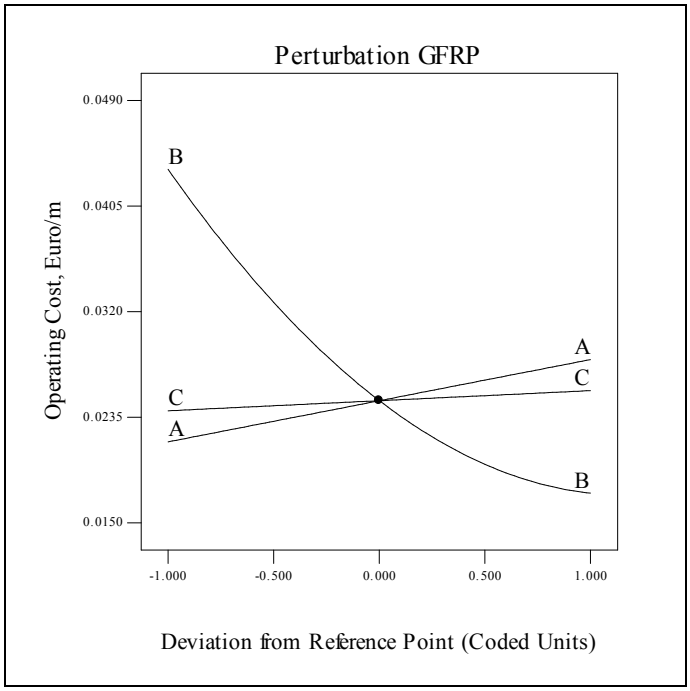

Fig. 5.55: Perturbation plots showing the effect of each factor on the operating cost for 3mm thick GFRP.

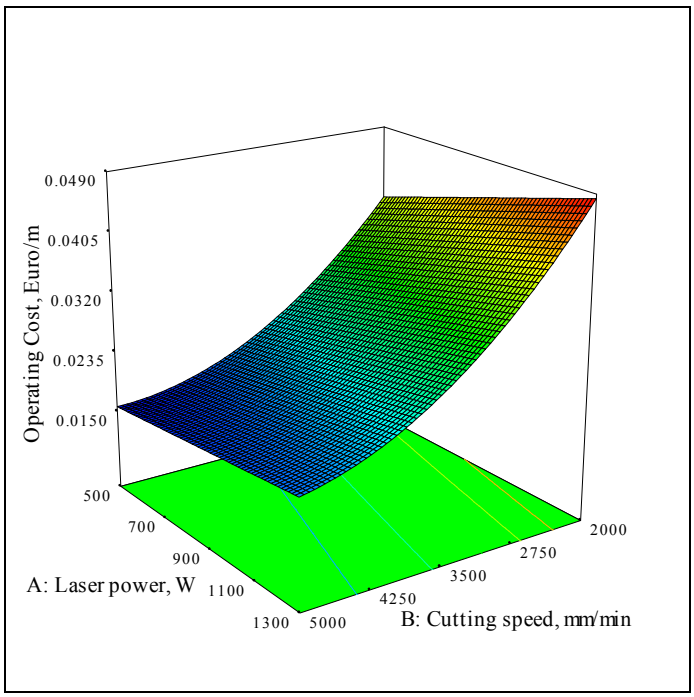

Fig. 5.56: 3D plots showing the effect of cutting speed and laser power on the operating cost for 3mm thick GFRP.

CHAPTER VI
OPTIMISATION

6. OPTIMISATION

Laser cutting is a multi-input and multi-output process that needs to be assessed carefully in order to achieve the most desirable results. Planning the fabrication of parts based on quality of the final cut surface alone may have important cost implications, which should be evaluated. Based on the previously presented results and discussion it is clear that there are many factors and their interactions, which affect the process. Thus, an in-depth optimisation is required. To run any optimisation it is important to know the following: the effect of each factor and its interaction effect with the other factors on the responses, the output of the process (i.e. responses) and finally the desirable criterion (i.e. the goal). In the numerical optimisation for this research two criteria were used. The difference between these two criteria is that in the first criterion there were no restrictions on the process input parameters and the output quality features were set to achieve the highest quality in terms of surface roughness and cut edge perpendicularity (referring to this criterion as Quality). In the second criterion, the cost of the cutting is the main issue, consequently, some restrictions have been put on the process input parameters which have an effect on the operating cost. Also, regarding the second criterion, the operating cost was set to be a minimum with no restrictions on the other responses (referring to this criterion as Cost). This multi-responses optimisation is solved via the desirability approach explained earlier in chapter 3, which is built in the Design expert software. Two types of optimisation layout are available in Design expert. The first one, the numerical optimisation feature, which finds a point or more in the factors domain that would maximise the overall desirability (i.e. objective function). The second one, the graphical optimisation, where the optimal range of each response has to be brought from the numerical optimisation results in order to present them graphically. The graphical optimisation allows visual selection of the optimal cutting conditions according to certain criterion. Graphical optimisation results in plots called overlay plots. These plots are extremely practical for technical use at the workshop and help the operator to choose the optimal values of the laser cutting parameters to achieve the desirable response values for each material. The green/shaded areas on the overlay plots are the regions that meet the proposed criteria.

6.1 Medical Grade Stainless Steel AISI 316L

For this material the two optimisation criteria are presented in Table 6.1. As seen in Table 6.1, each factor and response have been allocated a specific goal and importance. The nozzle diameter was set at 1.5 mm. This value was chosen because it was found to be the best nozzle diameter that would lead to an upper kerf width and a lower kerf width close to each other, and consequently, a square cut edge.

6.1.1 Numerical optimisation

Table 6.2 shows the optimal setting of the process parameters and the corresponding response values for both criteria for 2 mm AISI316L. It is clear that the roughness of cut section produced by using the setting of the first criterion is on average 65.8% smoother than the one produced by using the conditions of the second criterion. On the other hand, the cutting operating cost in the second criterion is on average 71% cheaper than that of the first criterion.

6.1.2 Graphical optimisation

As mentioned earlier the range of each response has been obtained from the numerical optimisation results in Table 6.2 to get the overlay plots. Figures 6.1 and 6.2 show green areas, which are the regions that comply with the first and second criteria respectively.

Table 6.1: Criteria for numerical optimisation of AISI316L.

Factor or response	First criterion (Quality)		Second criterion (Cost)	
	Goal	Importance	Goal	Importance
Laser power	Is in range	3	Minimise	5
Cutting speed	Is in range	3	Maximise	5
Focal position	Is in range	3	Is in range	3
N_2 pressure	Is in range	3	Minimise	3
Nozzle Diameter	Equal to 1.5	3	Minimise	5
Upper Kerf	Is in range	3	Is in range	3
Lower Kerf	Is in range	3	Is in range	3
Ratio	Target to 1	5	Is in range	3
Roughness	Minimise	5	Is in range	3
Operating cost	Is in range	3	Minimise	5

Table 6.2: Optimal cutting conditions as obtained by Design-Expert for 2 mm thick AISI316L.

	No.	A, kW	B, mm/min	C, mm	D, bar	E, mm	Upper kerf, mm	Lower kerf, mm	Ratio	Ra, mm	Cost, €/m	Desirability
1st criterion Quality	1	1.49	1635	-2.02	11.3	1.5	0.26	0.251	1	0.409	1.66	1
	2	1.49	1636	-2.01	11.4	1.5	0.26	0.251	1	0.402	1.67	1
	3	1.49	1650	-2.01	11.4	1.5	0.26	0.251	1	0.401	1.66	1
	4	1.49	1661	-2.02	11.4	1.5	0.258	0.25	1	0.409	1.63	1
	5	1.49	1538	-2	11.4	1.5	0.265	0.254	1	0.409	1.78	1
2nd criterion Cost	1	1.02	2575	-3.32	11.7	1	0.198	0.145	1.243	1.195	0.48	0.8311
	2	1.22	2968	-3.92	11.4	1	0.208	0.146	1.099	1.685	0.41	0.7927
	3	1.03	2106	-3.11	11.1	1	0.21	0.151	1.31	0.919	0.57	0.7754
	4	1.02	2831	-3.08	12.9	1	0.19	0.15	1.246	1.303	0.48	0.7721
	5	1.04	1900	-2.85	10.4	1	0.198	0.154	1.199	0.878	0.60	0.7625

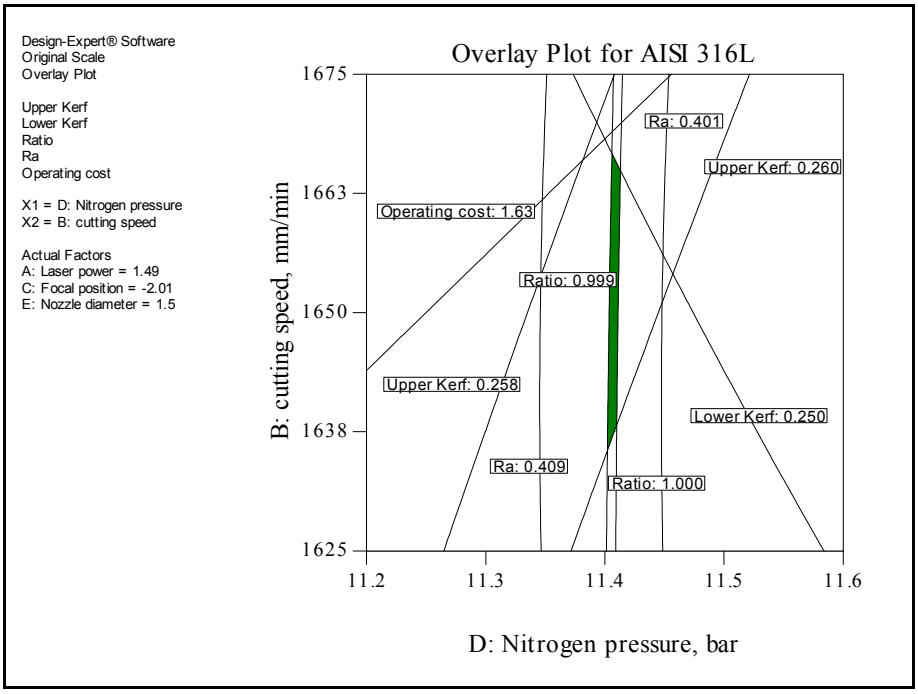

Fig. 6.1: Overlay plot shows the region of optimal cutting condition based on the first criterion for 2 mm AISI316L.

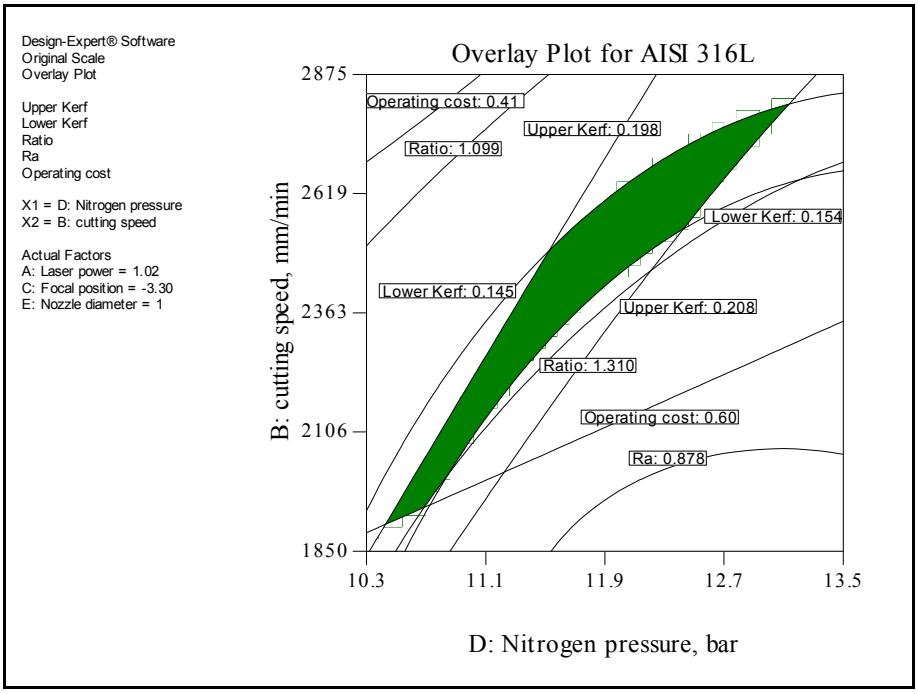

Fig. 6.2: Overlay plot shows the region of optimal cutting condition based on the second criterion for 2 mm AISI316L.

6.2 Ultra-High Molecular Weight Polyethylene UHMWPE

6.2.1 Numerical optimisation

For this polymeric material the two criteria are shown in Table 6.3, where each factor and response have been given a specific goal and importance.

Table 6.3: Criteria for numerical optimisation of UHMWPE.

Factor or response	First criterion (Quality)		Second criterion (Cost)	
	Goal	Importance	Goal	Importance
Laser power	Is in range	3	Minimise	5
Cutting speed	Is in range	3	Maximise	5
Focal position	Is in range	3	Is in range	3
Upper Kerf	Is in range	3	Is in range	3
Lower Kerf	Is in range	3	Is in range	3
Ratio	Maximise	5	Is in range	3
Roughness	Minimise	5	Is in range	3
Operating cost	Is in range	3	Minimise	5

6.2.1.1 Optimisation of 6 mm UHMWPE

Table 6.4 shows the optimal conditions of process factors and the corresponding response values for both criteria for 6 mm UHMWPE. It is notable that the roughness of the cut section achieved by applying the settings of the first criterion is on average 44% smoother than the one obtained using the settings of the second criterion, this improvement in the surface quality agree with the conclusions of Kurt [51]. Although the cutting cost is certainly higher in the first criterion, due to higher laser power and slower cutting speed, the quality of the cut section is better. In contrast, the percentage reduction in the operating cost is 50.7% if the setting of the second criterion was implemented.

6.2.1.2 Optimisation of 8 mm UHMWPE

Table 6.5 presents the optimal setting of process factors and the matching response values for both criteria for 8 mm UHMWPE. It is evident that the roughness of cut

section obtained using the setting of the first criterion is on average 33% smoother than the roughness produced by applying the conditions of the second criterion, which is in agreement with Kurt [51]. On the other hand, the cutting operating cost for the second criterion is on average 49.7% cheaper than that of the first criterion.

6.2.1.3 Optimisation of 10 mm UHMWPE

Table 6.6 lists the optimal setting of process factors and the corresponding response values for both criteria for 10 mm UHMWPE. It is obvious that the roughness of the cut section achieved using the settings of the first criterion is on average 41% smoother than the roughness obtained by applying the settings of the second criterion. However, a percentage reduction in the operating cost of 45.2% could be achieved if the second criterion was implemented.

Table 6.4: Optimal cutting conditions as obtained by Design-Expert for UHMWPE 6 mm.

	No.	A, W	B, mm/min	C, mm	Upper kerf, mm	Lower kerf, mm	Ratio	Ra, μm	Operating cost, €/m	Desirability
1st criterion Quality	1	1262	1000	-3.24	0.644	1.309	0.498	1.743	0.09	0.7753
	2	1267	1000	-3.24	0.645	1.307	0.499	1.746	0.09	0.7753
	3	1258	1000	-3.23	0.643	1.31	0.497	1.738	0.09	0.7753
	4	1269	1000	-3.24	0.645	1.307	0.498	1.745	0.09	0.7753
	5	1257	1000	-3.21	0.64	1.311	0.494	1.728	0.09	0.7751
2nd criterion Cost	1	800	1750	-2.32	0.402	0.885	0.457	2.503	0.04	1
	2	800	1750	-1.39	0.287	0.92	0.342	2.847	0.04	1
	3	800	1750	-2.51	0.424	0.878	0.48	2.493	0.04	1
	4	800	1750	-1.84	0.343	0.903	0.398	2.619	0.04	1
	5	800	1750	-1.50	0.3	0.916	0.355	2.782	0.04	1

Table 6.5: Optimal cutting conditions as obtained by Design-Expert for UHMWPE 8 mm.

	No.	A, W	B, mm/min	C, mm	Upper kerf, mm	Lower kerf, mm	Ratio	Ra, μm	Operating cost, €/m	Desirability
1st criterion Quality	1	1313	800	-5.48	0.738	1.307	0.552	1.853	0.11	0.7024
	2	1311	800	-5.48	0.738	1.307	0.552	1.853	0.11	0.7024
	3	1316	800	-5.49	0.739	1.304	0.554	1.861	0.11	0.7024
	4	1322	800	-5.46	0.737	1.307	0.551	1.847	0.11	0.7024
	5	1293	800	-5.51	0.739	1.306	0.554	1.86	0.11	0.7021
2nd criterion Cost	1	900	1400	-4.5	0.533	0.891	0.6	2.463	0.06	1
	2	900	1400	-3.43	0.399	0.965	0.437	2.811	0.06	1
	3	900	1400	-4.74	0.562	0.868	0.642	2.473	0.06	1
	4	900	1400	-3.64	0.425	0.954	0.465	2.693	0.06	1
	5	900	1400	-4.24	0.5	0.913	0.557	2.489	0.06	1

Table 6.6: Optimal cutting conditions as obtained by Design-Expert for UHMWPE 10 mm.

	No.	A, W	B, mm/min	C, mm	Upper kerf, mm	Lower kerf, mm	Ratio	Ra, mm	Operating cost, €/m	Desirability
1st criterion Quality	1	1450	700	-6.31	0.819	1.523	0.571	2.05	0.13	0.694
	2	1450	700	-6.26	0.815	1.526	0.567	2.025	0.13	0.6937
	3	1450	701	-6.23	0.812	1.528	0.564	2.009	0.13	0.6919
	4	1436	700	-6.29	0.817	1.522	0.569	2.048	0.13	0.6915
	5	1450	705	-6.3	0.818	1.524	0.568	2.051	0.13	0.6891
2nd criterion Cost	1	1100	1150	-5.5	0.685	0.988	0.706	2.882	0.07	1
	2	1100	1150	-5.76	0.712	0.973	0.73	2.922	0.07	1
	3	1100	1150	-5.28	0.664	1.001	0.686	2.892	0.07	1
	4	1100	1150	-4.96	0.631	1.019	0.656	2.976	0.07	1
	5	1100	1150	-5.07	0.642	1.013	0.666	2.938	0.07	1

6.2.2 Graphical optimisation

As mentioned earlier the range of each response has been chosen from the numerical optimisation results in Tables 6.5- 6.6. These ranges were brought into the graphical optimisation tab to draw the overlay plots. Figures 6.3 - 6.8 highlight green areas which are the regions that comply with the first and second criteria for UHMWPE. Fig. 6.3 and Fig. 6.4 are overlay plots for 6 mm UHMWPE. Figure 6.5 and Fig. 6.6 are overlay plots for 8 mm UHMWPE. Fig. 6.7 and Fig. 6.8 are overlay plots for 10 mm UHMWPE.

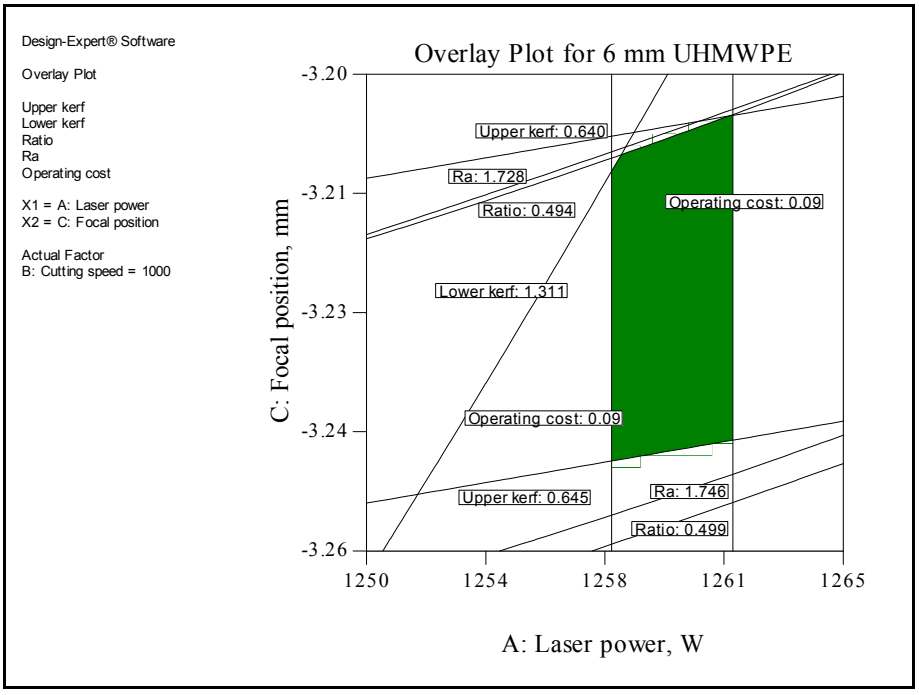

Fig. 6.3: Overlay plot shows the region of optimal cutting condition based on the first criterion for 6 mm UHMWPE.

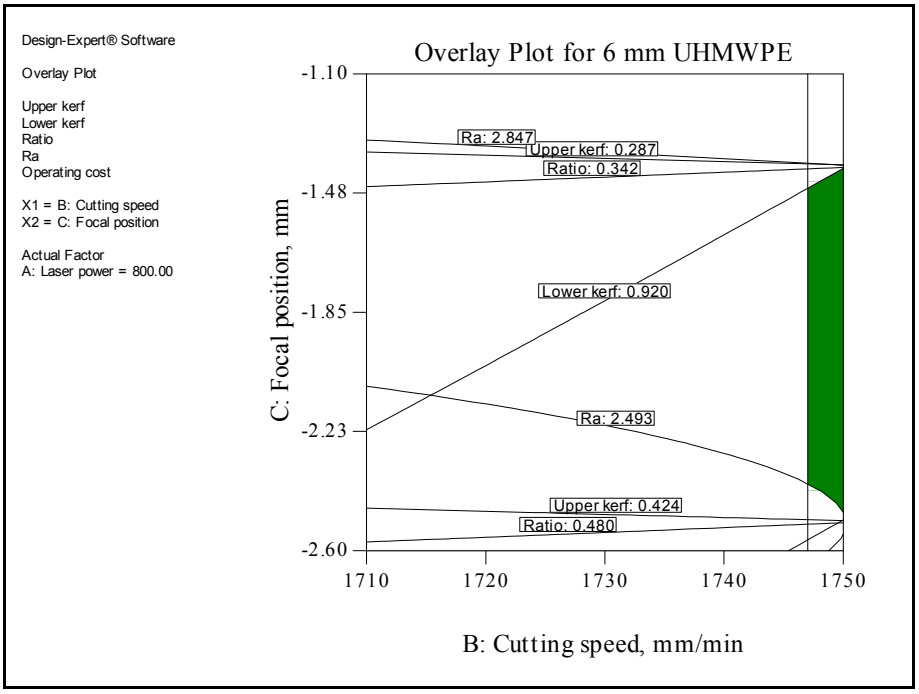

Fig. 6.4: Overlay plot shows the region of optimal cutting condition based on the second criterion for 6 mm UHMWPE.

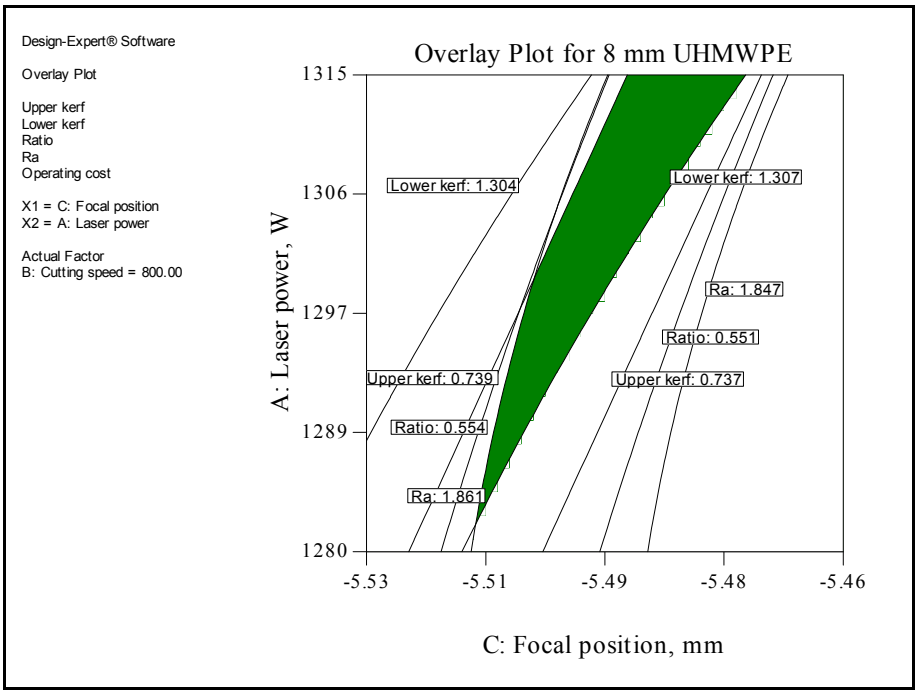

Fig. 6.5: Overlay plot shows the region of optimal cutting condition based on the first criterion for 8 mm UHMWPE.

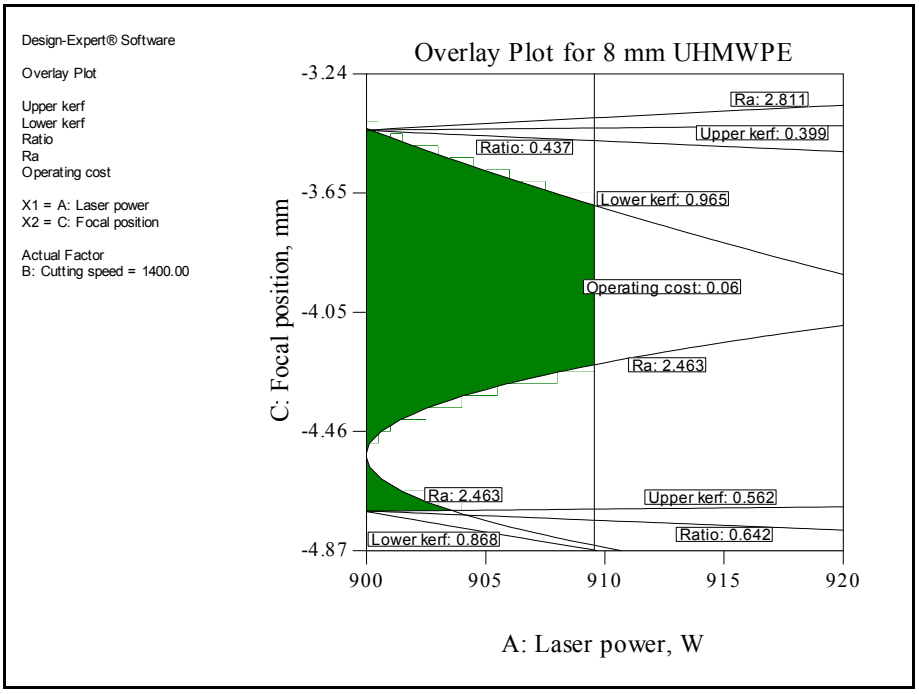

Fig. 6.6: Overlay plot shows the region of optimal cutting condition based on the second criterion for 8 mm UHMWPE.

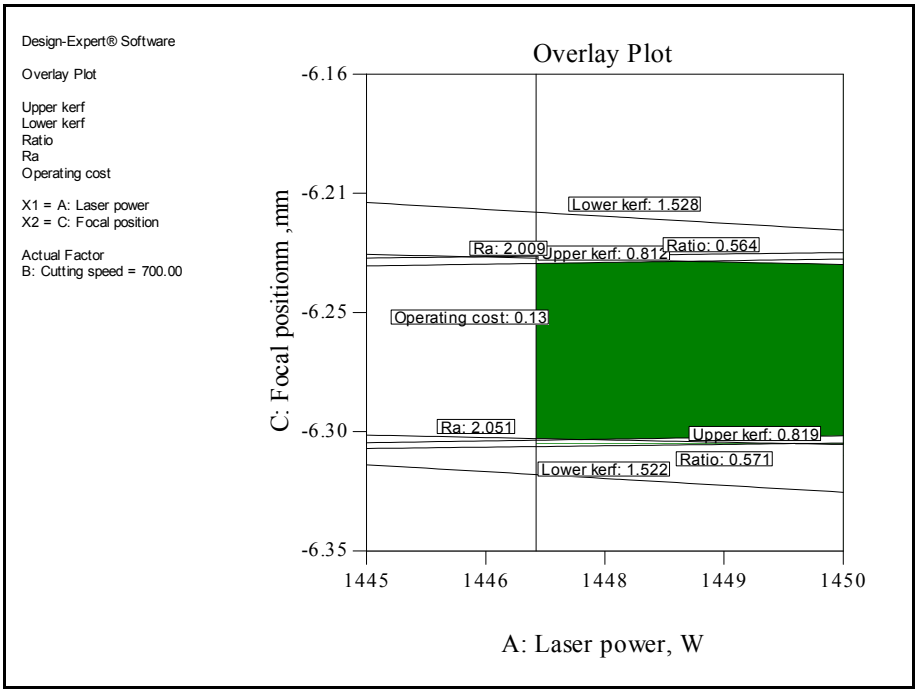

Fig. 6.7: Overlay plot shows the region of optimal cutting condition based on the first criterion for 10 mm UHMWPE.

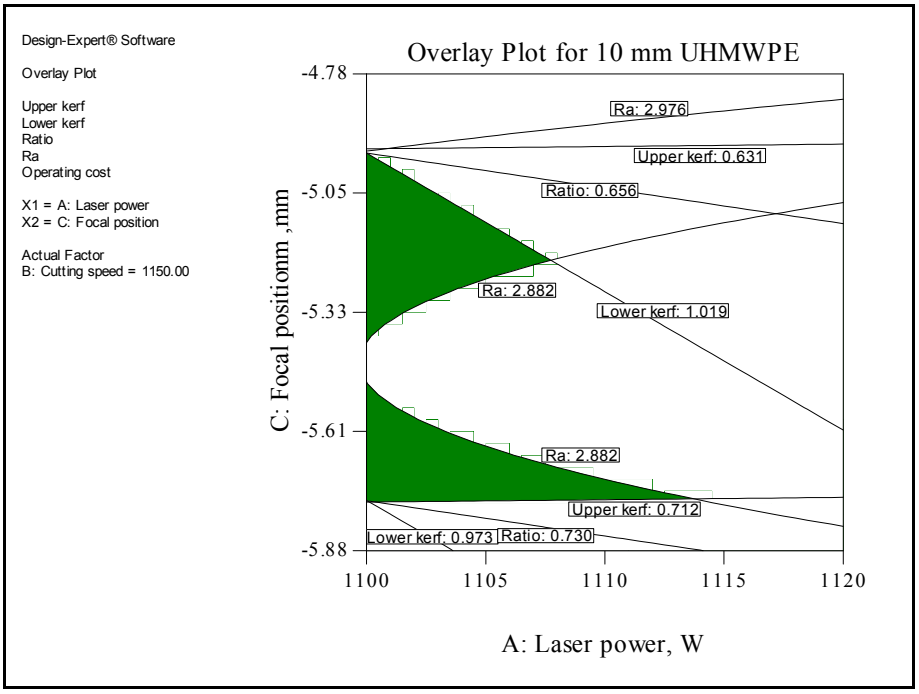

Fig. 6.8: Overlay plot shows the region of optimal cutting condition based on the second criterion for 10 mm UHMWPE.

6.3 Polymethyl Methacrylate PMMA

6.3.1 Numerical optimisation

The two numerical optimisation criteria are presented in Table 6.7. In these criteria each factor and response have been given a specific target. For this material the main aim is to minimise the roughness and achieve a square edge. Therefore, the HAZ was set to be within range as it conflicts with the roughness.

6.3.1.1 Optimisation of 2 mm PMMA

Table 6.8 demonstrates the optimal laser cutting setting of the process factors and the corresponding response values for both criteria for 2 mm PMMA. It was found that the roughness of the cut section produced using the setting of the first criterion is on average 75.6% smoother than the one produced using the setting of the second criterion. The cutting cost is definitely higher in the first criterion due to higher laser power and slower cutting speed, however, the quality of the cut section is better if the optimal factor combinations in the first criterion are used. On the other hand, a percentage

reduction of 72.3% in the operating cost could be achieved if the setting of the second criterion was employed.

Table 6.7: Criteria for numerical optimisation of PMMA.

Factor or response	First criterion (Quality)		Second criterion (Cost)	
	Goal	Importance	Goal	Importance
Laser power	Is in range	3	Minimise	5
Cutting speed	Is in range	3	Maximise	5
Air pressure	Is in range	3	Minimise	5
Focal position	Is in range	3	Is in range	3
Upper Kerf	Is in range	3	Is in range	3
Lower Kerf	Is in range	3	Is in range	3
HAZ	Is in range	3	Is in range	3
Ratio	Minimise	5	Is in range	3
Roughness	Minimise	5	Is in range	3
Operating cost	Is in range	3	Minimise	5

6.3.1.2 Optimisation of 4 mm PMMA

Table 6.9 presents the optimal laser cutting setting of the process parameters and the matching response values for both criteria for 4 mm PMMA. It is evident that the roughness of the cut section produced using the setting of the first criterion is on average 80.4% smoother than the one obtained using the setting of the second criterion. However, the percentage reduction in the operating cost is found to be 78.2% if the setting of the second criterion was implemented.

6.3.1.3 Optimisation of 6 mm PMMA

Table 6.10 shows the optimal laser cutting setting of the process parameters and the corresponding response values for both criteria for 6 mm PMMA. It is demonstrated that the roughness of the cut section produced by using the setting of the first criterion is on average 93.3% smoother than the roughness obtained using the setting of the second criterion. However, the cutting cost decreases by 16.8% if the second criterion is implemented.

Table 6.8: Optimal cutting conditions as obtained by Design-Expert for 2 mm PMMA.

	No.	A, W	B, mm/min	C, bar	D, mm	Upper kerf, mm	Lower kerf, mm	HAZ, mm	Ratio	Ra, μm	Operating cost, €/m	Desirability
1st criterion Quality	1	264	1500	0.8	-1	0.456	0.267	0.064	1.721	0.867	0.04	0.9817
	2	264	1500	0.8	-1	0.456	0.266	0.064	1.723	0.865	0.04	0.9814
	3	268	1533	0.8	-1	0.457	0.267	0.064	1.723	0.866	0.04	0.9814
	4	269	1537	0.8	-1	0.457	0.267	0.064	1.723	0.867	0.04	0.9813
	5	268	1500	0.8	-1	0.458	0.267	0.064	1.724	0.847	0.04	0.9812
2nd criterion Cost	1	100	5000	0.5	-1.57	0.449	0.143	0.035	2.927	3.558	0.01	1
	2	100	5000	0.5	-1.43	0.43	0.145	0.036	2.787	3.381	0.01	1
	3	100	5000	0.5	-2.99	0.66	0.152	0.025	4.14	4.088	0.01	1
	4	100	5000	0.5	-1.44	0.431	0.145	0.036	2.794	3.39	0.01	1
	5	100	5000	0.5	-2.56	0.597	0.143	0.028	3.831	4.193	0.01	1

Table 6.9: Optimal cutting conditions as obtained by Design-Expert for 4 mm PMMA.

	No.	A, W	B, mm/min	C, bar	D, mm	Upper kerf, mm	Lower kerf, mm	Ratio	Ra, μm	Operating cost, €/m	Desirability
1st criterion Quality	1	417	1200	1.0	-2.25	0.696	0.362	1.699	0.924	0.05	0.9674
	2	418	1200	1.0	-2.25	0.696	0.362	1.699	0.924	0.05	0.9674
	3	417	1200	1.0	-2.24	0.696	0.362	1.699	0.924	0.05	0.9674
	4	417	1200	1.0	-2.24	0.696	0.362	1.699	0.924	0.05	0.9674
	5	418	1201	1.0	-2.25	0.696	0.362	1.699	0.924	0.05	0.9673
2nd criterion Cost	1	200	5000	0.5	-2.55	0.654	0.197	3.263	4.742	0.01	1
	2	200	5000	0.5	-2.91	0.698	0.183	3.61	4.192	0.01	1
	3	200	5000	0.5	-3.78	0.804	0.171	4.459	3.978	0.01	1
	4	200	5000	0.5	-3.1	0.722	0.178	3.799	4.012	0.01	1
	5	200	5000	0.5	-2.38	0.633	0.205	3.094	5.124	0.01	1

Table 6.10: Optimal cutting conditions as obtained by Design-Expert for 6 mm PMMA.

	No.	A, W	B, mm/min	C, bar	D, mm	Upper kerf, mm	Lower kerf, mm	HAZ, mm	Ratio	Ra, μm	Operating cost, €/m	Desirability
1st criterion Quality	1	607	2901	0.5	-2.23	0.644	0.436	0.043	1.098	0.219	0.02	1
	2	623	2177	0.5	-2.6	0.728	0.462	0.046	1.224	0.223	0.03	1
	3	543	2232	0.6	-2.39	0.683	0.454	0.044	1.184	0.216	0.03	1
	4	533	2306	0.6	-2.06	0.637	0.46	0.044	1.106	0.218	0.03	1
	5	532	2283	0.5	-2.1	0.644	0.46	0.044	1.094	0.181	0.03	1
2nd criterion Cost	1	350	3600	0.5	-3.54	0.711	0.206	0.03	3.59	3.26	0.02	0.997
	2	350	3600	0.5	-2.83	0.626	0.234	0.031	2.94	2.96	0.02	0.997
	3	350	3600	0.5	-2.65	0.605	0.239	0.032	2.823	2.884	0.02	0.997
	4	350	3600	0.5	-3.17	0.667	0.223	0.031	3.214	3.103	0.02	0.997
	5	350	3600	0.5	-3.24	0.675	0.22	0.031	3.278	3.132	0.02	0.997

Table 6.11: Optimal cutting conditions as obtained by Design-Expert for 8 mm PMMA.

	No.	A, W	B, mm/min	C, bar	D, mm	Upper kerf, mm	Lower kerf, mm	Ratio	Ra, μm	Operating cost, €/m	Desirability
1st criterion Quality	1	800	1153	0.5	-4.19	0.968	0.609	1.618	0.676	0.07	0.9091
	2	800	1156	0.5	-4.18	0.968	0.61	1.617	0.676	0.07	0.9091
	3	800	1166	0.5	-4.19	0.969	0.607	1.622	0.675	0.07	0.9091
	4	800	1158	0.5	-4.19	0.969	0.609	1.619	0.676	0.07	0.9091
	5	800	1169	0.5	-4.18	0.967	0.608	1.619	0.676	0.07	0.9091
2nd criterion Cost	1	450	3200	0.5	-5.14	1.022	0.229	4.517	1.808	0.02	1
	2	450	3200	0.5	-4.84	0.986	0.235	4.212	1.745	0.02	1
	3	450	3200	0.5	-4.94	0.999	0.233	4.313	1.759	0.02	1
	4	450	3200	0.5	-5.19	1.028	0.228	4.569	1.824	0.02	1
	5	450	3200	0.5	-4.85	0.987	0.235	4.221	1.746	0.02	1

6.3.1.4 Optimisation of 8 mm PMMA

Table 6.11 presents the optimal laser cutting setting of the process parameters and the corresponding response values for both criteria for 8 mm PMMA. It is clear that the roughness of the cut section obtained by applying the setting of the first criterion is on average 62.6 % smoother than the roughness achieved by using the setting of the second criterion. However, the cutting cost will be reduced by 70.1 % if the setting of second criterion was employed.

6.3.2 Graphical optimisation

The green areas in Figs. 6.9 - 6.16 are the regions that comply with the first and second criteria for all thickness of PMMA.

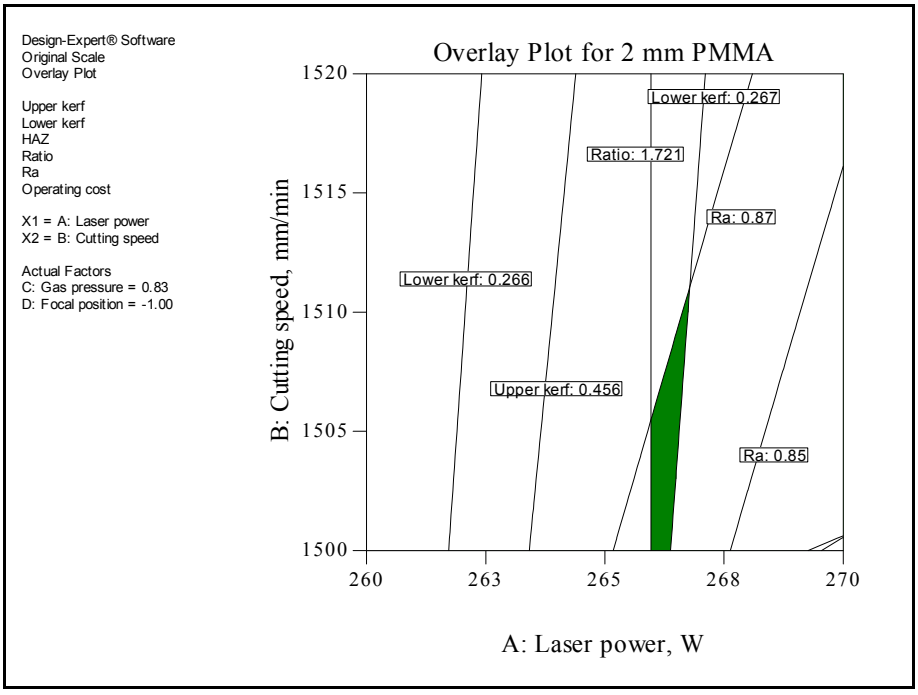

Fig. 6.9: Overlay plot showing the region of optimal cutting condition based on the first criterion for 2 mm PMMA.

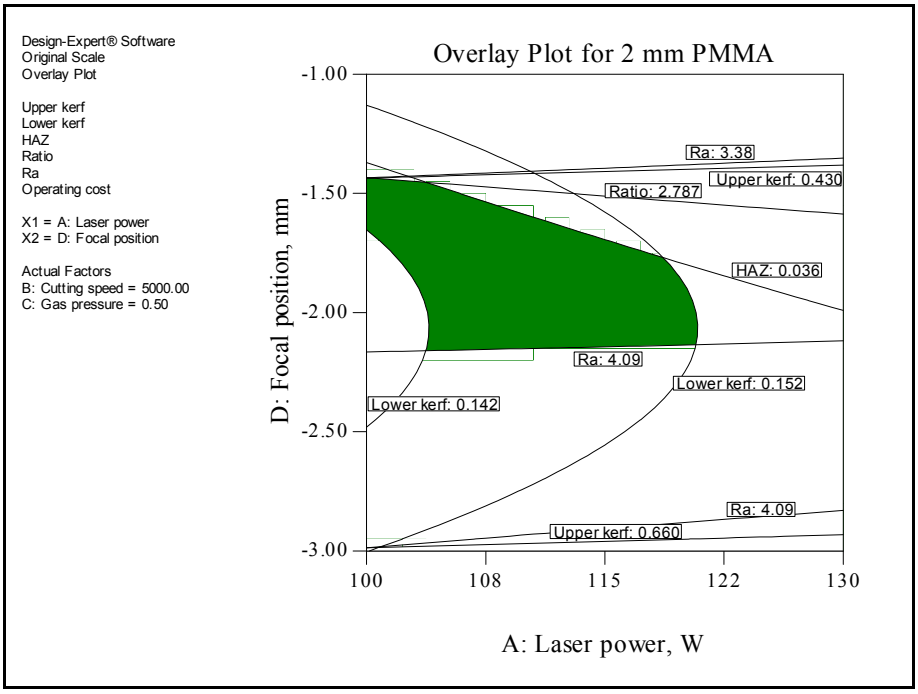

Fig. 6.10: Overlay plot showing the region of optimal cutting condition based on the second criterion for 2 mm PMMA.

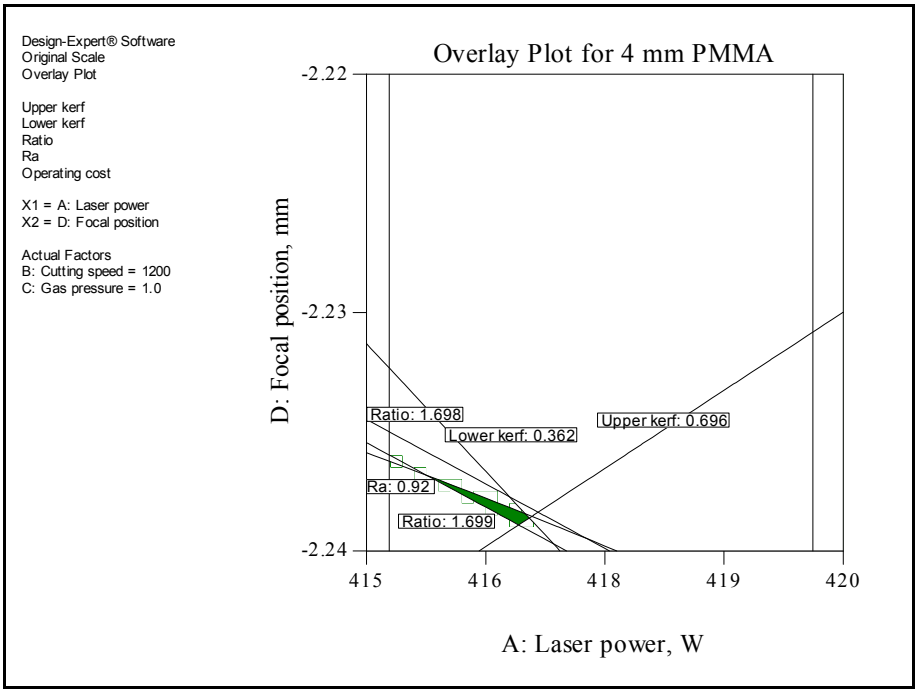

Fig. 6.11: Overlay plot showing the region of optimal cutting condition based on the first criterion for 4 mm PMMA.

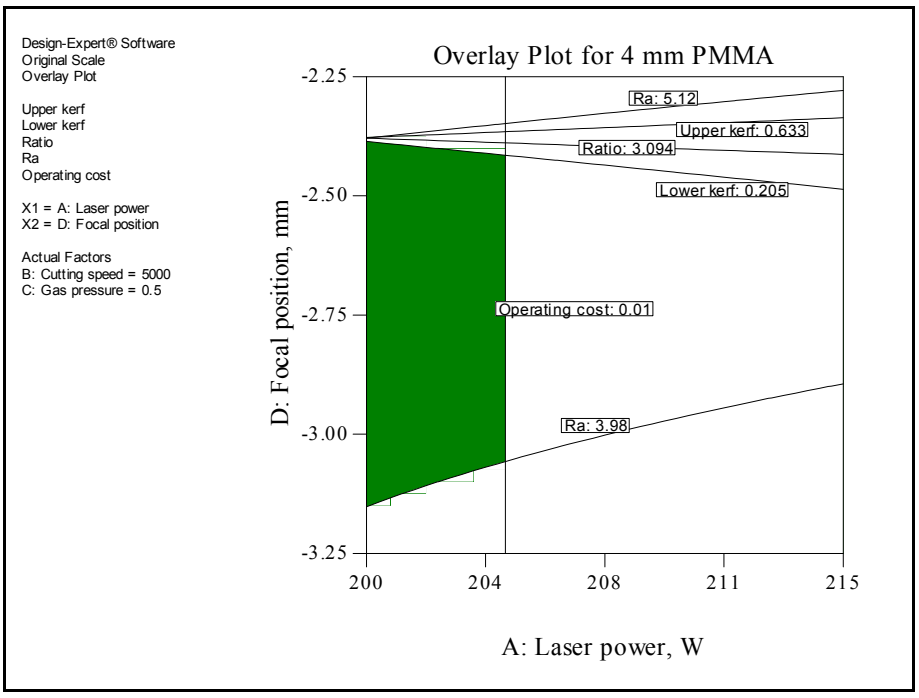

Fig. 6.12: Overlay plot showing the region of optimal cutting condition based on the second criterion for 4 mm PMMA.

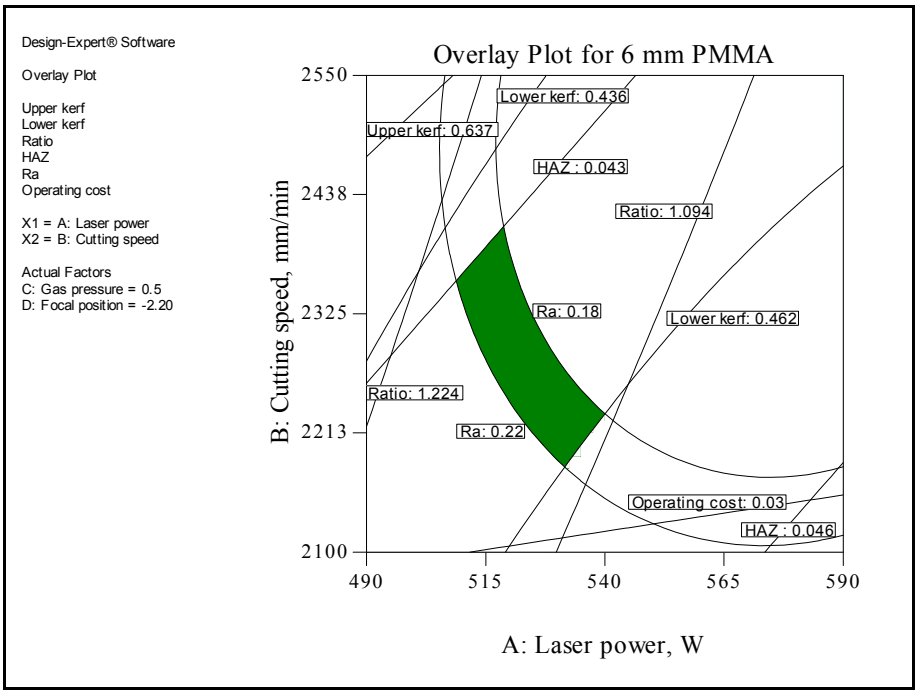

Fig. 6.13: Overlay plot showing the region of optimal cutting condition based on the first criterion for 6 mm PMMA.

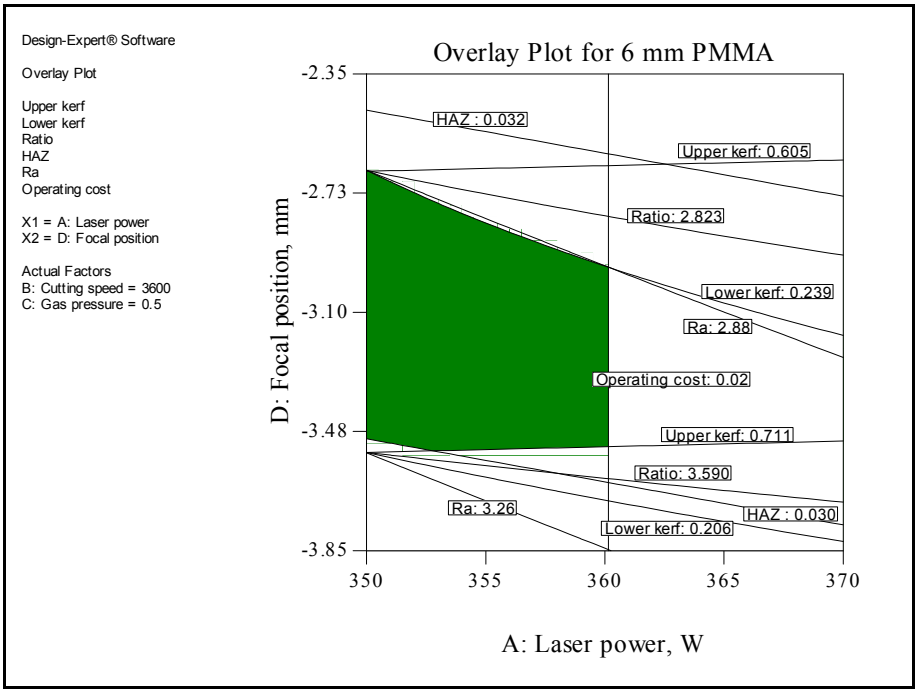

Fig. 6.14: Overlay plot showing the region of optimal cutting condition based on the second criterion for 6 mm PMMA.

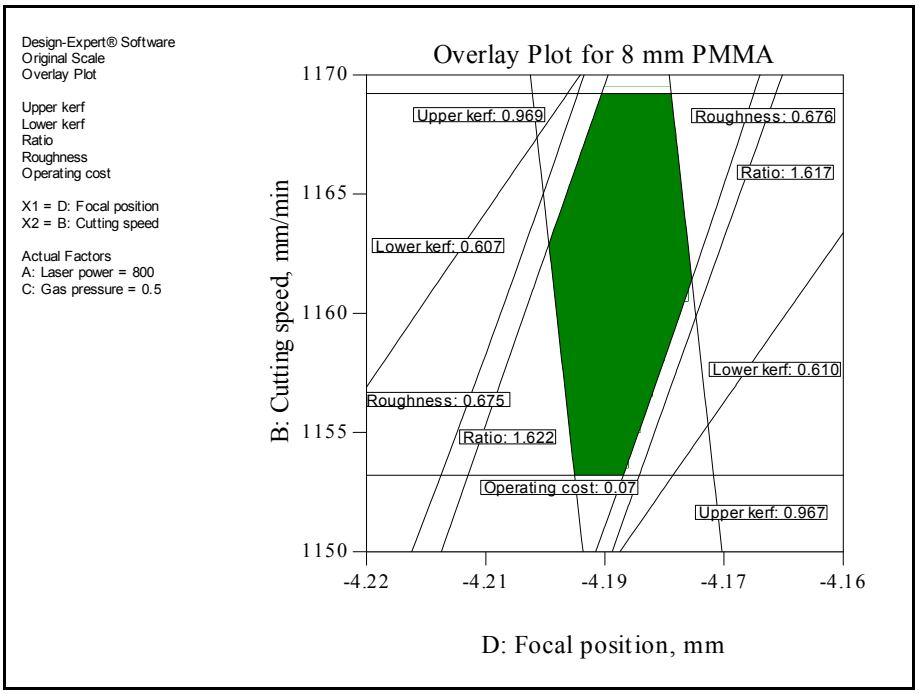

Fig. 6.16: Overlay plot showing the region of optimal cutting condition based on the first criterion for 8 mm PMMA.

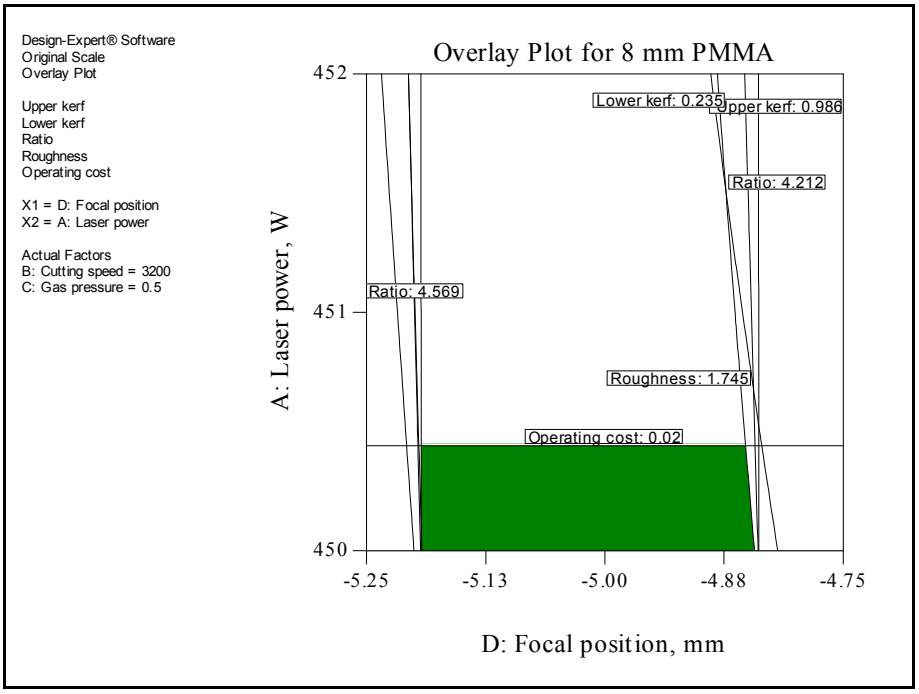

Fig. 6.16: Overlay plot showing the region of optimal cutting condition based on the second criterion for 8 mm PMMA.

6.4 Medium Density Fibre Board (MDF)

6.4.1 Numerical optimisation

The two numerical optimisation criteria are presented in Table 6.12. In these criteria each factor and response have been given a specific target and importance.

Table 6.12: Criteria for numerical optimisation.

Factor or response	First criterion (Quality)		Second criterion (Cost)	
	Goal	Importance	Goal	Importance
Laser power	Is in range	3	Minimise	5
Cutting speed	Is in range	3	Maximise	5
Air pressure	Is in range	3	Minimise	3
Focal position	Is in range	3	Is in range	3
Upper Kerf	Is in range	3	Is in range	3
Lower Kerf	Is in range	3	Is in range	3
Ratio	Target to 1	5	Is in range	3
Roughness	Minimise	5	Is in range	3
Operating cost	Is in range	3	Minimise	5

6.3.1.1 Optimisation of 4 mm MDF

Table 6.13 lists the optimal combinations of process factors and the corresponding response values for both criteria for 4 mm MDF. These optimal results are in good agreement with the results obtained by Barnekov et al. [73 and 74]. It is evident that the predicted ratio obtained using the optimal setting of the first criterion is on average 67.13 % less than the predicted ratio obtained using the optimal setting of the second criterion and theoretically equals 1, which means the cut edge is square. Also, the roughness of the cut section obtained using the setting of the first criterion is on average 41.38 % smoother than the roughness achieved using the optimal setting of the second criterion. However, the cutting operating cost for the first criterion is 131.72 % higher than the operating cost for the second criterion.

6.3.1.2 Optimisation of 6 mm MDF

The optimal setting of process factors for both criteria for 6 mm MDF are presented in Table 6.14. These optimal results are in fair agreement with the results obtained by Barnekov et al. [73 and 74] because the focal position is nearly on the surface. Concerning the quality of the cut section, the predicted ratio is on average 71.29% less than the ratio obtained in second criterion and in theory equals 1, which means the cut edge is square. Also, the roughness of the cut section obtained by applying the optimal settings of the first criterion is on average 41.57 % smoother than the roughness achieved in the second criterion. However, the cutting operating cost for the first criterion is 155.77 % higher than the operating cost of the second criterion.

Table 6.13: Optimal laser cutting setting as obtained by Design-Expert for 4 mm MDF.

	No.	A, W	B, mm/min	C, bar	D, mm	Upper kerf, mm	Lower kerf, mm	Ratio	Ra, µm	Cost, €/m	Desirability
1st criterion Quality	1	371	2440	3.1	-0.6	0.375	0.363	1	3.808	0.03	1
	2	363	2433	3.0	-0.5	0.374	0.362	1	3.805	0.03	1
	3	384	2452	3.0	-0.82	0.378	0.363	1	3.807	0.03	1
	4	382	2451	3.0	-0.79	0.377	0.363	1	3.809	0.03	1
	5	345	2366	3.1	-0.25	0.375	0.363	1	3.809	0.03	1
2nd criterion Cost	1	150	5000	3	-2.2	0.341	0.133	2.477	6.276	0.01	0.999
	2	150	5000	3	-1.82	0.308	0.126	2.283	6.158	0.01	0.999
	3	150	5000	3	-3.6	0.524	0.16	3.531	6.703	0.01	0.999
	4	150	5000	3	-3	0.433	0.148	3.014	6.52	0.01	0.999
	5	150	5000	3	-3.98	0.592	0.167	3.908	6.818	0.01	0.999

Table 6.14: Optimal laser cutting setting as obtained by Design-Expert for 6 mm MDF.

	No.	A, W	B, mm/min	C, bar	D, mm	Upper kerf, mm	Lower kerf, mm	Ratio	Ra, µm	Cost, €/m	Desirability
1st criterion Quality	1	481	2127	5.0	-1.24	0.453	0.382	1	4.994	0.03	1
	2	484	2181	4.3	-2.39	0.543	0.391	1	5.059	0.03	1
	3	491	2141	5.4	-1.79	0.477	0.389	1	5.169	0.03	1
	4	469	2003	4.0	-0.35	0.437	0.381	1	4.57	0.03	1
	5	417	2241	4.0	-0.01	0.408	0.338	1	5.03	0.03	1
2nd criterion Cost	1	270	5000	4	-2.83	0.343	0.151	2.91	8.365	0.01	0.9992
	2	270	5000	4	-4	0.466	0.14	3.984	8.614	0.01	0.9992
	3	270	5000	4	-2.91	0.35	0.15	2.973	8.382	0.01	0.9992
	4	270	5000	4	-3.14	0.373	0.149	3.17	8.432	0.01	0.9992
	5	270	5000	4	-4.38	0.512	0.135	4.381	8.692	0.01	0.9992

6.3.1.3 Optimisation of 9 mm MDF

Table 6.15 shows the optimal combinations of process factors and the corresponding response values for both criteria for 9 mm MDF. These optimal results are in fair agreement with the results obtained by Barnekov et al. [73 and 74] due to the fact that the focal position is nearly on the surface. The predicted ratio obtained for the first criterion is on average 65.39 % less than the ratio obtained for second criterion. Also, the roughness of the cut section for the first criterion is on average 32.25% smoother than the roughness achieved for the second criterion and in theory equals 1. However, the cutting operating cost for the first criterion is 158.14 % higher than the operating cost for the second criterion.

6.3.2 Graphical optimisation

The green areas in Figs. 6.17 - 6.22 are the regions that fulfil with the first and second criteria for all thickness of MDF.

Table 6.15: Optimal cutting setting as obtained by Design-Expert for 9 mm MDF.

	No.	A, W	B, mm/min	C, bar	D, mm	Upper kerf, mm	Lower kerf, mm	Ratio	Ra, µm	Cost, €/m	Desirability
1st criterion Quality	1	548	2027	4.6	-0.29	0.384	0.405	1	5.855	0.03	1
	2	577	2219	4.9	-0.05	0.368	0.382	1	5.861	0.03	1
	3	538	2075	5.7	-0.12	0.365	0.381	1	6.123	0.03	1
	4	516	2029	4.7	-0.1	0.357	0.386	1	5.888	0.03	1
	5	572	2032	4.1	-0.45	0.406	0.428	1	5.72	0.03	1
2nd criterion Cost	1	375	5000	4	-5.43	0.732	0.147	4.356	9.783	0.01	0.9995
	2	375	5000	4	-1.08	0.346	0.204	1.964	7.899	0.01	0.9995
	3	375	5000	4	-4.32	0.633	0.167	3.586	9.298	0.01	0.9995
	4	375	5000	4	-1.74	0.404	0.199	2.213	8.184	0.01	0.9995
	5	375	5000	4	-2.01	0.428	0.197	2.327	8.3	0.01	0.9995

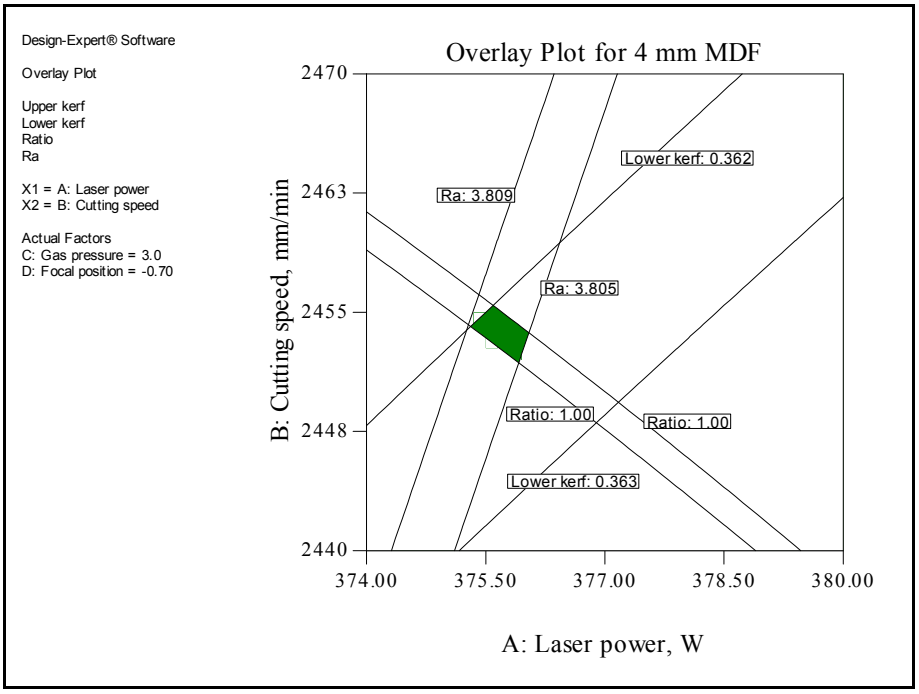

Fig. 6.17: Overlay plot showing the region of optimal cutting condition based on the first criterion for 4 mm MDF.

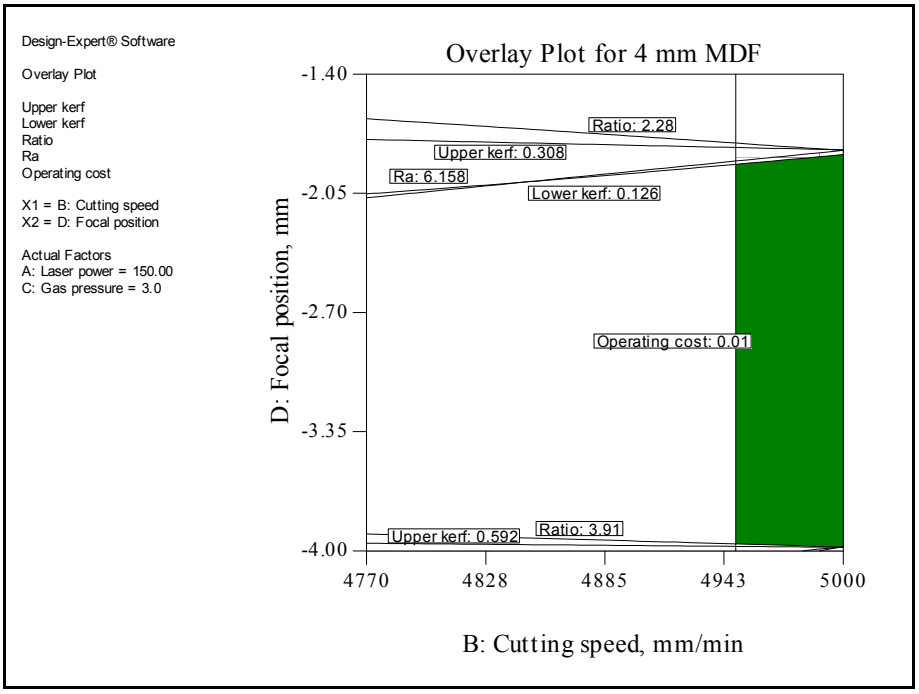

Fig. 6.18: Overlay plot showing the region of optimal cutting condition based on the second criterion for 4 mm MDF.

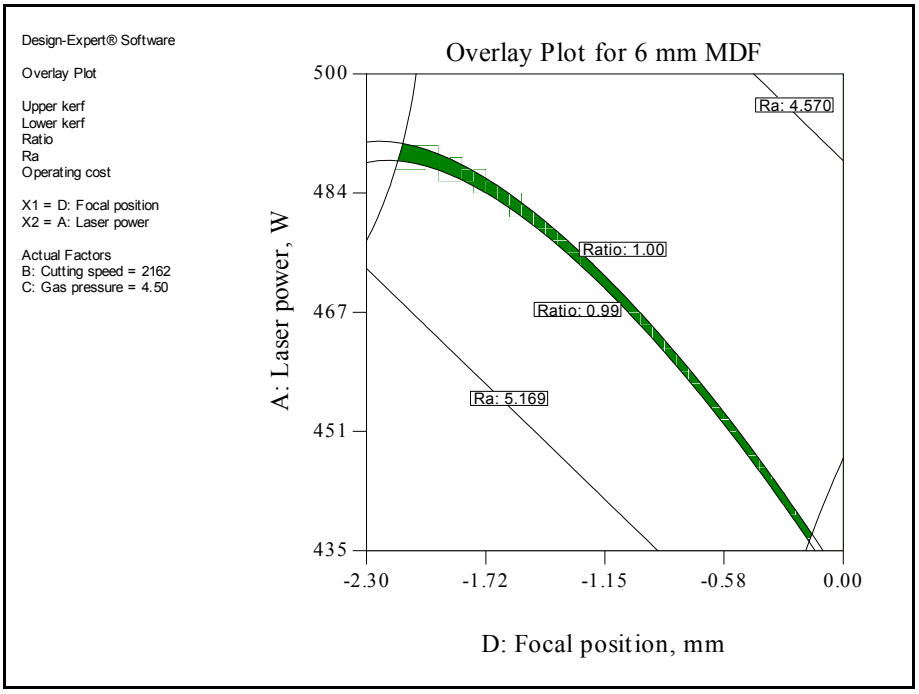

Fig. 6.19: Overlay plot showing the region of optimal cutting condition based on the first criterion for 6 mm MDF.

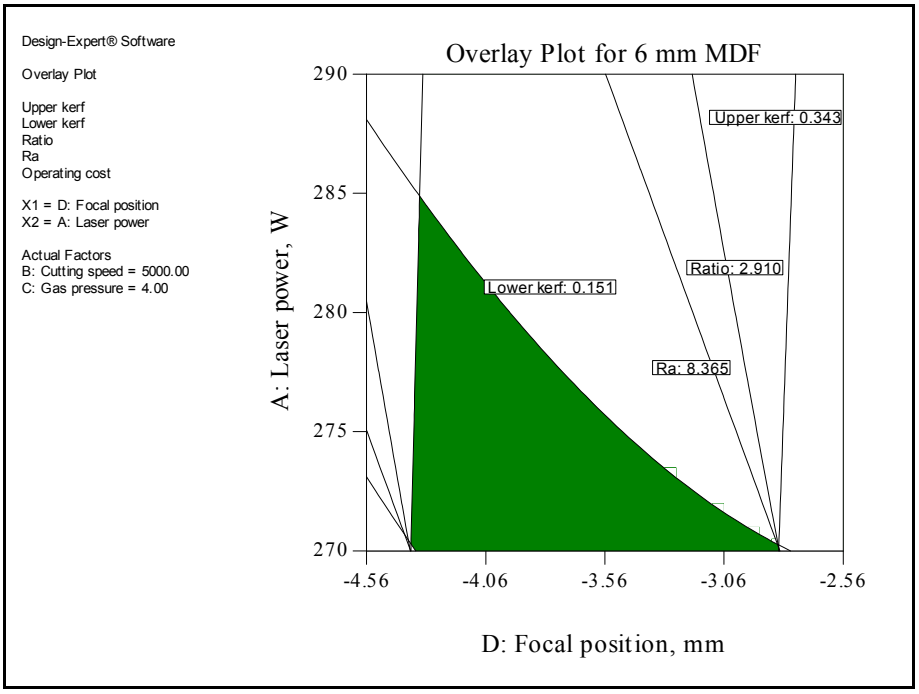

Fig. 6.20: Overlay plot showing the region of optimal cutting condition based on the second criterion for 6 mm MDF.

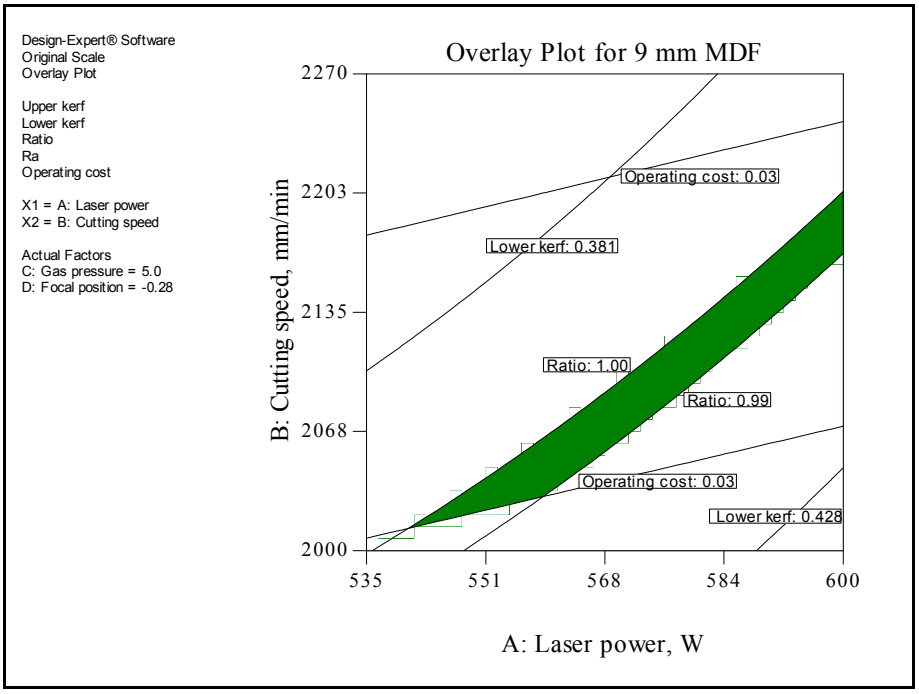

Fig. 6.21: Overlay plot showing the region of optimal cutting condition based on the first criterion for 9 mm MDF.

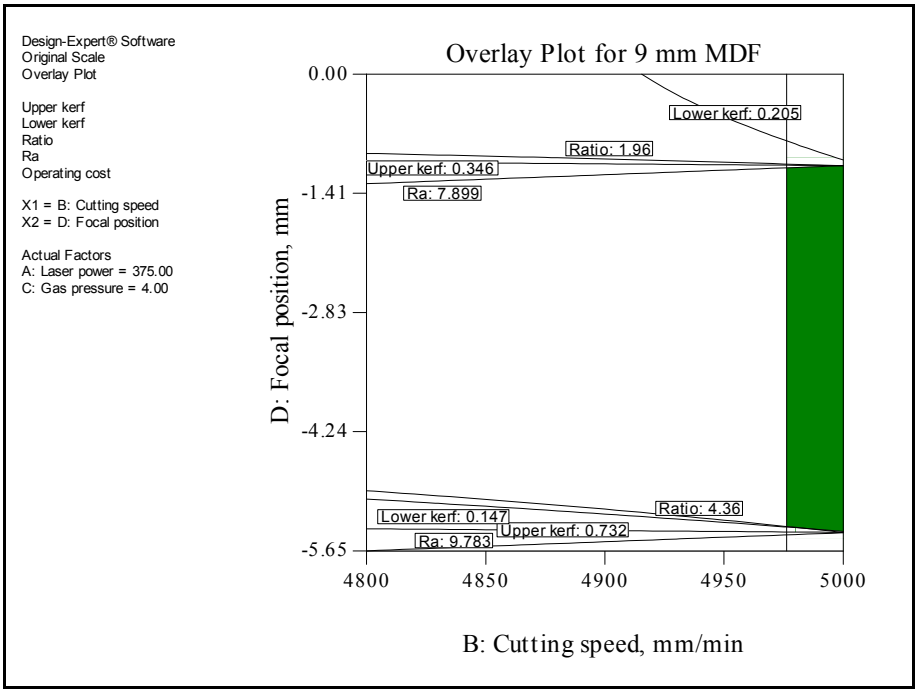

Fig. 6.22: Overlay plot showing the region of optimal cutting condition based on the second criterion for 9 mm MDF.

6.5 Glass-Fibre Reinforced Plastic GFRP

For this material the two optimisation criteria are presented in Table 6.16. Each factor and response have been given a specific goal and importance. For this composite material, the measurement of the surface roughness was not possible due to the inconsistency in the surface roughness values for some specimens and surface roughness values already out of the tester range for some other specimens.

6.5.1 Numerical optimisation

Table 6.17 shows the optimal laser cutting setting of the process parameters and the matching response values for both criteria for 3 mm GFRP. It is evident that the HAZ extent produced using the optimal setting of the first criterion is on average 13.7% smaller than the one produced by using the optimal setting of the second criterion setting. On the other hand, the cutting operating cost for the second criterion is on average cheaper than that of the first criterion by 10.5%.

6.5.2 Graphical optimisation

Figs. 6.23 and 6.24 show green areas which are the regions that meet the first and second criteria respectively.

Table 6.16: Criteria for numerical optimisation of GFRP.

Factor or response	First criterion (Quality)		Second criterion (Cost)	
	Goal	Importance	Goal	Importance
Laser power	Is in range	3	Minimise	5
Cutting speed	Is in range	3	Maximise	5
Air pressure	Is in range	3	Minimise	5
Focal position	Is in range	3	Is in range	3
Upper Kerf	Is in range	3	Is in range	3
Lower Kerf	Is in range	3	Is in range	3
HAZ	Minimise	5	Is in range	3
Ratio	Target to 1	5	Is in range	3
Operating cost	Is in range	3	Minimise	5

Table 6.17: Optimal cutting conditions as obtained by Design-Expert for 3 mm GFRP.

	No.	A, W	B, mm/min	C, bar	D, mm	Upper kerf, mm	Lower kerf, mm	HAZ, mm	Ratio	Operating cost, €/m	Desirability
1st criterion Quality	1	717	4845	3.8	-1.05	0.305	0.343	0.044	1	0.017	1
	2	727	4944	3.7	-1.21	0.312	0.346	0.043	1	0.017	1
	3	739	4972	3.7	-1.33	0.319	0.349	0.044	1	0.017	1
	4	733	4913	3.8	-1.27	0.316	0.346	0.043	1	0.017	1
	5	746	4797	4.0	-1.36	0.325	0.346	0.043	1	0.018	1
2nd criterion Cost	1	500	5000	2	-0.13	0.316	0.278	0.051	1.508	0.015	0.9995
	2	500	5000	2	-1.52	0.356	0.276	0.051	1.428	0.015	0.9995
	3	500	5000	2	-0.29	0.311	0.28	0.051	1.459	0.015	0.9995
	4	500	5000	2	-1.98	0.41	0.266	0.051	1.579	0.015	0.9995
	5	500	5000	2	-0.98	0.319	0.282	0.051	1.365	0.015	0.9995

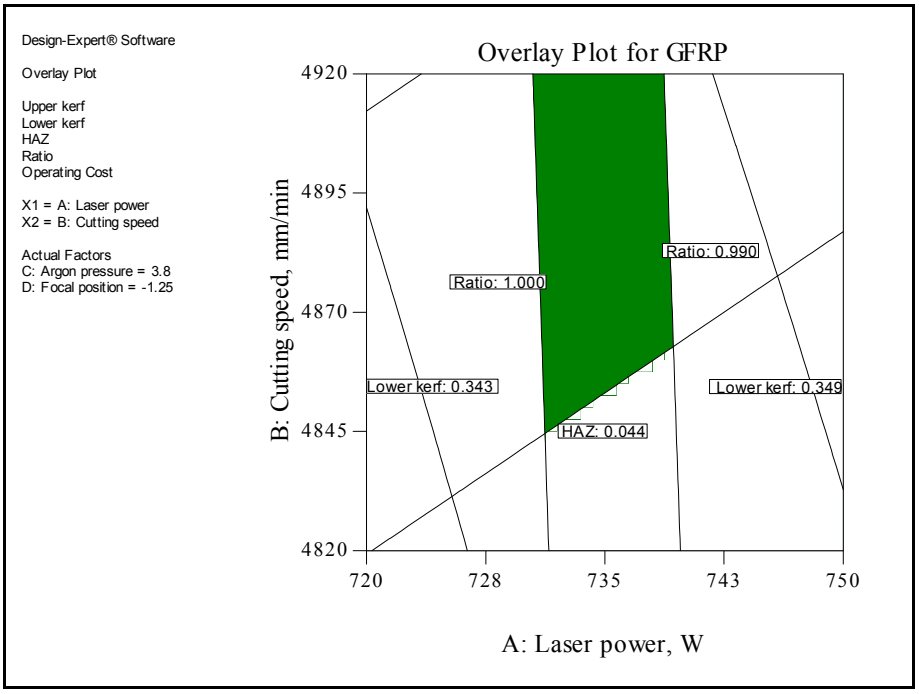

Fig. 6.23: Overlay plot showing the region of optimal cutting condition based on the first criterion for 3 mm GFRP.

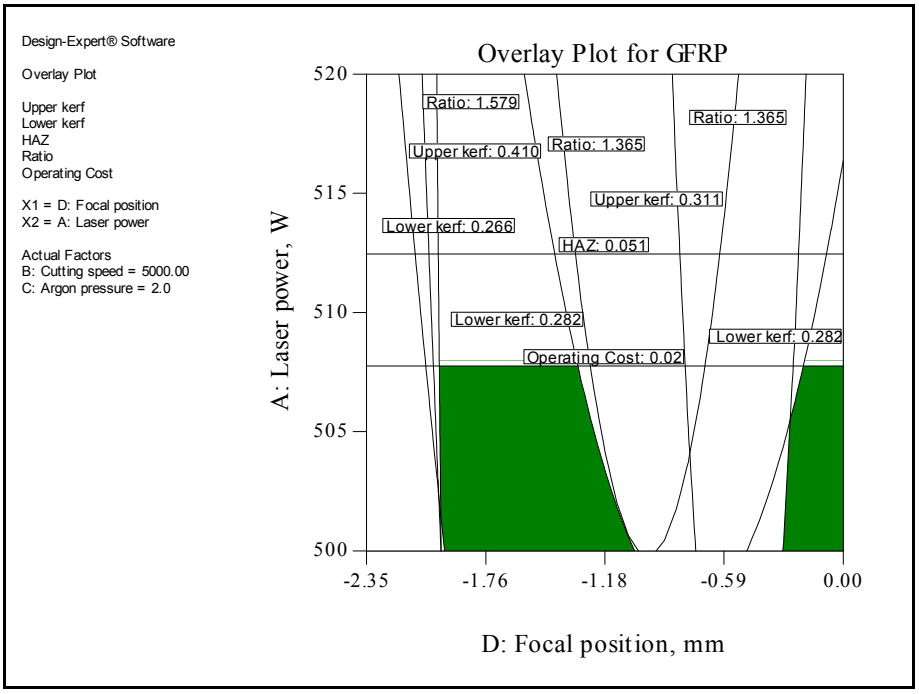

Fig. 6.24: Overlay plot showing the region of optimal cutting condition based on the second criterion for 3 mm GFRP.

CHAPTER VII
CONCLUSIONS AND RECOMMENDATIONS FOR FUTURE WORK

7. CONCLUSIONS AND RECOMMENDATIONS FOR FUTURE WORK

7.1 Conclusions

In this study the effect of the laser cutting process parameters were quantified using mathematical models. The models were developed using Design Expert software with the aim of assessing the main and interaction effects of the parameters on the quality of the cut section characteristics obtained under the experimental conditions, which were based on the experimental design. This contributed to an optimisation of the LBC process to produce cuts which fully satisfy the end user requirements. The developed mathematical models and the optimal solutions are applicable within the cutting parameters ranges considered. The conclusions drawn from the study are summarised below:

The literature review showed the current high interest in the application of RSM to the optimisation of different laser material processing techniques. In this work, seventy one mathematical models were successfully developed for five common engineering materials with different thicknesses. Also, the operating cost was estimated for all materials and successfully included in the optimisation. The cutting speed is the most significant factor affecting the operating cost followed by laser power and assist gas pressure. Furthermore, the influence of all parameters was established at their different levels for all materials and thicknesses. The upper kerf width is inversely proportional to the cutting speed and the focal point position and directly proportional to the other factors. In general, the lower kerf is similarly characterised, however, in this case, the lower kerf width is directly proportional to the focal position. The roughness value increases as the cutting speed increases and it decreases as the other parameters increases. The nozzle diameter, however, has no significant effect on the roughness. The HAZ decreases as the cutting speed and gas pressure increase, and it increases as the laser power and focal position increase.

Laser cutting of UHMWPE required high power, which ranged from 800 W to 1450 W, depending on the workpiece thickness. In addition, the higher cutting speed does not always improve the efficiency of the laser cutting process. For PMMA, as the thickness increases the effect of the factors becomes more obvious. The cut section of PMMA is of very high quality compared with the other materials.

The LBC process was optimised using Box-Behnken design and the desirability approach. The graphical optimisation using the overlay plots for all materials were preformed effectively. It was found that high quality or economical cut sections could be processed using the tabulated optimal settings. Finally, the developed models were built in VB program to enable the prediction of each response.

7.2 Recommendations for Future Work

The results in this thesis have contributed significantly to knowledge regarding LBC. The models developed and the understanding gained will prove valuable for future research carried out in this area. During the course of this work, further research and development steps that would contribute to improve of laser material processing have been identified. These recommendations are as follows:

1. Apply DOE to predict and optimise the laser cutting of other materials.
2. Investigate the effect of other parameters, for example, focusing lenses with different focal lengths and different nozzle designs.
3. Explore the effect of LBC parameters on other responses, such as mass removal, dross, striation frequency and formation of micro-cracks.
4. Compare the findings with the results of finite element analysis and computational fluid dynamics base techniques.

7.3 Main Contributions from this Work

- ✓ The investigation of three to five different laser cutting parameters simultaneously along with a material parameter (i.e. sheet thickness) using RSM.
- ✓ The estimation of the processing cost and the inclusion of it in the optimisation as a response, which has not been done previously in the laser cutting area.
- ✓ The provision of models which can easily predict various responses.
- ✓ The investigation of the ratio between the upper and lower kerfs.
- ✓ The identification of the effect of each parameter and their interactions on each response.
- ✓ The identification of sets of operating parameters which lead to either optimal quality or optimal process operating cost.
- ✓ Publication of several papers in peer-reviewed journals and international conferences.

LIST OF PUBLICATIONS

- **Peer-Reviewed Journal papers**

1. H. A. Eltawahni, A. G. Olabi and K. Y. Benyounis, Effect of process parameters and optimisation of CO_2 laser cutting of ultra high-performance polyethylene, Materials & Design, Volume 31, Issue 8, September 2010, Pages 4029-4038.

2. H. A. Eltawahni, A. G. Olabi and K. Y. Benyounis, Investigating the CO_2 laser cutting parameters of MDF wood composite material, Optics and laser Technology, Volume , 43, Issue 3, April 2011, pp. 684-659.

- **Conferences Papers**

3. A. G. Olabi and H. A. Eltawahni, Effect of co_2 laser cutting process parameters on the kerf width of AISI316, AMPT2008, Manama, Kingdom of Bahrain from November 2 - 5, 2008.

4. H. A. Eltawahni and A. G. Olabi, High power laser cutting of different materials- a literature review, IMC2008, DIT Dublin Ireland from September 3-5, 2008.

5. H. A. Eltawahni, A. G. Olabi and K. Y. Benyounis, Assessment and optimisation of CO_2 laser cutting process of PMMA, Proceedings of AMPT conference, 24-27 Oct, 2010 Paris-France.

- **Peer-Reviewed Journal Papers under Preparation**

6. H. A. Eltawahni, K. Y. Benyounis and A. G. Olabi, Overall optimisation of CO_2 laser cutting of AISI316L.
7. H. A. Eltawahni, K. Y. Benyounis and A. G. Olabi, Effect of high power CO_2 laser parameters on the roughness of PMMA.
8. H. A. Eltawahni, K. Y. Benyounis and A. G. Olabi, Assessment and optimisation of laser cutting of glass-fibre reinforced plastic.

REFERENCES

[1] http://inventors.about.com/od/lstartinventions/a/laser.htm accessed on May 2010.
[2] http://en.wikipedia.org/wiki/Laser accessed on Feb. 2010.

[3] G. Herziger, H. Weber, R. Poprawe, Laser Physics and Applications, Springer-Verlag Berlin Heidelberg, (2007).

[4] J. Powell, CO_2 Laser Cutting, 2nd Edition, Springer-Verlag Berlin Heidelberg, New York, (1998).

[5] J. F. Ready and D. F. Farson, LIA Handbook of Laser Materials Processing, Laser Institute of America Magnolia Publishing, Inc., 2001.

[6] G. Chryssolouris, Laser machining: Theory and practice, Speinger-Verlag, New York Inc. 1991.

[7] C. Dawes, Laser Welding, Abington Publishing, New York, NY, 1992.

[8] J. C. Ion, Laser processing of engineering materials, Elsevier Butterworth Heinemann, Linacre House, Jordan Hill, Oxford OX2 8DP, 2005.

[9] W. M. Steen, Laser material processing, 3rd Ed., Springer-Verlag London Limited, 2003.

[10] E. Kannatey-Asibn, Principles of laser materials processing, John Wiley & Sons, Inc., Hoboken, New Jersey, 2009.

[11] D. Havrilla and P. Anthony, Laser cutting Process Fundamentals and Troubleshooting, 2nd Printing, Rofin, 2003.

[12] http://www.mrl.columbia.edu/ntm/level2/ch02/images/dof.gif

[13] I. Uslan, CO_2 laser cutting: kerf width variation during cutting, Proc. Of IMechE, Vol. 219 part B, J. of Engineering Manufacture, 2005, pp. 572-577.

[14] J. N. Gonsalves and W. W. Duley, Cutting thin metal sheets with the cw CO_2 laser, J. of applied physics, Vol. 43, No. 11, 1972, pp. 4684-4687.

[15] B. S. Yilbas, Effect of process parameters on the kerf width during the laser cutting process, Proc Instn Mech Engrs, Vol. 215 part B, J. of Engineering Manufacture, 2001, pp. 1357-1365.

[16] S. L. Chen, Analysis and modelling of reactive three-dimensional high-power CO_2 laser cutting, Proc Instn Mech Engrs, Vol. 212 part B, J. of Engineering Manufacture, 1998, pp. 113-128.

[17] B. S. Yilbas, Experimental investigation into CO_2 laser cutting parameters, J. of Materials Processing Technology, Vol. 58, 1996, pp. 323-330.

[18] B. S. Yilbas, S. J. Hyder and M. Sunar, The Taguchi method for determining CO_2 laser cut quality, J. of Laser Applications, Vol. 10, No. 2, 1998, pp. 71-77.

[19] K. Abdel Ghany and M. Newishy, Cutting of 1.2 mm thick austenitic stainless steel sheet using pulsed and CW Nd-YAG laser, J. of Materials Processing Technology, Vol. 198, 2005, pp. 438-447.

[20] S. L. Chen, The effects of high-pressure assistant-gas flow on high-power CO_2 laser cutting, J. of Materials Processing Technology, Vol. 88, 1999, pp. 57-66.

[21] B. S. Yilbas, Laser cutting quality and thermal efficiency analysis, J. of Materials Processing Technology, Vol. 155-156, 2004, pp. 2106-2115.

[22] W. K. Hamoudi, The effects of speed and processing gas on the laser cutting of steel using a 2 kW CO_2 laser, Inter. J. for the Joining of Materials, Vol. 9, No. 1, 1997, pp. 31-36.

[23] P. S. Sheng and V. S. Joshi, Analysis of heat-affected zone formation for laser cutting of stainless steel, J. of Materials Processing Technology, Vol. 53, 1999, pp. 879-892.

[24] U. Dilthey, M. Faerber and J. Weick, Laser cutting of steel-cut quality depending on cutting parameters, J. of Welding in the World, Vol. 30, No. 9/10, 1992, pp. 275-278.

[25] M. L. Cadortte and H. F. Walker, Characterizing productivity of a 4 kW CO_2 laser cutting system for 0.25" mild steel using central composite methodology, J. of Industrial Technology, Vol. 22, No. 2, 2006, pp.2-8.

[26] J. Wang and W. C. K. Wong, CO_2 laser cutting of metallic coated sheet steels, J. of Materials Processing Technology, Vol. 95, 1999, pp. 164-168.

[27] P. D. Pietro and Y. L. Yao, An investigation into characterizing and optimizing laser cutting quality-a review, Inter. J. of Machine Tools and Manufacture, Vol. 34, No 2, 1994, pp. 225-243.

[28] N. Rajaram, J. Sheikh and S. H. Cheraghi, CO_2 laser cut quality of 4130 steel, J. of Machine Tools and Manufacture, Vol. 43, 2003, pp. 351-358.

[29] B. S. Yilbas, The analysis of CO_2 laser cutting, Proc Instn Mech Engrs IMechE, Vol. 211 part B, 1996, pp. 223-232.

[30] L. Li, M. Sobih and P. L. Crouse, Striation-free laser cutting of mild steel sheets, Annals of the CIRP, Vol. 56, No. 1, 2007, pp.193-196.

[31] G. V. S. Prasad, E. Siores and W. C. K. Wong, Laser cutting of metallic coated sheet steels, J. of Materials Processing Technology, Vol. 74, 1998, pp. 234-242.

[32] G. Simon and U. Gratzke, Theoretical investigations of instabilities in laser gas cutting, proceedings of SPIE 89, Vol. 1132, Paris, France, 1989, pp. 204-210.

[33] S. L. Chen, The effects of gas composition on the CO_2 laser cutting of mild steel, J. of Materials Processing Technology, Vol. 73, 1998, pp. 147-159.

[34] P. A. Atanasov, Some aspects of high-pressure N_2 assisted CO_2-laser cutting of metals, International symposium of Gas Flow and Chemical Lasers, Vol. 1810, 1992, pp. 628-631.

[35] J. Grum and D. Zuljan, Frequency analyses of a signal of IR radiation from the cutting front and surface profile height in laser cutting of austenitic stainless steel, J. of Laser in Engineering, Vol. 12, No. 1, 2002, pp. 59-80.

[36] J. Duan, H. C. Man and T. M. Yue, Modelling the laser fusion cutting process: III. Effects of various process parameters on cut kerf quality, J. of Physics D: Applied Physics, Vol. 34, 2001, pp. 2143-2150.

[37] B. S. Yilbas and M. Rashid, CO_2 laser cutting of Incoloy 800 HT alloy and its quality assessment, J. of Laser in Engineering, Vol. 12, No. 2, 2002, pp. 135-145.

[38] B. S. Yilbas and B. J. Abdul Aleem, Dross formation during laser cutting process, J. of Physics D: Applied Physics, Vol. 39, 2006, 1451-1461.

[39] M. Radovanovic and P. Dasic, Research on surface roughness by laser cut, the Annals of University "Dunarea De Jos" of Galati Fascicle VII, ISSN 1221-4590, Tribology, 2006, pp. 84-88.

[40] R. Neimeyer, R. N. Smith and D. A. Kaminski, Effects of operating parameters on surface quality for laser cutting of mild steel, J. of Engineering for Industry, Vol. 115, 1993, pp. 359-362.

[41] D. Schuocker, Dynamic phenomena in laser cutting and cut quality. J. of Applied Physics B: Lasers and Optics. Vol. 40, No. 1, 1986, pp. 9-14.

[42] C. S. Lee, A. Goel, and H. Osada, Parametric studies of pulsed-laser cutting of thin metal plates, J. of Applied Physics, American Institute of Physics, Vol. 58, No. 3, 1985, pp. 1339-1343.

[43] B. S. Yilbas, C. Karatas, I. Uslan, O. Keles, Y. Usta, Z. Yilbas, M. Ahsan, Wedge cutting of mild steel by CO_2 laser and cut-quality assessment in relation to normal cutting, J. of Optics and Lasers in Engineering, Vol. 46, No. 10, 2008, pp. 777-784.

[44] A. Lamikiz, L. N. L. de Lacalle, J. A. Sa´nchez, D. del Pozo, J. M. Etayo and J. M. Lo´pez, CO2 laser cutting of advanced high strength steels (AHSS), J. of Applied Surface Science, Vol. 242, 2005, pp. 362-368.

[45] C. Karatas, O. Keles, I. Uslan and Y. Usta, Laser cutting of steel sheets: influence of workpiece thickess and beam waist position on kerf size and stria formation, J. of Materials Processing Technology, Vol. 172, 2006, pp. 22-29.

[46] Y. P. Kathuria, Laser miroprocessing of metallic stent for medical therapy, J. of Materials Processing Technology, Vol. 170, 2005, pp. 545-550.

[47] A. Lamikiz, L. N. L. De lacalle, D. D. Pozo, J. M. Etayo and J. M. Lopez, Cutting parameters for the reduction in material degradation in the laser cutting of advanced high-strength steels, J. of Engineering Manufacture Proc. IMechE, Vol. 220 part B, 2006, pp. 877-882.

[48] F. Caiazzo, F. Curico, G. Daurelio, F. M. C. Minutolo, Laser cutting of different polymetric plastics (PE, PP and PC) by a CO_2 laser beam, Journal of Materials Processing Technology, Vol. 159, 2005, pp. 279-285.

[49] I. A. Choudhury and S. Shirley, laser cutting of polymeric materials: An experimental investigation, journal of Optics and Laser Technology, Vol. 42, 2010, pp. 503-508.

[50] J. P. Davim, C. Oliveira, N. Barricas and M. Conceicão, Evaluation of cutting quality of PMMA using CO_2 lasers, International Journal of Advanced Manufacturing Technology, Vol. 35, 2008, pp. 875-879.

[51] M. Kurt, Y. Kaynak, E. Bagei, H. Demirer and M. Kurt, Dimensional analyses and surface quality of laser cutting process for engineering plastics, Inter. J. of Manuf. Technology, Vol. 41, 2009, pp. 259-267.

[52] P. A. Atanasov and M. G. Baeva, CW CO_2 laser cutting of plastics, J. of SPIE Vol. 3092, 1997, pp. 772-775.

[53] J. Bahr, H. Barolff, A. E. Schwind, M. Thiele and G. Wiedemann, Laser cutting of plastic scintillator and light guid materials, J. of Nuclear Instruments and Methods in Physics Research, Vol. A274, 1989, pp. 145-151.

[54] J. P. Davim, N. Barricas, M. Conceicao and C. Oliverira, Some experimental studies on CO_2 laser cutting quality of polymeric materials, Journal of Materials Processing Technology, Vol. 198, 2008, pp. 99-104.

[55] P. Sheng and L. Cai, Predictive process planning for laser cutting, J. of Manufacturing systems, Vol. 17, No. 2, 1998, pp. 144-158.

[56] P. G. Berrir and F. N. Birkett, The drilling and cutting of Polymethyl methacrylate (Perspex) by CO_2 laser, J. of Optics and Lasers in Engineering, Vol. 1, 1980, pp. 107-129.

[57] L. Romoli, G. Tantussi and G. Dini, Layered laser vaporization of PMMA manufacturing 3D mould cavities, Annals of the CIRO, Vol. 56, No. 1, 2007, pp. 209-212.

[58] I. Black, Laser cutting of perspex, J. of Materials Science Letters, Vol. 17, 1998, pp. 1531-1533.

[59] V. Di Illio, V. Tagliferri and F. Veniali, Machining parameters and cut quality in laser cutting of aramid fibre reinforced plastics, J. of Materials Manufacturing Process, Vol. 5, No. 4, 1990, pp. 591-608.

[60] B. H. Zhou and S. M. mahdavian, Experimental and theoretical analyses of cutting nonmetallic materials by low power CO_2-laser, J. of Materials Processing Technology, Vol. 146, 2004, pp. 188-192.

[61] R. Nuss, Laser cutting of prim-polyurethane components in comparison with other cutting techniques, proceedings of 5th international conf. on Laser in Manufacturing, Spet. 13-14, 1988.

[62] V. Tagliaferri, A. Di Ilio and I. Crivelli Visconti, Laser cutting of fiber-reinforced polyesters, J. of Composites, Vol. 16, No. 4**,** 1985, pp. 317–325.

[63] G. Caprino and V. Tagliaferri, Maximum cutting speed in laser cutting of fiber reinforced plastics, J. of Machine Tool and manufacture, Vol. 28, No. 4, 1988, pp. 389-398.

[64] G. Caprino, V. Tagliaferri, L. Covelli, Cutting glass fibre reinforced composites using CO_2 laser with multimodal-Gaussian distribution, International J of Machine Tools and Manufacture, Vol. 35, No. 6, 1995, pp. 831-840.

[65] G. Caprino, V. Tagliaferri and L. Covelli, The importance of material structure in the laser of glass fibre reinforced plastic composite, J. of Engineering Materials and Technology, Vol. 117, 1995, pp. 133-138.

[66] A. A. Cenna, P. Mathew, Analysis and prediction of laser cutting parameters of fibre reinforced plastics (FRP) composite materials, International J. of Machine Tools and Manufacture, Vol. 42, No. 1, 2002, pp. 105-113.

[67] A. Goeke and C. Emmelmann, Influence of laser cutting parameters on CFRP part quality, J. of Physics Procedia, Vol. 5, 2010, pp. 253-258.

[68] A. Riveiro, B. Gómez, F. Quintero, F. Lusquiños, R. Comesaña and J. Pou, Parametric study on CO_2 laser cutting of carbon fibre reinforced plastic composite, Proceedings of 26th International Congress on Applications of Lasers and Electro-

Optics, ICALEO 2007, October 29 - November 1, 2007, Orlando, FL, United states.

[69] A. Dilio, V. Tagliaferri, Thermal damage in laser cutting of $(0/90)_{2s}$ aramid/epoxy laminates, Composites, Vol. 20, No. 2, 1989, pp. 115-119.

[70] P. Bamforth, K. Williams and M. R. Jackson, Edge quality optimisation for CO_2 laser cutting of nylon textiles, J. of Applied Thermal Engineering, Vol. 26, 2006, pp. 403-412.

[71] N. yusoff, S. R. Ismail, A. Mamat and A. A. Yazid, Selected Malaysian wood CO_2-laser cutting parameters and cut quality, American Journal of Applied Science, Vol. 5, No. 8, 2008, pp. 990-996.

[72] N. Hattori, Laser processing of wood, Mokuzai Gakkaishi, Vol. 41, No. 8, 1995, pp. 703-709.

[73] V. G. Barnekov, C. W. McMillin and H. A. Huber, Factors influencing laser cutting of wood, Forest Products Journal, Vol. 36, No. 1, 1986, pp. 55-58.

[74] V. G. Barnekov, H. A. Huber and C. W. McMillin, Laser machining of wood composites, Forest Products Journal, Vol. 39, No. 10, 1989, pp. 76-78.

[75] P. A. A. Khan, M. Cherif, S. Kudapa, V. G. Barnekov and K. Mukherjee, High speed, high energy automated machining of hardwoods by using a carbon dioxide laser, Proceedings of SPIE-ICALEO;91: Laser Materials Processing, 1722, San Jose, USA, Nov. 1991, pp. 238-252.

[76] K. Mukherjee, T. Grendawell, P. A. A. Khan and C. W. McMillin, Gas flow parameters in laser cutting of wood-nozzle design, Forest Products Journal, Vol. 40, No. 10, 1990, pp. 39-42.

[77] K. C. P. Lum, S. L. Hg and I. Black, CO_2 laser cutting of MDF, 1- Determination of process parameter settings, Journal of Optics and Laser Technology, Vol. 32, 2000, pp. 67-76.

[78] S. L. Hg , K. C. P. Lum and I. Black, CO_2 laser cutting of MDF, Estimation of power distribution, Journal of Optics and Laser Technology, Vol. 32, 2000, pp. 77-87.

[79] F. Letellier and G. J. Ramos, Determination of optimal focal position during CO_2 laser cutting of MDFB thick sheets to reduce side kerf curvature, ICALEO 2008, laser institute of America, 20- 23 Oct. 2008, Temecula, CA, United states, pp. 664-670.

[80] C. Tsai and H. Chen, Laser cutting of thick ceramic substrates by controlled fracture technique, J. of Materials Processing Technology, Vol. 136, 2003, pp. 229-239.

[81] L. Ji, Y. Yan, Y. Bao and Y. Jiang, Crack-free cutting of thick and dense ceramics with CO_2 laser by single-pass process, J. of Optics and Lasers in Engineering, Vol. 46, No. 10, 2008, pp. 785-790.

[82] I. Black, K. L Chua, Laser cutting of thick ceramic tile, J. of Optics & Laser Technology, Vol. 29, No. 4, 1997, pp. 193-205.

[83] I. Black, S. A. J. Livingstone, K. L. Chua, A laser beam machining (LBM) database for the cutting of ceramic tile , J. of Materials Processing Technology, Vol. 84, No. 1-3, 1998, pp. 47-55.

[84] L. Hong, L. Li, C. Ju, Investigation of cutting of engineering ceramics with Q-switched pulse CO2 laser, J. of Optics and Laser in Engineering, Vol. 38, 2002, pp. 279-289.

[85] L. M. Wee & P. L. Crouse & L. Li, A statistical analysis of striation formation during laser cutting of ceramics, International J. of Advanced Manufacturing Technology, Vol. 36, 2008, pp. 699–706.

[86] A. Grabowski, J. Sleziona and M. Nowak, Laser cutting of AlSi-alloy/SiCp composite-modelling of the cut kerf geometry, Proceedings of the SPIE - The International Society for Optical Engineering, Vol. 6598, 2007, pp. 65980H (5 pp.).

[87] L. Hong and L. Li, A study of laser cutting engineering ceramics, J. of Optics and Laser Technology, Vol. 31, 1999, pp. 531-538.

[88] M. Boutinguiza, J. Pou, F. Lusquiños, F. Quintero, R. Soto, M. Pérez-Amor, K. Watkins and W. M. Steen, CO_2 laser cutting of slate, J. of Optics and Lasers in Engineering, Vol. 37, No. 1, 2002, pp. 15-25.

[89] J. Jiao and X. Wang, Cutting glass substrates with dual-laser beams, J. of Optics and Lasers in Engineering, Vol. 47, No. 7-8, 2009, pp. 860-864.

[90] P. L. Crouse, L. Li and J. T. Spencer, Performance comparison of CO and diode 2 lasers for deep-section concrete cutting, J. of Thin Solid Films, Vol. 453-454, 2004, pp. 594-599.

[91] A. Ruggiero, L. Tricarico, A.G. Olabi and K. Y. Benyounis, Weld-bead profile and costs optimisation of the CO_2 dissimilar laser welding process of low carbon steel and austenitic steel AISI316, J. of Optics & Laser Technology, Vol. 43, No. 1, 2011, pp. 82-90.

[92] A. K. Dubey and V. Yadava, Multi-objective optimization of Nd:YAG laser cutting of nickel-based superalloy sheet using orthogonal array with principal component analysis, J. of Optics and Lasers in Engineering, Vol. 46, No. 2, 2008, pp. 124-132.

[93] A. K. Dubey and V. Yadava, Multi-objective optimisation of laser beam cutting process, Optics & Laser Technology, Vol. 40, No. 3, 2008, pp. 562-570.

[94] A. Sharma, V. Yadava, R. Rao, Optimization of kerf quality characteristics during Nd: YAG laser cutting of nickel based superalloy sheet for straight and curved cut profiles, J. of Optics and Lasers in Engineering, Vol. 48, No. 9, 2010, pp. 915-925.

[95] B. S. Yilbas, Laser cutting of thick sheet metals: Effect of cutting parameters on kerf size variations, J. of Materials Processing Technology, Vol. 201, 2008, pp. 285-290.

[96] R. Rao and V. Yadava, .Multi-objective optimization of Nd:YAG laser cutting of thin superalloy sheet using grey relational analysis with entropy measurement, J. of Optics and Laser Technology, Vol. 41, No. 8, 2009, pp. 922-930.

[97] A. K. Dubey and V. Yadava, Multi-objective optimization of Nd:YAG laser cutting of nickel-based superalloy sheet using orthogonal array with principal component analysis, J. of Optics and Lasers in Engineering, Vol. 46, No. 2, 2008, pp.124-132.

[98] A. K. Dubey and V. Yadava, Optimization of kerf quality during pulsed laser cutting of aluminium alloy sheet, J. of Materials Processing Technology, Vol. 204, No. 1-3, 2008, pp. 412-418.

[99] S. H. Lim, C. M. Lee and W. J. Chung, A study on the optimal cutting condition of a high speed feeding type laser cutting machine by using Taguchi method, International J. of Precision Engineering and Manufacturing, Vol. 7, No. 1, 2006, pp. 18-23.

[100] J. Mathew, G. L. Goswami, N. Ramakrishnan and N. K. Naik, Parametric studies on pulsed Nd:YAG laser cutting of carbon fibre reinforced plastics composites, J. of Materials Processing Technology, Vol. 89-90, 1999, pp. 198-203.

[101] E. Cicala, D. Zsivanov and A. Nichici, Off-line multiresponse optimization of gas jet assisted CO_2 laser cutting of polymettacrylate, Proceedings of the SPIE - The International Society for Optical Engineering, v 3405, No.1-2, 1998, pp. 293-298.

[102] J. C. H. Castaneda, H. K. Sezer and L. Li, Statistical analysis of ytterbium-doped fibre laser cutting of dry pine wood, Journal of Engineering Manufacture, 223 (part B) (2009) 775-789.

[103] C. W. McMillin and J. E. Harry, Laser machining of southern pine, Forest Products Journal Vol 21, No. 10, 1971, pp. 35–37.

[104] J. C. H. Castaneda, H. K. Sezer and L. Li, The effect of moisture content and tracheids orientation in fibre laser cutting of dry and wet pine wood, ICALEO 2009 - 28th International Congress on Applications of Lasers and Electro-Optics, Proceedings of 28th International Congress on Applications of Lasers and Electro-Optics, ICALEO 2009, Vol. 102, pp. 1409-1418.

[105] K. Huehnlein, K. Tschirpke and R. Hellmann, Optimization of laser cutting processes using design of experiments, J. of Physics Procedia, Vol. 5, No. 2, 2010, pp. 243-252.

[106] D. Dhupal, B. Doloi and B. Bhattacharyya, Modeling and optimization on Nd:YAG laser turned micro-grooving of cylindrical ceramic material, Optics and Lasers in Engineering, Vol. 47, No. 9, 2009, pp. 917-925.

[107] D. Guo, J. Chen, Y. Cheng, Laser cutting parameters optimization based on artificial neural network, Proceedings of 2006 International Joint Conference on Neural Networks, 16-21 July 2006, Vancouver, BC, Canada, 2007, pp. 1106-1111.

[108] G. Casalino, A. D. Ludovico, F. M. C. Minutolo and V. Sergi, laser cutting model bases on artificial intelligence, Congress proceedings of ICALEO 22nd international Congress on Applications of Laser and Electro-Optics, 13-16 Oct. 2003.

[109] G. Dixin, C. Jimin and C. Yuhong, Laser cutting parameters optimization based on artificial neural network, International Joint Conf. on Neural Networks, Sheraton Vancouver Wall Centre Hotel, Canada, July 16-21, 2006, pp. 1106-1111.

[110] M. J. Tsai , C. H. Li and C. C. Chen, Optimal laser-cutting parameters for QFN packages by utilizing artificial neural networks and genetic algorithm, J. of Materials Processing Technology, Vol. 208, No. 1-3, 2008, pp. 270-283.

[111] K. Y. Benyounis, A. H. Bettamer, A. G. Olabi and M. S. J. Hashmi, Prediction the impact strength of spiral-welded pipe joints in Submerged arc welding of low carbon steel, Proceedings of IMC21, Limerick 1-3-Sep. 2004, pp. 200-210.

[112] E. S. Ege, O. T. Inal and C. A. Zimmerly, Response surface study on production of explosive-welded aluminium-titanium laminates, J. of Materilas Science, Vol. 33, 1998, pp. 5327-5338.

[113] T. T. Allen, R. W. Richardson, D. P. Tagliabue and G. P. Maul, Statistical process design for robotic GMA welding of sheet metal, Welding Journal, AWS, May 2002, pp. 69-s – 77-s.

[114] K. Raghukandan, Analysis of the explosive cladding of Cu-low carbon steel plates, J. of Materials Processing Technology, Vol. 139, 2003, pp. 573-577.

[115] V. V. Murugan and V. Gunaraj, Effects of process parameters on angular distortion of gas metal arc welded structural steel plates, Welding Journal, AWS, Nov. 2005, pp. 165-s – 171-s.

[116] K. Y. Benyounis, A. G. Olabi and M. S. J. Hashmi, Estimation of mechanical properties of laser welded joints using RSM, Proceedings of IMC22, Institute of Technology Tallaght, Dublin- Ireland, 31 Aug.- 2 Sep. 2005, pp. 565-571.

[117] K. Y. Benyounis, A. G. Olabi and M. S. J. Hashmi, Residual stresses prediction for CO2 laser butt-welding of 304- stainless steel, Applied Mechanics and materials, Trans Tech publications, Vols. 3-4 , pp. 125-130..

[118] A. G. Olabi, K. Y. Benyounis, M. S. J. Hashmi, Application of RSM in describing the residual stress distribution in CO2 laser welding of AISI304, Strain Journal, Vol. 43, No. 1, 2007, pp. 37-46.

[119] K. Y. Benyounis, A. G. Olabi and M. S. J. Hashmi, Effect of laser welding parameters on the tensile-shear strength of AISI304 sheet, Published in AMPT2006 proceedings, July 30- Aug. 3, 2006, Ohio university, Athens, Ohio, USA.

[120] R. Koganti, C. Karas, A. Joaquin, D. Henderson, M. Zaluzec and A. Caliskan. Metal inert gas (MIG) welding process optimization for joining aluminium sheet material using OTC/DAIHEN equipment, Proceedings of IMECE'03, ASME Inter. Mech. Eng. Congress, Washington, D. C. , Nov. 15-21, 2003, pp.409-425.

[121] K. Y. Benyounis, A.G. Olabi, M. S. J. Hashmi, Multi-response optimization of CO_2 laser-welding process of austenitic stainless steel, J. of Optics & Laser Technology, Vol. 40, No. 1, 2008, pp. 76-87.

[122] K. Sampath, Constrains-based modelling Enables successful development of welding electrode specification for critical navy application, Welding journal, AWS, Aug. 2005, pp. 131-s -138-s.

[123] T. Pine, M. M. Lee, and T. B. Jones, Factors affecting torsional properties of box sections, J. of Ironmarking and Steelmarking, Vol. 25, n. 3, 1998, pp. 205- 209.

[124] M. P. Lightfoot, G. J. Bruce, N. A. McPherson and K. Woods, The application of artificial neural networks to weld-induced deformation in ship plate, Welding J., AWS and WRC, February 2005, pp. 23-s – 26-s.

[125] A.G. Olabi, G. Casalino, K. Y. Benyounis and M. S. J. Hashmi, An ANN and Taguchi algorithms integrated approach to the optimization of CO_2 laser welding, Advances in Engineering Software, Vol. 37, No. 10, 2006, pp. 643-648.

[126] Z. Sterjovski, D. Nolan, K. R. Carpenter, D. P. Dune and J. Norrish, Artificial neural network for modelling the mechanical properties of steels in various applications, J. of Materials Processing Technology, Vol. 170, No. 3, 2005, pp. 336-544.

[127] K. H. Christensen, T. SØrensen and J. K. Kristensen, Gas metal arc welding of butt joint with varying gap width on neural networks, J. of Science and Technology of welding and joining, Vol. 10, n.1, 2005, pp. 32-43.

[128] H. Okuyucu, A. Kurt and E. Arcaklioglu, Artificial neural network application to the friction stir welding of aluminium plates, J. of Materials & Design, Vol. 29, 2007, pp. 78-84.

[129] S. C. Tam, C. Y. Yeo, S. Jana, M. W. S. Lau, L. E. N. Lim, L. J. Yang, Y. M. Noor, Optimization of laser deep-hole drilling of Inconel 718 using the Taguchi method , J. Materials Processing Technology, Vol. 37, No. 1-4, 1993, pp. 741-757.

[130] S. Bandyopadhyay, H. Gokhale, J. K. S. Sundar, G. Sundararajan, S. V. Joshi, A statistical approach to determine process parameter impact in Nd:YAG laser drilling of IN718 and Ti-6Al-4V sheets, J. of Optics and Lasers in Engineering, Vol. 43, No. 2, 2005, pp. 163-182.

[131] J. Kamalu and P. Byrd, Statistical design of laser drilling experiments, Proceedings ICALEO '98: Laser Materials Processing Conference; Orlando, FL; USA; 16-19 Nov. Vol. B5, 1998, pp. 50-57.

[132] N. Masmiati and P. K. Philip, Investigations on laser percussion drilling of some thermoplastic polymers, J. of Materials Processing Technology, Vol. 185, 2007, pp. 198-203.

[133] M. Ghoreishi, O. B. Nakhjavani, Optimisation of effective factors in geometrical specifications of laser percussion drilled holes, J.of Materials Processing Technology, Vol. 196, No. 1-3, 2008, pp. 303-310.

[134] S. M. Karazi, A. Issa and D. Brabazon, Comparison of ANN and DoE for the prediction of laser-machined micro-channel dimensions, J. of Optics and Lasers in Engineering, Vol. 47, No. 9, 2009, pp. 956-964.

[135] O. B. Nakhjavani and M. Ghoreish, Multi criteria optimization of laser percussion drilling process using artificial neural network model combined with genetic algorithm, Materials & Manufacturing Processes, Vol. 21, No. 1-2, 2006, pp.11-18.

[136] K. Y. Benyounis, A.G. Olabi and M. S. J. Hashmi, Effect of laser welding parameters on the heat input and weld-bead profile, Journal of Materials Processing Technology, Vol. 164-165, 2005, pp. 978-985.

[137] M. J. Tsai and C. H. Li, The use of grey relational analysis to determine laser cutting parameters for QFN packages with multiple performance characteristics, Optics & Laser Technology, Vol. 41, No. 8, 2009, pp. 914-921.

[138] K. Y. Benyounis and A.G. Olabi, Optimization of different welding process using statistical and numerical approaches- A reference guide, Journal of Advances in Engineering Software, Vol. 39, 2008, pp. 483-496.

[139] D.C. Montgomery, Design and Analysis of Experiments, 2nd Ed, John Wiley & Sons, New York, (1984).

[140] A. I. Khuri and J.A. Cornell, *Response Surfaces Design and Analysis*, 2nd ed, Marcel Dekker, New York, (1996).

[141] Design-Expert software, V7, user's guide, Technical manual, Stat-Ease Inc., Minneapolis, MN, 2005..

[142] J. Antony, Design of experiments for engineers and scientists, Elsevier, 2003.

[143] G. E. P. Box and K. B. Wilson, On the experimental attainment of optimum conditions, J. of the Royal Statistical Society B13, 1951, pp. 1- 45.

[144] G. E. P. Box and D. W. Behnken, Some new three level designs for the study of quantitative variables, Technometrics, Vol. 2, n., 4, November 1960, pp. 455-475.

[145] http://www.itl.nist.gov/div898/handbook/pri/section3/pri3362.htm

[146] R. H. MYERS AND D.C. Montgomery, Response surface methodology- process and product optimization using designed experiment, John Wiley & Sons, 1995.

[147]http://www.worldstainless.org/NR/rdonlyres/1563541A-23AD-4869-A5BFD4F1FC963257/4929/Automotiveapplications.pdf (accessed on September 2009).

[148]http://www.automation.com/pdf_articles/RittalWhitePaper104StainlessSteelEnclosures.pdf (accessed on September 2009).

[149]http://academic.uprm.edu/~mgoyal/materialsmay2004/k04orthopaedic.pdf(accessed on September 2009).

[150] http://en.wikipedia.org/wiki/Ultra_high_molecular_weight_polyethylene(accessed on September 2009).

[151] Kurtz Steven M., the UHMWPE Handbook, Academic Press, New York, (2004) ISBN: 0124298516.

[152] http://en.wikipedia.org/wiki/Poly(methyl_methacrylate).

[153] M., A. Chiriac and I. Poeata, Hydroxyapatite thin films synthesized by pulsed laser deposition and magnetron sputtering on PMMA substrates for medical applications, Materials Science and Engineering: B, Vol. 169, No. 1-3, 2010, pp. 159-168.

[154] A. Kovaceic, M. Sreckovic, R. Gospavic, S. Ristic and P. Jovanic, Laser-PMMA interaction and mechanical stresses, J. of Acta Physica Polonica A, Vol. 112, N. 5, 2007, pp. 981-986.

[155] http://www.design-technology.org/mdf.htm (accessed on 10.2010)

[156] S. Hiziroglu, P. Kosonkorn, Evaluation of surface roughness of Thai medium density fibreboard, J. of Build Environ, Vol. 41, 2006, pp. 527–533.

[157] S. N. Kartal and F. Green, Decay and termite resistance of medium density fiberboard (MDF) made from different wood species, International Biodeterioration & Biodegradation, Vol. 51, No. 1, 2003, pp. 29-35.

[158] http://en.wikipedia.org/wiki/Glass-reinforced_plastic (accessed on 10.2010).

[159] K. Palanikumar, Modeling and analysis for surface roughness in machining glass fibre reinforced plastics using response surface methodology, J. of Materials & Design, Vol. 28, No. 10, 2007, pp. 2611-2618.

[160] Rofin DC 015 Slab laser operating manual, Serial No. 2042/2042, 2002.

[161] Mechtronic Technology in Motion, http://www.mechtronic.co.uk/about.html (Accessed on Sept.2010).

[162]http://visualbasic.about.com/od/applications/a/whatisvb.htm(accessed on 10.2010).

[163] http://en.wikipedia.org/wiki/Visual_Basic (accessed on 10.2010).

APPENDICES

APPENDIX – A (AISI316L)

A-1: Data for roughness of AISI316L.

Std	Roughness, mm				Std	Roughness, mm			
	1	2	3	Av.		1	2	3	Av.
1	0.730	0.776	0.869	0.792	24	0.532	0.620	0.583	0.578
2	0.741	0.697	0.757	0.732	25	0.967	1.117	1.016	1.033
3	2.045	1.276	1.624	1.648	26	0.414	0.487	0.541	0.481
4	0.784	0.758	0.870	0.804	27	0.830	0.801	0.875	0.835
5	1.384	1.937	1.884	1.735	28	0.455	0.467	0.424	0.449
6	0.434	0.305	0.444	0.394	29	0.715	1.009	1.101	0.942
7	2.321	2.440	1.722	2.161	30	0.716	0.527	0.617	0.620
8	0.530	0.811	0.737	0.693	31	0.582	0.617	0.546	0.582
9	1.034	0.777	1.089	0.967	32	0.631	0.829	0.771	0.744
10	0.727	0.796	0.678	0.734	33	0.715	0.792	0.758	0.755
11	0.924	0.827	0.860	0.870	34	0.576	0.695	0.631	0.634
12	0.877	0.779	0.785	0.814	35	0.627	0.622	0.841	0.697
13	1.834	1.492	1.573	1.633	36	0.659	0.478	0.428	0.522
14	0.774	0.866	1.089	0.910	37	1.224	1.088	1.320	1.211
15	0.635	0.606	0.754	0.665	38	0.704	0.702	0.822	0.743
16	0.458	0.364	0.405	0.409	39	0.844	0.878	0.927	0.883
17	0.539	0.477	0.651	0.556	40	0.419	0.426	0.593	0.479
18	0.619	0.613	0.599	0.610	41	0.679	0.796	0.797	0.757
19	0.698	0.505	0.696	0.633	42	0.524	0.662	0.653	0.613
20	0.412	0.459	0.600	0.490	43	0.514	0.548	0.622	0.561
21	0.807	0.787	0.605	0.733	44	0.544	0.771	0.767	0.694
22	1.012	1.010	1.095	1.039	45	0.556	0.667	0.579	0.601
23	0.819	0.752	0.773	0.781	46	0.767	0.588	0.694	0.683

A-2: Data for upper kerf of AISI316L.

Std	Upper kerf, mm				Std	Upper kerf, mm			
	1	2	3	Av.		1	2	3	Av.
1	0.290	0.308	0.290	0.296	24	0.212	0.152	0.176	0.180
2	0.341	0.324	0.311	0.325	25	0.199	0.192	0.200	0.197
3	0.245	0.214	0.208	0.222	26	0.230	0.242	0.232	0.235
4	0.270	0.265	0.189	0.241	27	0.247	0.260	0.247	0.251
5	0.278	0.264	0.247	0.263	28	0.309	0.322	0.312	0.314
6	0.212	0.256	0.195	0.221	29	0.248	0.235	0.321	0.268
7	0.295	0.299	0.286	0.293	30	0.234	0.241	0.251	0.242
8	0.281	0.261	0.253	0.265	31	0.308	0.309	0.297	0.305
9	0.289	0.309	0.301	0.300	32	0.259	0.262	0.268	0.263
10	0.192	0.191	0.199	0.194	33	0.241	0.238	0.231	0.237
11	0.311	0.329	0.324	0.321	34	0.262	0.302	0.279	0.281
12	0.229	0.218	0.223	0.223	35	0.265	0.273	0.277	0.272
13	0.259	0.276	0.256	0.264	36	0.301	0.298	0.309	0.303
14	0.311	0.304	0.306	0.307	37	0.294	0.323	0.328	0.315
15	0.192	0.204	0.193	0.196	38	0.212	0.207	0.213	0.211
16	0.229	0.280	0.183	0.231	39	0.344	0.389	0.316	0.350
17	0.201	0.198	0.189	0.196	40	0.253	0.268	0.272	0.264
18	0.261	0.264	0.268	0.264	41	0.328	0.322	0.325	0.325
19	0.260	0.256	0.246	0.254	42	0.296	0.320	0.319	0.312
20	0.287	0.292	0.288	0.289	43	0.295	0.288	0.285	0.289
21	0.321	0.328	0.315	0.321	44	0.269	0.322	0.313	0.301
22	0.255	0.248	0.247	0.250	45	0.314	0.293	0.299	0.302
23	0.304	0.310	0.313	0.309	46	0.284	0.301	0.306	0.297

A-3: Data for lower kerf of AISI316L.

Std	Upper kerf, mm				Std	Upper kerf, mm			
	1	2	3	Av.		1	2	3	Av.
1	0.222	0.210	0.176	0.203	24	0.186	0.170	0.191	0.182
2	0.231	0.230	0.219	0.227	25	0.251	0.323	0.199	0.258
3	0.142	0.150	0.149	0.147	26	0.198	0.168	0.152	0.173
4	0.219	0.253	0.175	0.216	27	0.157	0.162	0.167	0.162
5	0.193	0.154	0.203	0.183	28	0.194	0.183	0.188	0.188
6	0.210	0.273	0.188	0.224	29	0.157	0.143	0.164	0.155
7	0.244	0.208	0.201	0.218	30	0.195	0.194	0.188	0.192
8	0.197	0.096	0.178	0.157	31	0.155	0.194	0.198	0.182
9	0.209	0.286	0.203	0.233	32	0.225	0.215	0.207	0.216
10	0.139	0.122	0.173	0.145	33	0.217	0.197	0.186	0.200
11	0.203	0.195	0.174	0.191	34	0.233	0.227	0.229	0.230
12	0.181	0.162	0.158	0.167	35	0.150	0.183	0.180	0.171
13	0.176	0.202	0.175	0.184	36	0.182	0.196	0.180	0.186
14	0.215	0.207	0.213	0.212	37	0.195	0.197	0.200	0.197
15	0.200	0.245	0.174	0.206	38	0.197	0.192	0.168	0.186
16	0.251	0.292	0.193	0.245	39	0.161	0.198	0.181	0.180
17	0.156	0.104	0.181	0.147	40	0.170	0.178	0.173	0.174
18	0.211	0.206	0.210	0.209	41	0.209	0.265	0.265	0.246
19	0.176	0.141	0.195	0.171	42	0.156	0.154	0.168	0.159
20	0.196	0.183	0.191	0.190	43	0.198	0.145	0.161	0.168
21	0.243	0.278	0.218	0.246	44	0.163	0.175	0.164	0.167
22	0.222	0.210	0.176	0.203	45	0.161	0.166	0.156	0.161
23	0.231	0.230	0.219	0.227	46	0.182	0.171	0.168	0.174

APPENDIX – B (UHMWPE)

B-1: Data for upper kerf of 6 mm UHMWPE.

No.	1	2	3	4	5	Average
1	0.516	0.531	0.511	0.522	0.502	0.516
2	0.572	0.571	0.571	0.568	0.567	0.570
3	0.412	0.421	0.431	0.417	0.418	0.420
4	0.459	0.465	0.462	0.455	0.462	0.461
5	0.639	0.648	0.658	0.655	0.647	0.649
6	0.678	0.679	0.679	0.678	0.687	0.680
7	0.281	0.276	0.276	0.27	0.268	0.274
8	0.321	0.324	0.315	0.315	0.312	0.317
9	0.717	0.713	0.724	0.716	0.721	0.718
10	0.627	0.62	0.629	0.631	0.635	0.628
11	0.398	0.386	0.378	0.276	0.283	0.344
12	0.274	0.274	0.272	0.27	0.275	0.273
13	0.513	0.514	0.504	0.508	0.504	0.509
14	0.499	0.501	0.497	0.498	0.495	0.498
15	0.491	0.495	0.505	0.498	0.512	0.500
16	0.484	0.48	0.484	0.484	0.485	0.483
17	0.491	0.492	0.488	0.491	0.49	0.490

B-2: Data for lower kerf of 6 mm UHMWPE.

No.	1	2	3	4	5	Average
1	1.255	1.25	1.217	1.246	1.24	1.242
2	1.348	1.359	1.368	1.371	1.358	1.361
3	0.857	0.872	0.857	0.866	0.879	0.866
4	1.318	1.311	1.317	1.32	1.337	1.321
5	1.040	1.059	1.057	1.036	1.045	1.047
6	1.299	1.278	1.294	1.289	1.294	1.291
7	1.163	1.139	1.148	1.163	1.157	1.154
8	1.471	1.465	1.474	1.472	1.466	1.470
9	1.246	1.261	1.263	1.253	1.29	1.263
10	1.155	1.140	1.142	1.14	1.158	1.147
11	1.332	1.332	1.364	1.353	1.376	1.351
12	1.216	1.220	1.242	1.243	1.220	1.228
13	1.328	1.319	1.32	1.312	1.319	1.320
14	1.356	1.351	1.358	1.358	1.353	1.355
15	1.333	1.334	1.334	1.331	1.335	1.333
16	1.329	1.329	1.329	1.331	1.346	1.333
17	1.326	1.339	1.339	1.345	1.345	1.339

B-3: Data for roughness of 6 mm UHMWPE.

No.	1	2	3	4	5	Average
1	1.753	1.564	1.625	1.572	1.634	1.630
2	1.196	1.235	1.254	1.238	1.348	1.254
3	1.755	1.698	1.784	1.736	1.648	1.724
4	1.486	1.359	1.282	1.246	1.331	1.341
5	1.992	1.845	1.955	1.845	1.902	1.908
6	1.568	1.684	1.724	1.423	1.542	1.588
7	1.845	1.785	1.942	1.822	1.8362	1.846
8	1.642	1.452	1.458	1.542	1.562	1.531
9	1.942	1.722	1.885	1.762	1.834	1.829
10	1.664	1.589	1.756	1.687	1.722	1.684
11	1.587	1.642	1.622	1.782	1.564	1.639
12	1.842	1.775	1.687	1.856	1.621	1.756
13	1.521	1.442	1.456	1.447	1.546	1.482
14	1.245	1.456	1.387	1.423	1.429	1.388
15	1.394	1.418	1.339	1.384	1.357	1.378
16	1.656	1.452	1.557	1.523	1.568	1.551
17	1.452	1.234	1.23	1.475	1.457	1.370

B-4: Data for upper kerf of 8 mm UHMWPE.

No.	1	2	3	4	5	Average
1	0.567	0.574	0.582	0.575	0.573	0.574
2	0.665	0.662	0.660	0.663	0.662	0.662
3	0.529	0.512	0.514	0.517	0.521	0.519
4	0.564	0.566	0.551	0.557	0.566	0.561
5	0.746	0.771	0.764	0.75	0.745	0.755
6	0.780	0.768	0.778	0.789	0.757	0.774
7	0.407	0.41	0.407	0.409	0.408	0.408
8	0.433	0.443	0.458	0.454	0.437	0.445
9	0.782	0.777	0.770	0.774	0.779	0.776
10	0.760	0.758	0.743	0.758	0.762	0.756
11	0.467	0.462	0.479	0.467	0.473	0.470
12	0.382	0.385	0.367	0.363	0.399	0.379
13	0.585	0.604	0.605	0.589	0.615	0.600
14	0.58	0.572	0.585	0.576	0.575	0.578
15	0.606	0.574	0.578	0.578	0.579	0.583
16	0.582	0.605	0.597	0.580	0.600	0.593
17	0.592	0.589	0.589	0.581	0.577	0.586

B-5: Data for lower kerf of 8 mm UHMWPE.

No.	1	2	3	4	5	Average
1	1.376	1.375	1.374	1.366	1.348	1.368
2	1.419	1.43	1.437	1.418	1.412	1.423
3	0.862	0.86	0.862	0.861	0.866	0.862
4	1.41	1.412	1.414	1.415	1.416	1.413
5	1.006	0.999	0.989	0.996	1.008	1.000
6	1.281	1.288	1.273	1.297	1.3	1.288
7	1.282	1.292	1.293	1.303	1.301	1.294
8	1.522	1.536	1.528	1.522	1.53	1.528
9	1.238	1.233	1.239	1.237	1.241	1.238
10	1.019	1.003	1.02	1.014	1.026	1.016
11	1.49	1.492	1.482	1.484	1.471	1.484
12	1.321	1.335	1.349	1.325	1.337	1.333
13	1.353	1.393	1.372	1.356	1.376	1.370
14	1.378	1.369	1.376	1.366	1.37	1.372
15	1.387	1.387	1.384	1.387	1.389	1.387
16	1.349	1.368	1.35	1.372	1.371	1.362
17	1.372	1.351	1.386	1.376	1.365	1.370

B-6: Data for roughness of 8 mm UHMWPE.

No.	1	2	3	4	5	Average
1	2.356	2.321	2.324	2.358	2.205	2.313
2	1.614	1.787	1.768	1.647	1.601	1.683
3	2.424	2.556	2.547	2.314	2.154	2.399
4	2.157	1.986	1.995	2.235	2.145	2.104
5	2.712	2.689	2.645	2.728	2.749	2.705
6	2.353	2.335	2.351	2.248	2.205	2.298
7	2.959	3.058	2.984	2.956	2.977	2.987
8	2.574	2.665	2.526	2.647	2.562	2.595
9	2.247	2.476	2.428	2.498	2.341	2.398
10	2.698	2.795	2.795	2.786	2.756	2.766
11	2.127	2.045	2.257	2.254	2.105	2.158
12	2.789	2.684	2.723	2.782	2.624	2.720
13	1.725	1.745	1.653	1.523	1.758	1.681
14	1.956	2.024	1.856	1.845	1.986	1.933
15	1.756	1.968	1.784	1.826	1.657	1.798
16	1.658	1.756	1.582	1.553	1.958	1.701
17	1.735	1.986	1.662	1.674	1.752	1.762

B-7: Data for upper kerf of 10 mm UHMWPE.

No.	1	2	3	4	5	Average
1	0.725	0.739	0.736	0.724	0.725	0.730
2	0.738	0.734	0.738	0.737	0.734	0.736
3	0.71	0.692	0.682	0.681	0.674	0.688
4	0.702	0.701	0.709	0.708	0.708	0.706
5	0.857	0.843	0.851	0.852	0.853	0.851
6	0.895	0.877	0.877	0.87	0.871	0.878
7	0.556	0.552	0.555	0.556	0.551	0.554
8	0.589	0.572	0.577	0.586	0.575	0.580
9	0.877	0.874	0.873	0.872	0.875	0.874
10	0.842	0.849	0.846	0.844	0.848	0.846
11	0.559	0.556	0.57	0.656	0.56	0.580
12	0.541	0.557	0.533	0.541	0.543	0.543
13	0.729	0.715	0.712	0.705	0.717	0.716
14	0.714	0.721	0.72	0.706	0.714	0.715
15	0.742	0.727	0.707	0.705	0.712	0.719
16	0.692	0.693	0.678	0.694	0.691	0.690
17	0.706	0.701	0.708	0.706	0.697	0.704

B-8: Data for lower kerf of 10 mm UHMWPE.

No.	1	2	3	4	5	Average
1	1.438	1.458	1.448	1.433	1.438	1.443
2	1.589	1.598	1.596	1.591	1.593	1.593
3	0.930	0.926	0.928	0.920	0.930	0.927
4	1.493	1.950	1.960	1.489	1.486	1.676
5	1.188	1.233	1.235	1.238	1.237	1.226
6	1.458	1.464	1.450	1.460	1.465	1.459
7	1.421	1.416	1.424	1.411	1.42	1.418
8	1.661	1.652	1.655	1.666	1.662	1.659
9	1.390	1.392	1.393	1.395	1.390	1.392
10	1.221	1.186	1.185	1.17	1.204	1.193
11	1.604	1.595	1.601	1.600	1.603	1.601
12	1.278	1.289	1.286	1.275	1.279	1.281
13	1.475	1.481	1.480	1.471	1.473	1.476
14	1.478	1.474	1.476	1.466	1.470	1.473
15	1.478	1.473	1.458	1.770	1.450	1.526
16	1.450	1.444	1.459	1.495	1.467	1.463
17	1.470	1.458	1.476	1.481	1.495	1.476

B-9: Data for roughness of 10 mm UHMWPE.

No.	1	2	3	4	5	Average
1	2.457	2.289	2.356	2.378	2.402	2.376
2	1.824	1.864	1.673	1.845	1.786	1.798
3	2.986	2.987	3.034	2.845	2.897	2.950
4	2.418	2.412	2.358	2.315	2.217	2.344
5	3.684	3.473	3.582	3.462	3.406	3.521
6	2.982	2.845	2.759	2.994	2.978	2.912
7	3.562	3.458	3.442	3.374	3.352	3.438
8	2.978	3.055	3.12	3.142	2.998	3.059
9	2.896	2.989	2.986	2.986	2.889	2.949
10	3.562	3.359	3.428	3.358	3.429	3.427
11	2.976	2.745	2.685	2.994	2.976	2.875
12	3.568	3.397	3.375	3.256	3.252	3.370
13	2.227	2.108	2.356	2.045	2.152	2.178
14	2.256	2.452	2.356	2.342	2.245	2.330
15	2.423	2.156	2.228	2.156	2.254	2.243
16	2.259	2.108	2.149	2.116	2.101	2.147
17	2.356	2.254	2.205	2.145	2.113	2.215

APPENDIX – C (PMMA)

C-1: Data for upper kerf of 2 mm PMMA.

No.	1	2	3	4	5	Average
1	0.585	0.563	0.555	0.571	0.583	0.571
2	0.634	0.640	0.633	0.638	0.644	0.638
3	0.525	0.515	0.514	0.523	0.531	0.522
4	0.593	0.584	0.596	0.592	0.602	0.593
5	0.755	0.741	0.757	0.746	0.759	0.752
6	0.72	0.704	0.722	0.701	0.692	0.708
7	0.444	0.421	0.429	0.435	0.422	0.430
8	0.466	0.438	0.447	0.44	0.451	0.448
9	0.719	0.732	0.751	0.747	0.712	0.732
10	0.76	0.75	0.755	0.74	0.752	0.751
11	0.324	0.379	0.367	0.365	0.371	0.361
12	0.443	0.45	0.444	0.434	0.448	0.444
13	0.646	0.654	0.652	0.666	0.647	0.653
14	0.569	0.593	0.574	0.57	0.576	0.576
15	0.614	0.617	0.601	0.594	0.603	0.606
16	0.566	0.55	0.559	0.551	0.561	0.557
17	0.503	0.433	0.452	0.492	0.497	0.475
18	0.578	0.567	0.572	0.574	0.577	0.574
19	0.507	0.503	0.495	0.504	0.512	0.504
20	0.568	0.574	0.571	0.562	0.587	0.572
21	0.739	0.721	0.719	0.744	0.733	0.731
22	0.656	0.655	0.657	0.675	0.683	0.665
23	0.417	0.428	0.446	0.451	0.432	0.435
24	0.444	0.453	0.427	0.442	0.445	0.442
25	0.539	0.53	0.532	0.536	0.527	0.533
26	0.546	0.531	0.556	0.558	0.52	0.542
27	0.582	0.551	0.553	0.564	0.577	0.565
28	0.607	0.590	0.594	0.591	0.568	0.590
29	0.595	0.581	0.564	0.574	0.57	0.577

C-2: Data for lower kerf of 2 mm PMMA.

No.	1	2	3	4	5	Average
1	0.196	0.194	0.190	0.184	0.186	0.190
2	0.235	0.251	0.259	0.254	0.238	0.247
3	0.173	0.165	0.160	0.168	0.152	0.164
4	0.243	0.228	0.230	0.227	0.238	0.233
5	0.241	0.215	0.239	0.247	0.225	0.233
6	0.215	0.205	0.214	0.219	0.206	0.212
7	0.220	0.223	0.231	0.212	0.226	0.222
8	0.207	0.202	0.205	0.209	0.200	0.205
9	0.178	0.171	0.163	0.157	0.198	0.173
10	0.252	0.267	0.263	0.257	0.258	0.259
11	0.185	0.170	0.171	0.187	0.177	0.178
12	0.266	0.274	0.271	0.254	0.263	0.266
13	0.245	0.224	0.226	0.238	0.229	0.232
14	0.208	0.188	0.187	0.199	0.186	0.194
15	0.218	0.230	0.216	0.220	0.215	0.220
16	0.188	0.172	0.192	0.175	0.185	0.182
17	0.143	0.127	0.139	0.150	0.153	0.142
18	0.243	0.225	0.232	0.221	0.245	0.233
19	0.170	0.153	0.145	0.164	0.151	0.157
20	0.217	0.225	0.255	0.245	0.222	0.233
21	0.251	0.260	0.245	0.250	0.254	0.252
22	0.246	0.228	0.216	0.226	0.237	0.231
23	0.291	0.273	0.243	0.270	0.259	0.267
24	0.257	0.244	0.250	0.233	0.243	0.245
25	0.230	0.217	0.213	0.221	0.218	0.220
26	0.234	0.230	0.228	0.225	0.236	0.231
27	0.229	0.251	0.236	0.234	0.231	0.236
28	0.209	0.229	0.211	0.214	0.224	0.217
29	0.233	0.213	0.219	0.224	0.220	0.222

C-3: Data for HAZ of 2 mm PMMA.

No.	1	2	3	4	5	Average
1	0.048	0.042	0.035	0.039	0.044	0.042
2	0.049	0.049	0.051	0.052	0.05	0.050
3	0.032	0.04	0.036	0.032	0.037	0.035
4	0.041	0.039	0.038	0.036	0.04	0.039
5	0.042	0.045	0.043	0.039	0.038	0.041
6	0.032	0.031	0.034	0.035	0.028	0.032
7	0.054	0.056	0.049	0.053	0.051	0.053
8	0.021	0.02	0.022	0.027	0.023	0.023
9	0.028	0.02	0.022	0.02	0.021	0.022
10	0.043	0.051	0.048	0.04	0.044	0.045
11	0.025	0.024	0.026	0.028	0.023	0.025
12	0.05	0.045	0.05	0.045	0.044	0.047
13	0.064	0.077	0.054	0.07	0.072	0.067
14	0.051	0.047	0.052	0.045	0.059	0.051
15	0.037	0.036	0.034	0.033	0.03	0.034
16	0.036	0.04	0.037	0.044	0.038	0.039
17	0.03	0.033	0.035	0.028	0.027	0.031
18	0.048	0.042	0.043	0.046	0.047	0.045
19	0.034	0.03	0.029	0.027	0.023	0.029
20	0.041	0.034	0.031	0.037	0.033	0.035
21	0.059	0.063	0.051	0.055	0.054	0.056
22	0.035	0.037	0.038	0.036	0.035	0.036
23	0.069	0.061	0.064	0.065	0.066	0.065
24	0.039	0.041	0.04	0.042	0.042	0.041
25	0.042	0.043	0.046	0.036	0.037	0.041
26	0.044	0.042	0.046	0.043	0.04	0.043
27	0.048	0.042	0.044	0.047	0.052	0.047
28	0.045	0.042	0.043	0.04	0.038	0.042
29	0.038	0.045	0.05	0.048	0.043	0.045

C-4: Data for roughness of 2 mm PMMA.

No.	1	2	3	4	5	Average
1	4.133	4.094	4.005	3.972	3.852	4.011
2	1.206	1.576	1.248	1.247	1.124	1.280
3	5.542	5.162	5.562	5.336	5.348	5.390
4	6.242	6.297	6.124	5.874	5.876	6.083
5	1.582	1.927	1.765	1.842	1.642	1.752
6	3.705	2.813	3.257	3.318	3.175	3.254
7	1.717	2.473	2.115	2.068	2.148	2.104
8	2.612	2.646	2.584	2.663	2.578	2.617
9	5.753	5.265	5.621	5.473	5.472	5.517
10	2.423	2.367	2.385	2.386	2.378	2.388
11	3.576	3.451	3.642	3.725	3.421	3.563
12	2.255	3.005	2.644	2.427	2.384	2.543
13	0.974	0.791	0.872	0.921	0.776	0.867
14	4.883	4.685	4.682	4.823	4.745	4.764
15	2.104	2.788	2.337	2.528	2.442	2.440
16	5.266	5.337	5.337	5.246	5.429	5.323
17	2.471	2.535	2.482	2.553	2.618	2.532
18	1.007	0.965	0.996	0.972	0.856	0.959
19	4.577	3.891	4.338	4.276	4.421	4.301
20	3.684	3.916	3.795	3.826	3.782	3.801
21	1.587	1.378	1.523	1.446	1.437	1.474
22	6.030	5.873	5.872	5.894	5.689	5.872
23	1.256	1.816	1.457	1.652	1.555	1.547
24	5.302	5.980	5.553	5.643	5.489	5.593
25	4.616	3.940	4.325	4.198	4.178	4.251
26	4.389	4.351	4.286	4.338	4.322	4.337
27	3.964	3.856	3.875	4.124	3.872	3.938
28	3.938	4.658	3.598	4.356	4.412	4.192
29	3.581	3.937	3.776	4.215	3.475	3.797

C-6: Data for upper kerf of 4 mm PMMA.

No.	1	2	3	4	5	Average
1	0.700	0.674	0.694	0.703	0.690	0.692
2	0.760	0.755	0.778	0.784	0.775	0.770
3	0.635	0.633	0.615	0.629	0.628	0.628
4	0.725	0.742	0.734	0.732	0.723	0.731
5	0.908	0.879	0.915	0.997	0.881	0.916
6	0.805	0.811	0.838	0.819	0.833	0.821
7	0.671	0.676	0.672	0.667	0.673	0.672
8	0.539	0.526	0.530	0.521	0.519	0.527
9	0.764	0.772	0.771	0.751	0.766	0.765
10	0.896	0.874	0.852	0.869	0.876	0.873
11	0.541	0.551	0.546	0.550	0.539	0.545
12	0.615	0.605	0.601	0.613	0.604	0.608
13	0.744	0.785	0.788	0.778	0.794	0.778
14	0.769	0.777	0.790	0.792	0.796	0.785
15	0.744	0.739	0.745	0.748	0.753	0.746
16	0.691	0.662	0.670	0.673	0.688	0.677
17	0.670	0.673	0.624	0.668	0.653	0.658
18	0.830	0.821	0.804	0.816	0.803	0.815
19	0.690	0.673	0.657	0.685	0.670	0.675
20	0.789	0.768	0.772	0.759	0.769	0.771
21	0.900	0.891	0.885	0.898	0.899	0.895
22	0.852	0.819	0.827	0.833	0.816	0.829
23	0.688	0.679	0.693	0.696	0.683	0.688
24	0.594	0.591	0.599	0.592	0.589	0.593
25	0.681	0.686	0.680	0.676	0.688	0.682
26	0.700	0.694	0.692	0.699	0.694	0.696
27	0.730	0.708	0.726	0.716	0.708	0.718
28	0.703	0.686	0.699	0.691	0.705	0.697
29	0.705	0.702	0.693	0.687	0.692	0.696

C-7: Data for lower kerf of 4 mm PMMA.

No.	1	2	3	4	5	Average
1	0.280	0.277	0.281	0.263	0.290	0.278
2	0.310	0.348	0.322	0.351	0.355	0.337
3	0.158	0.153	0.173	0.181	0.201	0.173
4	0.269	0.251	0.242	0.267	0.254	0.257
5	0.209	0.211	0.204	0.212	0.219	0.211
6	0.197	0.210	0.203	0.194	0.205	0.202
7	0.303	0.302	0.307	0.309	0.316	0.307
8	0.311	0.302	0.306	0.320	0.312	0.310
9	0.167	0.160	0.164	0.159	0.170	0.164
10	0.238	0.251	0.241	0.243	0.247	0.244
11	0.213	0.199	0.216	0.230	0.220	0.216
12	0.367	0.363	0.355	0.348	0.354	0.357
13	0.285	0.264	0.290	0.269	0.286	0.279
14	0.262	0.224	0.232	0.241	0.245	0.241
15	0.248	0.263	0.259	0.250	0.258	0.256
16	0.228	0.237	0.226	0.224	0.254	0.234
17	0.168	0.170	0.199	0.171	0.196	0.181
18	0.263	0.267	0.256	0.270	0.261	0.263
19	0.191	0.194	0.198	0.196	0.202	0.196
20	0.259	0.261	0.272	0.267	0.277	0.267
21	0.285	0.282	0.294	0.288	0.284	0.287
22	0.207	0.192	0.195	0.209	0.206	0.202
23	0.346	0.358	0.367	0.372	0.366	0.362
24	0.294	0.258	0.261	0.288	0.274	0.275
25	0.236	0.242	0.248	0.253	0.254	0.247
26	0.237	0.264	0.230	0.240	0.247	0.244
27	0.243	0.237	0.226	0.233	0.245	0.237
28	0.226	0.225	0.246	0.233	0.242	0.234
29	0.247	0.219	0.230	0.232	0.225	0.231

C-8: Data for roughness of 4 mm PMMA.

No.	1	2	3	4	5	Average
1	1.945	1.756	1.603	2.092	1.827	1.845
2	1.357	1.425	1.014	1.374	1.142	1.262
3	7.241	7.145	6.916	7.088	6.862	7.050
4	5.952	6.183	5.846	6.143	6.127	6.050
5	1.439	1.306	1.472	1.248	1.422	1.377
6	4.363	3.854	3.986	4.245	4.105	4.111
7	1.203	1.021	1.326	1.247	1.145	1.188
8	5.055	4.310	4.986	4.571	4.446	4.674
9	2.475	2.682	2.754	2.621	2.748	2.656
10	2.368	2.064	2.175	2.358	2.175	2.228
11	4.916	4.816	5.142	4.856	4.685	4.883
12	3.105	2.756	2.775	2.998	2.753	2.877
13	0.892	0.948	1.105	0.891	0.879	0.943
14	2.949	2.745	2.768	2.943	2.842	2.849
15	1.103	1.121	1.254	1.142	1.121	1.148
16	8.175	8.956	8.849	8.034	8.418	8.486
17	1.947	1.504	1.845	1.652	1.649	1.719
18	0.986	0.829	0.993	0.842	1.058	0.942
19	3.228	2.856	3.337	3.145	2.923	3.098
20	2.594	2.894	2.653	2.851	2.743	2.747
21	1.142	0.997	1.060	1.091	1.082	1.074
22	5.728	5.648	5.211	5.844	5.601	5.606
23	0.662	0.746	0.762	0.631	0.621	0.684
24	7.628	7.552	7.338	7.804	7.453	7.555
25	1.900	1.445	1.590	1.443	1.754	1.626
26	1.531	1.200	1.458	1.334	1.204	1.345
27	1.426	1.815	1.682	1.745	1.775	1.689
28	1.624	1.490	1.452	1.528	1.246	1.468
29	1.628	1.761	1.472	1.235	1.248	1.469

C-9: Data for upper kerf of 6 mm PMMA.

No.	1	2	3	4	5	Average
1	0.817	0.822	0.821	0.815	0.824	0.820
2	0.929	0.922	0.931	0.930	0.935	0.929
3	0.756	0.743	0.731	0.755	0.738	0.745
4	0.775	0.758	0.776	0.780	0.773	0.772
5	1.053	1.045	1.030	1.048	1.041	1.043
6	0.929	0.910	0.940	0.933	0.932	0.929
7	0.676	0.685	0.681	0.679	0.680	0.680
8	0.700	0.698	0.699	0.704	0.701	0.700
9	0.977	0.961	0.940	0.946	0.949	0.955
10	1.035	1.032	1.025	1.033	1.038	1.033
11	0.589	0.570	0.595	0.574	0.601	0.586
12	0.614	0.625	0.621	0.611	0.619	0.618
13	0.870	0.862	0.874	0.870	0.865	0.868
14	0.629	0.643	0.620	0.630	0.634	0.631
15	0.873	0.895	0.893	0.896	0.894	0.890
16	0.713	0.674	0.686	0.690	0.704	0.693
17	0.755	0.765	0.760	0.751	0.769	0.760
18	0.865	0.852	0.860	0.850	0.857	0.857
19	0.743	0.732	0.728	0.721	0.723	0.729
20	0.847	0.837	0.833	0.827	0.821	0.833
21	1.031	1.043	1.046	1.032	1.042	1.039
22	1.060	0.996	0.999	1.000	1.002	1.011
23	0.659	0.682	0.688	0.694	0.681	0.681
24	0.589	0.585	0.596	0.582	0.588	0.588
25	0.838	0.837	0.830	0.843	0.838	0.837
26	0.845	0.829	0.834	0.830	0.843	0.836
27	0.782	0.802	0.804	0.792	0.788	0.794
28	0.820	0.824	0.834	0.840	0.833	0.830
29	0.762	0.774	0.777	0.772	0.770	0.771

C-10: Data for lower kerf of 6 mm PMMA.

No.	1	2	3	4	5	Average
1	0.330	0.296	0.321	0.298	0.323	0.314
2	0.414	0.412	0.411	0.412	0.421	0.414
3	0.162	0.204	0.209	0.175	0.186	0.187
4	0.340	0.323	0.353	0.345	0.346	0.341
5	0.222	0.216	0.249	0.228	0.259	0.235
6	0.260	0.254	0.269	0.277	0.252	0.262
7	0.449	0.436	0.444	0.440	0.441	0.442
8	0.293	0.295	0.281	0.296	0.289	0.291
9	0.182	0.194	0.200	0.196	0.170	0.188
10	0.233	0.214	0.238	0.245	0.239	0.234
11	0.329	0.311	0.335	0.340	0.320	0.327
12	0.479	0.451	0.467	0.451	0.459	0.461
13	0.402	0.401	0.400	0.407	0.392	0.400
14	0.309	0.297	0.295	0.289	0.300	0.298
15	0.385	0.421	0.402	0.371	0.363	0.388
16	0.257	0.283	0.271	0.275	0.288	0.275
17	0.268	0.264	0.262	0.273	0.275	0.268
18	0.397	0.397	0.401	0.395	0.402	0.398
19	0.232	0.243	0.224	0.244	0.235	0.236
20	0.328	0.341	0.322	0.349	0.323	0.333
21	0.269	0.286	0.280	0.285	0.284	0.281
22	0.213	0.177	0.198	0.199	0.203	0.198
23	0.559	0.570	0.578	0.576	0.556	0.568
24	0.336	0.323	0.302	0.345	0.346	0.330
25	0.384	0.381	0.385	0.386	0.380	0.383
26	0.371	0.374	0.376	0.366	0.377	0.373
27	0.383	0.405	0.395	0.389	0.383	0.391
28	0.394	0.386	0.377	0.375	0.374	0.381
29	0.389	0.402	0.379	0.386	0.384	0.388

C-11: Data for HAZ of 6 mm PMMA.

No.	1	2	3	4	5	Average
1	0.047	0.045	0.043	0.046	0.043	0.045
2	0.054	0.052	0.053	0.054	0.056	0.054
3	0.026	0.027	0.028	0.021	0.029	0.026
4	0.032	0.037	0.035	0.036	0.033	0.035
5	0.040	0.038	0.035	0.034	0.038	0.037
6	0.033	0.034	0.035	0.033	0.035	0.034
7	0.047	0.045	0.045	0.046	0.046	0.046
8	0.040	0.039	0.039	0.038	0.040	0.039
9	0.023	0.027	0.031	0.035	0.030	0.029
10	0.038	0.039	0.038	0.039	0.040	0.039
11	0.034	0.038	0.041	0.022	0.034	0.034
12	0.048	0.051	0.053	0.052	0.050	0.051
13	0.043	0.042	0.045	0.042	0.044	0.043
14	0.035	0.038	0.040	0.037	0.039	0.038
15	0.038	0.039	0.039	0.038	0.040	0.039
16	0.029	0.025	0.027	0.028	0.029	0.028
17	0.038	0.037	0.038	0.036	0.040	0.038
18	0.042	0.041	0.042	0.043	0.039	0.041
19	0.031	0.034	0.033	0.030	0.031	0.032
20	0.040	0.039	0.040	0.038	0.039	0.039
21	0.044	0.041	0.039	0.044	0.043	0.042
22	0.028	0.027	0.031	0.035	0.030	0.030
23	0.047	0.046	0.043	0.042	0.046	0.045
24	0.030	0.035	0.036	0.028	0.030	0.032
25	0.040	0.039	0.040	0.038	0.040	0.039
26	0.040	0.042	0.043	0.041	0.041	0.041
27	0.041	0.038	0.034	0.037	0.040	0.038
28	0.043	0.044	0.039	0.038	0.040	0.041
29	0.044	0.043	0.040	0.043	0.041	0.042

C-12: Data for roughness of 6 mm PMMA.

No.	1	2	3	4	5	Average
1	2.465	2.623	2.552	2.647	2.743	2.606
2	1.845	1.856	1.946	1.855	1.875	1.875
3	5.643	6.256	6.201	6.015	5.846	5.992
4	4.152	4.245	4.560	4.251	4.273	4.296
5	0.245	0.215	0.227	0.233	0.214	0.227
6	3.024	3.150	2.982	2.785	2.774	2.943
7	0.510	0.442	0.432	0.439	0.412	0.447
8	3.003	3.076	3.014	3.105	3.018	3.043
9	2.247	2.196	2.250	2.447	2.314	2.291
10	1.810	1.739	1.689	1.542	1.957	1.747
11	2.732	2.956	2.853	2.914	2.746	2.840
12	1.846	1.845	1.774	1.648	1.453	1.713
13	1.381	1.343	1.342	1.366	1.425	1.371
14	1.445	1.628	1.528	1.558	1.621	1.556
15	2.174	2.148	2.241	2.246	1.996	2.161
16	7.164	6.404	6.628	6.948	6.793	6.787
17	1.667	1.421	1.485	1.628	1.493	1.539
18	0.428	0.446	0.482	0.501	0.417	0.455
19	3.895	3.832	3.942	3.774	3.881	3.865
20	3.356	3.572	3.274	3.567	3.448	3.443
21	1.538	1.268	1.424	1.302	1.324	1.371
22	4.403	5.007	4.682	4.849	4.662	4.721
23	2.153	2.345	2.262	1.949	2.141	2.170
24	3.128	2.806	3.102	2.895	3.107	3.008
25	1.163	1.416	1.452	1.147	1.276	1.291
26	1.484	1.125	1.289	1.324	1.415	1.327
27	1.610	1.556	1.657	1.453	1.582	1.572
28	1.485	1.300	1.452	1.337	1.425	1.400
29	1.132	1.547	1.385	1.475	1.342	1.376

C-13: Data for upper kerf of 8 mm PMMA.

No.	1	2	3	4	5	Average
1	1.031	1.021	1.022	1.015	1.025	1.023
2	1.049	1.044	1.042	1.045	1.054	1.047
3	0.921	0.906	0.912	0.916	0.920	0.915
4	0.974	0.969	0.975	0.976	0.965	0.972
5	1.102	1.100	1.103	1.121	1.102	1.106
6	1.113	1.114	1.118	1.120	1.122	1.117
7	0.789	0.780	0.788	0.795	0.800	0.790
8	0.810	0.797	0.807	0.799	0.798	0.802
9	1.130	1.121	1.128	1.139	1.116	1.127
10	1.165	1.163	1.158	1.153	1.149	1.158
11	0.743	0.741	0.745	0.740	0.744	0.743
12	0.794	0.779	0.767	0.778	0.787	0.781
13	1.009	1.001	1.008	1.000	1.010	1.006
14	0.930	0.935	0.947	0.949	0.940	0.940
15	1.015	1.017	1.010	1.012	1.003	1.011
16	0.975	0.989	0.979	0.968	0.978	0.978
17	1.007	1.011	1.014	1.010	1.015	1.011
18	0.977	0.989	0.984	0.988	0.991	0.986
19	0.971	0.965	0.966	0.976	0.970	0.970
20	1.018	1.025	1.030	1.026	1.027	1.025
21	1.177	1.167	1.174	1.173	1.170	1.172
22	1.113	1.107	1.111	1.110	1.112	1.111
23	0.860	0.857	0.854	0.865	0.866	0.860
24	0.710	0.700	0.709	0.719	0.717	0.711
25	0.960	0.963	0.966	0.954	0.965	0.962
26	0.969	0.977	0.978	0.971	0.963	0.972
27	0.965	0.976	0.966	0.963	0.970	0.968
28	0.970	0.974	0.976	0.979	0.974	0.975
29	0.976	0.982	0.970	0.972	0.978	0.976

C-14: Data for lower kerf of 8 mm PMMA.

No.	1	2	3	4	5	Average
1	0.532	0.531	0.524	0.532	0.533	0.530
2	0.638	0.641	0.632	0.626	0.637	0.635
3	0.164	0.255	0.289	0.186	0.190	0.217
4	0.382	0.374	0.394	0.400	0.385	0.387
5	0.335	0.349	0.356	0.336	0.338	0.343
6	0.264	0.253	0.263	0.255	0.262	0.259
7	0.453	0.459	0.443	0.460	0.459	0.455
8	0.457	0.468	0.475	0.469	0.485	0.471
9	0.241	0.227	0.257	0.230	0.249	0.241
10	0.319	0.327	0.333	0.326	0.320	0.325
11	0.386	0.385	0.388	0.359	0.384	0.380
12	0.541	0.543	0.546	0.536	0.533	0.540
13	0.578	0.587	0.586	0.580	0.587	0.584
14	0.342	0.323	0.377	0.320	0.319	0.336
15	0.562	0.543	0.563	0.560	0.553	0.556
16	0.297	0.300	0.280	0.291	0.293	0.292
17	0.324	0.333	0.336	0.334	0.341	0.334
18	0.487	0.488	0.482	0.479	0.479	0.483
19	0.326	0.328	0.338	0.340	0.345	0.335
20	0.501	0.484	0.497	0.492	0.493	0.493
21	0.388	0.394	0.382	0.384	0.385	0.387
22	0.241	0.214	0.222	0.227	0.238	0.228
23	0.659	0.665	0.668	0.670	0.658	0.664
24	0.341	0.330	0.333	0.334	0.328	0.333
25	0.418	0.424	0.414	0.416	0.412	0.417
26	0.410	0.417	0.418	0.421	0.420	0.417
27	0.408	0.412	0.406	0.419	0.421	0.413
28	0.416	0.418	0.420	0.415	0.423	0.418
29	0.418	0.421	0.420	0.419	0.420	0.420

C-15: Data for roughness of 8 mm PMMA.

No.	1	2	3	4	5	Average
1	1.046	1.384	1.127	1.354	1.149	1.212
2	0.737	0.960	0.842	0.823	0.781	0.829
3	4.957	4.856	4.997	4.856	4.942	4.922
4	3.682	3.456	3.341	3.946	3.681	3.621
5	0.766	1.192	0.956	1.147	0.836	0.979
6	1.627	1.214	1.652	1.241	1.308	1.408
7	1.025	0.842	1.127	0.752	0.824	0.914
8	2.942	3.068	3.068	2.875	2.983	2.987
9	1.161	1.074	1.274	1.027	1.109	1.129
10	1.024	0.986	1.075	0.842	1.107	1.007
11	2.231	2.285	2.237	2.318	2.254	2.265
12	1.325	1.212	1.241	1.324	1.241	1.269
13	0.867	0.852	0.659	0.857	0.648	0.777
14	1.142	1.089	1.215	1.139	1.115	1.140
15	1.239	1.027	1.238	1.135	1.051	1.138
16	6.694	6.894	6.785	7.167	6.764	6.861
17	0.817	0.965	1.017	0.945	0.816	0.912
18	0.596	0.641	0.638	0.613	0.605	0.619
19	1.375	1.743	1.734	1.472	1.481	1.561
20	1.327	1.292	1.154	1.142	1.118	1.207
21	1.015	0.972	0.961	0.912	0.873	0.947
22	2.238	2.326	2.252	2.341	2.138	2.259
23	2.847	2.538	2.746	2.684	2.643	2.691
24	8.522	8.403	8.285	8.651	8.372	8.447
25	1.087	0.876	1.165	0.867	0.895	0.978
26	0.978	0.949	0.876	0.955	1.037	0.959
27	1.017	0.963	0.991	1.108	0.873	0.990
28	1.102	1.109	1.123	1.218	1.225	1.155
29	1.024	0.845	0.861	1.105	0.848	0.937

APPENDIX – D (MDF)

D-1: Data for upper kerf of 4 mm MDF.

No	upper kerf, mm					Average
	1	2	3	4	5	
1	0.355	0.328	0.316	0.311	0.320	0.326
2	0.444	0.440	0.432	0.428	0.430	0.435
3	0.260	0.282	0.271	0.275	0.246	0.267
4	0.323	0.329	0.333	0.331	0.324	0.328
5	0.692	0.705	0.701	0.675	0.695	0.694
6	0.642	0.616	0.626	0.621	0.620	0.625
7	0.349	0.333	0.324	0.325	0.297	0.326
8	0.310	0.297	0.299	0.291	0.311	0.302
9	0.619	0.648	0.629	0.636	0.631	0.633
10	0.653	0.678	0.680	0.667	0.659	0.667
11	0.273	0.279	0.292	0.283	0.294	0.284
12	0.375	0.352	0.337	0.351	0.364	0.356
13	0.440	0.462	0.451	0.442	0.455	0.450
14	0.370	0.368	0.387	0.378	0.380	0.377
15	0.416	0.419	0.420	0.433	0.413	0.420
16	0.375	0.385	0.369	0.382	0.384	0.379
17	0.368	0.371	0.356	0.370	0.378	0.369
18	0.434	0.461	0.440	0.436	0.446	0.443
19	0.342	0.320	0.323	0.345	0.337	0.333
20	0.406	0.419	0.409	0.404	0.405	0.409
21	0.682	0.690	0.670	0.685	0.673	0.680
22	0.659	0.635	0.651	0.638	0.637	0.644
23	0.352	0.324	0.337	0.330	0.335	0.336
24	0.326	0.345	0.331	0.342	0.333	0.335
25	0.405	0.398	0.390	0.404	0.403	0.400
26	0.393	0.379	0.354	0.365	0.381	0.374
27	0.417	0.428	0.413	0.406	0.423	0.417
28	0.409	0.412	0.405	0.403	0.422	0.410
29	0.425	0.042	0.411	0.410	0.413	0.340

D-2: Data for lower kerf of 4 mm MDF.

No.	Lower kerf, mm					Average
	1	2	3	4	5	
1	0.210	0.237	0.246	0.228	0.240	0.232
2	0.369	0.372	0.356	0.355	0.364	0.363
3	0.147	0.130	0.112	0.125	0.154	0.134
4	0.259	0.268	0.288	0.279	0.227	0.264
5	0.247	0.250	0.245	0.238	0.249	0.246
6	0.252	0.260	0.244	0.249	0.267	0.254
7	0.276	0.224	0.181	0.207	0.218	0.221
8	0.250	0.213	0.212	0.202	0.245	0.224
9	0.134	0.113	0.137	0.123	0.152	0.132
10	0.292	0.278	0.282	0.269	0.275	0.279
11	0.129	0.125	0.123	0.114	0.125	0.123
12	0.337	0.349	0.333	0.337	0.351	0.341
13	0.333	0.329	0.324	0.315	0.320	0.324
14	0.238	0.255	0.236	0.232	0.260	0.244
15	0.338	0.335	0.333	0.334	0.337	0.335
16	0.278	0.270	0.246	0.255	0.271	0.264
17	0.117	0.122	0.130	0.123	0.149	0.128
18	0.322	0.309	0.300	0.320	0.310	0.312
19	0.147	0.130	0.126	0.148	0.137	0.138
20	0.311	0.306	0.295	0.298	0.297	0.301
21	0.285	0.308	0.314	0.296	0.301	0.301
22	0.261	0.251	0.245	0.268	0.255	0.256
23	0.350	0.367	0.349	0.358	..348	0.356
24	0.251	0.230	0.204	0.199	0.228	0.222
25	0.235	0.244	0.256	0.236	0.255	0.245
26	0.260	0.236	0.261	0.249	0.254	0.252
27	0.255	0.256	0.224	0.226	0.238	0.240
28	0.259	0.265	0.260	0.254	0.264	0.260
29	0.262	0.248	0.263	0.250	0.251	0.255

D-3: Data for roughness of 4 mm MDF.

No.	Ra, μm					Average
	1	2	3	4	5	
1	6.286	5.428	5.915	5.818	5.840	5.857
2	3.721	3.897	3.842	3.864	3.720	3.809
3	7.008	6.748	6.876	6.872	6.879	6.877
4	5.162	5.174	5.215	5.202	5.186	5.188
5	5.889	5.680	5.741	5.842	5.772	5.785
6	6.404	6.826	6.624	6.612	6.611	6.615
7	4.709	4.502	4.624	4.322	4.420	4.515
8	5.262	5.138	5.177	5.216	5.188	5.196
9	6.255	7.434	6.942	6.926	6.742	6.860
10	5.241	5.240	5.372	5.271	5.261	5.277
11	5.260	5.791	5.475	5.527	5.325	5.476
12	4.278	4.318	4.316	4.342	4.235	4.298
13	4.515	3.976	4.211	4.312	4.227	4.248
14	5.855	6.156	6.145	6.001	5.912	6.014
15	5.355	6.338	5.944	5.645	5.855	5.827
16	5.817	6.017	5.984	5.785	5.964	5.913
17	5.107	5.039	4.954	5.104	5.211	5.083
18	4.358	4.172	4.251	4.143	4.158	4.216
19	5.921	6.345	6.242	5.998	6.220	6.145
20	5.982	5.969	5.897	5.973	5.982	5.961
21	6.134	5.219	5.847	5.347	5.768	5.663
22	6.084	6.674	6.842	6.442	6.528	6.514
23	4.478	4.522	4.475	4.251	4.322	4.410
24	5.662	5.497	5.348	5.446	5.521	5.495
25	5.089	5.482	5.241	5.314	5.141	5.253
26	5.965	5.842	5.945	6.174	5.747	5.935
27	6.742	6.107	6.447	6.124	6.273	6.339
28	5.754	5.882	6.164	5.894	5.786	5.896
29	5.539	7.267	6.547	6.228	6.257	6.368

D-4: Data for upper kerf of 6 mm MDF.

No.	upper kerf, mm					Average
	1	2	3	4	5	
1	0.523	0.540	0.530	0.529	0.525	0.529
2	0.599	0.594	0.597	0.580	0.571	0.588
3	0.302	0.396	0.386	0.301	0.304	0.338
4	0.405	0.382	0.408	0.406	0.405	0.401
5	0.966	0.950	0.956	0.964	0.960	0.959
6	0.915	0.914	0.910	0.907	0.906	0.910
7	0.338	0.332	0.326	0.319	0.322	0.327
8	0.318	0.326	0.332	0.329	0.323	0.326
9	0.825	0.851	0.827	0.821	0.809	0.827
10	0.984	0.971	0.988	0.992	0.981	0.983
11	0.303	0.306	0.307	0.297	0.308	0.304
12	0.380	0.385	0.357	0.372	0.383	0.375
13	0.566	0.544	0.545	0.565	0.562	0.556
14	0.435	0.426	0.437	0.440	0.429	0.433
15	0.481	0.488	0.487	0.490	0.478	0.485
16	0.546	0.523	0.522	0.539	0.536	0.533
17	0.495	0.498	0.491	0.483	0.493	0.492
18	0.538	0.540	0.555	0.546	0.548	0.545
19	0.550	0.539	0.536	0.525	0.547	0.539
20	0.585	0.571	0.575	0.576	0.580	0.577
21	0.916	0.922	0.917	0.915	0.912	0.916
22	0.851	0.826	0.850	0.845	0.830	0.840
23	0.365	0.364	0.370	0.370	0.355	0.365
24	0.330	0.327	0.347	0.339	0.335	0.336
25	0.570	0.559	0.557	0.555	0.560	0.560
26	0.445	0.443	0.446	0.466	0.442	0.448
27	0.467	0.461	0.474	0.470	0.464	0.467
28	0.571	0.568	0.562	0.570	0.572	0.569
29	0.546	0.537	0.548	0.545	0.551	0.545

D-5: Data for lower kerf of 6 mm MDF.

No.	Lower kerf, mm					Average
	1	2	3	4	5	
1	0.316	0.323	0.299	0.320	0.313	0.314
2	0.396	0.418	0.405	0.416	0.415	0.410
3	0.147	0.136	0.139	0.145	0.143	0.142
4	0.268	0.280	0.270	0.281	0.293	0.278
5	0.207	0.214	0.205	0.215	0.222	0.213
6	0.235	0.230	0.227	0.240	0.245	0.235
7	0.197	0.194	0.200	0.193	0.196	0.196
8	0.186	0.190	0.193	0.194	0.204	0.193
9	0.104	0.106	0.110	0.106	0.108	0.107
10	0.292	0.290	0.266	0.278	0.271	0.279
11	0.178	0.187	0.173	0.176	0.179	0.179
12	0.220	0.207	0.221	0.223	0.235	0.221
13	0.370	0.371	0.362	0.345	0.365	0.363
14	0.210	0.209	0.213	0.320	0.219	0.234
15	0.387	0.352	0.374	0.376	0.369	0.372
16	0.254	0.260	0.234	0.240	0.253	0.248
17	0.125	0.127	0.136	0.148	0.144	0.136
18	0.297	0.291	0.301	0.290	0.305	0.297
19	0.142	0.149	0.134	0.153	0.143	0.144
20	0.317	0.284	0.299	0.309	0.303	0.302
21	0.327	0.328	0.324	0.334	0.310	0.325
22	0.214	0.200	0.201	0.205	0.206	0.205
23	0.391	0.358	0.380	0.386	0.390	0.381
24	0.203	0.200	0.190	0.202	0.215	0.202
25	0.270	0.256	0.260	0.263	0.271	0.264
26	0.247	0.259	0.255	0.256	0.248	0.253
27	0.260	0.250	0.253	0.254	0.249	0.253
28	0.247	0.268	0.250	0.251	0.260	0.255
29	0.245	0.240	0.242	0.267	0.235	0.246

D-6: Data for roughness of 6 mm MDF.

No.	Ra, μm					Average
	1	2	3	4	5	
1	6.875	6.702	6.994	7.102	6.784	6.891
2	5.427	5.550	5.563	5.487	5.414	5.488
3	8.729	8.659	8.812	8.733	8.745	8.736
4	6.991	7.122	6.946	6.821	6.925	6.961
5	7.232	7.285	7.341	7.184	7.245	7.257
6	9.351	8.010	8.633	8.825	8.601	8.684
7	6.516	6.345	6.627	6.702	6.644	6.567
8	8.292	6.108	7.335	7.154	7.042	7.186
9	7.635	8.980	8.322	8.410	8.221	8.314
10	6.135	7.672	7.014	6.897	6.811	6.906
11	6.525	8.272	7.451	7.231	7.287	7.353
12	5.188	5.466	5.341	5.245	5.418	5.332
13	5.587	6.555	5.633	5.265	5.554	5.719
14	7.643	6.983	7.332	7.455	7.211	7.325
15	6.768	6.506	6.774	6.828	6.924	6.760
16	7.303	8.583	8.141	8.325	8.004	8.071
17	7.845	7.662	7.845	8.104	8.241	7.939
18	5.622	5.795	5.714	5.652	5.821	5.721
19	8.409	8.184	8.234	8.527	8.119	8.295
20	6.411	6.217	6.335	6.951	6.487	6.480
21	7.079	6.597	6.922	6.812	6.758	6.834
22	5.774	5.651	5.824	5.722	5.815	5.757
23	5.201	5.211	5.385	5.064	5.102	5.193
24	7.123	7.876	7.644	7.552	7.423	7.524
25	6.512	7.315	6.844	6.963	6.977	6.922
26	6.805	7.345	7.100	7.127	6.985	7.072
27	6.801	6.536	6.584	6.884	6.945	6.750
28	6.620	6.544	6.338	6.846	6.751	6.620
29	6.370	7.464	7.247	6.824	6.552	6.891

D-7: Data for upper kerf of 9 mm MDF.

	upper kerf, mm					Average
	1	2	3	4	5	
1	0.581	0.546	0.636	0.567	0.572	0.580
2	0.657	0.671	0.651	0.656	0.662	0.659
3	0.474	0.479	0.473	0.473	0.477	0.475
4	0.569	0.574	0.585	0.572	0.529	0.566
5	0.924	0.943	0.933	0.944	0.931	0.935
6	0.906	0.914	0.912	0.907	0.898	0.907
7	0.321	0.313	0.318	0.324	0.329	0.321
8	0.311	0.308	0.295	0.313	0.303	0.306
9	0.887	0.865	0.898	0.869	0.896	0.883
10	1.013	1.003	1.007	1.002	1.012	1.007
11	0.291	0.273	0.296	0.306	0.304	0.294
12	0.362	0.350	0.342	0.343	0.367	0.353
13	0.652	0.660	0.642	0.645	0.649	0.650
14	0.539	0.532	0.529	0.530	0.532	0.532
15	0.678	0.696	0.581	0.685	0.671	0.662
16	0.625	0.622	0.612	0.623	0.620	0.620
17	0.638	0.645	0.658	0.644	0.645	0.646
18	0.655	0.651	0.648	0.657	0.660	0.654
19	0.624	0.620	0.622	0.618	0.623	0.621
20	0.680	0.661	0.670	0.660	0.672	0.669
21	0.957	0.955	0.951	0.938	0.949	0.950
22	1.004	0.996	1.001	1.003	1.004	1.002
23	0.365	0.370	0.350	0.356	0.351	0.358
24	0.318	0.334	0.324	0.320	0.321	0.323
25	0.599	0.602	0.610	0.606	0.595	0.602
26	0.642	0.624	0.632	0.620	0.634	0.630
27	0.571	0.596	0.595	0.602	0.605	0.594
28	0.628	0.615	0.633	0.622	0.620	0.624
29	0.649	0.636	0.648	0.642	0.635	0.642

D-8: Data for lower kerf of 9 mm MDF.

	Lower kerf, mm					Average
	1	2	3	4	5	
1	0.338	0.340	0.328	0.353	0.331	0.338
2	0.455	0.475	0.487	0.475	0.452	0.469
3	0.195	0.166	0.161	0.179	0.197	0.180
4	0.270	0.285	0.261	0.283	0.275	0.275
5	0.210	0.199	0.203	0.181	0.169	0.192
6	0.197	0.202	0.194	0.200	0.203	0.199
7	0.221	0.217	0.243	0.214	0.226	0.224
8	0.202	0.222	0.205	0.221	0.219	0.214
9	0.170	0.122	0.126	0.111	0.132	0.132
10	0.256	0.264	0.241	0.259	0.277	0.259
11	0.222	0.196	0.191	0.194	0.201	0.201
12	0.261	0.242	0.235	0.241	0.230	0.242
13	0.432	0.435	0.425	0.436	0.430	0.432
14	0.204	0.215	0.190	0.186	0.205	0.200
15	0.390	0.416	0.419	0.409	0.415	0.410
16	0.196	0.198	0.206	0.220	0.192	0.202
17	0.172	0.188	0.179	0.167	0.183	0.178
18	0.308	0.314	0.296	0.297	0.305	0.304
19	0.178	0.177	0.185	0.168	0.172	0.176
20	0.291	0.310	0.324	0.326	0.317	0.314
21	0.350	0.365	0.371	0.380	0.343	0.362
22	0.145	0.139	0.134	0.146	0.138	0.140
23	0.389	0.375	0.360	0.371	0.360	0.371
24	0.200	0.208	0.194	0.201	0.212	0.203
25	0.210	0.205	0.196	0.197	0.194	0.200
26	0.206	0.195	0.210	0.208	0.198	0.203
27	0.181	0.184	0.200	0.199	0.214	0.196
28	0.209	0.236	0.199	0.230	0.190	0.213
29	0.199	0.198	0.219	0.215	0.252	0.217

D-9: Data for roughness of 9 mm MDF.

	Ra, Micro m					Average
	1	2	3	4	5	
1	8.346	8.454	8.157	7.894	8.254	8.221
2	7.524	7.657	7.957	7.873	7.997	7.802
3	9.780	9.674	10.142	9.365	9.491	9.690
4	8.869	8.787	9.102	8.873	8.641	8.854
5	8.248	10.520	9.543	9.541	9.445	9.459
6	11.220	9.553	10.648	10.325	10.254	10.400
7	6.156	6.478	6.431	6.258	6.314	6.327
8	7.767	6.919	7.456	7.354	7.218	7.343
9	10.627	9.954	10.732	10.422	10.320	10.411
10	9.360	9.420	9.345	9.335	9.241	9.340
11	7.345	6.935	7.346	7.423	7.241	7.258
12	6.397	6.305	6.457	6.237	6.358	6.351
13	7.568	7.275	7.654	7.254	7.136	7.377
14	8.222	9.125	8.742	8.521	8.761	8.674
15	8.372	8.846	8.754	8.824	8.948	8.749
16	9.837	9.816	9.887	9.578	9.995	9.823
17	7.405	7.623	7.534	7.632	7.413	7.521
18	7.856	7.843	7.832	7.747	7.946	7.845
19	9.426	9.435	9.114	8.904	8.745	9.125
20	8.560	8.462	8.154	8.316	8.114	8.321
21	8.626	9.748	9.047	9.278	9.225	9.185
22	10.653	11.165	10.992	10.768	10.882	10.892
23	6.448	5.971	6.381	6.142	6.214	6.231
24	7.925	8.154	8.137	7.856	7.894	7.993
25	8.636	8.142	8.571	8.286	8.273	8.382
26	8.985	9.242	8.854	8.672	8.424	8.835
27	7.487	8.856	8.145	8.245	7.627	8.072
28	9.452	7.561	8.831	8.458	8.233	8.507
29	9.386	8.961	8.935	8.985	9.228	9.099

APPENDIX – E (GFRP)

E-1: Data for upper kerf of 3 mm GFRP.

No.	Upper kerf, mm			Average, mm
	1	2	3	
1	0 .416	0.410	0.416	0.413
2	0.488	0.493	0.489	0.490
3	0.344	0.311	0.318	0.324
4	0.417	0.443	0.430	0.430
5	0.691	0.697	0.682	0.690
6	0.557	0.519	0.551	0.542
7	0.360	0.344	0.364	0.356
8	0.336	0.327	0.328	0.330
9	0.603	0.673	0.708	0.661
10	0.555	0.547	0.577	0.560
11	0.343	0.320	0.332	0.332
12	0.291	0.327	0.314	0.311
13	0.398	0.381	0.385	0.388
14	0.306	0.339	0.294	0.313
15	0.357	0.331	0.319	0.336
16	0.364	0.365	0.354	0.361
17	0.394	0.389	0.386	0.390
18	0.516	0.514	0.521	0.517
19	0.425	0.412	0.418	0.418
20	0.483	0.469	0.478	0.477
21	0.724	0.748	0.756	0.743
22	0.597	0.547	0.525	0.556
23	0.390	0.405	0.369	0.388
24	0.371	0.373	0.369	0.371
25	0.365	0.344	0.332	0.347
26	0.306	0.291	0.309	0.302
27	0.454	0.358	0.334	0.382
28	0.378	0.356	0.360	0.365
29	0.337	0.322	0.317	0.325

E-2: Data for lower kerf of 3 mm GFRP.

No.	Lower kerf, mm					Average, mm
	1	2	3	4	5	
1	0.335	0.312	0.348	0.328	0.355	0.336
2	0.423	0.453	0.472	0.451	0.489	0.458
3	0.334	0.293	0.271	0.280	0.310	0.298
4	0.376	0.368	0.370	0.385	0.364	0.373
5	0.368	0.292	0.372	0.350	0.359	0.348
6	0.327	0.269	0.295	0.298	0.293	0.296
7	0.398	0.407	0.438	0.399	0.402	0.409
8	0.383	0.385	0.379	0.412	0.340	0.380
9	0.222	0.237	0.206	0.294	0.274	0.247
10	0.384	0.337	0.338	0.339	0.358	0.351
11	0.211	0.184	0.183	0.188	0.269	0.207
12	0.388	0.394	0.408	0.387	0.374	0.390
13	0.404	0.396	0.411	0.409	0.454	0.415
14	0.446	0.411	0.367	0.387	0.401	0.402
15	0.436	0.446	0.472	0.462	0.378	0.439
16	0.377	0.341	0.312	0.325	0.399	0.351
17	0.270	0.209	0.227	0.191	0.196	0.219
18	0.423	0.418	0.386	0.411	0.438	0.415
19	0.317	0.318	0.303	0.289	0.302	0.306
20	0.405	0.465	0.429	0.449	0.496	0.449
21	0.311	0.326	0.329	0.336	0.318	0.324
22	0.314	0.303	0.352	0.382	0.343	0.339
23	0.485	0.414	0.406	0.444	0.410	0.432
24	0.390	0.384	0.381	0.425	0.403	0.397
25	0.386	0.347	0.320	0.354	0.348	0.351
26	0.373	0.382	0.340	0.400	0.381	0.375
27	0.376	0.385	0.328	0.353	0.383	0.365
28	0.392	0.359	0.329	0.353	0.357	0.358
29	0.398	0.320	0.336	0.337	0.378	0.354

E-3: Data for HAZ of 3 mm GFRP.

No.	HAZ			Average, mm
	1	2	3	
1	0.077	0.076	0.080	0.078
2	0.088	0.091	0.088	0.089
3	0.041	0.048	0.043	0.044
4	0.045	0.047	0.048	0.047
5	0.084	0.083	0.084	0.084
6	0.055	0.057	0.058	0.057
7	0.083	0.082	0.080	0.082
8	0.055	0.058	0.062	0.058
9	0.064	0.067	0.063	0.065
10	0.087	0.093	0.090	0.090
11	0.055	0.057	0.049	0.054
12	0.082	0.086	0.083	0.084
13	0.074	0.077	0.083	0.078
14	0.055	0.058	0.056	0.056
15	0.072	0.075	0.079	0.075
16	0.040	0.048	0.043	0.044
17	0.078	0.076	0.080	0.078
18	0.101	0.097	0.098	0.099
19	0.060	0.057	0.062	0.060
20	0.085	0.090	0.083	0.086
21	0.079	0.078	0.076	0.078
22	0.046	0.044	0.048	0.046
23	0.078	0.088	0.079	0.082
24	0.051	0.049	0.047	0.049
25	0.060	0.069	0.063	0.064
26	0.079	0.081	0.078	0.079
27	0.062	0.068	0.065	0.065
28	0.062	0.063	0.056	0.060
29	0.062	0.060	0.061	0.061

APPENDIX – F (EXPLANATION OF SOME TERMS)

- **Perturbation plot:**

The perturbation plot helps you compare the effect of all the factors at a particular point in the design space. The response is plotted by changing only one factor over its range while holding of the other factors constant. By default, Design-Expert software sets the reference point at the midpoint (coded 0) of all the factors. A steep slope or curvature in a factor shows that the response is sensitive to that factor. A relatively flat line shows insensitivity to change in that particular factor. If there are more than two factors, the perturbation plot could be used to find those factors that most affect the response. These influential factors are good choices for the axes on the contour plots.

- **Desirability**

Desirability is an objective function (D) that ranges from zero outside of the limits to one at the goal. The numerical optimization finds a point that maximizes the desirability function. For several responses and factors, all goals get combined into one desirability function as shown below:

$$D = \left(d_1^{r_1} \times d_2^{r_2} \times \ldots \times d_n^{r_n}\right)^{\frac{1}{\sum r_i}} = \left(\prod_{i=1}^{n} d_i^{r_i}\right)^{\frac{1}{\sum r_i}}$$

- **Importance**

In the desirability objective function D, each response can be assigned an importance relative to the other responses. Importance (r_i) varies from the least

important (+) a value of 1, to the most important (+++++) a value of 5. If varying degrees of importance are assigned to the different responses, the objective function is shown above:

- **Adequacy**

An adequate model means that the reduced model has successfully passed all the required statistical tests and can be used to predict the responses or to optimise the process etc.

- **Quality**

In the numerical optimisation, two criteria were implemented in this research. The first criterion was set to obtain the cutting conditions that would improve the quality of the cut section by obtaining smooth cut and square cut edge. As to refer to this first criterion the name ‘Quality’ was given.